12-2021

Development of Solution Blow Spun Nanofibers as Electrical and Whole Cell Biosensing Interfaces

Craig Levar Miller

DEVELOPMENT OF SOLUTION BLOW SPUN NANOFIBERS AS ELECTRICAL AND WHOLE CELL BIOSENSING INTERFACES

A Dissertation
Presented to
the Graduate School of
Clemson University

In Partial Fulfillment
of the Requirements for the Degree
Doctor of Philosophy
Bioengineering

---

by
Craig Levar Miller
December 2021

Accepted by:
Jordon A. Gilmore, PhD., Committee Chair
Jeffrey N. Anker, Ph.D.
William R. Harrell, Ph.D.
David K. Karig, Ph.D.
Joel Kidd, M.D.

ABSTRACT

Infectious pathogens place a huge burden on the US economy with more than $120 billion spent annually for direct and indirect costs for the treatment of infectious diseases. Rapid detection schemes continue to evolve in order to meet the demand of early diagnosis. In chronic wound infections, bacterial load is capable of impeding the healing process. Additionally, bacterial virulence production works coherently with bacterial load to produce toxins and molecules that prolongs the healing cycle. This work examines the use of nonwoven polymeric conductive and non-conductive nanofiber mats as synthetic biosensor scaffolds, drug delivery and biosensor interface constructs.

A custom-made nanofiber platform was built to produce solution blow spun nanofibers of various polymer loading. Antimicrobial nanofiber mats were made with the use of an *in-situ* silver chemical reduction method. Ceria nanoparticles were incorporated to provide an additional antioxidative property. Conductivity properties were examined by using silver and multi-walled carbon nanotubes (MWCNT) as a filler material. SBS parameters were adjusted to analyze electrical conductivity properties. Nanofiber mats were used to detect bacteria concentrations *in vitro*.

Protein adhesion to conductive nanofibers was studied using fluorescent antibodies and BCA assay. Anti-rabbit and streptavidin Alexa Flour 594 was used to examine the adsorption properties of SBS nanofiber mats. Enhancements were made to further improve interface design for specificity. SBS nanofiber electrodes were fabricated to serve as scaffold and detection site for spike protein detection.

Bacteria virulence production was examined by the detection of pyocyanin and quorum sensing molecules. The opportunistic pathogen, *Pseudomonas aeruginosa* is a nosocomial

pathogen found in immunocompromised patients with such as those with chronic wounds and cystic fibrosis. Pyocyanin is one of four quorum sensing molecules that the pathogen produces which can be detected electrochemically due to its inherent redox-active activity. SBS has been used to develop a sensing scheme to detect pyocyanin. This work also examines the use of a synthetic biosensor with a LasR based system capable of detecting homoserine lactone produced by *P. aeruginosa* and other common gram-negative pathogens. Genetic modifications were made to biosensor in order to replace a green, fluorescent reporter with a chromoprotein based reporter system for visual readout.

Additionally, work related to community service and outreach regarding the encouragement of middle school students to pursue Science, Technology, Engineering and Math (STEM) was conducted. Results from outreach program showed an increase in the STEM interest among a group of middle school students. There was a general trend with STEM career knowledge, STEM self-efficacy and the level of interest in STEM careers and activities. Military research was also done with the United States Army Medical Research Institute of Infectious Diseases (USAMRIID) to develop several assays for the detection of several highly infectious viruses and bacteria. Due to confidentiality, the work cannot be published in this manuscript.

DEDICATION

This work is dedicated to my wonderful and patient wife Eliza Miller who has been my number one supporter and encourager during these last several years at Clemson. I am incredibly lucky to have you by my side through the good and bad times. Especially, during my second year when I was first diagnosed. You always motivated me to continue this journey and fight through all the hard times. This entire process has made us much stronger as a couple and I am extremely excited about the next phase of our life.

I would like to thank my dad, Harold Miller, for all the encouragement and late-night pep talks. You were always just a phone call away and always gave me hope to keep looking forward to the things to come. Thank you for being my spiritual guide. I want to give a warm appreciation to my mother and father in-law, Frank, and Patricia Brown. You were truly both an extension of my dad and late mother, Betty Miller. Thank you for all the 4-hour trips from Holly Hill and your support during my time of recovery. This could not have been done without your support.

Finally, I dedicate my work to the S.C. national guard, especially the 151st Expeditionary Signal Battalion (ESB). Thank you for allowing me to focus on my work and research while also fulfilling my duties in the guard. “Everywhere to the End…Ever Forward!” Thank you to Dr. Bael and Dr. McClain for expeditiously and correctly diagnosing me and giving me the proper treatment for 100% healing from my diagnosis during my second year. Without your efforts I may not have been here to see this day come to fruition. I am extremely grateful to you, your team and the Team at Anderson Area Cancer Center for giving me the second chance at pursuing my dream.

ACKNOWLEDGMENTS

First, I give honor to God who is the head of my life and I thank him for the opportunity and the ability to pursue my doctoral degree and providing the means for me to finish this journey.

I want to give thanks to Dr. Jordon Gilmore for accepting me as one of your first PhD students. I hope that I have done enough to sustain the idea that The Citadel still produces men of high integrity and a will power that never ends. Thank you for not giving up on me and motivating me to stick with the process and see everything through to the end. Thank you, committee members for all of your guidance and expertise. Your contributions to my journey will have a lifelong impact on my life going forward. I would also like to thank George Wetzel at Anderson Materials Research Lab for all your help with the scanning electron projects and allowing me to gain a valuable skill set for future endeavors.

This work was funded through the Call Me Doctor™ Fellowship, COVID-19 SEED Grant, and the Clemson Dissertation Completion grant. I would like to give thanks to the leadership and committees from all funding sources.

TABLE OF CONTENTS

Page

LIST OF TABLES

LIST OF FIGURES

CHAPTER ONE

Select portions of this chapter was generated in collaboration with Clemson University doctoral student Elizabeth Gianino. A large portion has been published in *Antibiotics* 2019 and *Bioengineering* 2017.

INTRODUCTION

1.1 Clinical Relevance

The growing health concern of antibiotic resistance threatens the effective treatment of infectious diseases to include chronic wounds and acute infections. Multidrug-resistant (MDR) bacteria infect over 2.5 million people and cause over 35,000 deaths annually. (1) Bacteria utilize a complex quorum sensing (QS) communication scheme to modulate gene expression. QS networks control virulence, biofilm formation, and antibiotic resistance. Bacteria communicate in a QS network using autoinducers, where virulence is only executed when the extracellular accumulation of autoinducers reach a specific threshold. (2) The evolution of MDR bacteria could be attributed to the overuse of antibiotics. At the onset of a wound formation, broad-spectrum antibiotics are often prescribed. In the advanced stages of biofilm formation and virulence, bacteria enable and express resistance to antibiotic treatment. The use of antibiotics after the log growth phase, could also produce persister cells and future resistance. Antibiotic use has increased by 36% between 2000 and 2010. 80% of antibiotics in the U.S. are used for crops and livestock and can promote further resistance via horizontal gene transfer. (3) Antibiotics work by either degrading the cell wall/membrane, damaging DNA replication processes or deprivation of vital molecules. Bacteria can also be intrinsically or synthetically resistant such as gram-positive resistance to aztreonam and gram-negative to glycopeptides. Molecularly, resistance could occur by drug inactivation, receptor modification, drug efflux activation and/or attenuation of drug uptake. Activated drug efflux pumps facilitate any compounds toxic to the pathogen. (4,5) Biofilms contribute to the MDR pandemic by the reduction of drug uptake and facilitation of horizontal

gene transfer of resistance genes. Figure 1.1 shows biofilm formation and the mechanism of antibiotic resistance. The extracellular polymeric substance (EPS) provides a protection barrier from antibiotics and increases the probability of gene transformation. Pathogens contained in a biofilm community are 1000x more resistant than planktonic cells which would require a higher dosage of antibiotic regimen. (6,7)

Due to the rising antibiotic resistant crisis, there is still a need for point of care assessment tools capable of detecting infection. For example, Chronic, non-healing wounds of the lower extremity affect approximately 2.4 to 4.5 million people in the U.S. alone. (8) In the US alone, approximately, $25 billion is spent annually on the management of chronic wounds. (9) $28,000 is spent annually per Medicare beneficiary that requires wound care. These wounds are prevalent in adults with diabetes or vascular related diseases. Additionally, cost associated with an infected ulceration and amputation are estimated at $17,000 and $45,000, respectively. (10) Clinical signs of infection in the early stages are very limited and can often lead to improper use of antibiotics. (11,12) In some cases severe wound infections can have minimal systematic signs of infection. (13) The use of biosensors in pathogen detection would improve the rate of infection and reduce possible antimicrobial resistance. However, there is little to no systematic use of biosensors in wound care management. Limited biosensor use could be attributed to the lack of ease-of-use and accurate biosensors available for clinical use in wound diagnosis. The field of biosensing has made great strides.

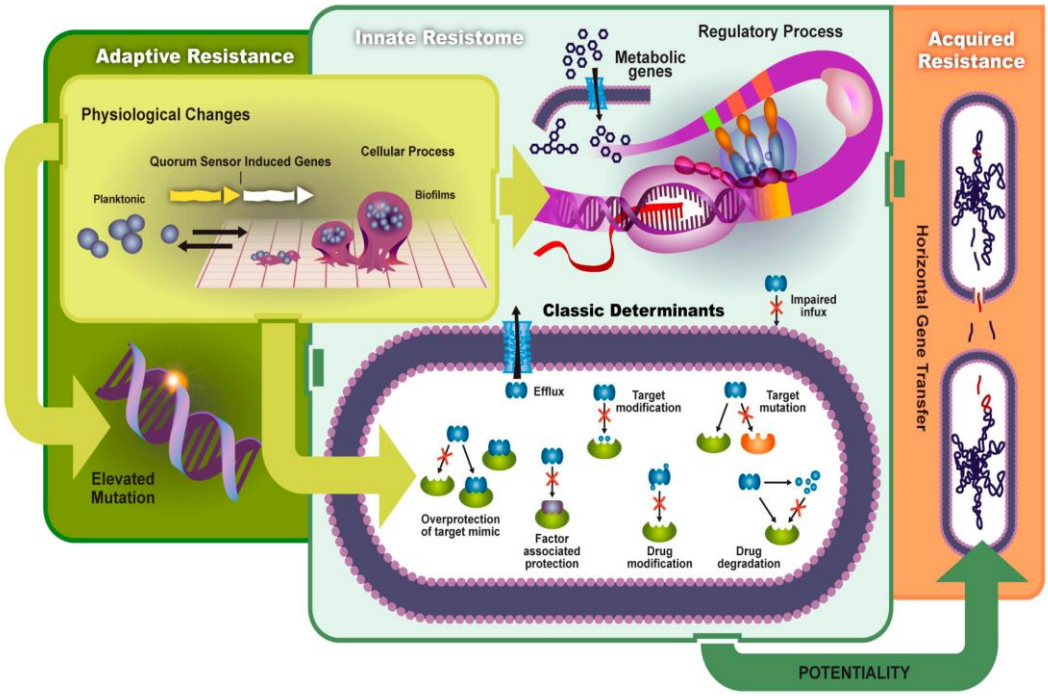

Figure 1.1 Development of Biofilm and antimicrobial resistance. Figure reproduced from Ref. (14).

1.2 ESKAPE and biothreat Pathogens

According to the Centers for Disease Control and Prevention (CDC), multidrug- resistant (MDR) bacteria infect approximately 2.8 million people, and cause over 35,000 deaths per year. (15) The acronym ESKAPE pathogens was given by the Infectious Diseases Society of America (IDSA) to a group of highly MDR bacteria: *Enterococcus faecium, Staphylococcus aureus, Klebsiella pneumoniae, Acinetobacter baumannii, Pseudomonas aeruginosa, and Enterobacter spp.* (14) The CDC has seen a significant increase in the rate of *P. aeruginosa* infections, which highlights the focus of chapter 3 on the detection of *P. aeruginosa* virulence. Pathogens can transfer genetic mutations and acquire antimicrobial genes via several pathways such as horizontal gene transfer. In response to the antibiotic resistance crises, the World Health Organization (WHO) acknowledged that there is a high priority to develop new antibiotics and therapeutics for ESKAPE pathogens. (16) However, according to WHO, there has been a steady decline in the development

of novel antibiotics for infectious diseases. (17) Antibiotics approved by the FDA has decreased between 1983-1987 and 2008-2012 from 16 to 2, respectively. Although this number has increased from 2 to 7 over 2013-2017, the Infectious Disease Society of America (IDSA) acknowledges that more work is needed to help mitigate MDR infections. Thus, IDSA created a collaborative initiative with other health organizations to advance the development of 10 new antibiotics. (18) The prevalence of MDR pathogens such as ESKAPE pathogens on the healthcare system shows the need to continue to find solutions for diagnostics and therapeutics.

1.3 Quorum Sensing

Both Gram-positive and Gram-negative strains utilize a complex quorum-sensing (QS) communication system to regulate gene expression. Bacterial quorum-sensing networks control biofilm formation, virulence factor production, bioluminescence, and antibiotic resistance (19). Quorum sensing depends on specific signaling molecules, called autoinducers, which accumulate in the extracellular space once the bacterial concentration reaches a specific threshold. Bacteria passively release or actively secrete low molecular weight acyl-homoserine lactones (AHLs) or autoinducing peptides (AIPs), respectively. AIPs are modified oligopeptides that can range from 5 to 17 amino acids (19). AHLs are neutral lipid molecules that contain a lactone ring with varying carbon side chains. The extent of hydrophobicity depends on the length of the side chains. Autoinducer-2 (AI-2) is an interspecies signaling molecule used in the formation and progression of biofilms with multicellular bacterial communities (19). AI-2 is a furanosyl borate diester used by several Gram-positive and Gram-negative species (20). The pseudomonas quinolone signal (PQS) is a separate class of autoinducer used specifically by *Pseudomonas aeruginosa* (*P. aeruginosa*) to regulate virulence. Figure 1.2 shows the chemical structure of some common autoinducing molecules. Once autoinducers reach a threshold, they bind to transcription factors in

the cytoplasm or cell membrane, activate gene expression, and produce more signaling molecules (21,22). Rapid detection of these signaling molecules could give clinicians an early indication of infection. Conventional detection methods used to quantify and identify autoinducers include the use of mass spectrometry (MS) and/or high-performance liquid chromatography (HPLC). These systems are used to examine the physical/chemical properties of autoinducers (23). MS and HPLC detection systems are highly accurate in the detection of autoinducers and are also used to validate novel biosensing schemes. Commonly used biosensor systems for in vitro and in vivo applications include the use of plasmids, chromosomes, or enzymes from reporter bacteria strains to detect a colorimetric, luminescence, or fluorescence signal (24). QS biosensors have the potential to detect bacterial virulence prior to the expression of resistant genes. Administration of antibiotics could be given at an optimal time to maintain antibiotic stewardship. Furthermore, QS biosensors could be used to screen for novel anti-virulent, antimicrobial, and/or quorum quenching molecules. Thus, further advancement and validation of these biosensors for in vitro and in vivo virulence detection could lessen the MDR bacteria epidemic.

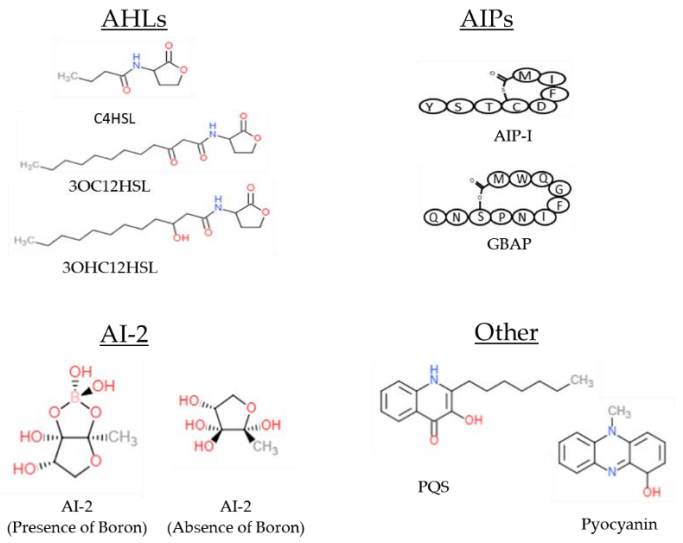

Figure 1.2 Chemical structure of common autoinducers discussed in this review. Figure reproduced from Ref. (25).

1.4 Development of Antibiotic Resistance in ESKAPE Bacteria

The development of multidrug-resistant ESKAPE strains could be attributed to the overuse of antibiotics. Broad-spectrum antibiotics are often prescribed as the first line of defense for wounds suspected of having significant bacterial colonization. However, when bacteria are in advanced stages of biofilm formation and virulence, governed by QS, these bacteria enable mechanisms for resistance to antibiotic treatment which begins the pathway for multidrug resistance. Administration of antibiotics during the stationary phase could also produce persister cells and future resistance. According to a study done with the IMS Health MIDAS database, there has been a 36% increase in antibiotic drug use between 2000 and 2010 (26). Moreover, approximately 80% of antibiotics in the U.S. are used in the agriculture industry in order to increase yield, quality, and profit. The use of antibiotics in crops and livestock can promote infections in humans and transfer-resistant genes to host pathogens (27). According to the World Health Organization, there has been a decrease in the development of approved antibiotics over the past few decades (28). Antibiotic approvals by the FDA decreased from 16 between 1983 and 1987 down to two between 2008 and 2012. Although this number has increased to seven between 2013 and 2017, the Infectious Diseases Society of America believes that more novel drugs are needed to reverse the MDR pandemic (29).

Most antibiotics work by destroying the bacteria cell wall, preventing DNA replication, inhibiting protein synthesis and/or by depriving the cell from vital nutrients. Bacteria can be intrinsically resistant or acquire specific antimicrobial resistance genes via horizontal gene transfer. For example, gram-positive pathogens are intrinsically resistant to aztreonam while gram-negative pathogens are resistant to glycopeptides and lipopeptides. From a molecular standpoint, bacteria resistance could be due to drug inactivation, target modification, activation of drug efflux,

and/or decreased drug uptake. Target pathogens can make surface modifications in order to prevent antibiotic attachment. Methicillin-resistant *S. aureus* prevents the binding of penicillin by synthesizing the penicillin-binding protein 2a through the *mecA* gene which binds to any drug with a β-lactam group. (4,5) Bacteria inactivates drugs by complete degradation or modification of a chemical group. Penicillin resistance in *S. aureus* is due to the synthesis of a β-lactamase called penicillinase. Hydrolyzation of the amide bond in penicillin and ampicillin inactivates the drugs. (5) Overexpressed efflux pumps transport toxic compounds which prevents the proper accumulation of antibiotics to kill the cell. Overexpression of the NorA efflux pump can lead to the resistance to tetracycline. Resistance via the efflux mechanism is seen mostly in gram-negative bacteria because gram-positive pathogens lack a lipopolysaccharide membrane. (4,5)

Biofilms contribute to the reduction of drug uptake and the formation of adaptive (environmental) resistance. Bacterial biofilm formation begins in the planktonic state where cells are motile until they attach to an adequate surface and bind with other cells. This initial adhesion state is weak, but further progression leads to the formation of an extracellular matrix composed of extracellular DNA, exopolysaccharides, and other proteins. Figure 2 shows a schematic of biofilm formation and antibiotic resistant pathways discussed in this section. QS plays a vital role in the production of the extracellular polymeric substance (EPS) and the release of virulent genes. The EPS enhances cell-cell communication and increases horizontal gene transfer. Pathogens contained in a mature biofilm structure is 1000 times more resistant than planktonic cells due to this increased QS efficiency. Persister cells, slow growth of bacteria, and poor antibiotic penetration decreases antimicrobial efficacy. Thus, higher concentration dosages are needed to reduce infection. (6,7)

1.5 QS in Gram-Positive Pathogens

Gram-positive bacteria utilize modified oligopeptides or autoinducing peptides (AIPs) that range from 5-17 amino acids long. (19) These AIPs are first produced in the cytoplasm of the bacterial cell. Then they are actively secreted from the cytoplasm by specific AIP transporters located in the cell membrane. Once the pathogens reach a concentration threshold in the extracellular environment, AIPs are detected by membrane-bound two-component sensor kinase receptors, which autophosporylates at histidines located in the cytoplasm. The interaction between AIPs and the sensor kinase receptors begins the activation of the respective quorum systems. (21,30)

Staphylococcus aureus (*S. aureus*) is a commensal microbe and human pathogen that has the potential to cause a wide range of infections. It is a key contributor of bacteremia, endocarditis, skin/soft tissue, and device-related infections. Accessory gene regulator (Agr) is the main QS system of *S. aureus.* (31) The Agr operon activates many toxins and degradative enzymes. (32–35) P2 and P3 promoters activate the RNAII and RNAIII divergent transcripts, respectively. P2 promotor activation results in the expression of *agrA*, *agrB*, *agrC*, and *agrD* genes. The *agrD* and *agrB* transcripts are responsible for the production and secretion of AIPs, respectively. The *agrD* gene encodes a precursor molecule and synthesizes extracellular QS AIPs. AgrB is needed to actively secrete autoinducers through the cell membrane via transmembrane proteins. A two-component signal transduction system is encoded by the *agrC* and *agrA* genes. AgrC histidine kinase sensor becomes phosphorylated once it binds to an AIP. AgrA is the response regulator to the *agrB* gene, which binds to the P2, P3, PSM□, and PSM□ peptide promotors leading to the production of toxins, surface proteins and exoenzymes. (33,34)

Enterococcus faecium (*E. faeciumi*) and *Enterococcus faecalis* (*E. faecalis*) are commensal organisms found in the gastrointestinal tract that has the potential to become virulent and cause nosocomial infections. (36) Similar to the Agr system, these bacteria primarily use the Fsr system to regulate its quorum sensing dependent virulence factors. This system contains four genes: *fsrA*,*fsrB*, *fsrC*, and *fsrD*. The *fsrD* and *fsrB* produces and secretes gelatinase biosynthesis-activating pheromone (GBAP), respectively. FsrC is the sensor histidine kinase that becomes phosphorylated after binding to GBAP, which activates the FsrA response regulator. (37) The activation of FsrA upregulates the expression of *fsrBCD*, *gelEsprE* and *ef1097*. (38–40)

Streptococcus pneumoniae (*S. pneumonia*) causes bloodstream infections, pneumonia, meningitis and acute otitis media. (41) These bacteria utilize two QS networks: Com and the Lux/AI-2. The Com pathway utilizes the competence-stimulating peptide (CSP) signaling molecule where its pre-cursor is synthesized by the *comc* gene, converted to CSP by the ComAB transporter and detected by the membrane-bound histidine kinase, ComD. The Lux/AI-2 system is like the system discussed above. Both systems are important in biofilm regulation. (42,43)

1.6 QS in Gram-Negative Pathogens

Gram-negative bacteria commonly use acyl-homoserine lactones as signaling molecules to regulate gene expression in a concentration-dependent manner. However, some strains produce additional non-homoserine lactone molecules, such as the PQS in *p. aeruginosa*. (44,45) Most gram-negative systems contain a LuxI/LuxR QS network homologs. LuxI is responsible for the synthesis of the acyl ghomoserine lactones (HSLs) that are passively diffused through the cell membrane. At high cell density levels, HSL ligand bind to highly specific LuxR-type transcriptional factors. Conversely, HSLs are degraded at a rapid rate at low cell density levels to avoid premature virulence activation. Binding of LuxR-type factors allows for the activation of

target virulence genes, auxillary QS networks, and the production of additional HSLs. HSL side carbon chains can range from short to long, where they can be 4 to 1 carbon chains long. (21)

The opportunistic pathogen, *P. aeruginosa*, could cause acute and chronic nosocomial infections in immunocompromised individuals. Infections are normally found in burn victims and patients with cystic fibrosis. (46,47) QS plays a vital role in the pathogenesis of this pathogen. *P. aeruginosa* consist of three major QS networks that function in a hierarchical manner. Upon activation of the Las system, the remaining networks (rhl and pqs) are positively regulated. Rhl is also upregulated by the pqs system. The compounds used to singnal the activation of each system are N-(3-oxododecanoyl)-L-homoserine lactone (3-oxo-C12-HSL), N-butanoyl-L-homoserine lactone (C4-HSL), and 2-heptyl-3-hydroxi-4-quinolone for the las, rhl, and pqs systems, respectively. The las and rhl systems are of the LuxR/LuxI type network as discussed in the above section. (48,49) *A. baumannii* are responsible for nosocomial infections to include pneumonia, endocarditis, skin, and wound infections. It uses acyl homoserine lactones ranging from 10 – 16 acyl side carbon chains. These lactones are medium to long chain AHLs. (50,51) Most strains produce and detect 3-hydroy-C12-homoserine lactone (3-oxo-C12-HSL) to regulate its QS circuit. Pathogenic *A. baumannii* strain M2 produces 3-oxo-C12-HSL and utilizes this lactone as its main signaling molecule. The QS circuit contains AbaI and AbaR that is similar to the LuxI and LuxR system found in *P. aurueginosa*. AbaI produces the AHL signaling molecules and AbaR is the corresponding receptor protein that is responsible for the expression of target QS genes. (50)

Klebsiella pneumoniae (K. pneumonia) is an important ESKAPE bacteria that is responsible for nosocomial, urinary tract, and surgical wound infections. (52,53) The QS system in *K. pneumonia* is less clear than the other ESKAPE pathogens. However, there is evidence that it utilizes type-two autoinducers or 4,5-dihydroxy-2,3-pentanedione (AI-2) and HSLs in its QS

circuit. (52–54) A report showed that K. pneumoniae isolates from a human tongue produced N-octanoylhomoserine lactone and N-3-dodecanoyl-L-homoserine lactone. (54) AI-2 is produced by a Luxs system, which is an enzyme found in several bacterial species. Thus, Al-2 is involved in interspecies QS communication and are found in both gram-negative and gram-positive bacteria. (55,56) There is little known about the transcriptional factors involved in the production of QS signaling molecules. Thus, this would be a great opportunity for further research.

Enterobacter. spp. QS network: *Enterobacter. spp*. is a family of gram-negative bacteria associated with nosocomial infections that has the ability to cause meningitis, septicemia, wound infection, and other complications. (57) There is little evidence about specific transcriptional factors involved in its virulence production. However, Zhou et al. and Yin et al. were able to isolate long and short chain HSLs, respectively. (58,59) This is an indication that *E. spp*. has the ability to synthesize and secrete HSLs using a LuxR-type QS network. (59) *Gram-negative bacteria Escherichia coli (E. coli*), *Salmonella typhimurium* (*S. typhimurium*), and *Vibrio harveyi* (*V. harveyi*) all has a LuxS/AI-2 system that utilizes type-2 autoinducer. Many strains of *E. coli* and *V. harveyi* are used in biosensors to detect type-2 QS systems in other strains. (60)

Table 1.1. QS networks and key players in ESKAPE bacteria.

Bacteria Strain	QS System	Main Signaling Molecules	Transcriptional Factor	QS Virulence Regulation	Ref.
S. aureus	Agr	AIP-I,II,III	AgrA	lipases, proteases, enterotoxins, superantigens, ureases	(24,33,34,61)
	LuxS	AI-2	LuxR-type	capsular polysaccharide synthesis	
E. faecium/E. faecalis	Fsr	GBAP	FsrABCD	Cytolysin, gelatinase	(24)
S. pneumoniae	Com	CSP	ComE	polysaccharide capsule, pneumolysin	(24,42,43)
	LuxS	AI-2	LuxR-type	Biofilm formation	

K. pneumoniae	LuxS	AI-2, 3OC10HSL, C8HSL	LuxR	Antibiotic resistance genes, biofilm formation	(24,52–54)
A. baumannii	Aba	3OC12HSL, C12HSL, C10HSL, C14HSL, 3OC13HSL, C16HSL	AbaI/AbaR	Biofilms, siderophore, lipopolysaccharides, superoxide dismutase	(24,50,51)
P. aeruginosa	Las	3OC12HSL	LasR/LasI	Elastase (lasB), staphylolysin (lasA), alkaline protease (aprA), exotoxin A (toxA), hydrogen cyanide synthase (hcnABC)	(24,48,49)
	Rhl	C4HSL	RhlR/RhlI	Rhamnolipid synthase (rhlAB), type 1 lectin (lecA), type II lectin (lecB), hcnABC, pyocyanin	
	PQS	2-heptyl-3hydroxy-4-quinolone (PQS)	PqsR	Pyocyanin, lecA, rhlAB, lasB	
	LuxS	AI-2	LuxR-type	Biofilm formation	
E. coli	LuxS	AI-2	LsRB	Chemotaxis towards AI-2	(60,62)
V. harveyi	LuxS	AI-2	LuxP	bioluminescence	(24)
E. spp.	LuxR-type	C12HSL, short-chain (C6) AHL molecules	LuxR	Biofilm formation	(58,59)

1.7 Fungal QS

Candida albicans is a the most prevalent human fungal pathogen that is normally commensal, but opportunistic organism affecting immunocompromised individuals. Many other fungal species do not cause diseases in humans. Infections of *C. albicans* include mucosal infection and oral-pharyngeal thrush, in immunocompromised women and AIDS patients, respectively. Other infections that it could cause are vaginal yeast, diaper rash, and medical implant infections. (63,64) *C. albicans* produces highly organized biofilms containing multiple types of cells such as

budding yeast, oval pseudophyphal, or hyphal cells all encased in an extracellular matrix. (65) Urinary and central venous catheters, pacemakers, and mechanical heart valves are highly susceptible to biofilm formation. After biofilm formation, infection is inevitable as the organism could release seeds in the bloodstream and lead to invasive organ infection and sepsis. (64–66) *C. albicans* is a polymorphism organism that utilize three different modes: yeast, pseudohyphae and pure hyphae. At concnetrations lower than 10^8 cells/mL, *C. albicans* develop into filamentous forms and into budding yeasts at higher concentrations. (63) In pseudohyphal cells, there is elongation of buds with attachment to mother cell which produces filaments of elongated buds with constrictions at the septal junction. Pure hyphae contain chains of tube-shaped cells that has no constriction at the septal junction. Pseudohyphae and pure hyphae have similar shape and elongation, but pseudohyphae extent of elongation can be random and different lengths. The three morphologies can be seen in Figure 1.3. Hyphal growth is considered to be the most important for virulence and is propagated by various external factors such as mammalian serum levels, acidic pH, L-proline, N-acetylglucosamine and increased CO_2 levels. The formation is also quorum sensing enabled. Yeast cells are capable of producing alcohol farnesol to act as a type of signaling molecule that can inhibit the formation of hyphae. (67,68) Farnesoic acid also acts as a quorum signal molecule if the strain lacks the ability to produce the isoprenoid farnesol molecule. Farnesol inhibits the conversion of the organism from yeast to mycelium and the inhibition of biofilm formation. Shirtliff et al. showed that farnesol concentrations between 40 to 100 μM was able to upregulate a number of genes and proteins that help protect the organism from oxidative stress. (69)

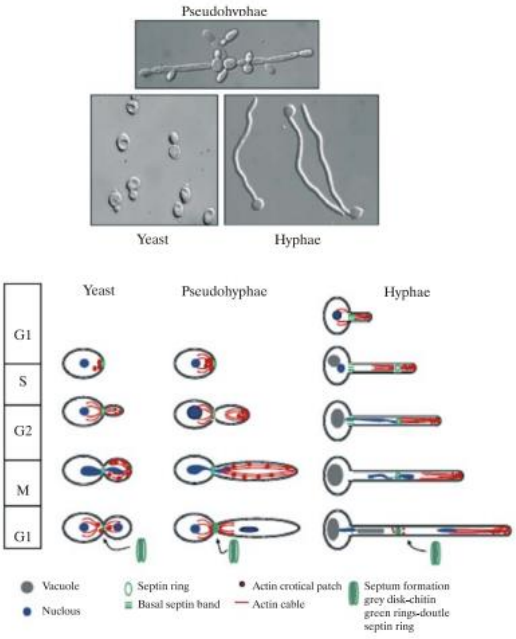

Figure 1.3. Growth morphologies of *C. albicans*. Figure reproduced with permission from Ref. (68).

1.8 Electrochemical detection schemes

Electrochemical detection allows the use of techniques capable of detecting molecules, proteins, and organisms with various detection methods. Dynamic detection schemes include electrochemical impedance spectroscopy (EIS), cyclic voltammetry (CV), and square-wave voltammetry (SWV). Electrochemical impedance spectroscopy is an alternating current (AC) technique that utilizes an applied fixed DC voltage with a superimposed AC voltage. The impedance and phase angle of the circuit undertest is measured as the frequency is fixed or varied. This technique measures the impedance as a function of frequency and applied voltage. Small changes in the testing medium induces a change in response. Figure 1.4 shows an impedance response of electrodes in phosphate buffer solution. Generally, electrode response shows more sensitivity over lower frequency ranges.

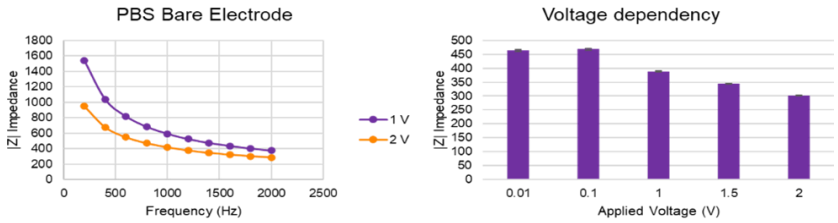

Figure 1.4. Phasor diagram and impedance response of electrodes in PBS.

The impedance response in aqueous media typically decreases as a function of the applied frequency. Impedance sensors have found many applications in wound monitoring research. Farrow et al. reported the development of a real-time impedance sensor that was able to detect the presence of *S. aureus* cultures by analyzing the normalized impedance profiles with respect to the frequency spectrum.

Cyclic voltammetry is an electrochemical technique that has been widely used and well-established. This technique is used to identify faradic current responses from redox active molecules. Voltammetry schemes scans the potential in a linear fashion over time and measures the current. Some common problems with cyclic voltammetry are reversible vs. irreversible redox reactions. Irreversible reactions are more complex to monitor than that of reversible reactions. The current produced in a pure electrochemical reaction depends highly on the scan rate (V/s) at the electrode surface. Cyclic voltammetry is typically used to characterize fabricated electrode materials.(70–72) However, it can also be used to detect rapid and sensitive changes in chemical molecules. Several authors have explored the use of cyclic voltammetry to detect changes and molecules in the brain such as dopamine and serotonin in real-time. (72,73) Potential step techniques utilize small pulsed potential overtime and measures the corresponding current examples include amperometric, Differential pulse voltammetry (DPV), and square wave voltammetry (SWV). Amperometric technique is typically used for applications to detect changes

in slower reactions such as the ones found in enzymatic detection schemes (i.e. glucose and glucose oxidase). SWV is a technique that utilizes high-speed potential scanning to measure current changes. This technique is ideal for applications that requires high sensitivity and can provide a means to reject background current due to the fast scans. This technique, compared to cyclic voltammetry, has a much lower limit of detection, and is used to detect redox reactions. In this reaction typical outputs include a peak current that is proportional to the concentration of redox active species.

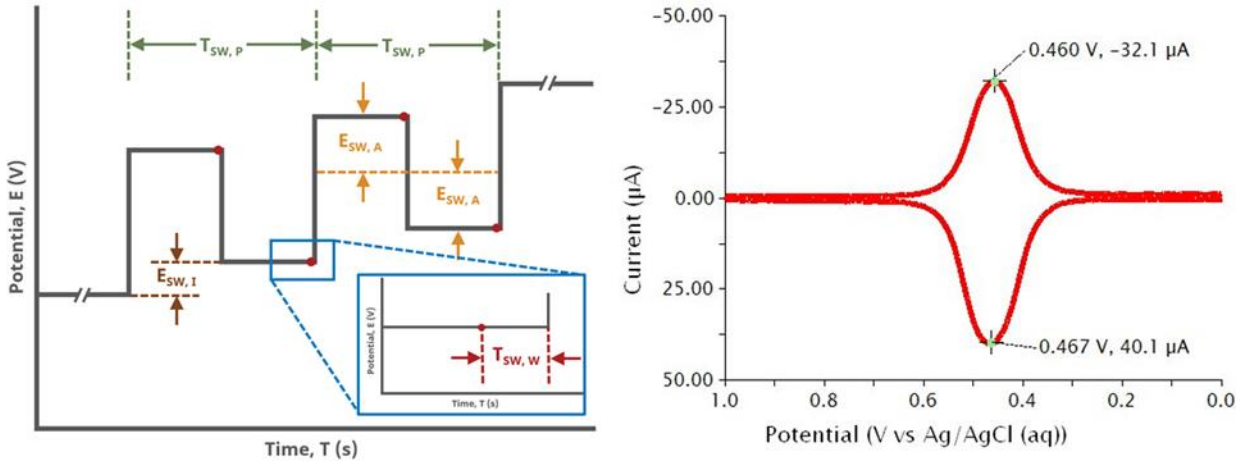

Figure 1.5. Square wave voltammetry applied potential and corresponding current response for the oxidation of 1mM solution of ferrocene in 0.1 M Bu_4NClO_4/CH_2CL_2. Figure reproduced from Ref. (74).

1.9 Biochemical Sensors

Biochemical sensors are designed for a specific analyte which makes them highly selective and sensitive. Ideally, a biosensor has a biorecognition element where the specified analyte binds to a transducer to change the chemical reaction or physical signal into an electrical signal, and a signal amplification and processing component (75). These sensors are complex, but very specific and promising in sensing the ulcer environment. Table 1.2 summarizes the sensors discussed in this section.

MMP sensors require the use of enzymes that are capable of catalyzing a specific biochemical reaction under a desired condition. Signal reduction from bio-fouling is a major concern as unwanted biological molecules interfere with the reaction (76). One of the most widely used types of protein assays is the enzyme-linked immunosorbent assay (ELISA). The ELISA consists of the immobilization of an antigen on a substrate, addition of a buffer solution, detection of a target analyte, and observation of the optical density via absorbance spectroscopy (77). Milne and colleagues created a device that was able to detect wound pH, moisture content and the MMP activity (78). The investigators created an ELISA sandwich assay to electrochemically detect the MMP activity in the wound site where they were able to detect MMP-9 concentrations between 0.1 - 100 ng/ml (78). Biela et al., were able to make a disposable MMP-9 sensor that relied on the degradation of a peptide cross-linker (79). The team used a microfabrication technique in order to fabricate 1.5 mm interdigitated gold electrodes with 0.1 mm thick gate channel (79). Their design models a standard semiconductor field effect transistor. They used electrochemical impedance spectroscopy to analyze the presence of MMP-9 where they were able to detect 200 ng/ml of MMP-9 within 5 minutes (79).

The sensing of UA is a promising methodology that uses enzymatic sensing techniques. Kassal and colleagues designed a wireless UA sensor by the use of screen printing and immobilization of uricase on a working electrode with a -0.3V operating voltage (80). The sensitivity coefficient of the sensor to 100-800 uM of UA was 2.4 nA/uM UA with an on board potentiostat compared to an electrochemical analyzer (80). The sensor remained highly selective for UA when compared to a control 400 uM UA solution. In the presence of common biological interferences and ascorbic acid the values of UA concentration decreased by 3% and 10%, respectively (80). Carbon fiber-based sensor electrodes have been developed by Sharp et al., to

detect uric acid levels electrochemically. The electrodes were modified with the application of a cellulose acetate permselective barrier to avoid biofouling. The team reported a sensitivity range of 0-500 μM for a linear fit (R^2 = 0.97) (81). RoyChoudhury and coworkers developed an enzymatic electrochemical sensor to detect uric acid changes in real-time by the immobolization of uricase and detecting the byproduct H2O2. The team was able to achieve a sensitivity of 0.14 μ/M-cm^2 and a limit of detection of 14 μM (82).

Most pH sensors utilize fluorescent or colorimetric agents to measure the pH level of solutions. This could be achieved by inserting a pH sensitive dye into the fiber matrix of a desired dressing. The pH range of the sensor depends on the receptor type where a hydroxyl groups or an amine groups are the main receptors of choice (83). McLister and Davis demonstrated the use of a poly-tryptophan modified carbon fiber composite to detect wound pH (84). They utilized square wave voltammetry to detect the pH of electrogenerated indolic quinone moieties and horse blood. The voltammograms varied with pH and fit to a linear model over a range of pH from 3 to 8 (R^2 = 0.993) (84). Akbari et al., fabricated a composite smart sensor that utilized alginate-based fibers that responded to changes in pH by changing colors. Microfluidic spinning method was used to fabricate alginate and glycerol solution with mesoporous particle beads into fibers. Fabricated fibers were placed in a PDMS chamber that received an inlet and outlet of solutions of varying pH of 6.5 to 8. The fibers changed color to dark red with basic and yellow with acidic solutions (85). Real-time sensing was achieved with the use of a smartphone camera and a custom MATLAB code to detect the pH of pig skin samples with the use of RGB values. The sensor values were within +-0.2 pH units compared to actual values (85). A hydrogel-based inductive pH sensor was used to detect pH changes in chronic wounds (86). The coils of the sensor were placed on the top and bottom surface of a folded substrate and a poly(vinyl alcohol)-poly(acrylic acid) pH-sensitive

hydrogel was sandwiched between the substrate surface. The coils' mutual inductance depended on the gap created by the hydrogel. The sensor displayed a linear response to pH in various buffer solutions between 1 to 8 (86).

Several sensors that detect the presence of bacteria have been developed by researchers using many of the same principles previously discussed. A team from the University of Rochester Medical Center fabricated a device using electrochemical multilayered porous silicon fibers [86, 87]. Lipid A was one of the target molecules and Tertryptophan ter-cyclopentane (TWTCP) was used as a receptor to bind to the target molecule, diphosphoryl lipid A [86, 87]. This binding created a change in the refractive index of the silicon that created an 8 nm shift in the wavelength of its photoluminescence peak. Gram-positive bacteria induced no change, but Gram-negative bacteria produced a small wavelength shift of 3-4 nm in the presence of bacteria. DeLouise tested the sensor on *E. coli* but failed to detect any changes due to a high rate of false negatives because of the pore blocking preventing target infiltration (88). A similar technique was used by Thet et al. where they demonstrated the use of colorimetric detection to identify the presence of bacteria. Hydrated agarose film containing 5, 6-Carboxyfluorescein dye vesicles were mixed with the agarose film. Compared to a 4-(2-hydroxyethyl)-1-piperazineethanesulfonic acid (HEPES) control group, detection of *S. aureus* and *P. aeruginosa* was seen with an intensity contrast approximately 20,000 and 35,000 fluorescence/a.u. after 24 hours. However, they were unable to detect any changes in *E. coli* or *E. faecalis* culture (89).

NO sensors measure the concentration of NO in a solution by the electroreduction or electrooxidation of NO. This could be accomplished by the utilization of a working electrode that has a potential of -0.5 to -1.4V (electroreduction) and 0.6 to 0.9V (electrooxidation) vs AG/AgCl (90). However, these electrodes experience biological interferences such as L-arginine, sodium

nitrate, sodium nitrite, oxygen, and hydrogen peroxide (90,91). Biological interference is filtered out by the inclusion of a transition metal or a metalloprotein such as hemoglobin (90). Most common sensors are of the Shibuki-style, solid permselective, and solid catalytic (78,91). The mentioned sensors are hard to utilize within a dressing and a custom sensor would be needed for application in chronic wounds. A novel method to electrically detect nitric oxide at subnanomolar levels was found by the use of a hemin-functionalized graphene field effect transistor (FET) (91). The device consisted of titanium-gold source, drain, and a solution gate. A PDMS channel was added to test the presence of NO in NONOate sodium in a NaOH solution. Presence of NONOate sodium at the device active site caused the conductance to gradually decrease from 160 uS to 135 uS with a half-life of 135 seconds (91). Figure 4 is an illustration of the Hemin-functionalized graphene FET. Furthermore, the sensor was able to detect as low as 0.3 nM of NO with a signal-to-noise ratio(SNR) of 3 (91)

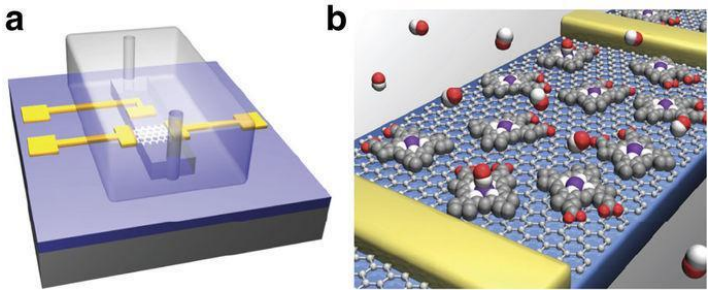

Figure 1.6. NO hemin-functionalized sensor. (a) PDMS channel with gold gate, source, and drain electrodes. (b) NO selective channel. Reprinted with permission from Ref. (91).

Oxygen sensors work similarly to NO sensors where the produced current is proportional to the given concentration of the solution. The Clark oxygen amperometric sensor is the most common type of oxygen biosensor (75). A wireless oxygen bandage sensor was fabricated by the use of a 3D printed polyrene-C dressing and the use of commercialized electronic components (92). Mostafalu and coworkers used a galvanic cell of 0.8V that was said to be proportional to the

reduced oxygen at the cathode and oxidized zinc at the anode. Ag and Zn electrodes were submerged in a potassium hydroxide electrolyte and capped off by a thin oxygen permeable PDMS top layer. The current from the oxygen sensor was amplified to 1-5V by an analog front-end, then read by a microcontroller with a 1 Hz sampling frequency. The signal was sent wirelessly to a monitor for data visualization and analysis. Current output from the sensor was 5-700 μA with an internal gain between 2.75-350K ohms. The ability to get such a wide range of output current and gain allows the sensor to be able to detect oxygen at different concentrations. The investigators reported current between 0.4-0.6 mA as oxygen concentration changed over 200-450 seconds (92).

1.10 Physical Sensors

Physical sensors incorporate the use of an analog-to-digital converter, amplifier and signal processing component to produce quantifiable data. Capacitive, resistive, and thermoelectric sensors are examples of physical sensors used in biomedicine. Physical sensors measure a parameter based on emergent phenomena or a cascade of metabolic activities. Thus, physical sensors are not as specific as biochemical sensors. However, they are widely used because of their ease of use and robustness.

Impedance sensors measure the resistance, reactance, and phase angle associated with the wound location by applying a small non-perturbing current and detecting the voltage that is produced. Due to the fact that chronic wounds have a higher level of bacteria, the conductance of the wound tends to be higher (93). Farrow et al. reported the development of a real-time impedance sensor that was able to detect the presence of *S. aureus* cultures by analyzing the normalized impedance profiles with respect to the frequency spectrum (94). The researchers developed a screen-printed sensor that contained Ag/AgCl electrodes inside of a 30mL bacterial test vial . They were able to detect S. *aureus* strains at levels of 5 x 10^7 CFU/ml (95). They also showed that

impedance measurements inhibited the growth of bacteria, due to the deposit of Ag ions in the culture (94). Ag is a widely acceptable antimicrobial molecule and the use of Ag in wound dressings has been demonstrated clinically (96).

Table 1.2 Sensor Used to Detect Biomarkers in Chronic Wounds

Sensor	**Sensitivity/Range**	**Biomarker**	**Method**	**Reference**
Elisa MMP Sensor	0.1-100 mg/ml	MMP-9	Electrochemical	(78)
Disposable MMP-9 Sensor	200 mg/ml	MMP-9	Electrochemical Impedance Spectroscopy	(79)
Smart Bandage UA Sensor	100 µM of UA	Uric Acid	Electrochemical	(80)
Carbon fiber sensor	0-500 µM	Uric Acid	Electrochemical	(81)
Wearable enzymatic sensor	0.14 µ/M-cm^2/ Range: 14 µM	Uric Acid	Electrochemical	(82)
Poly-tryptophan Carbon Fiber pH Sensor	pH of 3-8 (± 0.1)	pH	Voltammetry	(78)
Flexible Hydrogel pH sensor	pH of 5-8 (± 0.2)	pH	Fluorescent Spectroscopy/Image processing	(79)

Hydrogel pH sensor	pH of 1-8	pH	Electrical (LC circuit) and Chemical	(86)
Smart Bandage	Gram-Negative Bacteria, shift in wavelength by 3-4 nm	Gram-negative,-positive, *E. coli*, Lipid A	Electrochemical/ Optical Microcavity	(97)
Intelligent Hydrogel Dressing	Contrast of approximately 20,000 and 35,000 fluorescence/a.u. of *S. aureus and P aeruginosa*, respectively compared to HEPES	Bacteria (*S. aureus, P. aeruginosa, E. coli, E. faecalis*)	Electrochemical/ Fluorescent Spectroscopy	(89)
Hemin-Functionalized FET NO Sensor	0.3 nm of NO	Nitric Oxide	Bio-electrical	(91)
Oxygen Bandage Sensor	0.4-0.6 mA	Oxygen	Bio-electrical	(92)
Screen Printed Impedance Sensor	5 x 10^7 CFU/ml of *S. aureus*	*S. aureus*	Electrical	(94)
Inkjet Printed Impedance Sensor	N/A	Impedance	Electrical	(97)

Flexible Pt thermistor	2.7 Ω/°C	Temperature	Electrical	(98)
Wireless thermistor	17 Ω/°C at 35 °C	Temperature	Electrical	(99)
Flexible Low Power Sensor	0.2 °C temperature difference, 0.5 mmHg pressure, 3.0% RH	Moisture, Temperature, Pressure	Electrical	(100)
Inkjet Printed Smart Bandage	+- 2.3% capacitance, 8% quality factor, +- 2.6% resistance	Blood, pH, Resistance	Electrical (Capacitance and Resistance)	(101)

Swisher et al. designed a flexible, electronic device that non-invasively detects ulcers via impedance spectroscopy across a flexible electrode array in a rat model (97) They used inkjet printing to create gold-plated electrodes on a polyethylene naphthalene substrate where they used a LCR meter to detect the impedance between two locations on the array. The measurements were gathered in a scanning fashion, covering the entire sensor (97).This method effectively captures more surface area than a single two electrode measurement. The researchers compared the data from the LCR meter to a histology graph and showed that at 15kHz the threshold for tissue damage was seen when the impedance magnitude was 6K ohms and the phase angle was between -30 and 10 degrees (97). Figure 5 shows an image of the hydrogel impedance array sensor used for the study.

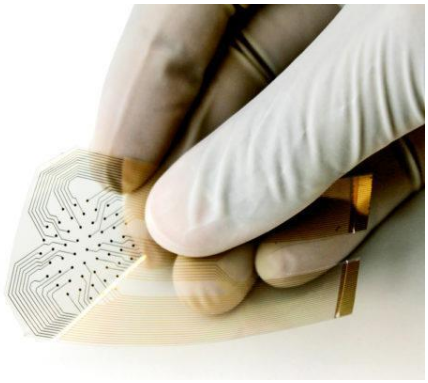

Figure 1.7. Flexible impedance sensor made via Inkjet Printing. Figure reproduced from Ref. (97)

The most commonly used temperature sensors are thermistors, thermocouples, resistive temperature detectors, and digital/analog thermometers. A thin, flexible micro-fabricated platinum resistor temperature sensor was fabricated by Kim and colleagues (98). Resistance-temperature curve shows that the sensor is linear for temperature in the range of 0 ℃ to 120 ℃ with a slope of 2.7 Ω/ ℃. Matzeu et al., developed a wireless thermistor sensor based on resistive carbon nanotube film and radio frequency identification (RFID) tag (99). The team did not find a linear relationship between temperature and resistance. At 35 ℃ they obtaned a slope of 17 Ω/℃ for their resistance-temperature curve. The sensor's measurement resolution was reported to be 0.2 ℃ (Matzeu).

Some sensors use a collection of modalities that are integrated on a single chip. Pressure, moisture, pH, irregular bleeding, and/or temperature are integrated on a single device in order to capture a holistic view of the wound. Mehmood et al., used a wireless sensor to inspect the wound's moisture level, temperature and pressure (100). They used commercially available devices such as the Honeywell HCZ-D5, Interlink Electronics FSR406, and Texas Instrument LM94021B for the moisture, temperature and pressure sensing, respectively. Under standard conditions and room temperature, they were able to detect a temperature difference of 0.2℃. They also detected very low resolution for pressure and moisture of 0.5mmHg and 3.0% RH, respectively. These values

are sensitive enough to detect a change in the chronic wound environment. In addition to sensing, a telemetry system was incorporated with the use of the ZigBee network protocol (100). ZigBee was used due to its ease of use for experimental verification of their device. However, Wi-fi Protected Access II(WPA2) protocol would be more ideal due to its inherent security and its use in the hospital settings (100). Farooqui and Shamim fabricated a disposable bandage via inkjet printing that used a double layer technique to measure the irregular bleeding, pH, and external pressure of a wound with wireless telemetry capabilities. This was achieved by detecting any significant changes to the initial capacitance and resistance (101). They were able to correlate the change in resistance, dielectric properties of blood and the change in distance to pH level, bleeding and pressure, respectively (101). Similar sensors were made that employed pressure sensors inside of shoes, such as the insole flexor force sensor used by Ostadabbas et al. (95).

1.11 Fabrication of electrochemical electrodes for biosensing

Biofabrication has evolved into a multifunctional fabrication tool that allows engineers to create an array of biosensors for a broad range of diagnostic applications. Biosensors include the use of a biorecognizing element to specifically transduce a signal proportional to the concentration or reaction at the active site. Immobilization techniques such as crosslinking is important as the detection limit of biosensors depend on this critical step. The majority of this work is on understanding and developing nonwoven biosensing interface materials for potential point-of-care applications. Nonwoven fibers are widely used in biosensing applications. The element of a biosensor includes the sample or target analyte. Commonly biological recognizing elements are nucleic acids or aptamers, whole cells, capture antibodies, enzymes, and bacteriophages. Antibodies are widely used biological recognizing agents used in biosensing applications. They are fabricated by the use of a host immune system, typically a rabbit or mouse for research

applications. The organism is injected with the antigen sample that is capable of evoking an immunogenic response. The organism proceeds to develop antibodies from this injection and produce polyclonal antibodies that are recovered directly from the serum. This is a highly careful and expensive process, but it is capable of producing proteins that are highly specific to the analyte of interest. Aptamers are short (20-60 nucleotides) single-stranded RNA or DNA oligonucleotides that are able to bind to target molecules or organisms with high affinity and specificity. Aptamers is a fairly new application that has been developed to fix the limitations of antibodies. Aptamers can be synthesized to target simple inorganic molecules, protein and protein complexes, and entire cells. Aptamer production is considered easier and cheaper to fabricate than antibodies because they do not require the use of live organisms and can be produced *in vitro* using the systematic evolution of ligands by exponential enrichment (SELEX) technology. The development of aptamers is a rapidly growing field that has found numerous applications. Developed aptamers for numerous targets are made available at public databases, such as the database at Aptagen located on their webpage (102,103). One drawback to the use of aptamers is the rapid degradation of them in nucleases in media which will decay rapidly. Methods have been developed to add modifications to aptamers to resist nuclease degradation. (102)

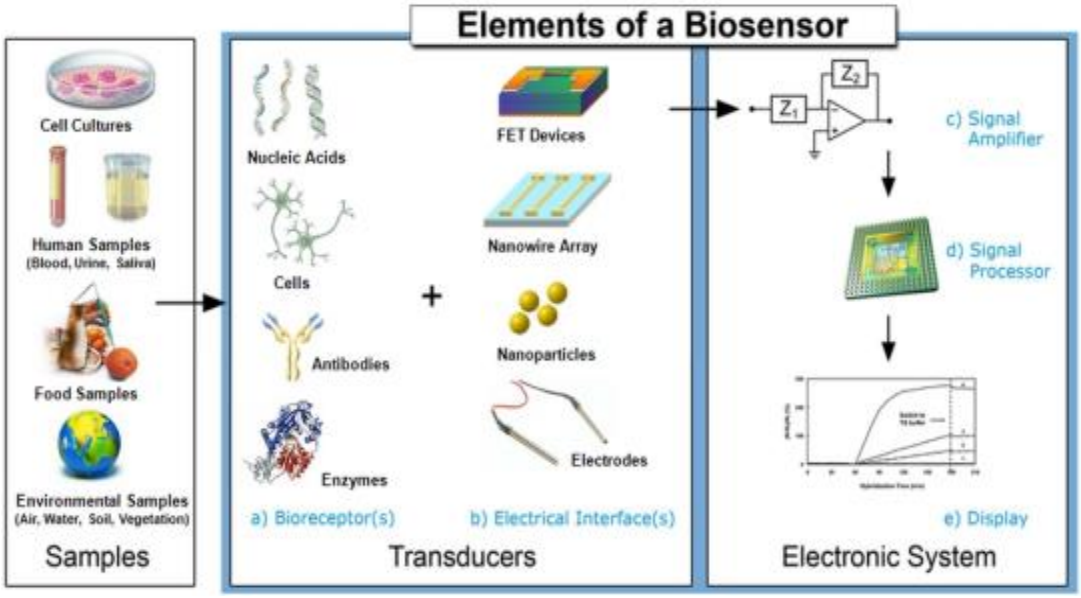

Figure 1.8. The elements of a biosensor from sample to electronic readout. Figure reproduced from Ref. (104).

The fabrication of transducers for biosensing applications are of utmost importance as they provide the site for the immobilization of biological agents capable of inducing an electrical change. The electrode size and dimensions must be at a scale that similar to the target analyte in order to make a sensitive enough detection scheme.

Nanofiber textile production has gained more interest in the past two decades compared to large diameter fiber textiles. (105–109) The reduction of fibers from a micron to a nanoscale dramatically increases the surface area to volume ratio, improves thermal acoustic insulation, increases water and lipid holding capacity, and modifies texture and appearance. (110–112) Moreover, nanofibers have shown great promise for use as tissue scaffolds, controlled release of drugs, and as a primary contact layer for wound dressings. (110,113–115) There are several techniques used to generate nanoscale fibers. Many of the techniques are derived from one another. Nonwoven is a sheet or mesh of fibers that are connected by physical entanglements without the

use of knitting. Melt spinning, melt blow spinning, electrospinning, wet spinning, and solution blow spinning are commonly used methods used to generate nonwovens.

Solution blow spinning is a fairly new technique first used in 2009 to produce nonwoven nanofiber composites (105) This technology utilizes key elements from electrospinning and melt blow spinning techniques to make *in situ* nonwoven nanofibers. Solution blow spinning creates nanofibers by the incorporation of a polymer dissolved within a volatile solvent. Two concentric fluid streams allow the flow of a polymer solution and compressed gas. Pressurized gas flows around the solution, creating fibers by stretching a polymer jet in the direction of air flow onto any substrate. The setup can is highly versatile and can be used in as a portable device or on a larger commercial scale. Solution blow spinning can deposit nanofibers on both planar and nonplanar substrates. The technique has tremendous potential for use in an array of applications to include wound healing. However, this technique has not been greatly exploited to generate substrates for point-of-care chronic infection biosensors. (106) SBS nanofibers mats have been shown to have similar mechanical strength as fibrin (1–10 MPa) or human skin (0.1–1 MPa). Polymeric dressings are the common material used in the management of chronic wounds and may contain natural or synthetic polymers, like cellulose or PLA, respectively. PLA is a hydrophobic, bioabsorbable, biocompatible, thermoplastic polymer that is used in an array of biomedical applications from scaffolds to biomolecular device fabrication. (116) Wound dressings that incorporates novel therapeutics decreases the bacterial load and facilitates proper healing. (117) Elemental silver and cerium nanoparticles can act as an antimicrobial and antioxidative agent. Silver ions are cytotoxic to bacteria cells through the blocking of the respiration process. (118) Ceria nanoparticles have the ability to attach to reactive oxygen species (ROS) and in order to reduce oxidative stress. (119)

Solution blow spinning can also be used to support conductive filler material to create a conductive fiber mat. Commonly used materials are Ag and carbon.

1.12 State-of-the-Art Biosensing for Quorum-Sensing Molecules

Conventional methods to verify the presence of QS signaling molecules and biosensor functionality includes the use of chromatography, mass spectrometry, or a combination of the two. High-performance liquid chromatography-tandem mass spectrometry (HPLC-MS/MS) procedure is most used to detect acyl-homoserine lactones, peptides and other biological relevant compounds. (120,121) HPLC-MS/MS combines the separation capabilities of HPLC and the detection technique of MS. Briefly, the analyte is passed through a chromatographic column and separated by HPLC then the components are transferred to a mass spectrometer where samples are converted to positively charged particles bombarded by electrons. Charged particles are detected by mass spectrometer and their mass-to-charge ratio is calculated. HPLC-MS/MS requires the use of ion detectors, mass analyzers, ion source, vacuum system and other highly expensive equipment. (122,123) HPLC-MS/MS is great for verifying the presence of quorum sensing signaling molecules and validating biosensor functionality. Many researchers utilize HPLC-MS/MS to detect short, medium and long chain homoserine lactones and autoinducing peptides secreted in bacterial cultures. (23,121,124–127)

Conventional screening methods provide a way to identify pathogens and diagnose most infections. However, their use can be time consuming and economically challenging in certain situation. The utilization of biosensors has several advantages over conventional methods. Most biosensors used to detect QS activity are cheap and easy to use. Point-of-care along with telemedicine can be used to diagnose chronic or acute infections in economically challenging areas. Sensors have been made to determine the bacterial load *in vitro.* (128–130) However, these

sensors are susceptible to common biological interferences. Additionally, biosensors were developed that utilizes antibodies or bacteriophages to specifically detect bacteria. (131–133) The incorporation of antibodies and/or bacteriophages solves the interference problem, but it does not guarantee that the captured bacteria are pathogenic. It was widely accepted that a bacterial load above 10^6 CFU/mL indicates the onset of infection. (134) However, many researchers believe that the release of virulence factors and biofilm production hinders the healing process and serves as a better indication of infection. (134–136) Bacterial colonization is only the presence of bacteria and the use of antibiotics before a "critically colonized" level could lead to antimicrobial resistance. (137) Virulent and/or critically colonized bacteria can be verified by the detection of toxins or QS signaling molecules. Genetically modified whole-cell based bacteria, cell-free transcriptional based reagents, aptasensors, and immunosensors are commonly used to detect these compounds *in vitro* or *in vivo*.

1.13 Gram-Positive Whole-Cell-Based QS biosensing

Autoinducing peptides (AIPs) are great targets for quorum sensing activity detection in gram-positive bacteria. Peptide-based biosensors have been used to target various molecules to include proteins, enzymes and nucleic acids by exploiting the selectivity of synthetic and natural peptides as enzymatic substrates. Cleavage between the analyte and peptide is verified through bio-conjugation with signal markers to produce a quantifiable output signal. (138) However, most AIP biosensing applications utilize a variety of engineered plasmids that has cognate AIP receptors and promotors that produce a measurable readout. Transcriptional based biosensing allows researchers to detect AIPs with high specificity and sensitivity. Thus, genetically engineered bacteria are the gold standard when detecting AIPs. (139) Several plasmids have been developed to detect CSP (Streptococcus spp. signaling molecules), synthesized by S. pneumonia. A lacZ

transcriptional reporter strain (S. mutant SMdC) was developed to assess the activity of comDE in response to CSP. The strain consisted of a comC mutant that prevents the production of CSP. A promoterless lacZ gene was used to fuse vectors pYH2 and pOMZ47 to the comDE and nlmAB promotors, respectively. Exogeneous CSP induced the expression of Beta-galactosidase (β-gal) in both mutans. Quorum sensing activity was assessed by the activation of β -gal as a percentage of maximal activation. A detection range was not determined from this study. (140,141)

A group from Norway developed two biosensors to quantify gelatinase biosynthesis-activating pheromone (GBAP) and cytolysin small subunit ($CylL_S$). (142) The $CylL_S$ biosensor was constructed by electroporation of the pSL101cylR2R1Pcyl vector into E. faecalis JH2-2. The GBAP biosensor was developed from the use of two vectors: pREG696luxP_{fsr}B45 and pREG696luxP_{gelE}. Biolumenescene was measured in $CylL_S$ inducing units (CIU) and GBAP inducing units (GIU). The authors found that the P_{gelE}-driven luxABCDE had a greater lux expression than the P_{fsr} promoter. The vector containing the P_{gelE} promoter was transformed into E. faecalis V583fsrB. Both biosensors were tested in E. faecalis cell-free supernatants that produced $CylL_S$ and GBAP. GBAP sensor displayed a bioluminescence equivalent to 320 and 5120 GIU in exponential phase and overnight cultures, respectively. This showed that GBAP activity was not responsible for the downregulation of the fsr circuit in the stationary growth phase. $CylL_S$ biosensor was also able to detect $CylL_S$ in cell-free supernatants during the exponential (640 CIU) and stationary (5120 CIU) growth phase. (142)

Most cell-based biosensors consist of non-pathogenic mutan bacteria derived from pathogenic strains. However, there still exist a risk when using such bacteria. Lubkowicz et al. reprogrammed the probiotic bacteria, Lactobacillus reuteri DSM20016 to detect AIP-I from S. aureus. The group designed two different reporter bacteria. Gibson assembly was used to construct

all plasmids. The agrCA genes and p3 promoter were amplified from the S. aureus RN 4220 strain. Plasmid pSIP409 was used to amplify the reporter GusA and can be seen in Figure 1.9. The second sensor consisted of the same sequence with a flipped slp-AgrCA site from the first designed plasmid. E. coli Top 10 was used to make plasmid copies and plasmids were transformed to L. reuteri via electroporation. The sensors innately produce glucuronidase. Therefore, the authors used p-nitrophenyl β-D-glucuronide (pNPGA), which hydrolyses in the presence of glucuronic acid. Sensor one was inversely proportional to AIP-I with a detection range between 10-1000 nM. However, sensor two was developed to address small inadvertent expression of GusA from sensor one when incubated with S. aureus cell lysate. Sensor two addressed a leaky GusA expression, had the same inverse response to AIP-I, but with a lower detection range of .5-1000 nM. (143)

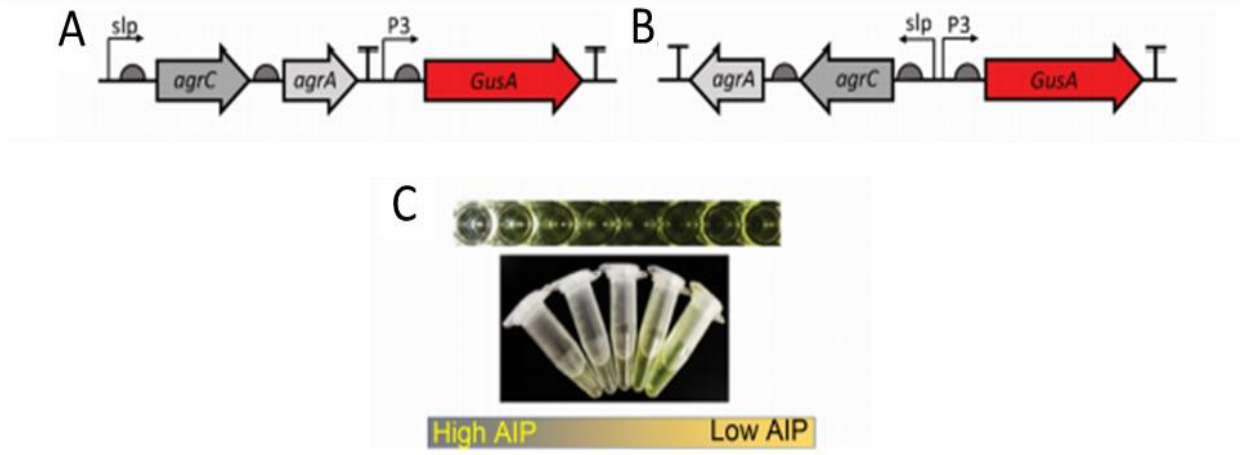

Figure 1.9. Probiotic biosensor schematic. (**A**) Sensor 1 with pSIP409 plasmid. (**B**) Sensor 2 with pSIP409 plasmid and a flipped *slp-agrC* fusion. (**C**) GusA reduction in the presence of high autoinducing peptides (AIPs). Figure reproduced from Ref. (143).

A variety of 11 different plasmids were created via the amplification of PCR promotors and subsequent vector ligation by Malone et al to detect *agr* expression. Plasmids developed by Yarwood et al. were used as base vectors for the construction all 11 plasmids. (144,145) The *asp23*

promotor and a YFP reporter gene was amplified from *S. aureus* SH1000 and pDB59 plasmid as templates, respectively. The resulting PCR products were processed and ligated into pDB59 to create the first plasmid, pAH5. Plasmids pAH6 and pAH1 were constructed with an *agr23* and *agr* P3 promotor, respectively, that expressed mCherry. The remaining plasmids were created with different promotors downstream a gene encoding various fluorescent proteins. Table 1.3 annotates all plasmids constructed in this study. The authors found that the ribosome binding site (RBS) played a role in protein expression. Due to the higher expression of protein (YFP), superoxide dismutase (*sod*) RBS and delta-toxin (*hld*) RBS, plasmids pAH16 (sod RBS) and pAH17 (hld RBS) were superior out of all plasmids. (144,146) Application of plasmids in *S. aureus* biofilm growth and fluorescence-activated cell sorting was also validated. (147) Two plasmids were generated to respond to exogeneous S. aureus peptides. E coli was used as a vehicle for plasmid construction and finalized plasmids were electroporated into *S. aureus* MN8. Plasmid pDB60 was transformed into a MN8 to construct an *agrD* mutant with *ermC*(erythromycin resistance cassete), *agrAC* and *agrB* P3. Plasmid pDB22 was constructed and contained a fusion of the agr P3 promotor downstream a gene encoding GFP. A second plasmid, pJY202 contained a fusion of the agr P2-P3 promotor in line with a gene encoding YFP. Average fluorescence were 4 times and 14 times higher than the required fluorescent signal needed for visualization. In a liquid media culture, both plasmids displayed an increase in fluorescence signal from late exponential to stationary growth phase. The group successfully examined biofilm formation under flow cytometry and what influence the Agr system had on antibiotic resistance. (145) Boles et al. constructed a plasmid, pAH9, with a *sarA* P1 promotor downstream from a *mCherry* gene using PCR amplification. The plasmid was subsequently transformed into S. Aureus SH1000. The researchers were able to use the reporter strain to show that low *agr* activity increased biofilm formation and AIPP-I causes

biofilm detachment. Planktonic and dispersed cells showed an increase sensitivity to the antibiotic, rifampicin. (147)

Table 1.3. Gram-positive detection schemes.				
Gram-Positive Detection Schemes				
Host Strain/Cell	**Plasmid/Biorecognizing Element**	**Reporter System**	**Molecules**	**Detection Range/LOD**
S. pneumoniae SMdC	pYH2-pOMZ47	LacZ reporter/β-gal	CSP	Not reported (140,141)
E. faecalis JH2-2	pSL101cylR2R1Pcyl	Bioluminescence	cytolysin	640 CIU (142)
E. faecalis MMH594	pREG696luxPfsrB45 and pREG696luxPgelE	Bioluminescence	GBAP	320 GIU (142)
L. reuteri DSM20016	pSIP409	GusA	AIP-I	10-1000 nM [77]
L. reuteri DSM20016	pSIP409 (w/flipped slp-AgrCA)	GusA	AIP-I	.5-1000 nM [77]
S. aureus SH1000	pAH1 (*agr* P3)	YFP, Cam	*agr* expression *agr* expression	Not reported [82], [83]
	pAH5 (SigB)	YFP, Cam		
	pAH6 (*asp23*)	mCherry, Cam		
	pAH7 (*agr* P3)	YFP, Erm		
	pAH8 (*agr* P3)	mCherry, Erm		
	pAH12 (*sarAP1*)	mCherry, Erm		
	pAH13 (tetracycline ind.)	GFP, Erm		
	pAH14 (*sarAP1*)	YFP, Erm		
	pAH15 (pAH14 w/*SarA* RBS)	YFP, Erm		
	pAH16 (pAH14 w/*sod* RBS)	YFP, Erm		
	pAH17 (pAH14 w/*hld* RBS)	YFP, Erm		
	pAH9 (*sarA* P1)	mCherry		

1.14 Gram-Negative Whole-Cell-Based QS biosensing

Agrobacterium tumefaciens (A. tumefaciens) is a gram-negative bacterium that infects plants by the growth of tumors via horizontal gene transfer. The bacteria, however, is not pathogenic to humans. A. tumefaciens utilize a TraI/TraR-type quorum sensing circuit to regulate

its virulence in plant species through the introduction of a tumor-inducing plasmid. Tumor-inducing plasmids maintains a copy of transfer DNA and regulates its conjugation. TraI is the synthase that synthesizes 3-oxo-C8-HSL and TraR is its transcriptional activator. (148) In order to detect HSLs, especially 3-oxo-C8-HSL, the synthase must be deleted or mutated. A. tumefaciens NT1 and NTL4 are commonly used as a host for several HSL biosensors with a broad detection range and can screen for medium and long chain HSLs. NT1 and NTL4 do not produce HSLs due to a mutation of the TraI synthase or a complete removal of the tumor inducing plasmid. NT1 strain that consist of a pZLR4 plasmid was used to detect several 3-oxo acyl-HSLs and 3-hydroxyl acyl-HSLs with different carbon side chains. The pZLR4 plasmid has traR and a traG::lacZ reporter. This plasmid allows for resistance to ampicillin and gentamicin. In the presence of X-Gal, the reporter strain produces β-galactosidase that then provides a blue color indicating the presence of HSLs listed in Table 1.4. (149,150) pZLR4 plasmid has been widely used by several researchers in NT1 and NTL4 strains. (149–153) A. tumefaciens A136 has been used to quantify several HSLs. Chambers et al. and Zhu et al. used pCF218-pMV26 and pCF218-pCF372 to screen and quantify HSLs, respectively. (154,155) Plasmid pMV26 has a PtraI promotor fused to reporter luxCDABE reporter. While plasmid pCF372 contains a PtraI promoter fused with a reporter lacZ gene. TLC bioassay reporter was used to detect the presence of 3OC10HSL, 3OC8HSL, and 3OC12HSL from the sputum samples of cystic fibrosis patients with the pCF372 plasmid. (155) Luminescence-based assay was used to quantify HSLs with various side carbon chains: C4HSL (25 nM), C6HSL (250 nM), C8HSL (0.25 nM), C10HSL, (25 nM), C12HSL (250 nM), 3OC6HSL, (20 pM), 3OC8HSL (0.2 pM), 3OC10HSL (0.02 pM), and 3OC12HSL (0.02pM). (155) Zhu et al. used A. tumefaciens to detect and quantify a broad range of HSLs using the TLC bioassay and β-galactosidase activity. Bacteriophage T7 was used to engineer a TraR protein expression system

in A. tumefaciens KYC55 using three plasmids: pJZ384, pJZ410, and pJZ372. Plasmid pJZ384 has a traR gene with a phage T7 promotor, pJZ410 has the phage T7 RNA polymerase gene and the last plasmid has a traI gene fused to reporter lacZ. Biosensor was able to detect 3 pM of 3OC8HSL by detecting the amount of β-galactosidase activity. TLC bioassay was used to detect several HSLs: 3OC6HSL (2.5 pM), 3OC8HSL (0.25 pM), 3OC12HSL (0.5 nM), 3hydroxylC6HSL (20 pM), 3hydroxylC8HSL (20 pM), 3hydroxylC6HSL (20 pM), C6HSL (100 pM), C8HSL (30 pM), and C10HSL (40 pM). The biosensor has greater sensitivity and lower detection limit than other A. tumefaciens biosensors. (156)

E. coli is widely used in detecting QS signaling molecules and its proteins and plasmids are used to derive cell-free lysates. Conveniently, E. coli is inherently absent of an HSL synthase gene. Most E. coli-based biosensors use a luxCDABE or β-galactosidase reporter system. Several biosensors based on a luxCDABE or lacZ reporter system have been developed in the latter half of the 20th Century. (157–159) Since the last two decades, many authors utilize E. coli-based plasmid systems. Recently a bioluminescent biosensor developed by Winson et al. was used to quantify HSLs. This sensor uses the JM109 E. coli strain as a host and harbors a pSB1075 plasmid. The psB1075 plasmid has a LasR receptor capable of activating a lux reporter in response to 3OC12HSL and other HSLs. As expected, there was a 10-fold signal reduction for every two-carbon side chain (C12HSL, C14HSL, and C16HSL) when compared to 3OC12HSL. The biosensor had a 10-fold increase in response to 10 nM of 3OC14HSL and 3OC16HSL than the cognate 3OC12HSL. The biosensor was able to detect 12 different non-cognate HSLs tested except for C18HSL. (160) Rai et al. designed a fluorescent biosensor capable of detecting synthetic HSLs. E. coli K-12-Z1 strain was used as a host to carry the pSB1A2 plasmid. The biosensor was able to detect 1μM of synthetic HSLs and was able to validate a computational model capable of showing

that promotor logic can be used to probe and predict QS activity. (161) Deng et al. found a way to quantify 3OC6HSL with a visible cherry fluorescence and determine biosensor location with a green fluorescence. The dual fluorescent whole-cell based sensor contains the plasmid pUCGMA2$T_{1-4,}$ which has three components: PnptII fused to gfp to indicate host biosensor, PahlI fused to mcherry to quantify 3OC6HSL, and the ahlR gene to encode HSL regulatory protein. The biosensor was able to detect $5x10^{-8}$ – $1x10^{-5}$ mol/L of HSL. (162) HSL concentrations were detected in real-time using E. coli fluorescent reporter bacteria. A plasmid encoding a gfpmut3 signal in the presence of HSLs was used to detect fluctuations of HSLs in real-time. E. coli MT102 cells containing the pJBA132 plasmid was able to detect the presence of 10 nM of 3OC6HSL in approximately 15 min via an epifluorescence microscope. The gfp signal had a 40 min. half-life, which allows this biosensor to be used in real-time detection schemes. Fluorescence in response to HSL dose was measured in liquid cultures at different time points to determine detection limit of various HSLs. Detection limits were 1 nM, 10 nM, 10 nM, 10 nM and 1000nM for 3OC6HSL, C6HSL, C8HSL, 3OC10HSL, and C4HSL, respectively. (163) A portable system was designed to detect C12HSL using a paper strip whole cell-based sensing. As can be seen in Figure 1.10, the biosensor can be used in point-of-care application to quantify infection. The pSDB1075 plasmid has a lacZ reporter that expresses β-galactosidase under the control of a lasI promotor. Plasmid was transformed into competent E. coli DH5α-T1. Reporter cells and chromogenic substrate X-gal (5-bromo-4-chloro-3-indolyl-β-d-galactopyranoside) were immobilized on filter paper via physical adsorption. Limit of detection was 10 nM of C12HSL for 90 min and 100 nM after 60 min of incubation. (164)

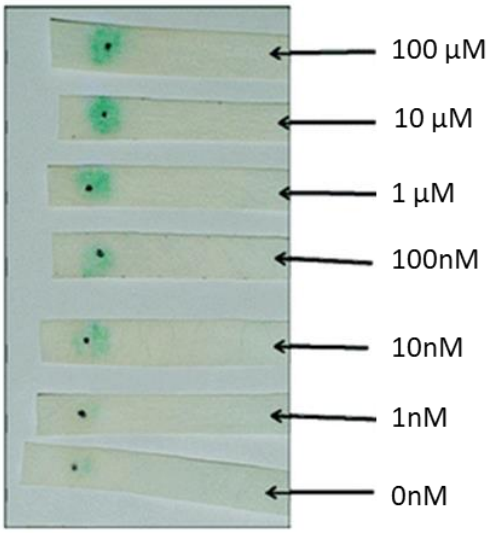

Figure 1.10. C12HSL *E. coli* DH5α-T1 paper biosensor. Figure reproduced from Ref. (164).

Several *Pseudomonas*-based biosensors have been constructed that utilizes a *lux*CDABE or *lacZ* reporter. *Pseudomonas spp.* Produce HSLs, so most sensors consist of plasmids with a mutating *lasI* or *rhII* HSL synthase gene. Massai et al. created a chromosomally integrated whole-cell biosensor that only bio-illuminates in the presence of 3OC12HSL and C4HSL. The sensor has a *lasI* mutant in the *P. aeruginosa* PA14 strain with a chromosomal copy of a P*rsaL* promoter fused to a *lux*iCDABE reporter. The detection range was 1.4 nM to 3 µM with a lower limit of detection for 3OC12HSL of 10 pM. The sensor responded to C4HSL with a lower detection limit of 10 µM (157). Dong et al. utilized a *Pseudomonas*-based whole-cell biosensor to show that *PprB* expression is essential for virulence production. *P. aeruginosa* mutant strain M71LZ was used to assess the production of β-galactosidase in the presence of HSLS. The strain contains a plasmid with *lacZ* fused to a *rsaL* promoter. The detection range was between 0.01 and 100 µM and 1.0 and 100 µM for 3OC12HSL and C4HSL, respectively. Additionally, the authors were able to show that a mutation in the *pprB* gene reduced gene expression (*lasI*, rhII, and *rhIR*) and 3C12HSL production. However, the *pprB* knockout strain was sensitive to C4HSL. This study shows that

PprB upregulates the production of 3OC12HSL in *P. aeruginosa* PAO1 (165). *P. fluorescens* is a bacterial species commonly cultured from human clinical samples and found in soil samples. There is a disparity in the literature as to whether *P. fluorescens* is pathogenic or not (166). Khan et al. developed a whole-cell-based biosensor to detect HSLs in *P. fluorescens* 2–79 culture supernatants. The *phzR* gene in the *P. fluorescens* genome can detect 3OC6HSL and the *phzA* gene upregulates the production of phenazines (redox-active metabolites). Production of phenazines gives their host a survival advantage in polymicrobial environments and has beneficial properties towards plants. Two plasmids (pSF105 and pSF107) were transformed in the *P. fluorescens* 1855. The *phzR* gene was cloned to a pSF105 plasmid. The pSF107 plasmid had a *phzR*-phzA dual promoter region. The *uidA* and *lacZ* reporters were placed upstream of the *phzR* and *phzA* promoter, respectively. The detection range of 3OC6HSL via β-galactosidase assay was between 10 and 10,000 nM. The biosensor was able to detect C6HSL and 3OC8HSL, but with a much lower sensitivity. The authors believe that the sensor is best for detecting 3OC6HSL. Additionally, it was noted that the 2–79 strain uses 3OC6HSL as its QS signal and PhzR activates *phzA* and *phzR* expression (167). Interspecies crosstalk was analyzed using two different biosensors. Two different plasmids were constructed and transferred (triparental mating) to *B. cepacia* H111-1 and *P. aeruginosa* PAO1-JP2 cells to specifically detect 3OC12HSL (pKRC12) and C8HSL (pASC8). Plasmid pKRC12 contains components from the *P. aeruginosa* PAO1 las system, which has a lasB fused together with gfp and the *lasR* gene under control by a *lac* promoter. The second plasmid, pASC8, utilized components from the *B. cepacia* H111 cep QS network. The plasmid has a gfp under the control of a cepi promoter and a *cepR* gene transcribed by a *lac* promoter. The detection range for plasmids in *P. aeruginosa* was both 25 nM for their respective HSL. The group was able to show that interspecies communication is a one-way direction in *P. aeruginosa* PAO1 and *B.*

cepacia H111 biofilm cultures. *B. cepacia* was able to recognize 3OC12HSL from *P. aeruginosa*, but the latter was unable to uptake HSLs from *B. cepacia* (168).

Reporter mammalian cells are of great interest. Mammalian cells such as fibroblasts are involved in the inflammatory response in chronic and acute infections. They are responsible for the destruction of damaged structural proteins and the creation of a new extracellular matrix (117). Fibroblast-like, monkey kidney COS-1 cells, were used to develop an in vitro mammalian reporter cell-culture system to detect the presence of C4HSL and 3OC12HSL (169). Reporter plasmids consisted of a LasBOX 1 sequence upstream of a *firefly luciferase* gene. Mammalian cells have different mechanisms to control transcriptional activity than that of prokaryotic cells. Therefore, the group incorporated a protein (T3N) with three copies of the VP16 transcriptional domain and the nuclear localization signal derived from an SV40 T antigen. Luciferase Assay Kit was used to detect luciferase activity in response to HSLS. Luciferase assay showed that reporter cells with a T3N module fused to RhIR had a three-fold signal increase vs. reporter cell with only an N module fused to RhIR in the presence of C4HSL (250 μM). T3N-LasR chimeric proteins were used to test time response to 3OC12HSL (250 μM) and C12HSL (750 μM) over a 48 h period. Although a higher concentration of C12HSL was needed for maximal effectiveness, both ligands induced a maximal response at 8 h with a significant drop off over the remaining 48 h. This inactivation could be due to AHL-inactivating enzymes or apoptosis of cells. This system could be used to assess mammalian cell response in the presence of active QS systems, screen for HSL mimics, or HSL inhibitors (169).

Whole-cell biosensing systems are very robust. However, cell-free systems also have their advantages. Cell-free systems allow the synthesis of proteins and contain the enzymes from eukaryotic or prokaryotic cells needed for transcription and translation (170). Kawaguchi et al.

utilized the *A. tumefaciens* NTL4 with pCF218 and pCF372 plasmids to make a cell-free assay system to detect QS HSLs. β-galactosidase activity was detected under 4 h in the presence of C6 HSL (30 nM), C7HSL (25 nM), C8HSL (20 nM), C10HSL (100 nM), C12HSL (200 nM), 3OC6HSL (17 nM), and 3OC8HSL (10 nM). However, the cell-free lysate was unable to detect C4HSL (171). USER-ligase DNA templates were used with *E. coli* S30 to generate libraries of DNA components for cell-free systems. PCR products were prepared using *PfuTurbo* C_x. PCR-amplified products were then circularized and used as DNA templates for cell-free systems via gfp production. All promoters and ribosome binding sites tested were able to express gfp in the presence of 3OC12HSL. Additionally, promoters and RBS had a similar response to HSLs in cell-free and cell-based extracts. However, two (J23100 and J23102) out of nine different promoter constructs had a significant increase in signal strength in the presence of 3OC12HSL. The group was also able to compare linear versus circular (plasmid) DNA cell-free systems to *E. coli*-based systems with the pSB1A2 plasmid. This in vitro approach allows one to rapidly investigate several different constructs for synthetic biology applications (172). The pSB1A2 plasmid developed by Chappel et al. was used to detect 3OC12HSL concentration levels in cystic fibrosis patients. The detection range of the biosensor was between 5 and 100 nM. Twenty *P. aeruginosa* positive samples were tested for HSL with LasRV biosensor and LC-MS. Biosensor had one false negative and one false positive out of the 20 samples. The two discrepancies could be due to molecular suppression or activation from interferents in samples (173).

Colorimetric methods for the detection of a wide range of HSLs typically consist of a *Chromobacterium violaceum* mutant. *C. violaceum* is a Gram-negative soil and water bacterium that produces violacein through the CviI/R QS circuit. Mclean et al. designed a *C. violaceum* mutant (*C. violaceum* CV026) that is incapable of synthesizing HSLs. The thin-layer

chromatography method is commonly used with this reporter strain. The biosensor is the most sensitive to C6HSL, but is able to detect C4HSL, C8HSL, 3OC6HSL, and 3OC8HSL (174). Furanosyl borate diester (AI-2) is a signaling molecule used by both Gram-positive and Gram-negative bacteria to regulate QS activity (151). *V. harveyi* BB170 reporter strains are commonly used to detect and quantify AI-2 molecules. This strain does not produce AI-2 due to a LuxS knockout nor sensitive to HSLs. The bioluminescence produced is due to AI-2 concentration and can be detected via the luminometer of the spectrometer (175).

Gram-Negative Aptamer-Based QS biosensing: There are not many developments in the use of aptamers to specifically detect QS signaling molecules or toxins produced by bacteria discussed in this review. Aptamer sensors include the use of fragmented DNA to detect cognate strands. Typically, a redox probe is used to detect the hybridization event between target and probe aptamer. Systematic evolution of ligands by exponential enrichment (SELEX) is a commonly used tool to develop highly specific aptamers for many applications. A group of aptamers was developed with a high affinity towards 3OC12HSL and C4HSL with a dissociation constant of 20 nM–35 nM and 25 nM–50 nM, respectively (176). These aptamers could be used to quench or detect HSLs released during infection. Sismaet used aptamers developed by Zhao et al. to electrochemically detect 3OC12HSL and C4HSL. Methylene blue was used as a redox label, which was attached to the aptamer probe. Once cognate ssDNA binds to the aptamer probe, the distance between the redox label and electrode surface increases. Thus, the peak current at a −0.25 V is inversely proportional to the HSL concentration. The range of detection for 3OC12HSL and C4HSL was between 0.1 and 100 μM (177).

Gram-Negative Electrochemical-Based QS biosensing: An electrochemical sensor was developed to detect the presence of β-galactosidase produced by the *A. tumefaciens* NTL4 reporter.

β-galactosidase hydrolyzes 4-aminophenyl β-D-galactopyranoside (PAPG) into p-aminophenol (PAP). PAP production was more sensitive than the detection of PAPG consumption. PAPG is irreversible, so any saturation in signal response is due to the complete consumption of PAPG. The concentration of 3OC12HSL was detected electrochemically *A. tumefaciens* 3OC12HSL spiked cultures. Limit of Detection in bacterial cultures was 2.5 and 3.6 pM in 2 h and 5 h of incubation, respectively (178). Other HSLs could be detected with this method due to NTL4 response to HSLs outlined in Table 1.4. The Rhl and PQS quorum systems are responsible for the upregulation of pyocyanin via *phz*ABCDEFG operons. Pseudomonas Quinolone Signal (PQS) is the QS molecule in the PQS system. Pyocyanin is synthesized from the chorismate precursor, which is converted to phenazine-1-carboxylic acid (PCA). The PhzM and PhzS enzymes convert two other precursors to upregulate the production of pyocyanin. PQS has an oxidation and reduction peak at +0.233 V and +0.178 V, respectively. Pyocyanin can be detected via electrochemically with symmetrical peaks at −0.16 V and an irreversible oxidation peak at +0.8 V (45).

Table 1.4. Gram-negative detection schemes.

Gram-Negative Detection Schemes				
Host Strain/Cell	**Plasmid/Biorecognizing Element**	**Reporter System**	**Molecules**	**Detection Range**
A. tumefaciens	pZLR4	LacZ reporter/β-gal	C6HSL C8HSL C10HSL C12HSL C14HSL 3OC6HSL 3OC8HSL 3OC10HSL 3OC12HSL 3OHC8HSL 3OHC6HSL	Mostly quantitative (149–153)

A. tumefaciens A136	pCF218-pMV26	luxCDABE reporter (Luminescence-based assay)	C4HSL C6HSL C8HSL C10HSL C12HSL 3OC6HSL 3OC8HSL 3OC10HSL 3OC12HSL	C4HSL (25 nM) C6HSL (250 nM) C8HSL (0.25 nM) C10HSL (25 nM) C12HSL (250 nM) 3OC6HSL (20 pM) 3OC8HSL (0.2 pM) 3OC10HSL (0.02 pM) 3OC12HSL (0.02pM) (154)
A. tumefaciens A136	pCF218-pCF372	LacZ reporter/β-gal	C6HSL 3OC6HSL 3OC8HSL	C6HSL (2.5 µM) 3OC6HSL (100 nM) 3OC8HSL (25 nM) (153)
A. tumefaciens KYC55	pJZ384, pJZ410, and pJZ372	LacZ reporter/β-gal	3OC6HSL 3OC8HSL 3OC12HSL 3OHC6HSL 3OHC8HSL 3OHC10HSL C6HSL C8HSL C10HSL	3OC6HSL (2.5 pM) 3OC8HSL (0.25 pM) 3OC12HSL (0.5 nM) 3hydroxylC6HSL (20 pM) 3hydroxylC8HSL (20 pM) 3hydroxylC10HSL (20 pM) C6HSL (100 pM) C8HSL (30 pM) C10HSL (40 pM) (156)
E. coli JM109	psB1075	luxCDABE/bioluminescent	C12HSL C14HSL	C12HSL (1nM-50µM)

			C16HSL 3OC12HSL 3OC14HSL 3OC16HSL 3OHC12HSL	C14HSL (10nM-50µM) C16HSL (100nM-5µM) 3OC12HSL (1nM-5µM) 3OC14HSL (10nM-50µM) 3OC16HSL (10nM-10µM) 3OHC12HSL (10µM - 50µM) (160)
E. coli K-12-Z1	pSB1A2	traI–luxCDABE	Synthetic HSL	1µM (155)
E. coli	pUCGMA2T	mCherry	3OC6HSL	5x10-8 – 1x10-5 mol/L (161)
E. coli MT102	pJBA132	gfpmut3	C4HSL C6HSL C8HSL 3OC6HSL 3OC10HSL	C4HSL (1µM) C6HSL (10nM) C8HSL (10nM) 3OC6HSL (1nM) 30C10HSL (10nM) (162)
E. coli DH5α-T1	pSDB1075	LacZ reporter/β-gal w/X-gal immobilized on filter paper	C12HSL	10nM @ 90 min. 100nM @ 60 min. (163)
P. aeruginosa PA14	pUCP18 and pMS402	luxiCDABE reporter	C4HSL 3OC12HSL	C4HSL (10 µM) 3OC12HSL (10 pM) (157)
P. aeruginosa M71LZ	pUCP19	LacZ reporter/β-gal	C4HSL 3OC12HSL	C4HSL (1.0 - 100 µM) 3OC12HSL (.01 – 100 µM) (165)
P. fluorescens 1855	pSF105 and pSF107	LacZ reporter/β-gal	3OC6HSL	10 – 10000 nM (167)
P. aeruginosa PAO1-JP2	pKRC12	GFP	3OC12HSL	25 nM (168)

P. aeruginosa PAO1-JP2	pASC8	GFP	C8HSL	25 nM (168)
monkey kidney COS-1	LasBOX 1 sequence	Luciferase	C4HSL 3OC12HSL	Not reported (169)
A. tumefaciens NTL4 (cell-free)	pCF218 and pCF372	β-gal	C6 HSL C7HSL C8HSL C10HSL C12HSL 3OC6HSL 3OC8HSL	C6 HSL (30 nM) C7HSL (25 nM) C8HSL (20 nM) C10HSL (100 nM) C12HSL (200 nM) 3OC6HSL (17 nM) 3OC8HSL (10 nM) (171)
E. coli extracts (cell-free)	pSB1A2	GFP	3OC12HSL	5 – 100 nM (173)
C. violaceum CV026	Sequenced on genome	violacein	C4HSL C6HSL C8HSL 3OC4HSL 3OC6HSL 3OC12HSL	C4HSL (1.8 nM) C6HSL (.01 nM) C8HSL (.44 nM) 3OC4HSL (73 nM) 3OC6HSL (.14 nM) 3OC12HSL (.83 nM) (175)
None	3OC12HSL and C4HSL aptamers	electrochemically w/Methylene blue	C4HSL 3OC12HSL	.1 – 100 μM (177)
None	A. tumefaciens NTL4 reporter	β-gal and PAPG/PAP electrochemical detection	3OC12HSL	2.5 pM (2hr) 3.6 pM (5 hr) (178)

1.15 Point-of-Care molecular based techniques

The development of polymerase chain reaction (PCR) in 1985 paved the way for genetic and molecular testing and diagnostics. The gene amplification technique has been used for a wide range of clinical applications to include genotyping, mutation detection, forensics, and diagnostics. (179,180) Currently PCR is an *in vitro* technique that is broadly used for the diagnosis of many diseases and infections.

PCR can be seen as an *in vitro* process of the DNA replication process that occurs during cell growth and division. There are three main steps in PCR process: thermal denaturation of the DNA target of interest, annealing of synthetic oligonucleotide sequence (primers), and extension of annealed primers by DNA polymerase. This process is repeated for several cycles, which doubles the number of products that is made. Each cycle produces a DNA template that can be used in the subsequent cycle. The product of the exponential PCR reaction is dsDNA. The amplification factor is given by equation 1:

$$(2^n\text{-}2n)x \qquad (1)$$

where n is the total number of cycles in the reaction, 2n is the product produced after the first and second cycle with undefined length, x is the number of original template copies. 100% efficiency is normally assumed, where the amplification factor is normally 2^n. For example, after 20 cycles there would be a 2^{20} -fold amplification of DNA target. The PCR process can be seen below in Figure 1.11. Proper thermal denaturation is required in order to allow primers to anneal and copy target DNA. Typical temperatures used are 94-97ºC. Annealing temperature require depends on the melting temperature (Tm) of primers. Higher GC content typically requires a higher annealing temperature. The required annealing temperature may be given by the manufacturer or may have to be determined experimentally. Typically, it is between 48-72ºC. The final step of extension

occurs at a temperature between 68-72ºC and is the longest step of the process. (181) PCR process requires precise temperature changes over time. Thermocyclers are used to automate and provide the require temperature needed to generate DNA products.

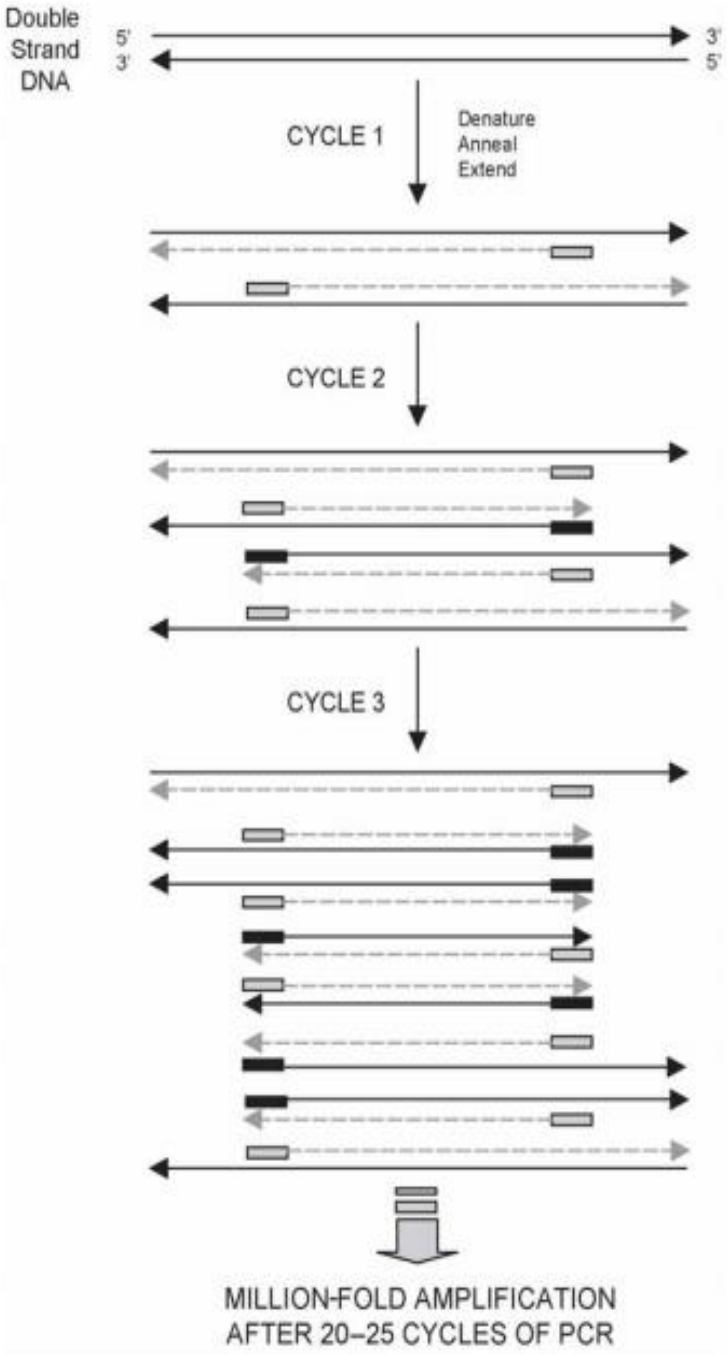

Figure 1.11. Illustration of PCR process. Figure reproduced from Ref. (182).

Several techniques can be used to analyze PCR products such as electrophoresis, restriction mapping, Real-time PCR etc. Electrophoresis is the most commonly and affordable method to assess products. Typically, Agarose gel is made to measure the length of DNA sequences between 100-10000 bp with the use of a reference DNA ladder. Restriction mapping can be used to verify the identity and or mutations of a product. Mass spectrometry has been used for many applications in molecular biology and can also be used to analyze PCR products. This technique can be used for mutation determination or genotyping. PCR products can also be quantified by the use of real-time PCR. A fluorescent probe is typically used to generate a signal once hybridization occurs. During each cycle, the probes cleave, and the relative fluorescence signal would increase. This method can be used to quantify products and also the original amount of DNA template in a sample. (182) Reverse transcriptase-PCR (RT-PCR) is another variation of PCR that is used to detect and quantify mRNA. Reverse transcriptase is used to catalyze DNA synthesis from and RNA template. The end-product of RT-PCR is called complementary DNA (cDNA). In RT-PCR, RNA template is degraded, and a dsDNA is produced, where PCR amplification follows the same process stated above. This technique is commonly used to diagnose and quantify RNA viral load or infections, such as coronavirus, or HIV (183).

Many developments have been made in molecular diagnostics to help overcome the limitation of PCR. PCR require a considerable amount of technical skill and relatively expensive equipment, which makes it less appealing point-of-care based diagnostic system. Loop-mediated isothermal amplification (LAMP) is a novel technique that was developed to help overcome the limitations of the PCR technique in terms of diagnostics and genotyping. This method combines the use of highly specific primers to rapidly detect target DNA in an isothermal reaction. Thus, no thermocycler is required to conduct the reaction. (184) LAMP exhibits increased sensitivity and

specificity due to a process that utilizes 4-6 primers that recognizes 6-8 distinct regions of DNA. The temperature used in this technique is between 60-65 ºC. 4 primers are required for correct amplification; Two outer primers: forward outer primer (F3) and backward outer primer (B3). Two inner primers: forward inner primer (FIP) and backward inner primer (BIP). Additionally, a DNA polymerase with dsDNA displacement activity is also required. Additional loop primers (forward loop primer and backward loop primer) can accelerate the reaction. LAMP reaction begins with the hybridization of FIP (primer with two target sequences specific to two separate regions on the template DNA) with the target DNA and the production of complementary strand synthesis. The forward outer primer (F3) begins strand displacement of the elongated FIP primer, which releases a ssDNA that serves as a template for the backward primers. BIP begins complementary strand synthesis and B3 displaces the elongated BIP primer. The ssDNA produced by the BIP elongation forms a stem-loop DNA structure on both sides. The stem-loop structure formed at this step is the starting point for exponential LAMP amplification. Self-priming and elongation on the F1 and B1 3’ end displaces the stem loop on the 5’ loop, subsequent unfolding and backfolding of new strands occurs. Cauliflower-like structures with long amplicons are generated after a few minutes under the optimal temperature. Additional forward loop and backward loop primers can be used to increase speed and amplification of the above reaction.

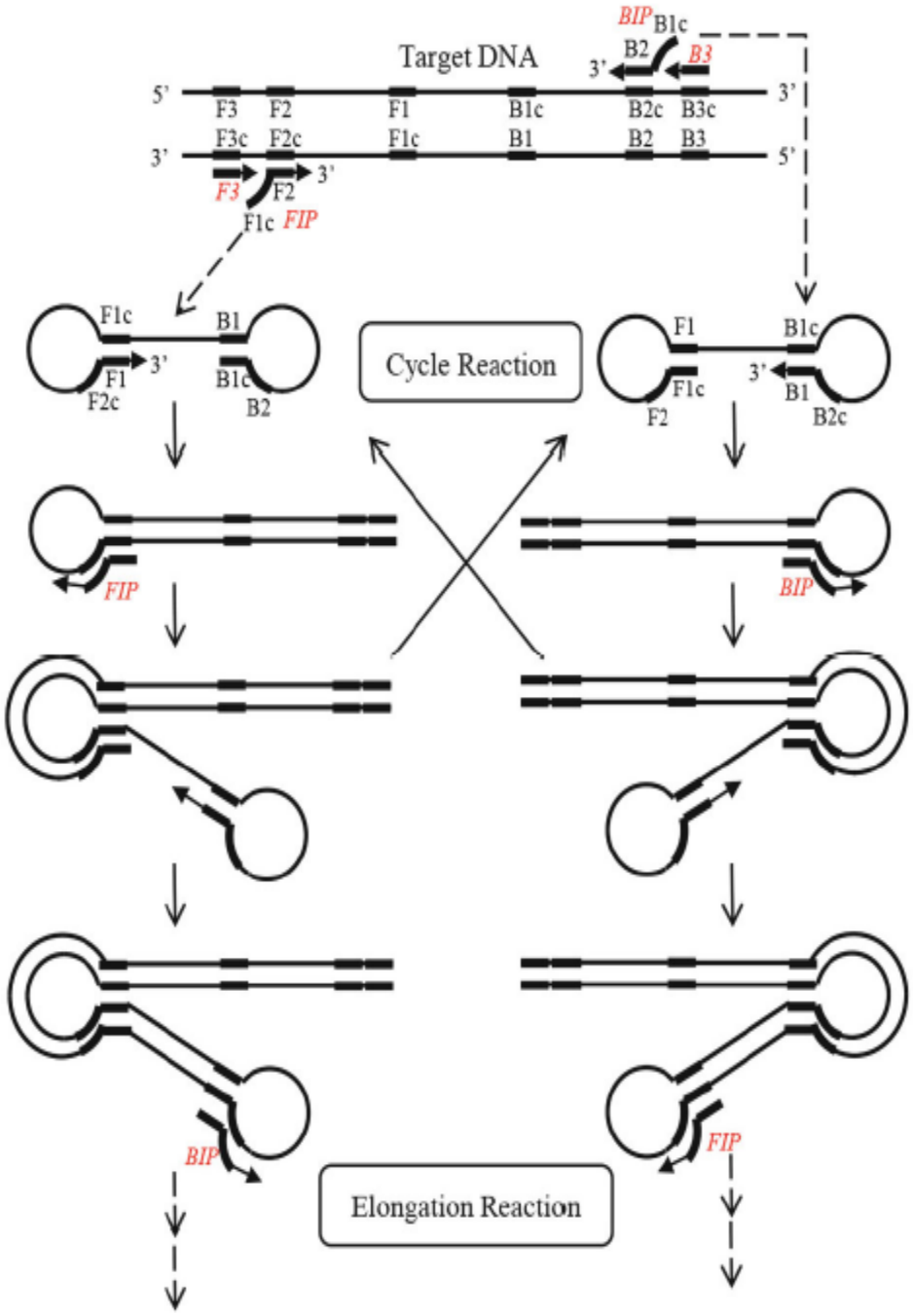

Figure 1.12. Illustration of loop-mediated isothermal amplification (LAMP) reaction. Figure reproduced from Ref. (185)

LAMP has been used to detect the novel coronavirus in several studies. A two stage LAMP assay was developed that could be deployed in closed tubes with both fluorescence and

colorimetric detection. This method was demonstrated with the use of spiked blood samples. LAMP assays developed was shown to have 10-fold greater sensitivity to target DNA than the use of RT-PCR assays. (186) The use of LAMP has also been shown to detect the coronavirus RNA from patient samples. Thi et al. utilized a two-color RT-LAMP assay to detect SARS-CoV-2 to detect the nucleocapsid gene. The group tested 768 pharyngeal swab samples and obtained a sensitivity of 97.5% and a specificity of 99.7%. Additional efforts were made to detect viral load without a RNA isolation step. The assay worked but had a lower sensitivity of 86% for a cycle threshold of less than 30min. (187) Figure 1.13 shows the LAMP colorimetric assay developed with the use of WarmStart Colorimetric RT-LAMP 2X Master Mix developed by New England Biolabs.

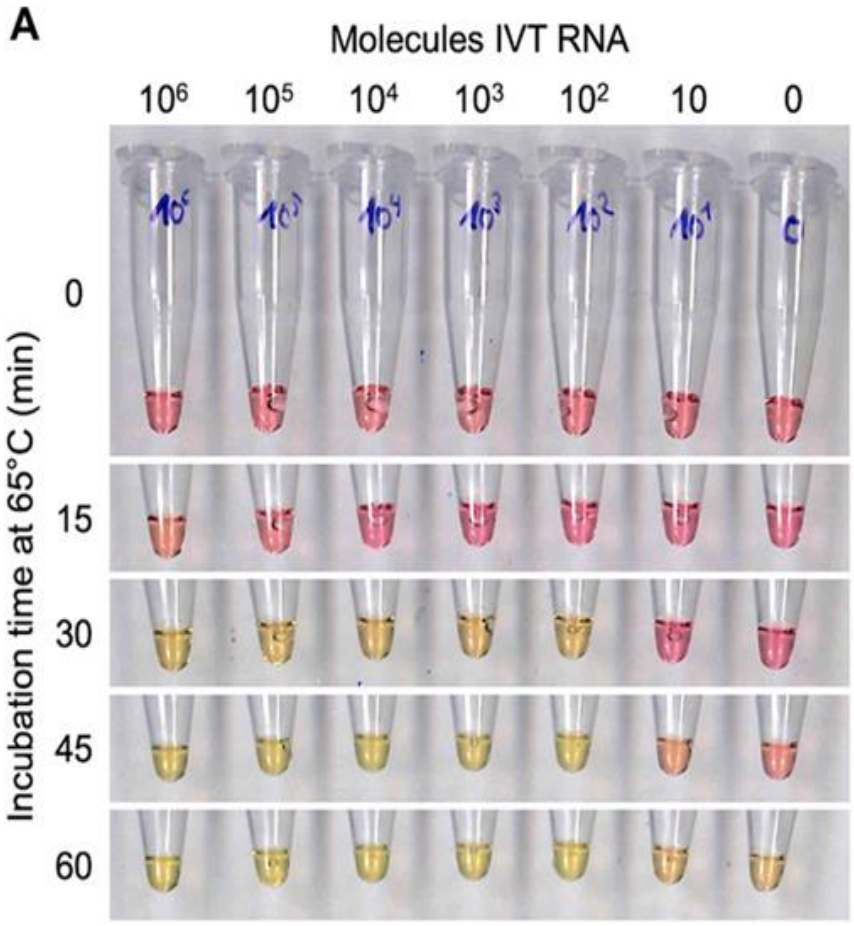

Figure 1.13. Colorimetric Sars-CoV-2 *N* gene LAMP assay. Figure reproduced from Ref. (187).

Several studies have also been published on exploring the use of LAMP detection scheme to detect the presence of bacterial load and infection. Shi et al. developed a protocol to rapidly detect *exoS* and *exoU* genes in *P. aeruginosa*. The team utilized two set of primers designed to amplify both genes. Assay utilized a 40min reaction under 63ºC. Detection limit for purified DNA was 100 fg. The team detected 107 river isolates for the detection of *P. aeruginosa*.

Multiplexing remains at the forefront of disease and infection control. In order to properly multiplex detection of pathogens, primers must be designed towards highly specific and conserved DNA targets. Kim et al. developed a custom multiplexed LAMP assay for the detection of *Mycobacterium tuberculosis* (MTB) and non-tuberculosis mycobacterium (NTM). This assay is relevant to be able to differentiate between species capable of causing tuberculosis (TB). Two different set of specific primers were developed. One set was designed to amplify the *IS6110* gene of MTB and the other for *rpoB* gene of several mycobacterium species. MTB was detected with a positive amplification from both genes. LAMP reagent kit from M-monitor was used to perform the reaction at 65 ºC for 60 min. Positive fluorescence was detected with Ct value. Sensitivity of multiplexed assay was 100% for MTB and 98.4% for NTM with a 100% specificity. (188) A multi-LAMP assay was developed to detect colistin resistance. Specifically, primer sets were made to detect the *mcr-1* through *mcr-5*. The sensitivity of assay was found via electrophoresis to be 10-fold greater than PCR. (189) Liu developed a duplex LAMP assay that targets two sequences to detect *Salmonella spp.* And *Vibro parahaemolyticus* capable of amplification from same reaction tube. Reaction of primers and target was done at 65 ºC for 60 min. The LAMP products were analyzed using melting curve technique. Products were distinguished based on the different melting temperatures (Tm). Tm value for *Salmonella spp.* And *Vibro parahaemolyticus* was 86.61

± 0.11 ºC and 83.8 ºC, respectively. There were no peaks for samples without the two species, suggesting no amplification and specific site binding from primers.

A single-tube internally controlled multiplexed Tth Endonuclease Cleavage TEC-LAMP assay was developed to detect *Streptococcus pneumoniae*, *Neisseria meningitidis* and *Haemophilus influenzae*. The assay incorporates Tth endonuclease IV with a novel TEC primer under normal LAMP conditions. (190) Tth endonuclease IV is a thermostable DNA AP endonuclease that catalyzes the cleavage of DNA at AP sites. This endonuclease leaves a 1 nucleotide gap with a 3'-hydroxyl and a 5' deoxyribose phosphate termini. TEC primer was forward inner primer (FIP) with an abasic site flanked with a 5' fluorophore with an internal thymine-based quencher. Internally controlled multiplex TEC-LAMP utilized FAM, Cy5, HEX, and CYAN probes for the three organisms with an internal amplification control. Initially, dsDNA is dissociated with primer and TEC primer hybridization. Next step, dsDNA is formed via inner primer strand extension. Once the newly formed inner primer linked ssDNA forms loop structures, the abasic site of TEC probe cleaves to the Tth endonuclease IV enzyme. The next cycle forms a new dsDNA and a nicking enzyme fully dissociates the TEC primer fluorophore from quencher to produce a fluorescent signal. Outer primer strand displacement extension displaces the next dsDNA to produce stem loop structures. This process is repeated leading to rapid exponential amplification. The assay was used on clinical samples and was shown to have a 92.3% and 100% sensitivity and specificity, respectively (190).

1.16. Future Direction

Biosensing applications are mostly done at the lab bench top. Most efforts may be dedicated to making these platforms more wearable. Mainly enzymatic biosensing is popular, but Aptamers are also of growing interest as opposed to the use of antibodies. Most cell-based and

cell-free systems are derived from pathogenic species. Although they are genetically modified to minimize virulence, they could induce an immune response by the host if used directly at an infection site. In order to develop in situ autoinducing whole-cell or cell-free systems, non-pathogenic bacteria should be used. Fluorescence is a commonly used reporter technique. An excitation source and a dark enclosure are needed to quantify fluorescence. Alternatively, other methods such as colorimetric, aptamers with electrochemistry, or odor emission reporter systems could be used for in situ applications. Interestingly, novel aptamers have been developed to specifically bind to autoinducing analogs. However, the number of reported aptamer-based sensors are extremely limited and further work could be done to synthesize more aptamers for QS biosensing applications. The detection of autoinducers produced by pathogenic bacteria would give clinicians information about the type and stage of infection, which would minimize the progression of antimicrobial resistance.

1.17 References

1. Preventrion. C for DC and. About Antibiotic Resistance. 2019.
2. Ng WL, Bassler BL. Bacterial quorum-sensing network architectures. Vol. 43, Annual Review of Genetics. NIH Public Access; 2009. p. 197–222.
3. Van Boeckel TP, Gandra S, Ashok A, Caudron Q, Grenfell BT, Levin SA, et al. Global antibiotic consumption 2000 to 2010: An analysis of national pharmaceutical sales data. Lancet Infect Dis. 2014 Aug 1;14(8):742–50.
4. C Reygaert W. An overview of the antimicrobial resistance mechanisms of bacteria. AIMS Microbiol. 2018;4(3):482–501.
5. Pantosti A, Sanchini A, Monaco M. Mechanisms of antibiotic resistance in Staphylococcus aureus. Future Microbiol. 2007;2(3):323–34.
6. Mohammad Reza S. Bacterial Biofilm and its Clinical Implications. Ann Microbiol Res. 2018;2(1).
7. Flemming HC, Wingender J. The biofilm matrix. Nat Rev Microbiol. 2010;8(9):623–33.
8. Frykberg RG, Banks J. Challenges in the Treatment of Chronic Wounds. Adv Wound

Care. 2015 Sep;4(9):560–82.

9. Livingstone M, Miller C, Gilmore J. Comparing PLA, Ag, and Ceria Nanofiber Composites for Antibacterial Efficacy in Chronic Wounds. Biomed Sci Instrum. 2020;56(1).

10. Dahiru I, Amaefule K, Okpe I, Ibrahim A, Muazu S. An overview of diabetic foot disease. Niger J Basic Clin Sci. 2016;13(1):1.

11. Alves C, Casqueiro J, Casqueiro J. Infections in patients with diabetes mellitus: A review of pathogenesis. Indian J Endocrinol Metab. 2012;16(7):27.

12. Powlson AS, Coll AP. The treatment of diabetic foot infections. Vol. 65, Journal of Antimicrobial Chemotherapy. Oxford Academic; 2010. p. iii3–9.

13. Oliver TI, Mutluoglu M. Diabetic Foot Ulcer. StatPearls. StatPearls Publishing; 2020.

14. Schroeder M, Brooks BD, Brooks AE. The complex relationship between virulence and antibiotic resistance. Genes (Basel). 2017;8(1).

15. Preventrion. C for DC and. About Antibiotic Resistance [Internet]. 2019. Available from: https://www.cdc.gov/drugresistance/about.html

16. World Health Organization. Global priority list of antibiotic-resistant bacteria to guide research, discovery, and development of new antibiotics. [Internet]. 2017 [cited 2021 Jun 13]. Available from: http://www.cdc.gov/drugresistance/threat-report-2013/

17. World Health Organization. No time to wait: securing the future from drug-resistant infections. World Heal Organ Geneva, Switz. 2019;

18. Talbot GH, Jezek A, Murray BE, Jones RN, Ebright RH, Nau GJ, et al. The infectious diseases society of America's 10 × '20 initiative (10 new systemic antibacterial agents US food and drug administration approved by 2020): Is 20 × '20 a possibility? [Internet]. Vol. 69, Clinical Infectious Diseases. Oxford University Press; 2019 [cited 2021 Jun 13]. p. 1–11. Available from: https://academic.oup.com/cid/article/69/1/1/5305275

19. Ng W, Bassler BL. Bacterial Quorum-Sensing Network Architectures. Annu Rev Genet. 2009;43.

20. Dickschat JS. Quorum sensing and bacterial biofilms. Vol. 27, Natural Product Reports. The Royal Society of Chemistry; 2010. p. 343–69.

21. Rutherford ST, Bassler BL. Bacterial quorum sensing: Its role in virulence and possibilities for its control. Cold Spring Harb Perspect Med. 2012;2(11):1–26.

22. Bassler BL. How bacteria talk to each other: Regulation of gene expression by quorum sensing. Curr Opin Microbiol. 1999;2(6):582–7.

23. Gould TA, Herman J, Krank J, Murphy RC, Churchill MEA. Specificity of acyl-homoserine lactone synthases examined by mass spectrometry. J Bacteriol. 2006;188(2):773–83.

24. Bhardwaj AK, Vinothkumar K. Quorum Sensing vs Quorum Quenching: A Battle with No End in Sight. New Delhi: Springer India. 2015. 9–22 p.

25. Miller C, Gilmore J. Detection of Quorum-Sensing Molecules for Pathogenic Molecules Using Cell-Based and Cell-Free Biosensors. Antibiotics [Internet]. 2020 May 1 [cited 2021 Nov 15];9(5). Available from: /pmc/articles/PMC7277912/

26. Van Boeckel TP, Gandra S, Ashok A, Caudron Q, Grenfell BT, Levin SA, et al. Global antibiotic consumption 2000 to 2010: An analysis of national pharmaceutical sales data. Lancet Infect Dis. 2014;14(8):742–50.

27. Bartlett JG, Gilbert DN, Spellberg B. Seven ways to preserve the Miracle of antibiotics. Clin Infect Dis. 2013;56(10):1445–50.

28. Resistance ICG on A. No time to wait: SECURING THE FUTURE FROM DRUG-RESISTANT INFECTIONS. Artforum Int. 2019;

29. Talbot GH, Jezek A, Murray BE, Jones RN, Ebright RH, Nau GJ, et al. The infectious diseases society of America's 10 × '20 initiative (10 new systemic antibacterial agents US food and drug administration approved by 2020): Is 20 × '20 a possibility? Clin Infect Dis. 2019;69(1):1–11.

30. Ali L, Goraya MU, Arafat Y, Ajmal M, Chen JL, Yu D. Molecular mechanism of quorum-sensing in Enterococcus faecalis: Its role in virulence and therapeutic approaches. Int J Mol Sci. 2017;18(5).

31. Tong SYC, Davis JS, Eichenberger E, Holland TL, Fowler VG. Staphylococcus aureus infections: Epidemiology, pathophysiology, clinical manifestations, and management. Clin Microbiol Rev. 2015;28(3):603–61.

32. Le KY, Otto M. Quorum-sensing regulation in staphylococci-an overview. Front Microbiol. 2015;6(OCT):1–8.

33. Yarwood JM, Schlievert PM. Quorum sensing in Staphylococcus infections. J Clin Invest. 2003;112(11):1620–5.

34. Gomes-Fernandes M, Laabei M, Pagan N, Hidalgo J, Molinos S, Villar Hernandez R, et al. Accessory gene regulator (Agr) functionality in Staphylococcus aureus derived from lower respiratory tract infections. PLoS One. 2017;12(4):1–14.

35. Novick RP. Autoinduction and signal transduction in the regulation of staphylococcal virulence. Mol Microbiol. 2003;48(6):1429–49.

36. Pinkston KL, Gao P, Diaz-Garcia D, Sillanpää J, Nallapareddy SR, Murray BE, et al. The

Fsr quorum-sensing system of Enterococcus faecalis modulates surface display of the collagen-binding MSCRAMM Ace through regulation of gelE. J Bacteriol. 2011;193(17):4317–25.

37. Dundar H, Brede DA, La Rosa SL, El-Gendy AO, Diep DB, Nes IF. The fsr quorum-sensing system and cognate gelatinase orchestrate the expression and processing of proprotein EF_1097 into the mature antimicrobial peptide enterocin O16. J Bacteriol. 2015;197(13):2112–21.

38. Shankar J, Walker RG, Ward D, Horsburgh MJ. The enterococcus faecalis exoproteome: Identification and temporal regulation by fsr. PLoS One. 2012;7(3):1–9.

39. Thurlow LR, Thomas VC, Narayanan S, Olson S, Fleming SD, Hancock LE. Gelatinase contributes to the pathogenesis of endocarditis caused by Enterococcus faecalis. Infect Immun. 2010;78(11):4936–43.

40. Thomas VC, Thurlow LR, Boyle D, Hancock LE. Regulation of autolysis-dependent extracellular DNA release by Enterococcus faecalis extracellular proteases influences biofilm development. J Bacteriol. 2008;190(16):5690–8.

41. Centers for Disease Control and Preventrion. Pneumococcal Disease. 2019;

42. Galante J, Ho A, Tingey S, Charalambous B. Quorum Sensing and Biofilms in the Pathogen, Streptococcus pneumoniae. Curr Pharm Des. 2014;21(1):25–30.

43. Yadav MK, Vidal JE, Go YY, Kim SH, Chae SW, Song JJ. The LuxS/AI-2 quorum-sensing system of Streptococcus pneumoniae Is required to cause disease, and to regulate virulence- and metabolism-related genes in a rat model of middle ear infection. Front Cell Infect Microbiol. 2018;8(MAY):1–16.

44. Lin J, Cheng J, Wang Y, Shen X. The Pseudomonas quinolone signal (PQS): Not just for quorum sensing anymore. Front Cell Infect Microbiol. 2018;8(JUL):1–9.

45. Oziat J, Gougis M, Malliaras GG, Mailley P. Electrochemical Characterizations of four Main Redox–metabolites of Pseudomonas Aeruginosa. Electroanalysis. 2017;29(5):1332–40.

46. Preventrion. C for DC and. Healthcare-associated Infections. 2019; Available from: https://www.cdc.gov/hai/organisms/pseudomonas.html

47. Bielecki P, Glik J, Kawecki M, Martins Dos Santos VAP. Towards understanding Pseudomonas aeruginosa burn wound infections by profiling gene expression. Biotechnol Lett. 2008;30(5):777–90.

48. Lee J, Zhang L. The hierarchy quorum sensing network in Pseudomonas aeruginosa. Protein Cell. 2014;6(1):26–41.

49. Higgins S, Heeb S, Rampioni G, Fletcher MP, Williams P, Cámara M. Differential

regulation of the phenazine biosynthetic operons by quorum sensing in Pseudomonas aeruginosa PAO1-N. Front Cell Infect Microbiol. 2018;8(JUL):1–13.

50. Saipriya K, Swathi CH, Ratnakar KS, Sritharan V. Quorum-sensing system in Acinetobacter baumannii: a potential target for new drug development. J Appl Microbiol. 2019;

51. Niu C, Clemmer KM, Bonomo RA, Rather PN. Isolation and characterization of an autoinducer synthase from Acinetobacter baumannii. J Bacteriol. 2008;190(9):3386–92.

52. De Araujo C, Balestrino D, Roth L, Charbonnel N, Forestier C. Quorum sensing affects biofilm formation through lipopolysaccharide synthesis in Klebsiella pneumoniae. Res Microbiol. 2010;161(7):595–603.

53. Balestrino D, Haagensen JAJ, Rich C, Forestier C. Characterization of type 2 quorum sensing in Klebsiella pneumoniae and relationship with biofilm formation. J Bacteriol. 2005;187(8):2870–80.

54. Yin WF, Purmal K, Chin S, Chan XY, Koh CL, Sam CK, et al. N-Acyl homoserine lactone production by Klebsiella pneumonia isolated from human tongue surface. Sensors. 2012;12(3):3472–83.

55. Pereira CS, Thompson JA, Xavier KB. AI-2-mediated signalling in bacteria. FEMS Microbiol Rev. 2013;37(2):156–81.

56. Xu L, Li H, Vuong C, Vadyvaloo V, Wang J, Yao Y, et al. Role of the luxS quorum-sensing system in biofilm formation and virulence of Staphylococcus epidermidis. Infect Immun. 2006;74(1):488–96.

57. Eugene Sanders WE, Sanders CC. Enterobacter spp.: Pathogens poised to flourish at the turn of the century. Clin Microbiol Rev. 1997;10(2):220–41.

58. Zhou J, Lao YM, Ma ZP, Cai ZH. Genome sequence of Enterobacter sp. ST3, a quorum sensing bacterium associated with marine dinoflagellate. Genomics Data. 2016;7:195–9.

59. Yin WF, Purmal K, Chin S, Chan XY, Chan KG. Long chain N-acyl homoserine lactone production by Enterobacter sp. isolated from human tongue surfaces. Sensors (Switzerland). 2012;12(11):14307–14.

60. Surette MG, Miller MB, Bassler BL. Quorum sensing in Escherichia coli, Salmonella typhimurium, and Vibrio harveyi: A new family of genes responsible for autoinducer production. Proc Natl Acad Sci U S A. 1999;96(4):1639–44.

61. Zhao L, Xue T, Shang F, Sun H, Sun B. Staphylococcus aureus AI-2 quorum sensing associates with the KdpDE two-component system to regulate capsular polysaccharide synthesis and virulence. Infect Immun. 2010;78(8):3506–15.

62. Hegde M, Englert DL, Schrock S, Cohn WB, Vogt C, Wood TK, et al. Chemotaxis to the

quorum-sensing signal AI-2 requires the Tsr chemoreceptor and the periplasmic LsrB AI-2-binding protein. J Bacteriol. 2011;193(3):768–73.

63. Albuquerque P, Casadevall A. Quorum sensing in fungi – a review. Med Mycol [Internet]. 2012 May 1 [cited 2021 Jul 10];50(4):337–45. Available from: https://academic.oup.com/mmy/article/50/4/337/1178656

64. Nobile CJ, Johnson AD. Candida albicans Biofilms and Human Disease. Annu Rev Microbiol [Internet]. 2015 Oct 15 [cited 2021 Jul 10];69(1):71. Available from: /pmc/articles/PMC4930275/

65. J C, DM K, PK M, LL H, T M, MA G. Biofilm formation by the fungal pathogen Candida albicans: development, architecture, and drug resistance. J Bacteriol [Internet]. 2001 [cited 2021 Jul 10];183(18):5385–94. Available from: https://pubmed.ncbi.nlm.nih.gov/11514524/

66. Seddiki SML, Boucherit-Otmani Z, Boucherit K, Badsi-Amir S, Taleb M, Kunkel D. Assessment of the types of catheter infectivity caused by Candida species and their biofilm formation. First study in an intensive care unit in Algeria. Int J Gen Med [Internet]. 2013 [cited 2021 Jul 10];6:1. Available from: /pmc/articles/PMC3549679/

67. JM H, EC J, AD L, JJ T, B J, R S, et al. Quorum sensing in the dimorphic fungus Candida albicans is mediated by farnesol. Appl Environ Microbiol [Internet]. 2001 Jul [cited 2021 Jul 10];67(7):2982–92. Available from: https://pubmed.ncbi.nlm.nih.gov/11425711/

68. Kim J, Sudbery P. Candida albicans , a major human fungal pathogen. J Microbiol 2011 492 [Internet]. 2011 May 3 [cited 2021 Jul 10];49(2):171–7. Available from: https://link.springer.com/article/10.1007/s12275-011-1064-7

69. Shirtliff ME, Krom BP, Meijering RAM, Peters BM, Zhu J, Scheper MA, et al. Farnesol-Induced Apoptosis in Candida albicans. Antimicrob Agents Chemother [Internet]. 2009 Jun [cited 2021 Jul 10];53(6):2392. Available from: /pmc/articles/PMC2687256/

70. Jackson BP, Dietz SM, Wightman RM. Fast-scan cyclic voltammetry of 5-hydroxytryptamine. Anal Chem [Internet]. 2002 [cited 2021 Jul 11];67(6):1115–20. Available from: https://pubs.acs.org/doi/abs/10.1021/ac00102a015

71. Akiyama A, Kato T, Ishii K, Yasuda E. In vitro measurement of dopamine concentration with carbon fiber electrode. Anal Chem [Internet]. 2002 Jul 1 [cited 2021 Jul 11];57(8):1518–22. Available from: https://pubs.acs.org/doi/abs/10.1021/ac00285a006

72. Kumar SS, Mathiyarasu J, Phani KLN, Yegnaraman V. Simultaneous determination of dopamine and ascorbic acid on poly (3,4-ethylenedioxythiophene) modified glassy carbon electrode. J Solid State Electrochem 2005 1011 [Internet]. 2005 Aug 2 [cited 2021 Jul 11];10(11):905–13. Available from: https://link.springer.com/article/10.1007/s10008-005-0041-7

73. Stamford JA, Palij P, Davidson C, Trout SJ. Fast cyclic voltammetry: neurotransmitter

measurement in “real time” and “real space.” Bioelectrochemistry Bioenerg. 1995 Oct 1;38(2):289–96.

74. Spinner N. Square Wave Voltammetry (SWV) [Internet]. 2021 [cited 2021 Nov 17]. Available from: https://pineresearch.com/shop/kb/software/methods-and-techniques/voltammetric-methods/square-wave-voltammetry/

75. Touhami A. Biosensors and Nanobiosensors: Design and Applications. Nanomedicine. 2015;374–400.

76. Rocchitta G, Spanu A, Babudieri S, Latte G, Madeddu G, Galleri G, et al. Enzyme biosensors for biomedical applications: Strategies for safeguarding analytical performances in biological fluids. Sensors (Switzerland). 2016;16(6).

77. Thiha A, Ibrahim F. A colorimetric Enzyme-Linked Immunosorbent Assay (ELISA) detection platform for a point-of-care dengue detection system on a lab-on-compact-disc. Sensors (Switzerland). 2015;15(5):11431–41.

78. Milne SD, Connolly P, Hamad H Al, Seoudi I. Development of wearable sensors for tailored patient wound care. 2014 36th Annu Int Conf IEEE Eng Med Biol Soc EMBC 2014. 2014;618–21.

79. Biela A, Watkinson M, Meier UC, Baker D, Giovannoni G, Becer CR, et al. Disposable MMP-9 sensor based on the degradation of peptide cross-linked hydrogel films using electrochemical impedance spectroscopy. Biosens Bioelectron. 2015;68:660–7.

80. Kassal P, Kim J, Kumar R, De Araujo WR, Steinberg IM, Steinberg MD, et al. Smart bandage with wireless connectivity for uric acid biosensing as an indicator of wound status. Electrochem commun. 2015;56:6–10.

81. Sharp D, Forsythe S, Davis J. Carbon Fibre Composites : Integrated Electrochemical Sensors for Wound Management Submitted to : 2007;44(August):1–22.

82. RoyChoudhury S, Umasankar Y, Bhansali S. A wearable electrochemical sensor to monitor progression of wound healing. ECS Trans. 2017;80(10):1345–53.

83. Staneva D, Betcheva R, Chovelon JM. Fluorescent benzo[de]anthracen-7-one pH-sensor in aqueous solution and immobilized on viscose fabrics. J Photochem Photobiol A Chem. 2006;183(1–2):159–64.

84. McLister A, Davis J. Molecular Wiring in Smart Dressings: Opening a New Route to Monitoring Wound pH. Healthcare. 2015;3(3):466–77.

85. Tamayol A, Akbari M, Zilberman Y, Comotto M, Lesha E, Serex L, et al. Flexible pH-Sensing Hydrogel Fibers for Epidermal Applications. Adv Heal Mater. 2016;5(6):711–9.

86. Sridhar V, Takahata K. A hydrogel-based passive wireless sensor using a flex-circuit inductive transducer. Sensors Actuators, A Phys. 2009;155(1):58–65.

87. Whelan J. Smart bandages diagnose wound infection. Drug Discov Today. 2002;7(1):9–10.

88. DeLouise LA. Smart bandage - A hydrogel supported optical microcavity sensor. 2005 NSTI Nanotechnol Conf Trade Show - NSTI Nanotech 2005. 2005;1:51–4.

89. Thet NT, Alves DR, Bean JE, Booth S, Nzakizwanayo J, Young AER, et al. Prototype Development of the Intelligent Hydrogel Wound Dressing and Its Efficacy in the Detection of Model Pathogenic Wound Biofilms. ACS Appl Mater Interfaces. 2016;8(24):14909–19.

90. Privetta BJ, Shinb JH, Schoenfisch MH. Tutorial Review: Electrochemical Nitric Oxide Sensors for Physiological Measurements. Chem Soc Rev. 2010;14(4):384–99.

91. Jiang S, Cheng R, Wang X, Xue T, Liu Y, Nel A, et al. Real-time electrical detection of nitric oxide in biological systems with sub-nanomolar sensitivity. Nat Commun. 2013;4:1–7.

92. Mostafalu P, Lenk W, Dokmeci MR, Ziaie B, Khademhosseini A, Sonkusale SR. Wireless Flexible Smart Bandage for Continuous Monitoring of Wound Oxygenation. IEEE Trans Biomed Circuits Syst. 2015;9(5):670–7.

93. Utz ER, Elster EA, Tadaki DK, Gage F, Perdue PW, Forsberg JA, et al. Metalloproteinase Expression is Associated with Traumatic Wound Failure. J Surg Res. 2010;159(2):633–9.

94. Farrow MJ, Hunter IS, Connolly P. Developing a real time sensing system to monitor bacteria in wound dressings. Biosensors. 2012;2(2):171–88.

95. Ostadabbas S, Saeed A, Nourani M, Pompeo M. Sensor architectural tradeoff for diabetic foot ulcer monitoring. Proc Annu Int Conf IEEE Eng Med Biol Soc EMBS. 2012;6687–90.

96. LaRiviere CA, Goldin AB, Avansino J. Silver toxicity with the use of silver-impregnated dressing and wound vacuum-assisted closure in an immunocompromised patient. J Am Col Certif Wound Spec. 2011;3(1):8–12.

97. Swisher SL, Lin MC, Liao A, Leeflang EJ, Khan Y, Pavinatto FJ, et al. Impedance sensing device enables early detection of pressure ulcers in vivo. Nat Commun. 2015;6:1–10.

98. Kim DH, Wang S, Keum H, Ghaffari R, Kim YS, Tao H, et al. Thin, flexible sensors and actuators as “instrumented” surgical sutures for targeted wound monitoring and therapy. Small. 2012;8(21):3263–8.

99. Matzeu G, Losacco M, Parducci E, Pucci A, Dini V, Romanelli M, et al. Skin temperature monitoring by a wireless sensor. IECON 2011 - 37th Annu Conf IEEE Ind Electron Soc. 2011;3533–5.

100. Mehmood N, Hariz A, Templeton S, Voelcker NH. A flexible and low power telemetric sensing and monitoring system for chronic wound diagnostics. Biomed Eng Online. 2015;14(1):1–17.

101. Farooqui MF, Shamim A. Low Cost Inkjet Printed Smart Bandage for Wireless Monitoring of Chronic Wounds. Sci Rep. 2016;6:1–13.

102. Lakhin AV, Tarantul VZ, Gening LV. Aptamers: Problems, Solutions and Prospects. Acta Naturae [Internet]. 2013 [cited 2021 Jul 11];5(4):34. Available from: /pmc/articles/PMC3890987/

103. NK N, WK M, L Y. In vitro selection of protein-binding DNA aptamers as ligands for biosensing applications. Methods Mol Biol [Internet]. 2009 [cited 2021 Jul 11];504:399–415. Available from: https://pubmed.ncbi.nlm.nih.gov/19159108/

104. Biosensors - ScienceAid [Internet]. [cited 2021 Jul 11]. Available from: https://scienceaid.net/Biosensors

105. Medeiros ES, Glenn GM, Klamczynski AP, Orts WJ, Mattoso LHC. Solution blow spinning: A new method to produce micro- and nanofibers from polymer solutions. J Appl Polym Sci [Internet]. 2009 Aug 15 [cited 2020 Dec 10];113(4):2322–30. Available from: https://onlinelibrary.wiley.com/doi/full/10.1002/app.30275

106. Daristotle JL, Behrens AM, Sandler AD, Kofinas P. A Review of the Fundamental Principles and Applications of Solution Blow Spinning. ACS Appl Mater Interfaces. 2016 Dec;8(51):34951–63.

107. Greiner A, Wendorff JH. Electrospinning: A fascinating method for the preparation of ultrathin fibers. Vol. 46, Angewandte Chemie - International Edition. John Wiley & Sons, Ltd; 2007. p. 5670–703.

108. Ramakrishna S, Fujihara K, Teo WE, Lim TC, Ma Z. An introduction to electrospinning and nanofibers. An Introduction to Electrospinning and Nanofibers. World Scientific Publishing Co.; 2005. 1–382 p.

109. Subbiah T, Bhat GS, Tock RW, Parameswaran S, Ramkumar SS. Electrospinning of nanofibers. J Appl Polym Sci. 2005 Apr;96(2):557–69.

110. Huang ZM, Zhang YZ, Kotaki M, Ramakrishna S. A review on polymer nanofibers by electrospinning and their applications in nanocomposites. Compos Sci Technol. 2003 Nov 1;63(15):2223–53.

111. Hunley MT, Long TE. Electrospinning functional nanoscale fibers: a perspective for the future. Polym Int [Internet]. 2008 Mar 1 [cited 2020 Aug 23];57(3):385–9. Available from: http://doi.wiley.com/10.1002/pi.2320

112. Fedorova N, Pourdeyhimi B. High strength nylon micro- and nanofiber based nonwovens via spunbonding. J Appl Polym Sci [Internet]. 2007 Jun 5 [cited 2020 Aug

23];104(5):3434–42. Available from: http://doi.wiley.com/10.1002/app.25939

113. Martins A, Araújo J V., Reis RL, Neves NM. Electrospun nanostructured scaffolds for tissue engineering applications. Nanomedicine. 2007 Dec;2(6):929–42.

114. Sell S, Barnes C, Smith M, McClure M, Madurantakam P, Grant J, et al. Extracellular matrix regenerated: Tissue engineering via electrospun biomimetic nanofibers. Vol. 56, Polymer International. John Wiley & Sons, Ltd; 2007. p. 1349–60.

115. Chen JP, Chang GY, Chen JK. Electrospun collagen/chitosan nanofibrous membrane as wound dressing. Colloids Surfaces A Physicochem Eng Asp. 2008 Feb;313–314:183–8.

116. Miller CL, Stafford G, Sigmon N, Gilmore JA. Conductive nonwoven carbon nanotube-PLA composite nanofibers towards wound sensors via solution blow spinning. IEEE Trans Nanobioscience. 2019 Apr;18(2):244–7.

117. Gianino E, Miller C, Gilmore J. Smart Wound Dressings for Diabetic Chronic Wounds. Bioengineering. 2018;5(3):1–26.

118. Dakal TC, Kumar A, Majumdar RS, Yadav V. Mechanistic basis of antimicrobial actions of silver nanoparticles. Front Microbiol. 2016 Nov;7(NOV):1831.

119. Walkey C, Das S, Seal S, Erlichman J, Heckman K, Ghibelli L, et al. Catalytic properties and biomedical applications of cerium oxide nanoparticles. Vol. 2, Environmental Science: Nano. Royal Society of Chemistry; 2015. p. 33–53.

120. Pitt JJ. Principles and Applications of Liquid Chromatography- Mass Spectrometry in Clinical Biochemistry. Clin Biochem Rev. 2009;30(February):19–34.

121. Purohit AA, Johansen JA, Hansen H, Leiros HKS, Kashulin A, Karlsen C, et al. Presence of acyl-homoserine lactones in 57 members of the Vibrionaceae family. J Appl Microbiol. 2013;115(3):835–47.

122. Pratima NA. Liquid Chromatography-Mass Spectrometry and Its Applications: A Brief Review. Arch Org Inorg Chem Sci. 2018;1(1):26–34.

123. Scientific C. Mass Spectrometry Fundamental LC-MS Introduction. 2004;1–24.

124. Yang Y, Zhou M, Hardwidge PR, Cui H, Zhu G. Isolation and characterization of N-acyl homoserine lactone-producing bacteria from cattle rumen and swine intestines. Front Cell Infect Microbiol. 2018;8(MAY):1–10.

125. Gless BH, Bojer MS, Peng P, Baldry M, Ingmer H, Olsen CA. Identification of autoinducing thiodepsipeptides from staphylococci enabled by native chemical ligation. Nat Chem. 2019;11(5):463–9.

126. Junio HA, Todd DA, Ettefagh KA, Ehrmann BM, Kavanaugh JS, Horswill AR, et al. Quantitative analysis of autoinducing peptide I (AIP-I) from Staphylococcus aureus

cultures using ultrahigh performance liquid chromatography-high resolving power mass spectrometry. J Chromatogr B Anal Technol Biomed Life Sci. 2013;930:7–12.

127. Kalkum M, Lyon GJ, Chait BT. Detection of secreted peptides by using hypothesis-driven multistage mass spectrometry. Proc Natl Acad Sci U S A. 2003;100(5):2795–800.

128. Miller C, Stiglich M, Livingstone M, Gilmore J. Impedance-Based Biosensing of Pseudomonas putida via Solution Blow Spun PLA: MWCNT Composite Nanofibers. Micromachines. 2019;10(12).

129. Bellitti P, Bona M, Fontana S, Sardini E, Serpelloni M. Study toward the integration of a system for bacterial growth monitoring in an automated specimen processing platform. Lect Notes Electr Eng. 2019;539:445–54.

130. Cristina Pablos, Javier Marugán, Sandra Cristóbal, Rafael van Grieken. Implications of Electrical Impedance-Based Microbiological Technology in Pork Meat Processing Industry for the Rapid Detection and Quantification of Salmonella Spp. J Food Sci Eng. 2017;7(1):1–16.

131. Lei KF. Review on impedance detection of cellular responses in micro/nano environment. Micromachines. 2014;5(1):1–12.

132. Farooq U, Wajid Ullah M, Yang Q, Wang S. Applications of Phage-Based Biosensors in the Diagnosis of Infectious Diseases, Food Safety, and Environmental Monitoring. Biosens Environ Monit. 2019;1–18.

133. Singh A, Poshtiban S, Evoy S. Recent advances in bacteriophage based biosensors for food-borne pathogen detection. Sensors (Switzerland). 2013;13(2):1763–86.

134. Sibbald RG, Orsted HL, Schultz G, Keast DH. Preparing the wound bed 2003: focus on infection and inflammation. 2003;(May 2014).

135. Stojadinovic A, Carlson JW, Schultz GS, Davis TA, Elster EA. Topical advances in wound care. Gynecol Oncol [Internet]. 2008;111(2 SUPPL.):S70–80. Available from: http://dx.doi.org/10.1016/j.ygyno.2008.07.042

136. Bjarnsholt T, Kirketerp-Møller K, Jensen PØ, Madsen KG, Phipps R, Krogfelt K, et al. Why chronic wounds will not heal: A novel hypothesis. Wound Repair Regen. 2008;16(1):2–10.

137. Yussof SJM, Omar E, Pai DR, Sood S. Cellular events and biomarkers of wound healing. Indian J Plast Surg. 2012;45(2):220–8.

138. Liu Q, Wang J, Boyd BJ. Peptide-based biosensors. Talanta. 2015;136:114–27.

139. Verbeke F, De Craemer S, Debunne N, Janssens Y, Wynendaele E, Van de Wiele C, et al. Peptides as quorum sensing molecules: Measurement techniques and obtained levels in vitro and in vivo. Front Neurosci. 2017;11(APR):1–18.

140. Syvitski RT, Tian XL, Sampara K, Salman A, Lee SF, Jakeman DL, et al. Structure-activity analysis of quorum-sensing signaling peptides from Streptococcus mutans. J Bacteriol. 2007;189(4):1441–50.

141. Tian X, Syvitski RT, Liu T, Livingstone N, Jakeman DL, Li YH. A method for structure-activity analysis of quorum-sensing signaling peptides from naturally transformable streptococci. Biol Proced Online. 2009;11(1):207–26.

142. La Rosa SL, Solheim M, Diep DB, Nes IF, Brede DA. Bioluminescence based biosensors for quantitative detection of enterococcal peptide - Pheromone activity reveal inter-strain telesensing in vivo during polymicrobial systemic infection. Sci Rep. 2015;5:8339.

143. Lubkowicz D, Ho CL, Hwang IY, Yew WS, Lee YS, Chang MW. Reprogramming Probiotic Lactobacillus reuteri as a Biosensor for Staphylococcus aureus Derived AIP-I Detection. ACS Synth Biol. 2018;7(5):1229–37.

144. Malone CL, Boles BR, Lauderdale KJ, Thoendel M, Kavanaugh JS, Horswill AR. Fluorescent reporters for Staphylococcus aureus. J Microbiol Methods [Internet]. 2009;77(3):251–60. Available from: http://dx.doi.org/10.1016/j.mimet.2009.02.011

145. Yarwood JM, Bartels DJ, Volper EM, Greenberg EP. Quorum Sensing in Staphylococcus aureus Biofilms. J Bacteriol. 2004;186(6):1838–50.

146. Franke GC, Dobinsky S, Mack D, Wang CJ, Sobottka I, Christner M, et al. Expression and functional characterization of gfpmut3.1 and its unstable variants in Staphylococcus epidermidis. J Microbiol Methods. 2007;71(2):123–32.

147. Malone CL, Boles BR, Lauderdale KJ, Thoendel M, Kavanaugh JS, Horswill AR. Fluorescent reporters for Staphylococcus aureus. J Microbiol Methods. 2009;77(3):251–60.

148. Subramoni S, Nathoo N, Klimov E, Yuan ZC. Agrobacterium tumefaciens responses to plant-derived signaling molecules. Front Plant Sci. 2014;5(JUL):1–12.

149. Cha C, Gao P, Chen YC, Shaw PD, Farrand SK. Production of acyl-homoserine lactone quorum-sensing signals by gram-negative plant-associated bacteria. Mol Plant-Microbe Interact. 1998;11(11):1119–29.

150. Farrand SK, Qin Y, Oger P. Quorum-sensing system of Agrobacterium plasmids: Analysis and utility. Methods Enzymol. 2002;358:452–84.

151. Steindler L, Venturi V. Detection of quorum-sensing N-acyl homoserine lactone signal molecules by bacterial biosensors. FEMS Microbiol Lett. 2007;266(1):1–9.

152. Nievas F, Bogino P, Sorroche F, Giordano W. Detection, characterization, and biological effect of quorum-sensing signaling molecules in Peanut-nodulating bradyrhizobia. Sensors. 2012;12(3):2851–73.

153. Luo ZQ, Su S, Farrand SK. In situ activation of the quorum-sensing transcription factor TraR by cognate and noncognate acyl-homoserine lactone ligands: Kinetics and consequences. J Bacteriol. 2003;185(19):5665–72.

154. Zhu J, Beaber JW, Moré MI, Fuqua C, Eberhard A, Winans SC. Analogs of the autoinducer 3-oxooctanoyl-homoserine lactone strongly inhibit activity of the TraR protein of Agrobacterium tumefaciens. J Bacteriol. 1998;180(20):5398–405.

155. Chambers CE, Visser MB, Schwab U, Sokol PA. Identification of N-acylhomoserine lactones in mucopurulent respiratory secretions from cystic fibrosis patients. FEMS Microbiol Lett. 2005;244(2):297–304.

156. Zhu J, Chai Y, Zhong Z, Li S, Winans SC. Agrobacterium Bioassay Strain for Ultrasensitive Detection of. Appl Environ Microbiol. 2003;69(11):6949–53.

157. Massai F, Imperi F, Quattrucci S, Zennaro E, Visca P, Leoni L. A multitask biosensor for micro-volumetric detection of N-3-oxo-dodecanoyl-homoserine lactone quorum sensing signal. Biosens Bioelectron [Internet]. 2011;26(8):3444–9. Available from: http://dx.doi.org/10.1016/j.bios.2011.01.022

158. Swift S, Karlyshev A V., Fish L, Durant EL, Winson MK, Chhabra SR, et al. Quorum sensing in Aeromonas hydrophila and Aeromonas salmonicida: Identification of the Luxri homologs AhyRi and AsaRi and their cognate N- acylhomoserine lactone signal molecules. J Bacteriol. 1997;179(17):5271–81.

159. Pearson JP, Gray KM, Passador L, Tucker KD, Eberhard A, Iglewski BH, et al. Structure of the autoinducer required for expression of Pseudomonas aeruginosa virulence genes. Proc Natl Acad Sci U S A. 1994;91(1):197–201.

160. Winson MK, Swift S, Fish L, Throup JP, Jørgensen F, Chhabra SR, et al. Construction and analysis of luxCDABE-based plasmid sensors for investigating N-acyl homoserine lactone-mediated quorum sensing. FEMS Microbiol Lett. 1998;163(2):185–92.

161. Rai N, Anand R, Ramkumar K, Sreenivasan V, Dabholkar S, Venkatesh K V., et al. Prediction by promoter logic in bacterial quorum sensing. PLoS Comput Biol. 2012;8(1).

162. Deng X, Zhuang G, Ma A, Yu Q, Zhuang X. Construction of a dual fluorescence whole-cell biosensor to detect N-acyl homoserine lactones. J Environ Sci (China) [Internet]. 2014;26(2):415–22. Available from: http://dx.doi.org/10.1016/S1001-0742(13)60407-6

163. Andersen JBO, Heydorn A, Hentzer M, Eberl LEO, Geisenberger O. gfp-Based N-Acyl Homoserine-Lactone Sensor Systems for Detection of Bacterial Communication. Microbiology. 2001;67(2):575–85.

164. Struss A, Pasini P, Ensor CM, Raut N, Daunert S. Paper strip whole cell biosensors: A portable test for the semiquantitative detection of bacterial quorum signaling molecules. Anal Chem. 2010;82(11):4457–63.

165. Dong YH, Zhang XF, Soo HML, Greenberg EP, Zhang LH. The two-component response regulator PprB modulates quorum-sensing signal production and global gene expression in Pseudomonas aeruginosa. Mol Microbiol. 2005;56(5):1287–301.

166. Scales BS, Dickson RP, Lipuma JJ, Huffnagle GB. Microbiology, genomics, and clinical significance of the Pseudomonas fluorescens species complex, an unappreciated colonizer of humans. Clin Microbiol Rev. 2014;27(4):927–48.

167. Khan SR, Mavrodi D V, Jog GJ, Suga H, Farrand SK. Activation of the phz Operon of Pseudomonas uorescens 2-79 Requires the LuxR Homolog PhzR, N-(3-OH-Hexanoyl)-. Society. 2005;187(18):6517–27.

168. Riedel K, Hentzer M, Geisenberger O, Huber B, Steidle A, Wu H, et al. N-acylhomoserine-lactone-mediated communication between Pseudomonas aeruginosa and Burkholderia cepacia in mixed biofilms. Microbiology. 2001;147(12):3249–62.

169. Shiner EK, Reddy S, Timmons C, Li G, Williams SC, Rumbaugh KP. Construction of a bacterial autoinducer detection system in mammalian cells. Biol Proced Online. 2004;6(1):268–76.

170. Tinafar A, Jaenes K, Pardee K. Synthetic Biology Goes Cell-Free. BMC Biol. 2019;17(1):1–14.

171. Kawaguchi T, Yung PC, Norman RS, Decho AW. Rapid screening of quorum-sensing signal N-acyl homoserine lactones by an in vitro cell-free assay. Appl Environ Microbiol. 2008;74(12):3667–71.

172. Chappell J, Jensen K, Freemont PS. Validation of an entirely in vitro approach for rapid prototyping of DNA regulatory elements for synthetic biology. Nucleic Acids Res. 2013;41(5):3471–81.

173. Wen KY, Cameron L, Chappell J, Jensen K, Bell DJ, Kelwick R, et al. A Cell-Free Biosensor for Detecting Quorum Sensing Molecules in P. aeruginosa-Infected Respiratory Samples. ACS Synth Biol. 2017;6(12):2293–301.

174. McClean KH, Winson MK, Fish L, Taylor A, Chhabra SR, Camara M, et al. Quorum sensing and Chromobacterium violaceum: Exploitation of violacein production and inhibition for the detection of N-acylhomoserine lactones. Microbiology. 1997;143(12):3703–11.

175. Winzer K, Hardie KR, Burgess N, Doherty N, Kirke D, Holden MTG, et al. LuxS: Its role in central metabolism and the in vitro synthesis of 4-hydroxy-5-methyl-3(2H)-furanone. Microbiology. 2002;148(4):909–22.

176. Zhao ZG, Yu YM, Xu BY, Yan SS, Xu JF, Liu F, et al. Screening and anti-virulent study of N-acyl homoserine lactones DNA aptamers against Pseudomonas aeruginosa quorum sensing. Biotechnol Bioprocess Eng. 2013;18(2):406–12.

177. Sismaet HJ. DEVELOPMENT AND OPTIMIZATION OF ELECTROCHEMICAL SENSORS TO DETECT BACTERIAL PATHOGENS FOR POINT-OF-CARE APPLICATIONS. Thesis. 2017;(May).

178. Baldrich E, Muñoz FX, García-Aljaro C. Electrochemical detection of quorum sensing signaling molecules by dual signal confirmation at microelectrode arrays. Anal Chem. 2011;83(6):2097–103.

179. Speers DJ, Ryan S, Harnett G, Chidlow G. Diagnosis of malaria aided by polymerase chain reaction in two cases with low-level parasitaemia. Intern Med J [Internet]. 2003 Dec 1 [cited 2021 Jun 7];33(12):613–5. Available from: https://onlinelibrary.wiley.com/doi/full/10.1111/j.1445-5994.2003.00500.x

180. Speers DJ. Clinical applications of molecular biology for infectious diseases. Clin Biochem Rev [Internet]. 2006 Feb [cited 2021 Jun 7];27(1):39–51. Available from: http://www.ncbi.nlm.nih.gov/pubmed/16886046

181. Polymerase Chain Reaction (PCR) | NEB [Internet]. [cited 2021 Jun 7]. Available from: https://www.neb.com/applications/dna-amplification-pcr-and-qpcr/polymerase-chain-reaction-pcr

182. Dennis YM, Rossa L, Chiu WK, Chan KCA. Clinical Applications of PCR Methods in Molecular Biology^{TM} 336. Humana Press Inc.; 2006.

183. Farkas DH, Holland CA. Overview of Molecular Diagnostic Techniques and Instrumentation. In: Cell and Tissue Based Molecular Pathology. Elsevier Inc.; 2009. p. 19–32.

184. Notomi T, Mori Y, Tomita N, Kanda H. Loop-mediated isothermal amplification (LAMP): principle, features, and future prospects. J Microbiol. 2015;53(1):1–5.

185. Zheng Z, Cheng Z. Advances in Molecular Diagnosis of Malaria. Adv Clin Chem. 2017 Jan 1;80:155–92.

186. El-Tholoth M, Bau HH, Song J. A Single and Two-Stage, Closed-Tube, Molecular Test for the 2019 Novel Coronavirus (COVID-19) at Home, Clinic, and Points of Entry. 2020 Feb 19 [cited 2021 Jun 7]; Available from: /articles/preprint/A_Single_and_Two-Stage_Closed-Tube_Molecular_Test_for_the_2019_Novel_Coronavirus_COVID-19_at_Home_Clinic_and_Points_of_Entry/11860137/1

187. Dao Thi VL, Herbst K, Boerner K, Meurer M, Kremer LPM, Kirrmaier D, et al. A colorimetric RT-LAMP assay and LAMP-sequencing for detecting SARS-CoV-2 RNA in clinical samples. Sci Transl Med [Internet]. 2020 Aug 12 [cited 2021 Jun 7];12(556):7075. Available from: http://stm.sciencemag.org/

188. Kim J, Park BG, Lim DH, Jang WS, Nam J, Mihn DCC, et al. Development and evaluation of a multiplex loop-mediated isothermal amplification (LAMP) assay for differentiation of Mycobacterium tuberculosis and non-tuberculosis mycobacterium in

clinical samples. PLoS One [Internet]. 2021 Jan 1 [cited 2021 Jun 7];16(1 January). Available from: /pmc/articles/PMC7787462/

189. Zhong LL, Zhou Q, Tan CY, Roberts AP, El-Sayed Ahmed MAEG, Chen G, et al. Multiplex loop-mediated isothermal amplification (Multi-LAMP) assay for rapid detection of mcr-1 to mcr-5 in colistin-resistant bacteria. Infect Drug Resist [Internet]. 2019 [cited 2021 Jun 7];12:1877–87. Available from: /pmc/articles/PMC6613457/

190. Higgins O, Clancy E, Cormican M, Boo TW, Cunney R, Smith TJ. Evaluation of an internally controlled multiplex Tth endonuclease cleavage loop-mediated isothermal amplification (TEC-LAMP) assay for the detection of bacterial meningitis pathogens. Int J Mol Sci [Internet]. 2018 Feb 9 [cited 2021 Jun 7];19(2):524. Available from: www.mdpi.com/journal/ijms

CHAPTER TWO

Select portions of this chapter was generated in collaboration with Clemson University undergraduate and master student: Madison Stiglich and Mark Livingstone, respectively. Some results in this chapter have been published in *NanoBioscience* and *Micromachines* 2019.

THE FABRICATION OF SOLUTION BLOW SPUN CONDUCTIVE AND ANTIMICROBIAL NANOFIBER MATS

2.1 Introduction

The use of nonwoven nanofiber mats provides a pathway to develop low-cost conductive and antimicrobial nanofibers for biosensing and therapeutic applications. Nanofiber textile production has gained more interest in the past two decades compared to large diameter fiber textiles. (1–5) The reduction of fibers from a micron to a nanoscale dramatically increases the surface area to volume ratio, improves thermal acoustic insulation, increases water and lipid holding capacity, and modifies texture and appearance. (6–8) nanofibers have shown great promise for use as tissue scaffolds, controlled release of drugs, and as a primary contact layer for wound dressings. (6,9–11) There are several techniques used to generate nanoscale fibers. Many of the techniques are derived from one another. Nonwoven is a sheet or mesh of fibers that are connected by physical entanglements without the use of knitting. Melt spinning, melt blow spinning, electrospinning, wet spinning, and solution blow spinning are commonly used methods used to generate nonwovens.

Non-woven nanofibers have various uses in many biomedical applications to include tissue engineering, wound dressings, drug delivery systems, and cell scaffolds. Most biomedical applications utilize nanofibers that are biocompatible and biodegradable. PLA is a biodegradable, bioabsorbable, biocompatible, thermoplastic polymer that is widely used in various biomedical applications ranging from tissue engineering scaffolds to biomolecular sensing device fabrication. (12,13) PLA belongs to the aliphatic polyester family made from α-hydroxy acids. Additionally,

the lactic acid known as 2-hydroxypropanoic acid can be produced by the fermentation of sugars from renewable resources through *Lactobacillus spp.* PLA has found uses in various applications to include medical, packaging, drug delivery systems, and the textile industry. Textiles to include dressings are made via melt spinning, electrospinning, or through the emerging solution blow spinning method (SBS).

Solution blow spinning is a fairly new technique first used in 2009 to produce nonwoven nanofiber composites (1) SBS is a fiber fabrication technique that utilizes pressurized inert gas to evaporate a volatile solvent from a polymer-solvent solution. This method creates in situ fibers on planar and non-planar substrates with a very inexpensive setup. SBS fiber mats have demonstrated similar mechanical properties as fibrin (1–10 MPa) or human skin (0.1–1 MPa). (2) This technology utilizes key elements from electrospinning and melt blow spinning techniques to make *in situ* nonwoven nanofibers. Solution blow spinning creates nanofibers by the incorporation of a polymer dissolved within a volatile solvent. Two concentric fluid streams allow the flow of a polymer solution and compressed gas. Pressurized gas flows around the solution, creating fibers by stretching a polymer jet in the direction of air flow onto any substrate. The setup can is highly versatile and can be used in as a portable device or on a larger commercial scale. Solution blow spinning can deposit nanofibers on both planar and nonplanar substrates. The technique has tremendous potential for use in an array of applications to include wound healing. However, this technique has not been greatly exploited to generate substrates for point-of-care chronic infection biosensors. (2) SBS nanofibers mats have been shown to have similar mechanical strength as fibrin (1–10 MPa) or human skin (0.1–1 MPa). Polymeric dressings are the common material used in the management of chronic wounds and may contain natural or synthetic polymers, like cellulose or PLA, respectively. PLA is a hydrophobic, bioabsorbable, biocompatible, thermoplastic polymer

that is used in an array of biomedical applications from scaffolds to biomolecular device fabrication. (14) Wound dressings that incorporates novel therapeutics decreases the bacterial load and facilitates proper healing. (15) Elemental silver and cerium nanoparticles can act as an antimicrobial and antioxidative agent. Silver ions are cytotoxic to bacteria cells through the blocking of the respiration process. (16) Ceria nanoparticles have the ability to attach to reactive oxygen species (ROS) and in order to reduce oxidative stress. (17) Solution blow spinning can also be used to support conductive filler material to create a conductive fiber mat. Commonly used materials are Ag and carbon.

Conductive nanofibers can be produced with both MWCNT and/or Ag. Carbon is a tetravalent element that forms the key bonds in all organic and living organisms. Many of these compounds and organisms form carbon-carbon bonds also called covalent bonds that are identified as the strongest bonds between one or two atoms. Diamond, amorphous carbon and graphene are the most abundant type of allotropes of carbon. Graphene is the 2-D allotrope of carbon (hexagonal lattice) and makes up the structure of CNTs. (18) Graphene has four bonds: three σ bonds and one π bond. The structure also has a tightly packed ensemble of atoms that give rise to a sp2 hybridization. Each atom's π bond is unpaired which allows the flow of free electrons throughout the entire structure. CNTs mechanical and electrical properties all depend on its physical structure. Single-walled carbon nanotubes (SWCNTs) are the simplest form of CNTs as they are one-layer of rolled up graphene (diameter = 1 nm); Multi-walled carbon nanotubes (MWCNTs) consist of multiple layers of SWCNT cylinders. (19) Figure 2.1 is a depiction of both SWCNTs and MWCNTs. Electron mobility depends on nanotube's diameter, helicity angle and indices. CNTs can exhibit metallic and semiconducting behavior where the Eg = 0.8 eV/diameter. Figure 2.2 shows an illustration of the chiral configuration among CNTs. The image can be adopted for a

MWCNT configuration, but with a multilayered configuration of SWCNT. There are three different orientations: 1) Armchair, 2) zigzag, and 3) chiral. Zigzag and chiral are mainly semiconducting, modifications to diameter and indices could cause them to be metallic like. Armchair nanotubes always behave like a metal conductor. Synthesis of SWCNTs and MWCNTs are done via arc discharge, laser ablation, or chemical vapor deposition. Where arc discharge is the simplest and inexpensive. Laser ablation generates the highest yield but is the most expensive. Chemical vapor deposition is the most commonly used and are used to generate aligned carbon nanotubes. (20)

Figure 2.1. 3D image of SWCNT (left) and MWCNT (right) (20)

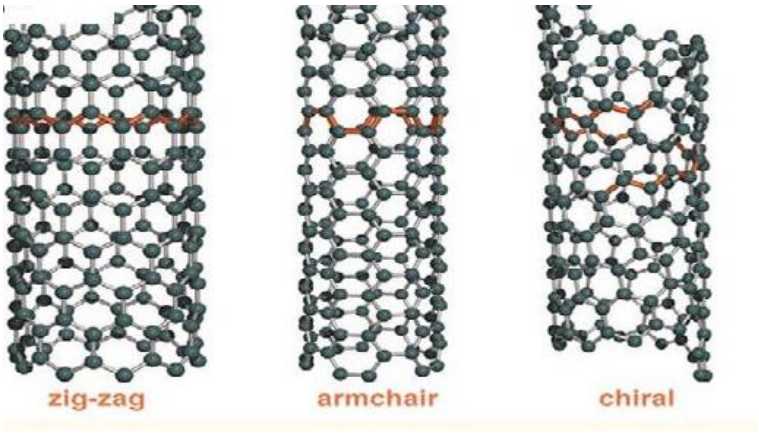

Figure 2.2. Chirality of SWCNT. (20)

Elemental silver has found many applications other than conductive material such as jewelry, hand tools, currency, and as antibacterial agents for many different applications. Silver has been used for many decades as a disinfectant material for medical applications such as surgical tools for routine operations. Since the early years of medicine, silver-based material was used for the storage of water and wine because it was thought that the element would serve as a preservative over a period of time. Additionally, the great philosopher, Hippocrates acknowledged that silver residue has a strong potential application for wound healing and for the treatment of ulcers. The silver salt, silver nitrate, was used as a therapeutic for ulcer treatment in the 17^{th} and 18^{th} centuries. The antimicrobial activity of silver was established during the 19^{th} century. However, similar to the use of bacteriophages, the discovery and development of antibiotics in the 1940s. Currently, silver and its salts are still used as antimicrobial materials for various biomedical applications to include burn treatment. (21)

There are many ways to fabricate elemental silver or silver nanoparticles via chemical synthesis. Some ancient examples include the bronze Lycurgus cup from the 9^{th} century and the metallic luster from the 15^{th} century. (21) Majority of silver nanoparticle synthesis is done via wet chemical procedure using either the Lee-Meisel or Creighton method. The Lee-Meisel method utilizes $AgNO_3$ as a precursor and sodium citrate as the reducing agent. This method generates silver nanoparticles of various sizes and has a broader size distribution. (22) Currently, the most common silver nanoparticle synthesis method is the Creighton method. This method consists of the use of $AgNO_3$ as a precursor and $NaBH_4$ as the reducing agent. This method can generate silver nanoparticles of various sizes and has a narrower size distribution. (23) The reduction of silver salts can produce uncontrollable silver growth. The presence of stabilizing agents such as polymers can protect nanoparticles from the environment and also precent agglomeration. (21) Figure 2.3

is an illustration for the wet chemical reduction of $AgNO_3$ to produce silver nanoparticles through nucleation and growth. Silver nanoparticle synthesis can also be completed via vapor reduction method by utilizing the vapor of a strong reducing agent to generate silver nanoparticles in a dry reduction procedure.

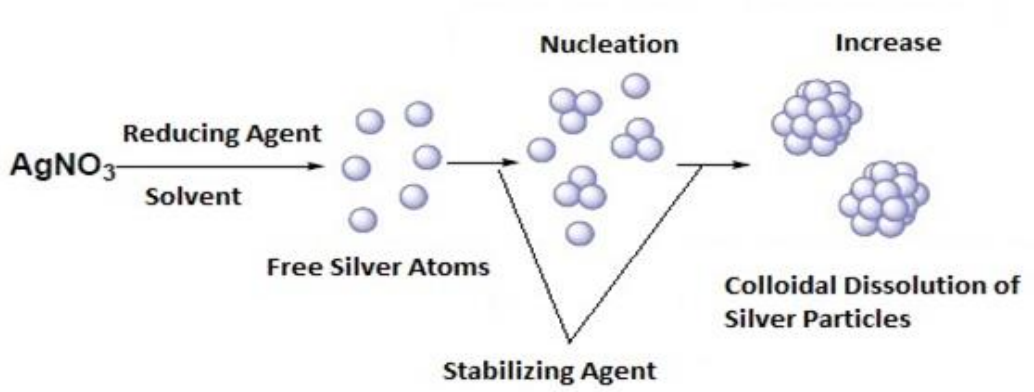

Figure 2.3. Silver nanoparticle formation via chemical reduction of $AgNO_3$ salt. Figure reproduced from (24).

As stated earlier, the antimicrobial properties of silver have been established since the 19th century. This antibacterial affect can be seen at relatively low concentrations. Elemental silver ions possess a positive charge that has a high affinity towards proteins, DNA and RNA molecules, which can interfere bacterial metabolic processes. The mechanism of the silver nanoparticle bactericidal effect was studied by Morones et al. by scanning electron microscopy. (25) There is a very strong bactericidal effect with smaller nanoparticles (1-10 nm) against several pathogens such as *Escherichia coli*, *Staphylococcus aureus* and *Listeria monocytogenes*. The attachment of the nanoparticles to the cell membrane blocked permeability which affects the function of membrane-bound proteins. Silver nanoparticles were also shown to have bactericidal properties towards methicillin-resistant *S. aureus* (MRSA) microorganism. Additionally, silver nanoparticles can release Ag ions and possess similar bactericidal mechanisms as elemental silver ions. Silver

nanoparticle size determines the antibacterial potential. Smaller nanoparticles have shown to have a much greater bactericidal effect and a much lower cytotoxicity effect. (21)

Chronic wounds are often sites of excessive bacterial colonization, leading to infection, delayed healing, amputation, and/or mortality (26). *Staphylococcus aureus*, *Enterococcus faecalis*, *Pseudomonas aeruginosa* are common pathogens found in non-healing wounds, where concentrations above 10^5 colony forming units (CFU)/ gram (g) have the potential to impede the healing process (27) Commonly, bacteria seek to invade the epidermis layer and excrete toxins and virulence factors into the bloodstream. Most of these organisms produce biofilms, a community of bacteria highly resistant to common treatment therapies. Biofilms become resistant through a phenomenon called quorum sensing. This communication system modifies gene expression via cell-to-cell communication among neighboring bacteria cells. These sensing systems are regulated by a set of molecules called autoinducers (AIs) or autoinducer peptides (AIPs) whose concentration is a function of cell population density (27,28). Bioluminescence, virulence factors, sporulation, and biofilm formation depend on the upregulation of AIs. These toxins have the potential to cause problems such as tissue damage, abscess, cellulites, osteomyelitis, or amputation (29). This requires clinicians to find ways to prevent the onset of infection (30). *Psuedomonas putida (P. putida)* is a part of the pseudomonas fluorescens species and is a Gram-negative, rod-shaped bacterium (30). Under UV light, it fluoresces a yellow green dye called pyoverdine (30,31). *P. putida* prefers a moist environment; w*ounds* with high exudate levels provide the environment for colonization (30). This microorganism is a common nosocomial agent found on medical devices, implants, and mucous membranes of patients (30). Hence, amputees, or patients with stents, pacemaker, etc. are at a higher risk. In the past, *P. putida* was thought to be nonpathogenic in Homo Sapiens, but it has been recognized as a cause for true

infection over the past few decades (30). In this study, *P. putida* is used to test analyze the use of solution blow spun nanofiber mats as a transducer for impedance sensing.

There is a need to quantify wound infection status and fabrication of technology that would enable in situ detection of bacterial load. Early detection would allow clinicians to treat infections in its earlier stages and avoid antimicrobial resistance to empirical antibiotics (15). Impedance based technology provides quantifiable information by the application of an alternating input signal and measurement of the system responding magnitude and phase angle. Previously, bioimpedance has been deployed to assess wound status in human and animal subjects (32,33). Monitoring of cell number, viability and metabolic activity have all been monitored via impedance response (34–36). Impedance microbiology is a technique that correlates resistance and reactance values to biological phenomena. Resistance is proportional to the ionic concentration of the extracellular fluid at the electrode surface, while reactance correlates to cell mass and is a good indicator of cell proliferation at the electrode surface (34–36). For this study we define the complex impedance is expressed in polar form as seen in Equation (1).

$$Complex\ Impedance\ (Z) = |Z|e^{j\Theta} \qquad (1)$$

Where |Z| is the magnitude and Θ is the phase angle of the complex impedance. Figure 1 gives a mathematical representation of impedance and the equivalent circuit of the sensing area. Where C_{dl} is the double layer capacitance that is determined by the capacitance of the cell membrane. R_{sol} is the solution resistance. Thus, impedance biosensors could quantify cell proliferation by calculating the equivalent impedance of the wound environment. Wearable sensor modalities should be flexible, adequately conform to wound geometry and limit shear stress induced at the wound surface.

$$\text{Magnitude} = \sqrt{{R_{sol}}^2 + {X_c}^2}$$

$$Phase\ Angle = \tan^{-1}\frac{X_c}{R_{sol}}$$

$$X_c = \frac{1}{J\omega Cdl}$$

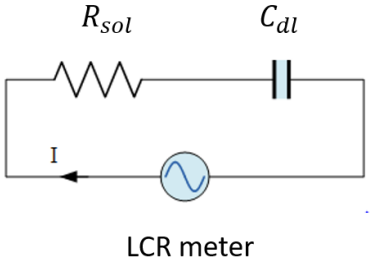

Figure 2.4. Schematic Diagram of impedance microbiology theory.

In this chapter, we first used PLA and multi-walled Carbon nanotubes (MWCNT) to generate nanoscale fibers that overlap to create reliably conductive fiber mats via SBS. We conducted a characterization study based on the parameters associated with SBS and the concentration of PLA in conjunction with MWCNT.

In a second study we utilized silver and ceria nanoparticles to examine the antimicrobial efficacy against *Pseudomonas aeruginosa* and the antioxidative efficacy against its respective toxin, pyocyanin. PLA, PLA/Silver nanoparticles (AgNPs), PLA/Ceria nanoparticles (CNPs), and PLA/AgNPs/CNPs nanofiber composites were fabricated via SBS. The protocol employed allows for in situ nanofiber fabrication, silver nanoparticle nucleation and growth, and ceria integration in the fiber composites. Silver nitrate was incorporated into the solution and the SBS nanofiber mats were reduced with ethylene glycol vapor to generate antimicrobial elemental silver. Cerium nitrate salt was also incorporated in the solution to generate antioxidative SBS nanofiber mats. Nanofiber mats were characterized for geometry and elemental composition via SEM, tensile strength, and surface tension. Antimicrobial efficacy was assessed with a three-day optical density and biofilm production assay. Antioxidative efficacy was assessed by measuring pyocyanin reduction using electrochemical detection with a commercial electrochemical electrode and potentiostat.

To examine the potential of impedance and conductive nanofibers, we used impedance to detect the presence and concentration of *P. putida in vitro* via a label-free, antibody-free method using poly-l-lactide (PLA):Multi-walled Carbon Nanotube-Solution Blow Spun-Printed Circuit Board (PLA:MWCNT-SBS-PCB) transducers. The frequency used for all measurements was 200 Hz and kept at a constant value during testing cycles. 24-hour real-time impedance measurements were taken on bacteria culture with an initial concentration ranging from 10^3-10^7 CFU/mL to examine any changes in impedance values. A calibration curve was constructed to display bacterial concentration as a function of the change in the magnitude and phase angle values. Instantaneous testing was done on culture media to examine the feasibility of rapid bacteria detection with PLA:MWCNT-SBS-PCB transducers. PPLA:MWCNT-SBS-PCB transducers were able to rapidly quantify planktonic bacterial load through the measurement of impedance magnitude and phase angle over a one-minute testing cycle. Impedance based bacterial sensing has been utilized in the past to identify and quantify bacterial load (37–43). However, none has included the use of conductive nonwoven nanofibers as the main transduction component, which have the potential for customizable shape and size for *in situ* incorporation. Other studies utilize fabrication techniques that would render the use of impedance sensing in a clinical setting too expensive, such as photolithography. PLA:MWCNT-SBS-PCB transducers are less expensive than such methods and are produced in significantly less time. This fabrication technique could be incorporated into a wound dressing or on a wearable sensor substrate by solution blow spinning a layer onto the substrate directly. The fibers act as the transducer themselves due to the porosity of the fiber mat which enables the detection of the impedance change as bacteria and other cells interact and alter the fiber orientation. The first portion of this work focused on the development of a solution blow spinning apparatus capable of producing nanofibers of varying polymer loading. SBS parameters

were varied to characterize the conditions that produced the more superior nanofiber construct, electrically. Results from this study give implications into the successful development of conductive nanofibers for impedance-based sensing.

Research questions:

1. To what extent does changing SBS parameters affect overall conductivity of scaffolds as reported by 4-point probe measurements?
2. How does multi-walled carbon nanotube/PLA SBS nanofiber composite affect silver ion release and antimicrobial efficacy?
3. To what extent does SBS nanofiber mats allow for monitoring the growth and detection of bacterial load?

2.2 Materials and Methods

2.2A Solution blow spun nanofiber preparation

Polymer solutions were made by dissolving PLA pellets (Mn = 75,000 g/mol, Jam Plast Inc., Ellisville, MO, USA) into the desired solvent, being Chloroform ($CHCl_3$ CAS 67-66-3, Sigma Aldrich, St. Louis, MO, USA) or Dichloromethane (CH_2Cl_2 CAS 75-09-2, Sigma Aldrich) to generate final concentrations. After which the solution was vigorously stirred until complete dissolution of pellets. The inclusion of MWCNT (CAS 308068-56-6, Sigma Aldrich) to the prepared solution was added as a (w/w %) of PLA. Afterwards, the solution was sonicated for 5–10 minutes to encourage nanotube dispersion. The SBS apparatus used in this work was built in-house using a Paasche flow pencil (Paasche Airbrush, Chicago, IL 600634 USA), compressed nitrogen (N_2) gas, stepper-motor driven collector spool, and an Arduino for control. The diameter of the nozzle flow pencil was 1.06 mm. The pencil was connected to a compressed nitrogen tank gas regulator and a syringe pump. The flow pen was kept at a constant working distance of 21 cm

from the collector spool. Figure 2.5 shows the SBS system setup. As the system began, nitrogen gas flowed through the concentric nozzle of the flow pen and the solution was pumped by the syringe pump through a second nozzle in the flow pen. The solution was then blown towards the rotating collector surface by the pressurized gas forcing solvent evaporation.

2.2B MWCNT-Silver nanoparticle SBS fabrication

Fibers were made from solutions containing PLA and Chloroform using a feed rate of 100/hr., air pressure of 30 psi and deposited on glass slides fixated on a rotating collector drum. The fiber matrix containing MWCNT, and PLA only were then used as a stabilizing matrix for in situ silver nanoparticle nucleation. Due to hydrophobic nature of nonwoven PLA samples, ethanol solution was used to introduce OH- groups to surface. A previously prepared solution of $AgNO_3$, Deionized water and ethanol was dropped on the mesh vie dropwise. Elemental silver was grown by reducing the solution with a solution of sodium borohydrate ($NaBH_4$), deionized water (50% v/v), and ethanol (50% v/v). The molarity ratio between $AgNO_3$ and $NaBH_4$ was 4/1. The reduced fiber mat was then rinsed with DI water and dried for future tests. For vapor synthesis, Silver nitrate and cerium (III) nitrate hexahydrate (Sigma Aldrich, St. Louis, MO, USA) was dissolved in DI water and added to chloroform-PLA solution. After which the solution was vigorously stirred for 4 hours. Then the solution was sonicated for 5–10 minutes to encourage solution homogeneity. Fibers were generated using a flow rate of 100mL/hr at 30 psi for 30 min. silver and cerium nanoparticle nucleation was done via ethylene glycol vapor at 125 C for 20 min. Fibers containing cerium nanoparticles were submerged in hydrogen peroxide for 30 min to obtain more ceria nanoparticles in the 3+ oxidation state.

2.2C MWCNT-SBS-PCB board fabrication

Fiber mats were fabricated via solution blow spinning conductive solutions onto 10 cm x 25 cm printed circuit boards (PCBs). PCB boards were made by printing a positive mask on PCB sheets. Sheets were melted on PCB surface. Next, boards were submerged in a fresh solution of 1:1 ratio of white vinegar and hydrogen peroxide. Table salt was then added to solution as needed. Fibers were generated using a 115 mL/hr flow rate at a pressure of 30 psi. In order to use MWCNT-SBS-printed circuit boards (PCBs) as the main transducer in an impedance study, linearity between current and voltage is important.

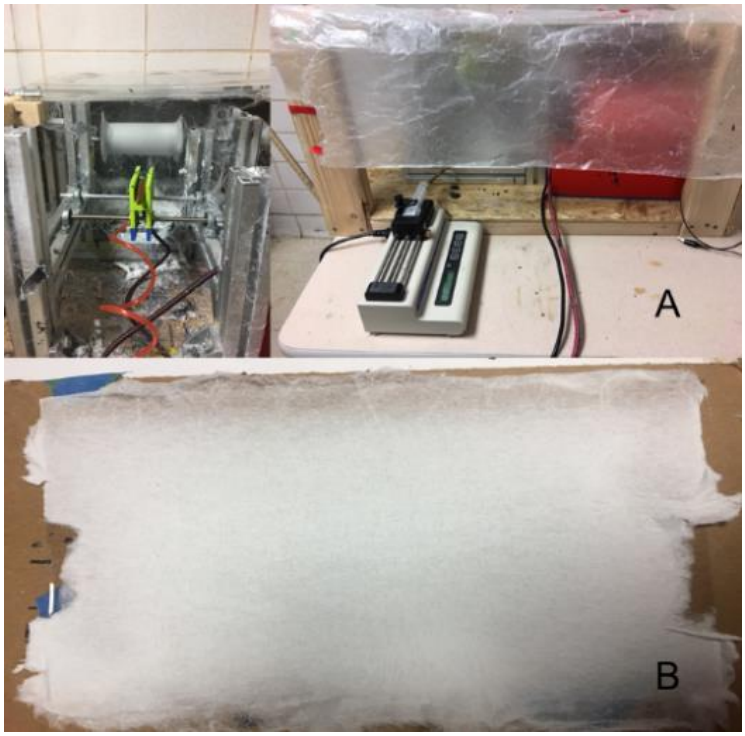

Figure 2.5. Setup (A) Solution blow spinning apparatus (B) SBS PLA nanofiber mat (12% w/v)

2.2D Morphological Characteristics & Surface Composition

S3400N variable pressure scanning electron microscope was used to examine nanofiber morphology. Fibers deposited on aluminum foil or polyethylene glycol sheets were cut to

approximately 5x5 mm. Samples were anchored to mount specimen holder using double sided carbon tape. All samples were subjected to a 5 min platinum coating procedure to provide a conductive coating for imaging. Average diameter and cross-sectional size were measured. Images captured were analyzed by Aztec (Oxford Instruments, Concord, MA, USA) to determine the intensity of silver and cerium elements within each sample. Surface composition of fibers were determined using a S3400N variable pressure SEM to measure the amount of elemental Silver, Carbon and/or Ceria contained in each sample. The images captured were analyzed by Aztec (Oxford Instruments, Concord, MA, USA) to determine the intensity of elements within each sample. Silver ion release was assessed on an inductively coupled plasma-optical emission spectrometer (Spectro Arcos ICP-OES; Spectro Analytical Instruments a division of Ametek Kleve, Germany) equipped with a UV-Plus Purifier gas cleaning system with argon gas flow and a Cetac autosampler. The instrument was calibrated using commercially available ICP standard solutions (from Inorganic Ventures) between each use. A check standard was analyzed along with samples to ensure calibration. For sample prep, 500mg of sample was placed in a 50 mL digestion tube. 1x5 mL of HNO_3 was added to tubes. Samples were digested on heating block at 125C, while adding 3 mL of 30 H_2O_2. After cooling, samples were then diluted with 50mL of DI water and shaken. Aliquots were placed in a test tube for elemental analysis.

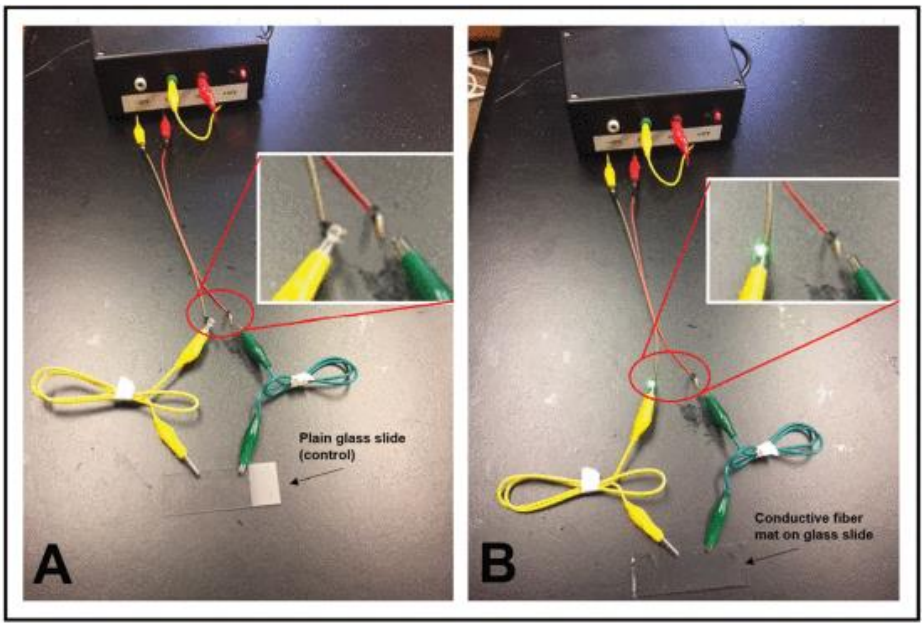

Figure 2.6. LED circuit with glass slide (A) and with conductive fiber mat (8%/10% PLA/MWCNT) deposited on glass slide (B).

2.2E Surface Contact Angle

Contact angle of water on each sample was measured using a Krüss Easy Drop (Krüss, Hamburg, Germany) that was equipped with a Model camera. Samples were prepared on a glass slide and a constant 2 or 4 μL deionized water was dropped onto the surface of fibers through a glass syringe. Sessile drop method was used to determine the shape of water on the surface and to calculate angles between the water and fiber surface. Angle measurements were calculated using the tangent two (t2) method in DSA-1 software (Krüss). Measurements were completed at 25°C with a relative humidity of 53%.

2.2F Tensile Testing

Tensile Testing: Instron (Instron, Norwood, MA, USA) testing system, equipped with a 50 N load cell was used to measure the mechanical properties of each sample. Test strips of 10 mm by 25 mm, according to the ASTM D 5035. An extension rate of 10 mm/min was used, and the Bluehill analysis software (Instron) was used to measure the tensile stress (Pa).

2.2G Cell Culture procedure

Pseudomonas aeruginosa (PAO1) was cultured in lysogeny broth overnight at 37 C. Antimicrobial efficacy was assessed by transferring an aliquot of culture media (1mL) to a 12 well plate. 1 x 1.5 mm of each sample was placed in a culture well. The optical density value was measured with Nano Drop 600 spectrometer over 3 days. Disc Diffusion method was employed to assess antimicrobial activity. The distance between fiber samples and bacterial growth was measured after a 24-hour growth cycle. The greater the distance is an indication of fiber mat antimicrobial efficacy. Antioxidative efficacy was measured by analyzing the reduction of 50 mM of pyocyanin via square wave voltammetry.

2.2H Impedance and electrical measurements

Conductivity of PLA fibers with added MWCNT was measured using a 4-point probe system, current source, and digital multimeter. Samples prepared on a glass slide were used to detect the degree of conductivity at 3 different locations. Voltage ranging from 1–2mV was applied across the sample and the current was measured to determine resistivity in the formula below. The conductivity was derived from the inverse of the result of equation (2):

$$\rho = VI \times C.F.1 \times C.F.2 \times t \quad (2)$$

Where, t (cm) is the thickness of mat, V (V) is the voltage applied, I (A) is the change in current and $C.F._1$ and $C.F._2$ are correction factors which were 4.3947 and 1, respectively. A custom 2-point probe system was used to measure the I-V curves of ten different transducers. The applied voltage ranged from -500mV to 500mV and the induced current was measured. The average resistance of the PCBs was 220 ± 16 Ω (n=5). All 10 boards tested showed a linear dependence between the applied voltage and the measured current. Given the importance of an accurate initial resistance, consistently generating large numbers of fiber mat-coated boards proved to be difficult. Out of 50

boards, roughly 30 fell into the above range. In order to test the use of MWCNT-SBS-PCBs as the main transducer, only fiber mats falling in the above range were used to start testing. Figure 2.7 shows a graphical representation of the test setup used to continuously detect the presence of bacteria in vitro. A parallel connection between three petri dishes was made in order to test multiple samples under the same condition. 10x25cm MWCNT-SBS-PCB transducers were placed flat in the petri dishes and a connection was made through the top of the petri dishes, on the backside of the boards to the LCR meter. This setup provided consistent impedance sensing results with minimal drift current, while maintaining conditions commonly used to culture microbial and mammalian cells. For instantaneous testing, one transducer was placed in a beaker and 2 mL of bacterial culture was added to assess concentration levels. Data from the instantaneous test was graphed vs. its starting concentration. Impedance of the bacterial pathogen cultured on petri dishes was measured using a 1V sine wave at 200 Hz. 200 Hz was found to be the most sensitive and gave a greater change in impedance than higher frequencies. Re-calibration of the LCR meter and new fiber mat transducers were used in each testing cycle. All measurements were performed at room temperature under a custom-made enclosure to ensure minimal media evaporation. Cycle duration was set to 10 points per minute to allow continuous 24-hour monitoring. The 24-hour test is a simulation of a real-time point-of-care (POC) diagnostic approach that could be used to monitor wound progression at home. Instantaneous, one-minute testing cycle was done using one transducer in a beaker with 2 mL of culture media to assess the response time of transducers.

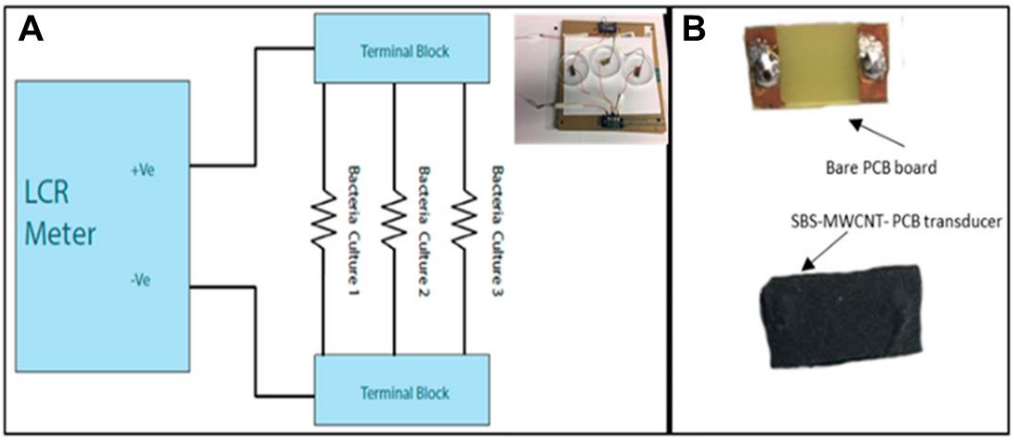

Figure 2.7. A) Equivalent circuit of Impedance Test Circuit. B) Front view of PCB board and SBS-PCB transducer.

2.2I Modified SBS mask method

A mask transfer method was used to deposit carbon over PCB board with a modified design. Briefly, desired design was created in solid works and made on PCB board as previously discussed. The same design was used as a template to laser cut an acrylic plastic mask. Acrylic mask was then placed over PCB boards with a glass slide spacer. An I&J printer was used as a holder for SBS airbrush in order to deposit PLA/MWCNT over PCB pattern.

2.3 Results and Discussion

Conductive MWCNT SBS nanofibers

Figure 2.8 shows SEM images of SBS PLA/MWCNT nanocomposite fibers fabricated with 8% w/v of PLA and 10% w/w MWCNT. Fibers formed with Dichloromethane produced thicker fibers than the Chloroform group. This could be due to the observation that Dichloromethane has a higher surface tension than that of Chloroform. With respect to fibers spun in Chloroform, these data showed a smaller overall fiber diameter that became increasingly uniform across all samples with the addition of increasing concentrations of MWCNT.

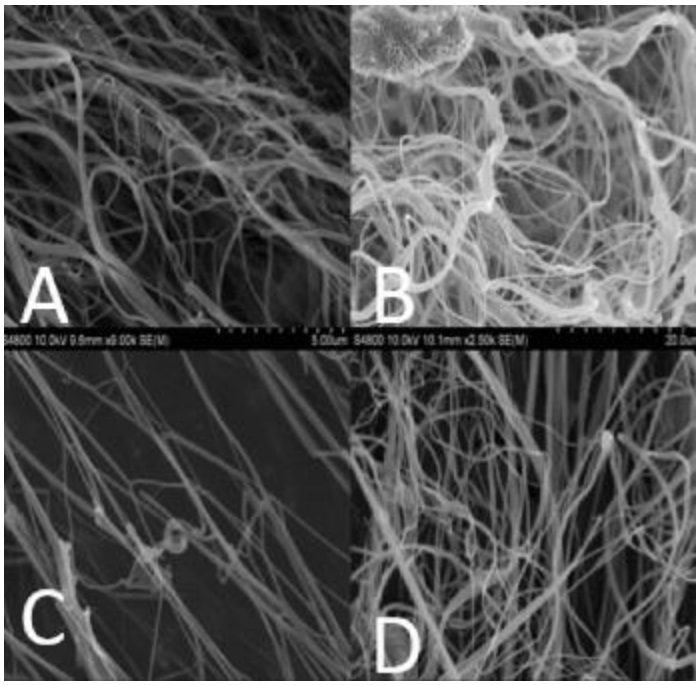

Figure 2.8. SEM of PLA and PLA/MWCNT composite nanofibers via SBS. All samples shown above were made using 50psi and 388 mL/min. A) 8% PLA(CHL), avg. diameter of 167.39 ± 42.77. B) 8% PLA(DCM), avg. diameter of 562.60 ± 295.14. C) 8% PLA with 10% MWCNT (CHL), avg. diameter of 158.40 ± 80.93. D) 8% PLA with 10% MWCNT (DCM), avg. diameter of 444.65 ± 140.78.

Addition of filler content also created smoother fibers with a decrease in the amount of corpuscular shaped bodies. Minimum and maximum diameters were 74.25 ± 42.71 and 781.12 ± 337.1 nm, respectively. Where, 4% PLA with 20% MWCNT produced the smallest diameter size where we hypothesized that fiber diameter would have a positive correlation with polymer concentration. This is a result of using higher MWCNT content with a lower PLA concentration. As can be seen in Figure 2.9, fiber diameter increased with increasing polymer concentration compared to the Chloroform group (α=0.05) using ANOVA and LSD method. With the exception to the 4% Chloroform and 4% Dichloromethane groups, which showed no significant difference in average diameter values.

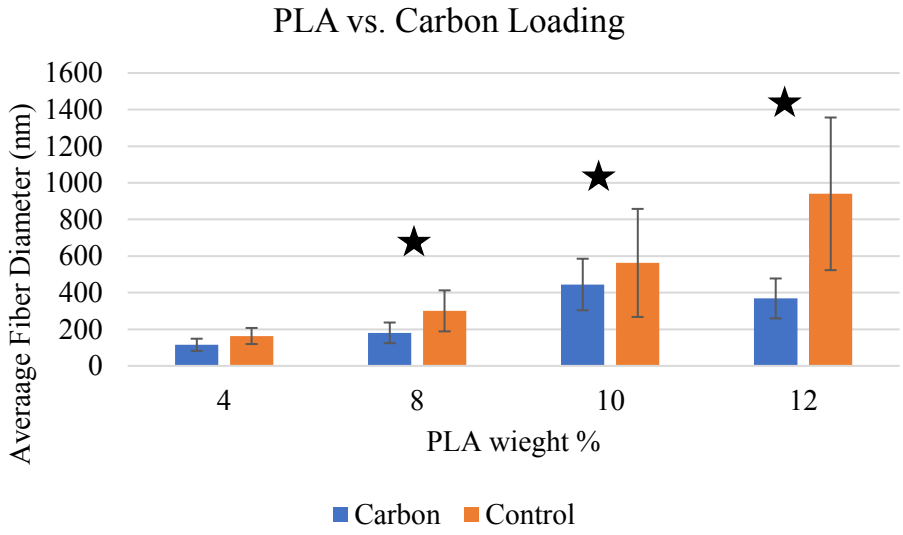

Figure 2.9 Average fiber diameter of MWCNT loaded PLA fiber mats.

Surface Composition data was used to verify the extent of carbon wt.% in each sample. As expected, the addition of MWCNT content significantly increased the average carbon content in the nanofiber mats. As seen in Figure 2.10, the Chloroform group displayed an increase in carbon content with increasing MWCNT. However, the Dichloromethane group (data not shown) did not display this same response. There was no significant difference when MWCNT content was added. This could be a result of poor nanotube dispersion within the polymer solution. As a result, Chloroform was used as the solvent of choice for further fabrication and analysis of conductive nanofiber mats.

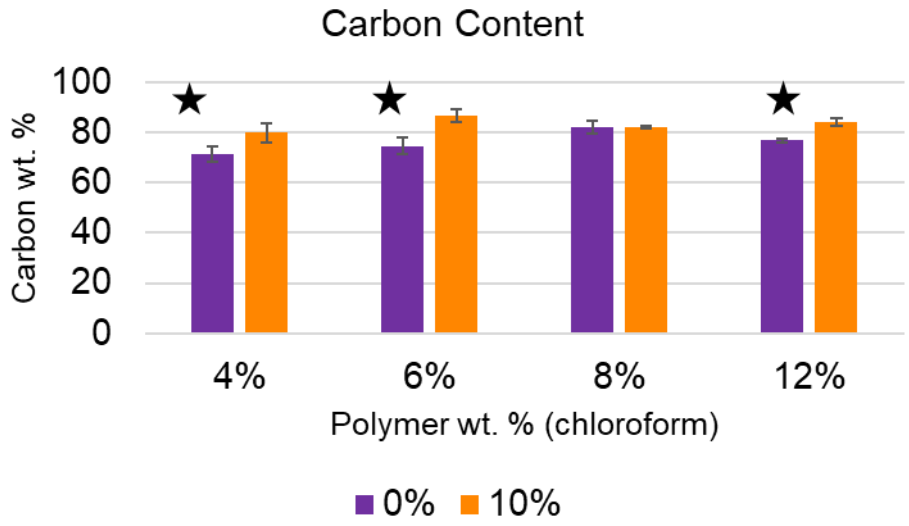

Figure 2.10 Carbon content of Fiber mesh with increasing polymer concentration and addition of 10% MWCNT.

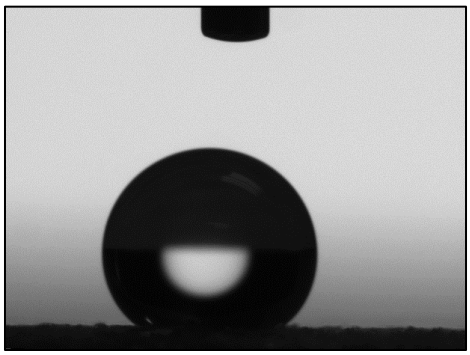

Figure 2.11 Contact angle sessile test on 8% w/v PLA with 10% MWCNT contact. Measured angle was 133.1 and 132 on the left and right liquid-fiber surface, respectively

Contact angle is important as it shows the extent of hydrophilicity of the nanofiber mat. This is of utmost importance when it comes to immobilization of proteins and cell adhesion. Fibers made from 4%/10% - PLA/MWCNT using Chloroform were highly porous due to the decrease in fiber cross over. Further addition of MWCNT (15, 20, 25%) in the 4% group increased the hydrophobicity. Increasing nanotube concentration in the 6 and 12% yielded an increase in hydrophilicity when 10% MWCNT was added to both solvent groups. However, contact angles

for 8%/10% PLA/MWCNT increased for both solvent groups when compared to the 8% w/v PLA control group. Figure 2.11 shows a water contact angle test on 8% w/v PLA and 10% w/w MWCNT content.

Further work was done to examine the use of MWCNT with and without added filler material. Silver (Ag) was chosen due to its ease of immobilization and integration in textile material. Also, the conductivity of elemental silver is much higher than that of carbon. The first study examined the use of a wet chemical synthesis of silver on the surface of SBS nanofiber mats. This method is similar to the physical adsorption method for the immobilization of common biological agents. $AgNO_3$ was used as a precursor for salt nucleation between 0 – 640 mM. A solution of silver nitrate ($AgNO_3$), deionized water, and ethanol were added dropwise to the fiber mat. $AgNO_3$ was reduced with a solution containing sodium borohydride, deionized water, and ethanol via dropwise. The reduction of $AgNO_3$ is shown in equation (3).

$$AgNO_3 + NaBH_4 \rightarrow Ag + \frac{1}{2}H_2 + \frac{1}{2}B_2H_6 + NaNO_3 \qquad (3)$$

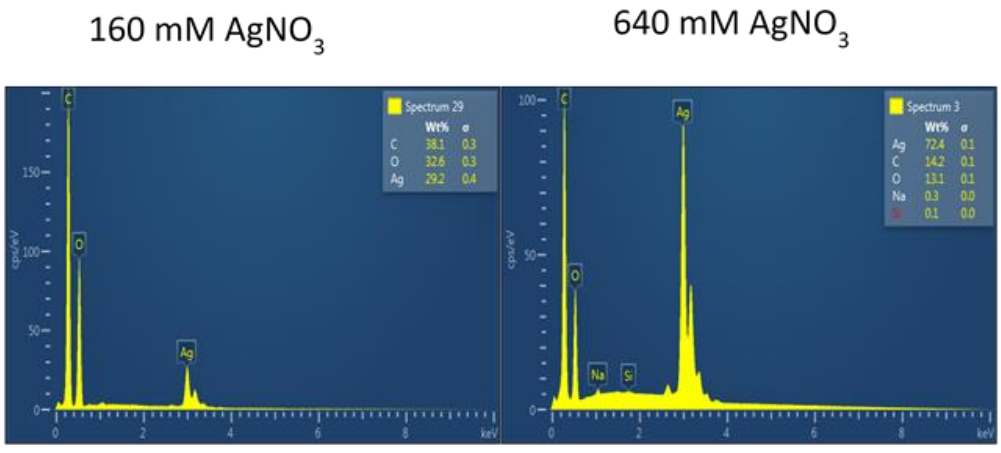

Figure 12. Energy Dispersive Spectroscopy (EDS) analysis on 160mM and 640 mM $AgNO_3$ groups

SBS fiber mats were successfully infused with silver. Similar to the incorporation of MWCNT, the addition of AgNO3 increased the conductivity, exponentially. There was a percolation threshold at approximately 300 mM of $AgNO_3$ where additionally Ag loading significantly increased conduction of fiber mats. SBS PLA:Ag nanofibers with 2.5 M of AgNO3 had a conductivity of 3,800 S/cm. Energy dispersive spectroscopy was used to detect Ag loading in PLA mesh. As seen in Figure 2.12, additional $AgNO_3$ loading increased the energy peak corresponding to elemental Ag. The incorporation of carbon loading with Ag was also examined between 0-640 mM of $AgNO_3$. As seen in Figure 2.13, carbon loading increased the conductivity of fiber mats with a similar percolation response at approximately 300 mM.

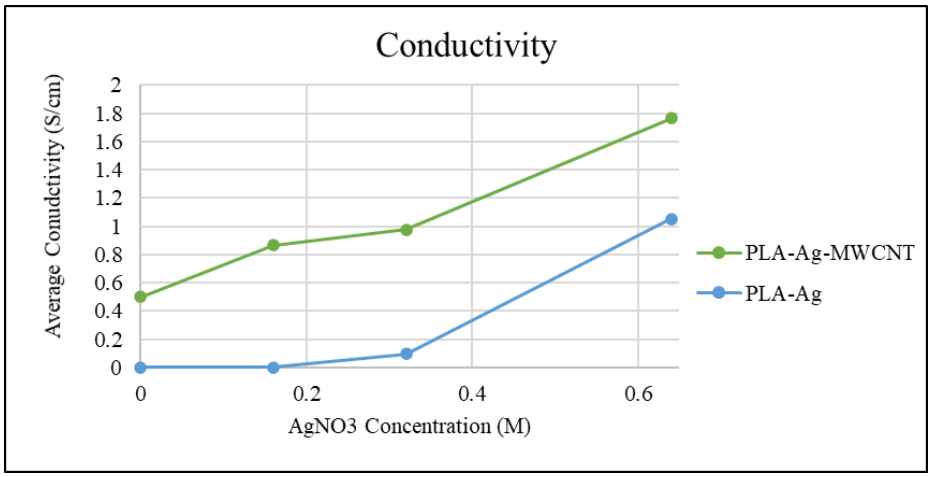

Figure 2.13. SBS Ag Study. Conductivity of Ag impregnated fiber mats

Additionally, SBS PLA:Ag and PLA:MWCNT:Ag fiber mats were used in an antimicrobial study against *Pseudomonas Putida*. 6% w/v was used for PLA:Ag and PLA:MWCNT composites, respectively. Silver ion released from fiber mats were characterized via wet ash digestion using nitric acid (HNO_3) and digesting using hydrogen peroxide (H_2O_2) at 125 C. Aliquots were placed in test tubes inductively coupled plasma mass spectrometry analysis. There was a significant difference between all groups with the except for the 160 and 320 mM PLA:Ag group as seen in Figure 2.14A. As can be seen from Figure 2.14C, fiber mats were used

in a disk diffusion test. Bacterial cultures were grown over 24 hours in a petri dish with an initial concentration of 10^7 CFU/mL. The diameter of the non-growing region was measured. There was a characteristic response like the conductivity curves. After 640 mM of $AgNO_3$ addition, there was an increase in the diameter of non-growth region. Optical density (not shown) assays were done to determine antimicrobial activity in liquid cultures. All treatment groups prevented the growth of bacteria in liquid cultures. As seen in Figure 2.14, there was a greater response with the use of MWCNT in the PLA and Ag composite. This could be due to higher surface roughness that could increase material loading. (44)

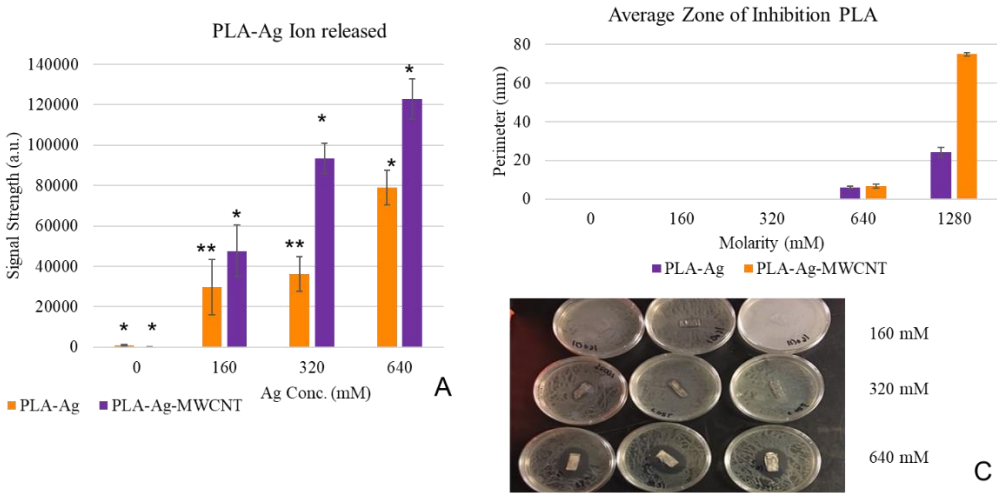

Figure 2.14. SBS silver study. (A) Silver Ion released from fiber mats using inductively coupled plasma mass spectrometry analysis (B) Antimicrobial efficacy of fiber composites via zone inhibition method (C) Images showing zone of inhibition of fiber mats

Silver reduction via wet chemical reduction of $AgNO_3$ produced highly conductive non-woven SBS fiber mats. However, this method produces silver nanofibers with extremely high silver content which could present metal toxicity in therapeutic applications. Vapor reduction of $AgNO_3$ was analyzed to determine the therapeutic efficacy. Morphological Characteristics & Surface Composition: All samples were similar in morphology and there was no significant difference between treatment groups. Figure 2.15 shows the composition data from each treatment

group. Fiber diameter of PLA composite was 788 nm. Fiber diameter decreased to 428 nm and 669 nm with the inclusion of silver nanoparticles and cerium nanoparticles, respectively.

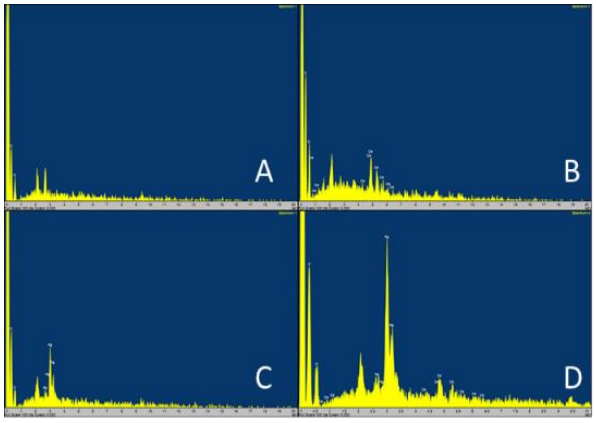

Figure 2.15. SEM images frontal with EDX graphs. A) PLA. B) PLA-Ce. C) PLA-Ag. D) PLA-Ag-Ce.

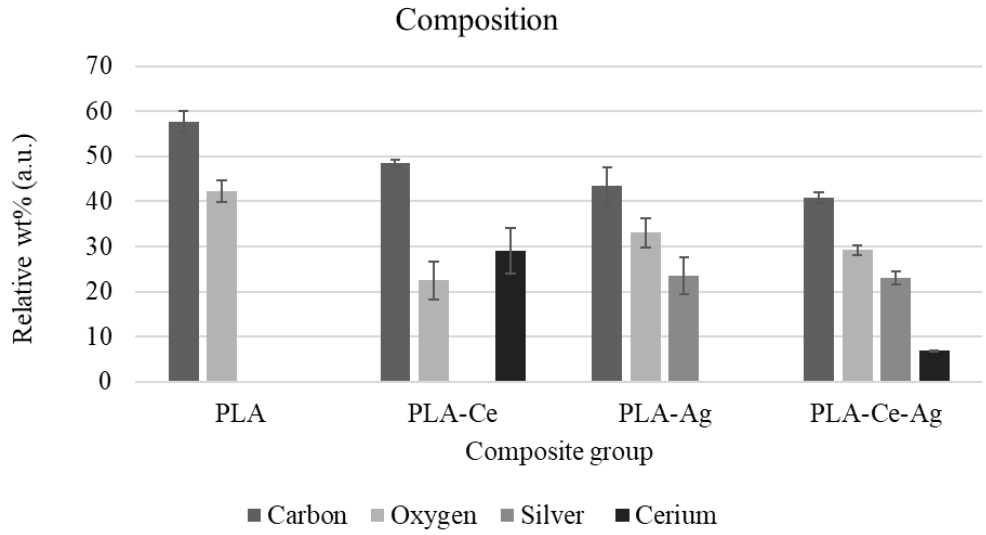

Figure 2.16. Nanofiber composition. There was not a significant difference in the silver content of PLA-Ag and PLA-Ag-Ce group. ($P < 5\%$.)

Surface Contact Angle: Overall, all fiber groups showed hydrophobicity with an angle greater than 100 degrees. Both the control and cerium treatment group had contact angle of 140 degrees. The inclusion of silver nanoparticles caused the contact angle to slightly decrease to 137 and 135 degrees for the PLA-Ag and PLA-Ag-Ce treatment groups.

3-day Optical Density Assay: Figure 2.17A shows an image of bacterial cultures on day 3 of the OD assay. The first row to the last was the control, PLA-Ag, PLA-Ce and PLA-Ag-Ce treatment group. Cultures containing fibers with Ag remained clear of bacteria throughout the entire duration. The PLA-Ce group allowed growth of bacteria, but was slightly antimicrobial. Samples containing Ag were bactericidal and prevented the growth of *P. aeruginosa*. Whereas the PLA-Ce group was bacteriostatic by through day 2 and 3. Figure 6 shows the optical density of P. *aeuruginosa* over a 3-day period. All cultures containing silver stayed constant and inhibited the growth of bacteria. Cultures containing only the PLA-Ce increased over 24 hours then there was a slight decrease after 48 hours indicating antimicrobial activity.

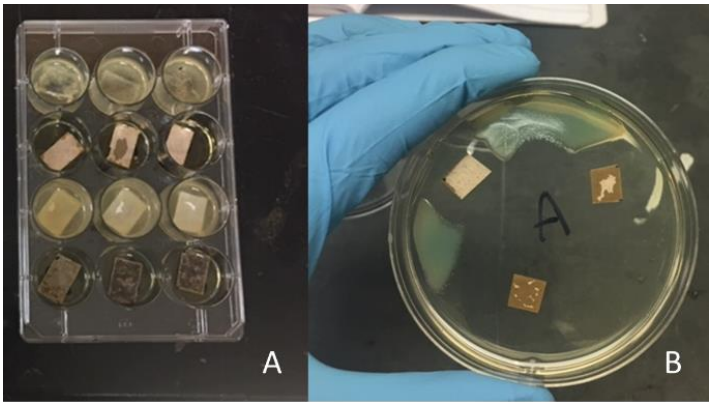

Figure 2.17. Antibacterial assay and disk diffusion. A) Day 3 of OD assay. B) Disc Diffusion of PLA-Ag Composite.

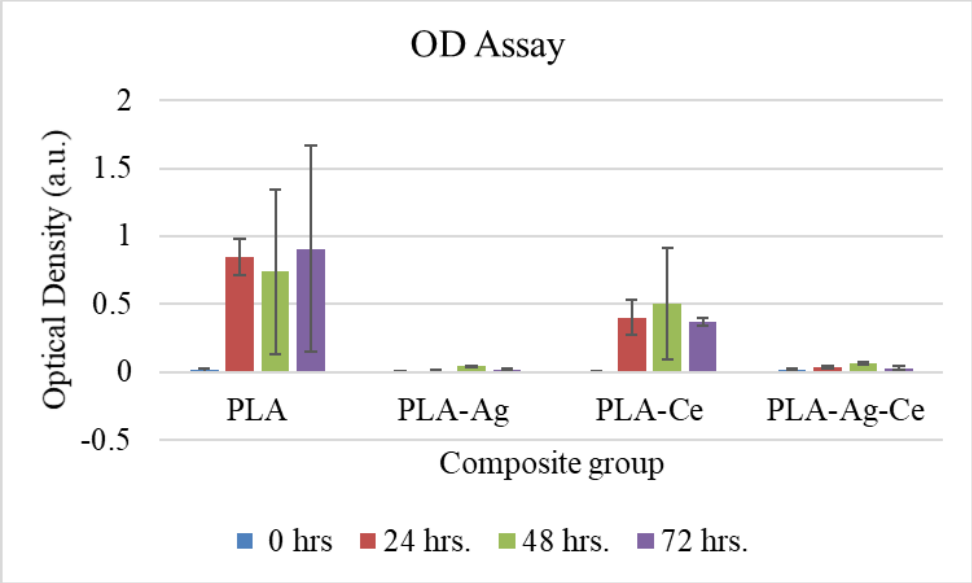

Figure 2.18. 3-Day OD assay. There was a significant difference between PLA and PLA-Ce on hour 24 and 72. ($P < 5\%$.)

Disc Diffusion: PLA control group showed confluent bacteria growth in petri dish. PLA-Ce treatment group showed little to no antimicrobial activity against PA. The inclusion of silver increased the antimicrobial efficacy. The distance measured from fiber to bacterial colonies in the PLA-Ag and PLA-Ag-Ce groups was 2.6 and 1.3 mm, respectively. Ceria nanoparticles occupied more space in the fiber mesh. Therefore, there is a slight decrease in silver content. This accounts for the increase in antimicrobial activity in the PLA-Ag group vs. the PLA-Ag-Ce composite.

Pyocyanin reduction: The activation of cerium to the 3+ oxidation state allows it to be more antioxidative. This can be seen in Figure 2.19. The groups with cerium reduced the pyocyanin production the most. Nanofiber containing only cerium decreased pyocyanin the most at 16.18%. The PLA-Ag-Ce group reduced pyocyanin by 15.66%. This response was similar to the disc diffusion response. Where additional silver in the PLA-Ag-Ce group had a lower antioxidative response than the PLA-Ce group. Pyocyanin reduction can be seen in Figure 2.19.

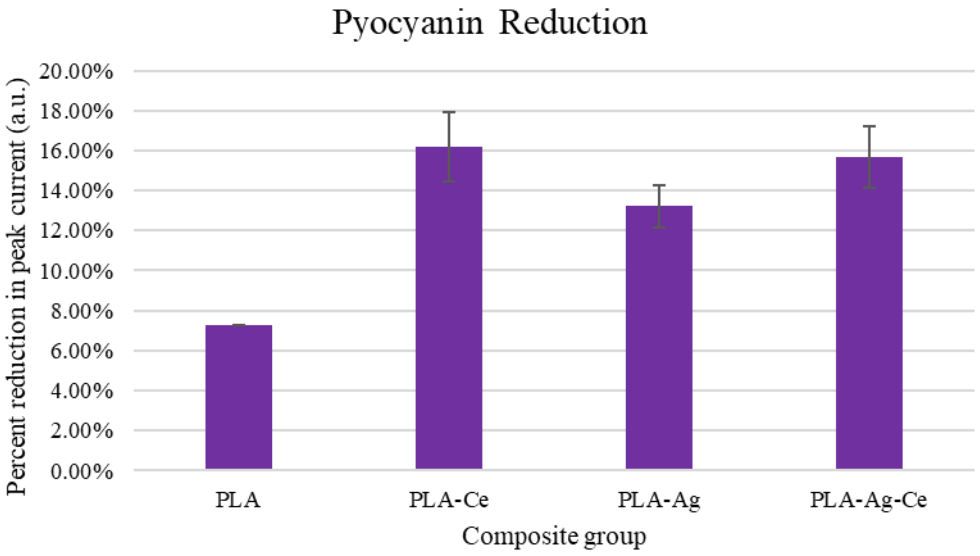

Figure 2.19. Pyocyanin assay. There was a significant reduction in peak current from each treatment group. ($P < 5\%$.)

The use of MWCNT to generate nanofibers was chosen as the best option for biosensor development. The use of silver impregnated nanofibers provided nanofibers with a more superior electrical performance than MWCNT/PLA nanofibers only. However, the Ag nanofibers released excess amount of elemental Ag as seen in the silver release study. This could potential interfere with electrical signal and interact with target analytes. Ag nanofibers have potential as a antimicrobial layer for various applications such as wound dressings. The vapor silver reduction method was examined to determine the use of a dry fabrication method of silver impregnation. Additionally, vapor silver reduction method was antimicrobial against *P. aeuruginosa*. For further efforts towards biosensing developments, MWCNT was used as the filler material where copper and screen-printed arrays were used as the underlaying conduction layer. Two methods were used to generate the electrodes for bacteria detection efforts. One method utilized the pattern of a PCB board with a SBS sheet over the entire surface. The second layer explored the use of a mask transfer technique to produce nanofibers overlaying the copper pattern on the PCB. As can be seen in Figure 2.20, the mask transfer method was able to produce nanofibers with a resolution of 2 mm.

At lower dimensions, there is clogging of the acrylic mask and poor pattern transfer. 2 mm was used as the resolution limit due to the fact that dimensions lower than this limit produced patterns that stuck to the surface of the silver pattern but lifted upon lifting of mask. As seen in Table 2.1 an increase in the coating layers produced a smaller surface resistance. 2% PLA loading group produced lower values as expected. Lower PLA loading allowed for greater MWCNT to reach substrate surface.

Table 2.1 Resistance values from SBS mask transfer method.			
2%	**Resistance**	**4%**	**Resistance**
A – 1	2056.67 Ω	A – 1	2300.33 Ω
A – 4	239.33 Ω	A – 4	328.67 Ω
B – 1	1343.33 Ω	B – 1	3400.00 Ω
B – 4	162.33 Ω	B – 4	247.00 Ω
C – 4	199.00 Ω	C – 4	217.33 Ω

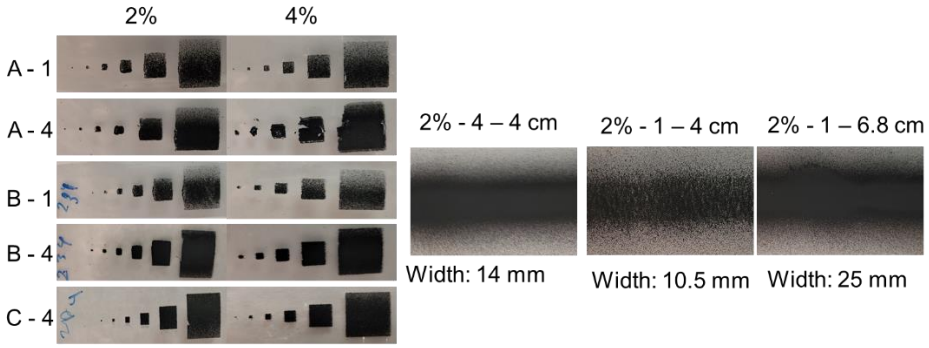

Figure 2.20 SBS mask transfer measurements.

24-hour Continuous Impedance Sensing

Transducers falling in the range of 220 +/- 15% Ω were used in all sensing conditions. The average starting impedance for the parallel setup before testing was 73.7 Ω with phase angle -

.0228° ± 2.93 Ω at 0. 0072°. The sensing cycle for the 24-hour measurement began 30 seconds after inoculation of pre-determined concentration. Figure 2.21 shows the impedance values of the experimental groups. The measured values were averaged out over each hour. The highest concentration tested (10^7 CFU/mL) had the highest corresponding impedance magnitude and the lowest phase angle value after 24 hours of testing. This is an indication of higher cell density in the local testing area. The effect of bacterial growth on transducers dominated the magnitude response over the testing cycle. A small amount of the change in magnitude response can be attributed to media evaporation (across all groups). The variation in the control was 5% and treatment groups varied by 16%, 20%, and 41% for the 10^3, 10^5, and 10^7 concentrations, respectively. The magnitude in the 10^7 group was lower than the 10^5 group, but increased to a higher value after five hours. This response could be due to lower media conductivity caused by planktonic/mobile bacteria in the lag phase. Over the 24-hour testing cycle, magnitude values for all treatment groups increased, which is an indication of log phase bacterial growth. There was also a change in the slope in all treatment groups where the point of change occurred earlier for higher concentrations.

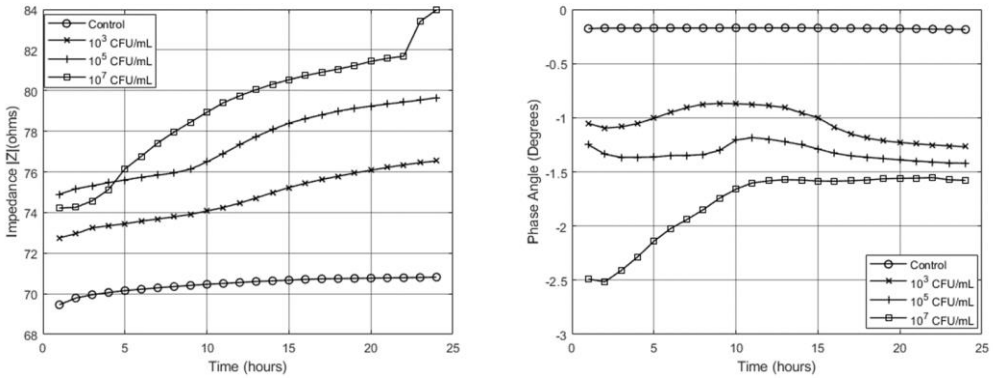

Figure 2.21. A) 24-hour impedance phase angle. B) 24-hour impedance magnitude.

There was a significant difference in the phase angle values between all groups within the first hour of testing ($n = 3$, $p < 5\%$). Higher concentrations gave rise to a more negative phase angle value in all treatment groups. Values for all treatment groups increased over the first 5 hours. After this gradual increase, there is a shift in the response where phase angle values start to stabilize and decrease slightly. Again, this change occurs at an earlier time for higher concentrations. This response is due to bacterial cell adhesion to the electrode surface. As cells continue to grow and populate the testing area, the cell membrane and biofilm orientation give rise to a decreasing phase angle. Magnitude and phase values can be used as a dual validation. This is where impedance can be exploited. This would allow quantification of bacterial concentration load based on two parameters as opposed to only one.

Instantaneous Metabolic Sensing

Further work was done to assess this method in an instantaneous fashion. For chronic wound applications it is worth noting that in any situation, there will always be a population of mature, multi-species bacteria. Instantaneous testing was done on the same concentrations as the above procedure where 2mL of culture media was used. This method was used to assess the determination of bacterial concentration with MWCNT-SBS-PCB transducers. Impedance magnitude response over the one-minute testing cycle had a negative correlation with bacterial concentration. This response is due to the dispersion of planktonic cells in the culture media. Therefore, the media is more conductive with more bacteria. As a result, magnitude values decrease. Phase angle values responded similarly to the continuous testing. Equation 3 and 4 was validated against an unknown concentration. There was a 3% and 1% error between the theoretical magnitude and phase values, respectively, from Equations 3 and 4 and the measured impedance values from the unknown concentration. Unknown concentration was validated with optical density after impedance measurements. The slope from the instantaneous test was -.36 and -3.4

for the phase and magnitude, respectively. The slope for the magnitude and phase from Figure 2.21 was .89 and -.27, respectively. This shows that the instantaneous testing was more sensitive than the continuous cycle. This could be due to faster ionic movement in the liquid phase of the instantaneous test setup as compared to the solid media. Based on the slope of the equation from the standard curves of Figure 2.22 both the magnitude and phase were more sensitive for the instantaneous test. This test shows that bacteria respond like capacitors in the planktonic growth phase and in the biofilm growth phase. Future studies are needed to assess MWCNT-SBS-PCB instantaneous impedance response to biofilm cultures.

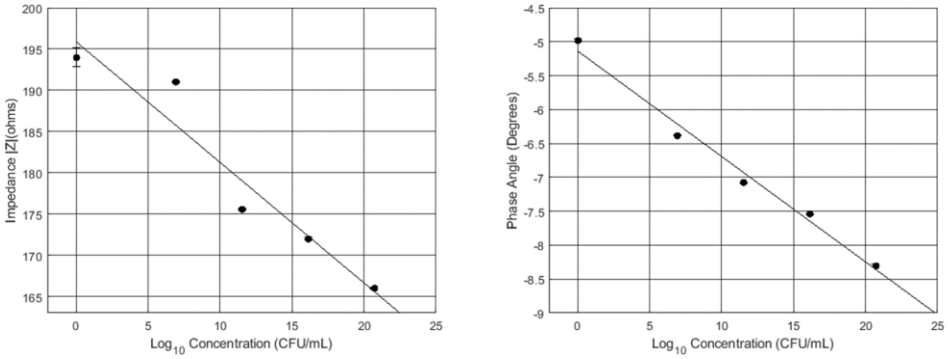

Figure 2.22. Calibration Curve. Using MWCNT-SBS-PCB transducers to instantaneously detect bacterial concentration.

Additional endpoint measurements of *P. putida* KT2440 was tested over a wider concentration range to detect the presence of lower concentrations of bacteria in DI water suspensions. As the media conductivity plays a major role in the detection of bacteria using a nonfunctionalized approach. Therefore, the use of DI water along with the use of a patterned two electrode configuration was used to examine the use of SBS based transducers for bacteria detection in DI water. PCB boards were fabricated using the modified SBS pattern transfer method

to generate an electrode pattern. Figure 2.23 shows the electrodes used in this experiment. The black region is insulation ink that was added to the middle portion of electrodes.

Concentration (CFU/mL)	0	$100x10^{5}$	$100x10^{6}$	$300x10^{6}$	$100x10^{7}$	$300x10^{7}$	$100x10^{8}$	$300x10^{8}$	$100x10^{9}$	$300x10^{9}$	$100x10^{10}$
Graph designator	0	1	2	3	4	5	6	7	8	9	10

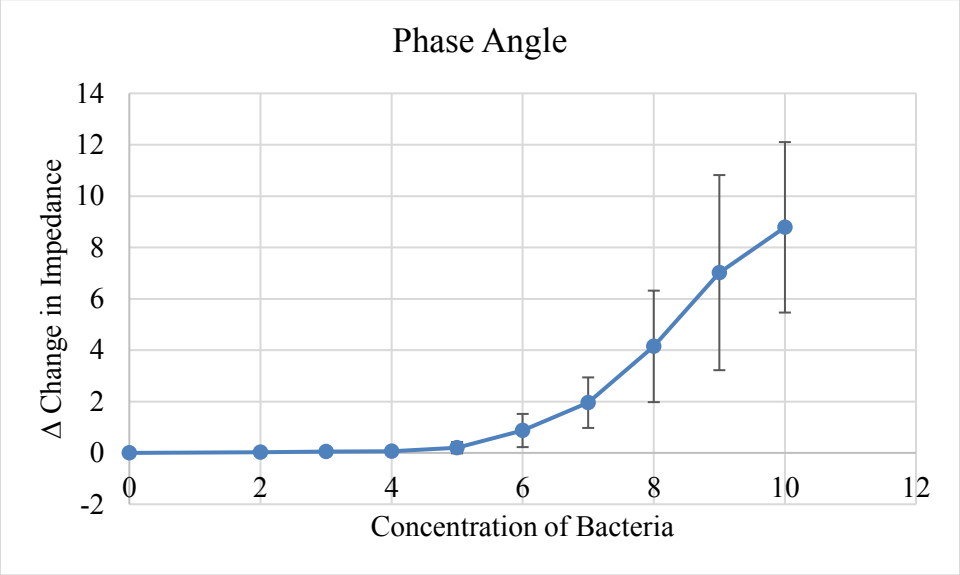

Figure 2.23 Phase angle response of *P. putida* with SBS PLA/MWCNT patterned electrodes.

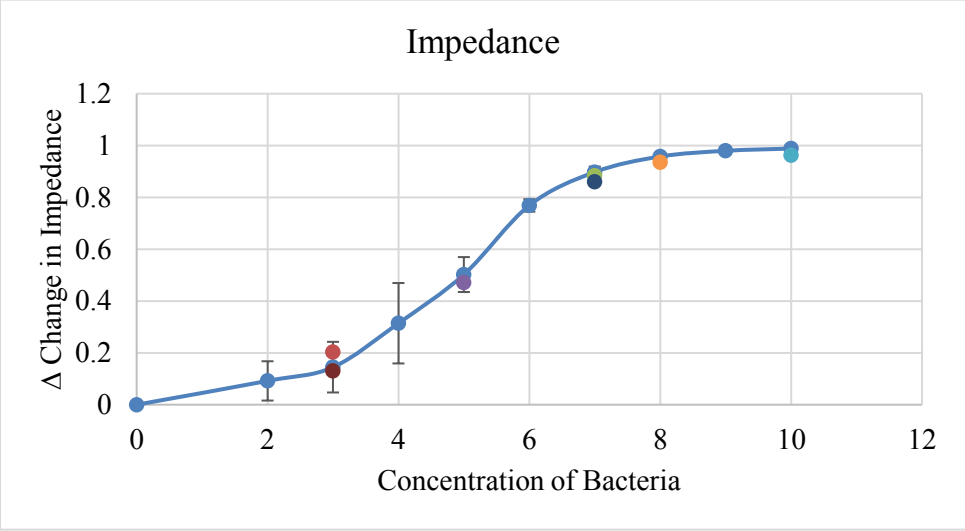

Figure 2.24 Impedance magnitude response of *P. putida* with SBS PLA/MWCNT patterned electrodes.

Additional instantaneous impedance testing was done over a wider concentration range to determine SBS response to bacteria in suspended cultures. As can be seen in Figure 2.23, the phase angle response of was negligible over lower concentrations of bacteria. Once the bacteria concentration reached a point of [5], the phase angle response reduced to more negative values as demonstrated in the initial experiments. In order to capture the impedance response over various runs, the change in impedance and phase angle values compared to the negative control was used as an measure of bacteria concentration. The variability in the phase angle can be seen more drastically at higher concentrations. The impedance magnitude response can be seen in Figure 2.24, where the change in magnitude can be seen at an earlier concentration than the phase angle. The linear range of detection is between 300 x 10^6 – 100 x 10^8 CFU/mL where there is a saturation in the response at around 300x10^8 CFU/mL. Standard curve of Impedance magnitude response was tested with various concentrations of bacteria. Unknown concentrations of bacteria was tested to determine the accuracy of the standard curve in Figure 2.24, Results of 7 concentrations of bacteria can be seen in Figure 2.24, annotated with a different color scheme. Additionally, Table 2.2 has the corresponding percentage error of concentrations tested. Lower concentrations tested showed a higher percent error against the calibration curve generated. Concentrations that were verified to be higher than 100 x 10^7 CFU/mL showed a percent error less than 5% as outlined in Table 2.2. Testing concentrations at 100 x 10^6 CFU/mL produced higher percent error rates. This is due to the fact that higher bacteria concentrations allow for a greater conduction of media and producing a greater change in impedance response. The 100 x 10^8 CFU/mL concentration allowed produces a saturated response and can be seen as the curves begin to reach an equilibrium region where higher concentrations of bacteria produce little to no change in impedance.

Table 2.2. Expected concentration values and percentage error of tested samples.		
Sample number	Concentration	percent error
1	5	6.04%
2	7	1.57%
3	3	28.88%
4	10	2.63%
5	8	2.26%
6	7	4.13%
7	3	9.70%

2.4 Conclusion

Solution blow spun conductive fiber mats have been successfully fabricated with characterization of polymer concentration, conductive MWCNT concentration, and the effects of solvent choice. The use of PLA and MWCNT are unique in that they are both biodegradable and biocompatible. Impedance spectroscopy was used to detect the physical interaction of the coating with the culture media and bacteria population. Solution blow spinning has been used to generate conductive fiber transducers capable of detecting the presence and concentration of bacteria in a LB media culture. This technology has the potential to provide rapid, real-time quantitative data about the bacterial activity in a culture media. Additionally, this method provides an economical method to generate biosensors capable of detecting infection. Continuous monitoring (24-hour testing) provided a way to simulate bacterial growth in a culture environment over a longer period, and may have applications in long term, remote patient monitoring and telehealth. Long-term monitoring allows for the time-wise characterization of the change in impedance as bacterial colonization and biofilm formation begin to surround transducers. Instantaneous measurements (1-minute testing) were able to detect the presence of bacteria within seconds and would be useful in point-of-care clinical applications where immediate quantification is important for diagnosis.

Conductive fiber mats will be used as a coating in biosensor construct fabrication. Selective sensing will be developed by functionalizing the coating surface with bio-recognition elements (i.e. antibodies, enzymes, or signaling molecules). Impedance spectra provides rapid, quantifiable information about bacterial growth and could be used as a valid analytical and diagnostic tool in wound care clinical settings. Further work needs to be done in order to increase the accuracy of continuous impedance sensing with SBS nanofiber mats. Furthermore, improvements must be made in order to accurately mass-produce transducers with a defined electrode pattern.

2.5 References

1. Medeiros ES, Glenn GM, Klamczynski AP, Orts WJ, Mattoso LHC. Solution blow spinning: A new method to produce micro- and nanofibers from polymer solutions. J Appl Polym Sci [Internet]. 2009 Aug 15 [cited 2020 Dec 10];113(4):2322–30. Available from: https://onlinelibrary.wiley.com/doi/full/10.1002/app.30275
2. Daristotle JL, Behrens AM, Sandler AD, Kofinas P. A Review of the Fundamental Principles and Applications of Solution Blow Spinning. ACS Appl Mater Interfaces. 2016 Dec;8(51):34951–63.
3. Greiner A, Wendorff JH. Electrospinning: A fascinating method for the preparation of ultrathin fibers. Vol. 46, Angewandte Chemie - International Edition. John Wiley & Sons, Ltd; 2007. p. 5670–703.
4. Ramakrishna S, Fujihara K, Teo WE, Lim TC, Ma Z. An introduction to electrospinning and nanofibers. An Introduction to Electrospinning and Nanofibers. World Scientific Publishing Co.; 2005. 1–382 p.
5. Subbiah T, Bhat GS, Tock RW, Parameswaran S, Ramkumar SS. Electrospinning of nanofibers. J Appl Polym Sci. 2005 Apr;96(2):557–69.
6. Huang ZM, Zhang YZ, Kotaki M, Ramakrishna S. A review on polymer nanofibers by electrospinning and their applications in nanocomposites. Compos Sci Technol. 2003 Nov 1;63(15):2223–53.
7. Hunley MT, Long TE. Electrospinning functional nanoscale fibers: a perspective for the future. Polym Int [Internet]. 2008 Mar 1 [cited 2020 Aug 23];57(3):385–9. Available from: http://doi.wiley.com/10.1002/pi.2320
8. Fedorova N, Pourdeyhimi B. High strength nylon micro- and nanofiber based nonwovens via spunbonding. J Appl Polym Sci [Internet]. 2007 Jun 5 [cited 2020 Aug 23];104(5):3434–42. Available from: http://doi.wiley.com/10.1002/app.25939
9. Martins A, Araújo J V., Reis RL, Neves NM. Electrospun nanostructured scaffolds for tissue engineering applications. Nanomedicine. 2007 Dec;2(6):929–42.

10. Sell S, Barnes C, Smith M, McClure M, Madurantakam P, Grant J, et al. Extracellular matrix regenerated: Tissue engineering via electrospun biomimetic nanofibers. Vol. 56, Polymer International. John Wiley & Sons, Ltd; 2007. p. 1349–60.

11. Chen JP, Chang GY, Chen JK. Electrospun collagen/chitosan nanofibrous membrane as wound dressing. Colloids Surfaces A Physicochem Eng Asp. 2008 Feb;313–314:183–8.

12. Da Silva Parize DD, De Oliveira JE, Foschini MM, Marconcini JM, Mattoso LHC. Poly(lactic acid) fibers obtained by solution blow spinning: Effect of a greener solvent on the fiber diameter. J Appl Polym Sci [Internet]. 2016 May 10 [cited 2021 Jun 15];133(18). Available from: https://onlinelibrary.wiley.com/doi/full/10.1002/app.43379

13. Zheng W, Li J, Zheng YF. Preparation of poly(l-lactide) and its application in bioelectrochemistry. J Electroanal Chem. 2008 Sep 1;621(1):69–74.

14. Miller CL, Stafford G, Sigmon N, Gilmore JA. Conductive nonwoven carbon nanotube-PLA composite nanofibers towards wound sensors via solution blow spinning. IEEE Trans Nanobioscience. 2019 Apr;18(2):244–7.

15. Gianino E, Miller C, Gilmore J. Smart Wound Dressings for Diabetic Chronic Wounds. Bioengineering. 2018;5(3):1–26.

16. Dakal TC, Kumar A, Majumdar RS, Yadav V. Mechanistic basis of antimicrobial actions of silver nanoparticles. Front Microbiol. 2016 Nov;7(NOV):1831.

17. Walkey C, Das S, Seal S, Erlichman J, Heckman K, Ghibelli L, et al. Catalytic properties and biomedical applications of cerium oxide nanoparticles. Vol. 2, Environmental Science: Nano. Royal Society of Chemistry; 2015. p. 33–53.

18. Pacios Pujadó M. Carbon Nanotubes as Platforms for Biosensors with Electrochemical and Electronic Transduction [Internet]. Berlin, Heidelberg: Springer Berlin Heidelberg; 2012 [cited 2021 Jun 15]. (Springer Theses). Available from: http://link.springer.com/10.1007/978-3-642-31421-6

19. Handbook of Nanomaterials Properties. Handbook of Nanomaterials Properties. Springer Berlin Heidelberg; 2014.

20. Eatemadi A, Daraee H, Karimkhanloo H, Kouhi M, Zarghami N, Akbarzadeh A, et al. Carbon nanotubes: Properties, synthesis, purification, and medical applications. Nanoscale Res Lett [Internet]. 2014 Aug 13 [cited 2021 Jun 15];9(1):1–13. Available from: http://www.nanoscalereslett.com/content/9/1/393

21. García-Barrasa J, López-De-luzuriaga JM, Monge M. Silver nanoparticles: Synthesis through chemical methods in solution and biomedical applications. Cent Eur J Chem [Internet]. 2011 Feb 1 [cited 2021 Jun 15];9(1):7–19. Available from: https://www.degruyter.com/document/doi/10.2478/s11532-010-0124-x/html

22. Lee PC, Meisel D. Adsorption and surface-enhanced Raman of dyes on silver and gold sols. J Phys Chem [Internet]. 1982 [cited 2021 Jun 15];86(17):3391–5. Available from: https://pubs.acs.org/sharingguidelines

23. Creighton JA, Blatchford CG, Albrecht MG. Plasma resonance enhancement of Raman

scattering by pyridine adsorbed on silver or gold sol particles of size comparable to the excitation wavelength. J Chem Soc Faraday Trans 2 Mol Chem Phys [Internet]. 1979 Jan 1 [cited 2021 Jun 15];75(0):790–8. Available from: https://pubs.rsc.org/en/content/articlehtml/1979/f2/f29797500790

24. Vega-Baudrit J, Gamboa SM, Rojas ER, Martinez VV. Synthesis and characterization of silver nanoparticles and their application as an antibacterial agent. Int J Biosens Bioelectron [Internet]. 2019 Oct 22 [cited 2021 Nov 17];Volume 5(Issue 5). Available from: https://medcraveonline.com/IJBSBE/IJBSBE-05-00172.php

25. Morones JR, Elechiguerra JL, Camacho A, Holt K, Kouri JB, Ramírez JT, et al. The bactericidal effect of silver nanoparticles. Nanotechnology [Internet]. 2005 Oct 1 [cited 2021 Jun 15];16(10):2346–53. Available from: https://pubmed.ncbi.nlm.nih.gov/20818017/

26. Bader MS. Diabetic foot infections. Med Manag Infect Dis. 2003;581–98.

27. Siddiqui AR, Bernstein JM. Chronic wound infection: Facts and controversies. Clin Dermatol. 2010;28(5):519–26.

28. Kalia VC. Quorum Sensing vs Quorum Quenching: A Battle with No End in Sight. Quorum Sensing vs Quorum Quenching: A Battle with no end in Sight. Springer; 2015. 7–22 p.

29. Edwards R HK. Bacteria and wound healing. Infect Dis (Auckl). 2004;17(2):91–6.

30. Carpenter RJ, Hartzell JD, Forsberg JA, Babel BS, Ganesan A. Pseudomonas putida war wound infection in a US Marine: A case report and review of the literature. J Infect. 2008;56(4):234–40.

31. Mandell GL, Douglas RG, Bennett JE. Principles and practice of infectious diseases. Volume 2. Vol. (I-XXXII+1. 1979.

32. Swisher SL, Lin MC, Liao A, Leeflang EJ, Khan Y, Pavinatto FJ, et al. Impedance sensing device enables early detection of pressure ulcers in vivo. Nat Commun. 2015;6:1–10.

33. Lukaski HC, Moore M. Bioelectrical impedance assessment of wound healing. J Diabetes Sci Technol. 2012;6(1):209–12.

34. Lei KF. Review on impedance detection of cellular responses in micro/nano environment. Micromachines. 2014;5(1):1–12.

35. Bancalari E, Bernini V, Bottari B, Neviani E, Gatti M. Application of impedance microbiology for evaluating potential acidifying performances of starter lactic acid bacteria to employ in milk transformation. Front Microbiol. 2016;7(October):1–11.

36. Szulcek R, Bogaard HJ, van Nieuw Amerongen GP. Electric cell-substrate impedance sensing for the quantification of endothelial proliferation, barrier function, and motility. J Vis Exp. 2014;(85):1–12.

37. Safavieh M, Pandya HJ, Venkataraman M, Thirumalaraju P, Kanakasabapathy MK, Singh

A, et al. Rapid Real-Time Antimicrobial Susceptibility Testing with Electrical Sensing on Plastic Microchips with Printed Electrodes. ACS Appl Mater Interfaces. 2017;9(14):12832–40.

38. Tingley K, Bukhtia A, Li Y, Nasir M, Bou-akl T. Impedance Analysis and Antibody Immobilization to Differentiate Methicillin- Resistant Staphylococcus Aureus. 2008;(9):1–10.

39. Maalouf R, Fournier-Wirth C, Coste J, Chebib H, Saïkali Y, Vittori O, et al. Label-free detection of bacteria by electrochemical impedance spectroscopy: Comparison to surface plasmon resonance. Anal Chem. 2007;79(13):4879–86.

40. Bellitti P, Bona M, Fontana S, Sardini E, Serpelloni M. Study toward the integration of a system for bacterial growth monitoring in an automated specimen processing platform. Lect Notes Electr Eng. 2019;539:445–54.

41. Cristina Pablos, Javier Marugán, Sandra Cristóbal, Rafael van Grieken. Implications of Electrical Impedance-Based Microbiological Technology in Pork Meat Processing Industry for the Rapid Detection and Quantification of Salmonella Spp. J Food Sci Eng. 2017;7(1):1–16.

42. Wawerla M, Stolle A, Schalch B, Eisgruber H. Impedance microbiology: Applications in food hygiene. J Food Prot. 1999;62(12):1488–96.

43. Zhu T, Pei Z, Huang J, Xiong C, Shi S, Fang J. Detection of bacterial cells by impedance spectra via fluidic electrodes in a microfluidic device. Lab Chip. 2010;10(12):1557–60.

44. Sakti SP, Santjojo DJDH, Saputri SN, Am A'. Improvement of Biomolecule Immobilization on Polystyrene Surface by Increasing Surface Roughness. J Biosens Bioelectron. 2012;3(3):119.

CHAPTER THREE

MULTI-WALLED CARBON NANOTUBE SOLUTION BLOW SPUN NANOFIBER IMMUNOSENSOR INTERFACE DEVELOPMENT

3.1 Introduction

Biofabrication has evolved into a multifunctional fabrication tool that allows engineers to create an array of biosensors for a broad range of diagnostic applications. Biosensors include the use of a biorecognizing element to specifically transduce a signal proportional to the concentration or reaction at the active site. Immobilization techniques such as crosslinking is important as the detection limit of biosensors depend on this critical step. Nonwoven fibers are widely used in biosensing applications. Stereolithography is a widely used 3D printing modality due to its high resolution. In 1956, Dr. Leland C. Clark used early fabrication techniques to create a long-term continuous oxygen sensor. This sensor is thought to be one of the first biosensors made. Clark's main goal was to find a simple way to quantify circulating, venous and arterial blood in real-time. (1) Molecular and serology tests are currently the two main biosensing platforms for COVID-19 detection. However, there have been detection schemes developed using electrochemical impedance testing Electrochemical immunosensors were developed to accurately detect the Middle East respiratory syndrome (MERS) with a detection range of 0.001 – 100 ng/mL. (2) Most of these electrochemical assays are made from highly complicated and expensive processes such as photolithography. Pathogenic Immunosensors can be validated several ways. One common way is to first verify functionalized surface with primary Ab/blocking agent versus the baseline signal in a redox test solution. Successively add antigen to electrode surface (incubate) followed by a wash step and measure the change in current or impedance with respect to baseline.

The immobilization of capture molecules such as proteins, antibodies, and aptamers play a vital role in the performance of immunoassays. Immunoassays depend on the orientation and

availability of antibodies. Immunodiagnostics and biosensors developed for pathogenic antigen detection and quantification from samples utilize recognition proteins such as antibodies. Biosensor performance depends on the sufficient immobilization of the capture element on a solid support surface with sufficient surface density and the maximization of antigen capture event. Antibodies are considered biorecognizing elements because they have binding sites specific to the antigen of interest. They have a molecular mass of approximately 150kDa with dimensions at around 14x10x4 nm. (3) Antibodies consist of two fragment antigen binding regions and a fragment crystallizable region known as Fab and Fc, respectively. There is an additional Fab region that is joined by a $F(ab')_2$ fragment. It is worth noting that the Fab and Fc region of the antibody are different in composition, isoelectric point and physical structure. The Fab region generally has a higher molecular mass than the attached Fc portion. The best antibody orientation is such that the Fc region is facing down on the substrate of interest. This orientation is considered as the end-on orientation and would allow for maximal antibody antigen complex interaction. Physical adsorption methods and spontaneous chemical immobilization of antibodies can generate antibodies in random orientations. Head-on orientation prevents antigen binding as the Fab region is blocked by the surface interaction. (3) As can be seen from Figure 3.1, the orientation of antibodies on a surface can take many forms which can ultimately affect protein site availability. The best strategy for immobilization of antibodies will depend on the nature of the assay design and solid substrate that is used for the system. Many aspects of the immobilization methodology can influence the functionality of the fixed antibodies. Protein denaturation and conformational changes during the immobilization process can reduce the immune-sensor activity and response. Antibodies that are non-specifically or randomly adsorbed unto the surface of the sensing support

experience the greatest inactivation. The modification of antibodies, especially on the Fab region, can also affect the function of the proteins.

Oriented immobilization of antibodies has been used in immunoassays in order to solve the issue of non-specific and randomized binding. This in turn can increase immunoassay response to target antigen. Studies have shown that oriented antibodies, with Fab regions exposed to the solution phase containing target antigen, generate better response than randomized antibodies. (3)

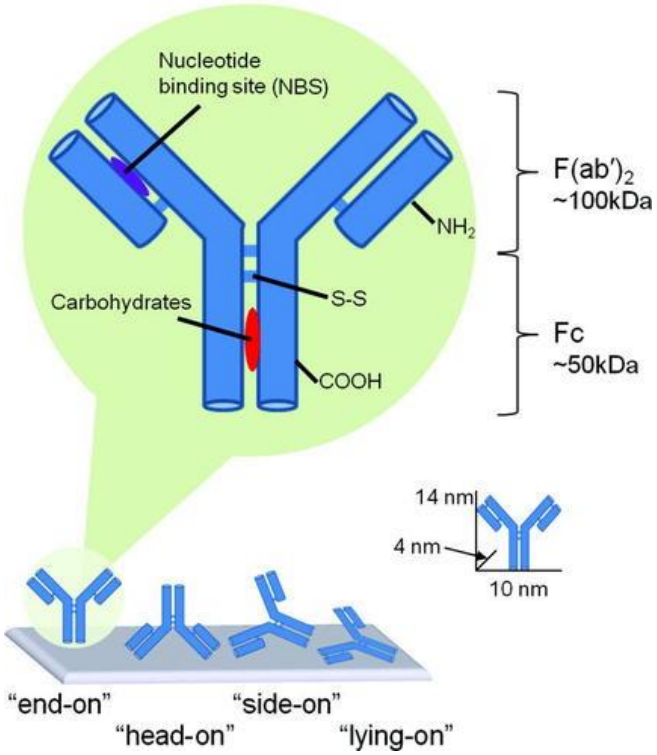

Figure 3.1. Antibody orientation on solid surface and chemical groups. Figure reproduced from Ref. (3)

The Physical adsorption method of immobilization is the most used method in traditional immunoassay technologies. This method depends on the hydrophobic, electrostatic, and weak van deer Waals forces between the antibodies and the contact surface of the support. Mainly, the hydrophilic and hydrophobic interactions are the main players between antibody and substrate attraction. The physical adsorption method provides the most simplistic method of immobilization

of proteins to a solid surface. However, this method is the least to control and antibodies can be immobilized in a random orientation resulting in denaturation or loss of functionality in subsequent testing steps. Butler et al. found that greater than 90% and 75% of monoclonal and polyclonal anti-fluorescyl antibodies denatured by physical adsorption immobilization technique. Additionally, the authors found that only less than 10% of proteins immobilized were active for antigen binding. (4) However, this method has been found in many applications to include ELISA and biosensors. Physical adsorption is used due to being the cheapest and its ease of use.

Chemical immobilization strategies include the use of strategies to form a chemical bond between solid surface and recognizing element surface groups such as streptavidin-biotin, aldehydes, and silanes immobilization method. Streptavidin and biotin interaction is a non-covalent strategy that utilizes the enzymatic interaction to form a strong bond with very high affinity of approximately $1x10^{-15}$ M. This binding is also considered resistance to detergents, organic solvents, and temperature and pH fluctuations. Streptavidin is approximately 70 kDa and has four binding sites for biotin interaction. (5) Antibody or aptamer surface can be modified with biotin to form an interaction that forms a stable, oriented conjugation. Covalent binding with glutaraldehyde (GA) can be used to immobilize capture molecules via amine groups. GA can crosslink with antibodies by other means, it has an aldehyde residue on both of its 5-carbon chain that can be used as an arm-linker between two molecules with an amine. (6) The use of glutaraldehyde has been explored with the use of organosilanes such as 3-Aminopropyl)triethoxysilane (APTES) which is capable of forming hydroxyl groups on the solid surface of immobilization. The use of APTES can provide stable bonds. APTES immobilization on electrode surface has been explored and its potential to immobilize antibodies on surface of glassy carbon electrodes has been examined by a few researchers. (7–9) Specifically, Badruzaman

et al. utilizaed APTES and GA at a concentration of 2% and 2.5%, respectively to immobilize rabbit IgG on screen printed carbon electrode for electrochemical applications. (9) APTES provides an ease of immobilization strategy, but there are few applications with the use of screen-printed electrodes and more applications with glassy carbon use. Thus, APTES is mainly used for polystyrene, glass, and silica surfaces. Another strategy is the use of EDC/NHS crosslinker method. This method has been the most widely used way to functionalize proteins on various surfaces to include gold, screen printed carbon, platinum. (10–14) This method is also used to provide biotin and other surface modifications to the amine groups of antibodies and capture molecules. 1-ethyl-3-(3-dimethylaminopropyl)carbodiimide (EDC) is a water-soluble carbodiimide that is capable of reacting with carboxylic acid groups on the surface of antibodies to produce O-acylisourea intermediates. (14) These intermediates can reduce antigen-antibody yield. The use of N-hydroxysuccinimide (NHS) rapidly reacts with these O-acylisourea intermediates which creates reactive esters to increase reaction yield. The NHS ester is then capable of reacting with the amine group of biological agents via covalent bond. (15) For this reaction, carboxyl activation is required to pretreat surface. Polymers with carboxyl groups such as PLA or poly(methyl methacrylate) (PMMA) can be used without pretreatment. (16) Hydroxyl surface treatment methods are used to introduce carboxyl groups to the surface of solids without these carboxyl containing polymers. These methods include plasma treatment, carboxyl salts and solvents. (17,18) Parkash et al. explored the use of screen printed carbon electrode to immobilize anti-Dengue NS1 capture using EDC/NHS with a carboxymethyldextran pretreatment step. (10)

Additional efforts can be made to increase the antigen-biological agent reaction by using microspheres to encourage binding. Many immunoassays have been developed with the use of microspheres as a substrate for capture biological immobilization. (19,20) Proteins adsorb onto

polystyrene rapidly and permanently. (21) The use of microspheres provides a surface with a high surface area which can result in efficient coupling of biological agents. This chapter assess the use of an electrochemical impedance assay with solution blow spun nanofibers. The production of cost-effective nanofibers has found applications in biosensing applications. Nanofibers have been used to facilitate the immobilization of proteins on the surface. Additional efforts were made to assess the performance of system with polystyrene microspheres. Now that we have established that we can make conductive nano-composites to measure bacterial biosensors. Therefore, we wanted to make this sensor more specific. However, this project was interrupted by the pandemic (COVID-19) this was an opportunity to use the developed technology to detect COVID in an immunosensing platform.

Research questions:

1. Develop a low-cost biosensor interface for potential point-of-care immunosensor applications.
2. To what extent does UV/Ozone and salinization treatment affect protein adsorption on SBS conductive material?
3. To what extent does blocking and antibody concentration affect impedance change?

3.2 Materials and Methods

3.2A Protein Adhesion Analysis

To assess the extent of protein adhesion to the surface of solution blow spun nanofibers. Pristine PLA and conductive MWCNT/PLA nanofibers were produced and used for protein adhesion to surface layer. The protein immobilization protocol is outlined in Figure 3.2. Nanofiber mats were produced from previously made polymer solutions with a chloroform solvent. The pristine PLA group consisted of a 12% w/v and the MWCNT/PLA group consist of a 4% w/v of

PLA and 10% w/v of MWCNT with respect to the PLA content. Samples were made using the I&J printer system. I&J system contains consist of a microcontroller-based stage and a holder with controllable height and speed of stage and holder. The holder speed was set at 10 mm/sec with a airbrush distance of approximately 15cm from the surface. Equal amounts of nanofibers were deposited on Polyethylene Terephthalate (PET) film. Samples were then allowed to dry for 1 hour under ambient conditions until further use. To understand how proteins would adhere to the fabricated nanofibers, a study was conducted. This study employed the Bicinchoninic Acid assay (BCA, Pierce BCA Protein Assay Kit, Life Technologies) for protein adhesion assessment. This assay utilizes a colorimetric method to non-selectively detect the presence of protein within a given sample. The assay utilizes the reduction of Cu^{+2} to Cu^{+1} by the presence of proteins, which produces a colorimetric change from a premixed green solution to a purple-colored reaction mixture. The mixture displays a strong adsorbance near 562 nm that is proportional to the protein concentration. Albumin serum (2mg/mL) were physically or chemically adsorbed to nanofibers with different PLA and MWCNT weight percentages. 4% w/v PLA was used as this was the desired concentration to use with the construction of the electrode configuration. 12% w/v PLA was used in order to assess protein adsorption and immobilization methodology with higher polymer loading. Initially, physical adsorption was used as the base method to adsorb proteins on the surface of nanofibers using different time points. Chemical adsorption was also used to assess the use of a more permanent immobilization method. Glutaraldehyde was used as a fixative for chemical immobilization of albumin serum proteins as this fixative is known to form a bond with free amine groups on the surface of proteins. Initial studies utilized a 30min and 1hour soak time for BCA analysis. Glutaraldehyde percentage used was 25%. All samples were done in triplicate for statistical analysis of protein adsorption. The use of higher PLA loading gave a higher signal

response due to PLA nanofibers serving as a scaffold. Carbon loading decreased the amount of protein adsorbed on the surface via physical adsorption method. Additionally, increasing soak time showed a greater change in signal response with all groups with the exception to the 4% control. Chemical adsorption with 25% glutaraldehyde (GA) significantly increased the adsorption potential in both the 4% and 12% groups.

Additional efforts were made to visually assess the adhesion of proteins to the surface of nanofibers. Alexa Flour 594 anti-rabbit and Alexa flour 594 streptavidin was used as a test to assess the adsorption of protein to the surface of pristine PLA (12% w/v) and PLA_MWCNT (4%_10%). For glutaraldehyde treated nanofibers, various percentages of glutaraldehyde (0% - 10%) was used to immobilize fluorescent streptavidin. Glutaraldehyde was diluted to the desired percentage using phosphate buffer solution, pH 7.2. The solutions were made and stored at a 2ºC up to 3 months. Glutaraldehyde was added to surface of MWCNT/PLA nanofiber mats via dropwise method and allowed to incubate at room temperature for 1 hour. Afterward, excess glutaraldehyde was rinsed off surface with DI water and allowed to dry. APTES was used in the immobilization of streptavidin to assess the effect of salinization on the attachment of proteins to the surface. The effect of UV/Ozone treatment on the surface of samples was also assessed. As seen in Figure 3.2, UVO treatment activates the treated surface in order to produce more hydrophilic surfaces. The salinization concentration was adopted from Sabdin et al. Where APTES treatment became highly unstable at concentrations above 2% w/v. Preliminary tests were done to confirm this response with SBS MWCNT/PLA nanofiber mats. Thus, the APTES concentration was kept constant within this chapter at 2% w/v. APTES was added to the surface of samples at 1:1 volume ratio to GA. Samples were allowed to soak for 1 hour at room temperature and allowed to dry before imaging samples. EVOS microscope was used to image samples compared to a

negative control. ImageJ was used to assess the relative fluorescent intensity between samples and negative control.

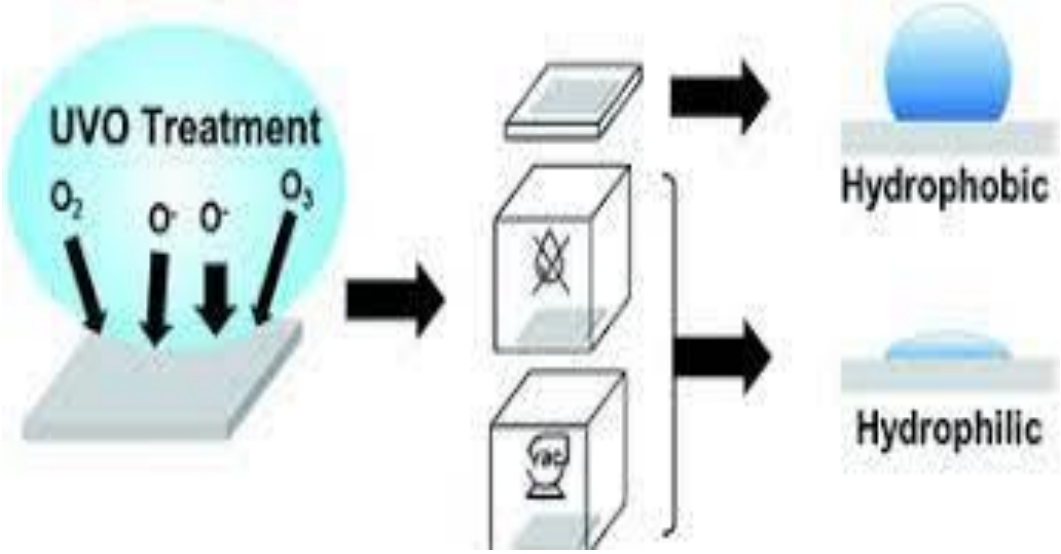

Figure 3.2. Workflow for the fabrication of SBS MWCNT/PLA based electrodes for biosensing applications. Figure reproduced from Ref. (22)

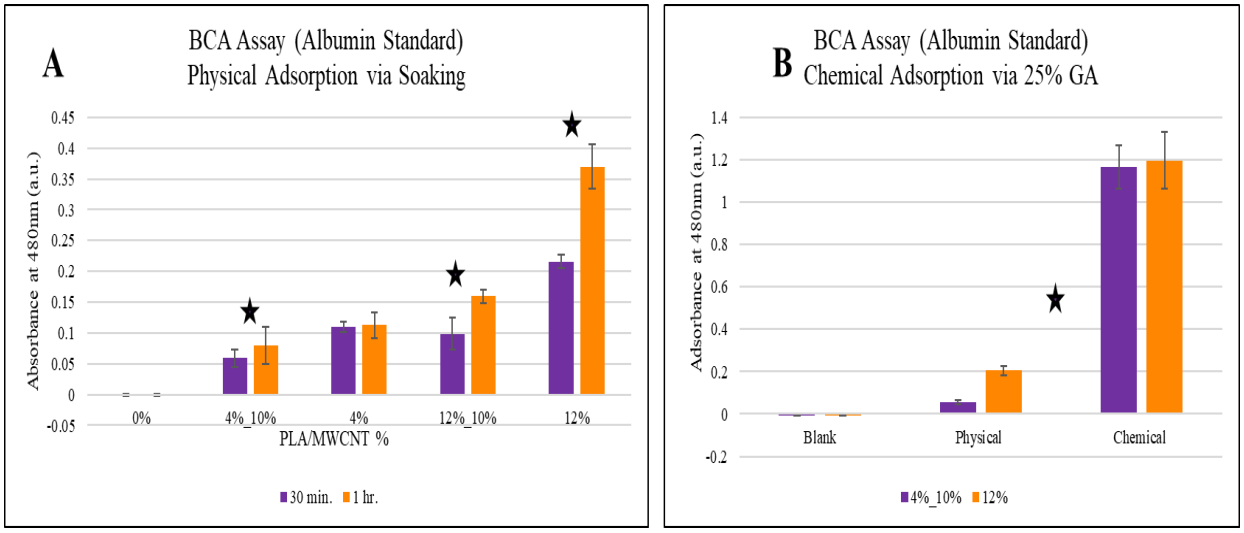

Figure 3.3. BCA assay of PLA SBS constructs A) BCA assay using albumin standard (2mg/mL) via physical adsorption. B) BCA assay using albumin standard (2mg/mL) via physical adsorption vs. chemical adsorption.

3.2B Electrode Fabrication

Electrode fabrication was done using SBS as the main method of fabrication with MWCNT/PLA nanofiber mats. This was done in order to explore the use of a rapid and affordable method to fabricate electrochemical biosensor electrodes for various applications. Nanofibers are inherently electrically unstable. In order to combat this, silver screen printing ink was used as a conductive underlying layer for electrodes. First, the electrode design was created and a photoemulsion mask was made in order to provide a positive mask for screen printing. Poly(ethylene) glycol (PEG) was used as the substrate for both the silver underlayer and the SBS nanofiber layer. PEG film was cleaned prior to screen printing silver ink. A similar mask as the silver mask was laser printed on acrylic plastic and used for depositing SBS MWCNT/PLA nanofibers over silver layer utilizing the I&J printer system. The workflow for electrode fabrication can be seen in Figure 3.4.

Figure 3.4. Modified fabrication of biosensing electrodes.

3.2C Pilot electrical response

In order to assess the electrical signal, Keithley 2400 source meter was and IO Rodeostat potentiostat was used to detect current flow after immobilization steps. Surface resistance was measured before and after each immobilization step (with a dry step) with source meter. Physical versus chemical immobilization was used to assess current change as seen in Figure 11A. Chemical adsorption with GA showed a consistent decrease with each immobilization step (1: Bare; 2: 10%

Anti-goat serum; 3: 10% non-fat milk; 4:50% Goat serum). During step 3, the current flow increased with physical adsorption, which could be due to the primary IgG washing off of surface due to a weaker bond to electrode surface. Amperometric measurements were taken using the chemically immobilized IgG in the same fashion within a 50mM potassium ferrocyanide solution in PBS (pH = 7.2). As seen in Figure 3.5A, the current flow decreases with the addition of Anti-goat serum, blocking, and goat serum (5%,10%). Additionally, in Figure 3.5B, there is an oversaturated response with the chronoamperometric response with the initial cycle. This is a result of the PLA polymer surface activation by phosphate buffer solution. Over time the signal naturally decreases and fluctuates as can be seen in the images. Further testing in this chapter was done to examine the fluctuation in signal and ways to overcome this response by surface modifications, increase testing time, and or increasing the biological agent and target interaction in an effort to increase signal strength.

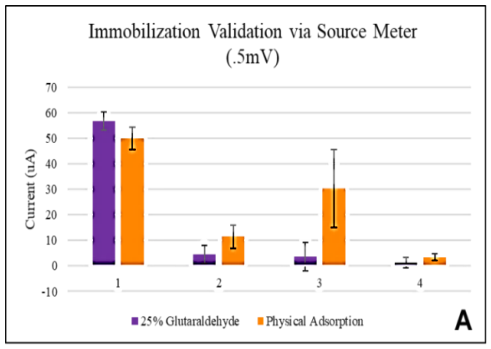

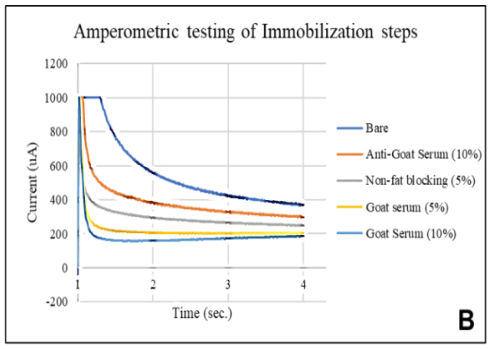

Step	25% Glutaraldehyde Response	Physical Adsorption (soaking) Response
Bare	56.67 uA	50.00 uA
Antibody (1/10)	4.50 uA	11.47 uA
Block (10% Milk)	3.67 uA	30.33 uA
Serum (50%)	1.18 uA	3.40 uA

Step	Response after 4 sec.
Bare	373.4 uA
Anti-goat serum (1/10)	297.2 uA
Non-fat milk (5%)	248.3 uA
Goat serum (5%)	204.5 uA
Goat serum (10%)	186.7 uA

Figure 3.5. Pilot electrical response of SBS electrodes (A) Change in current flow due to immobilization modification: 1-Bare; 2-10% Anti-goat serum; 3: 10% non-fat milk; 4: 50% Goat serum (B) Amperometric response to immobilization modification in 50 mM of potassium ferrocyanide

3.2D Electrical Analysis of protein adsorption

Electrical performance of electrode towards target antigen was tested in phosphate buffer solution. Initial antibody response to target antigen was testing in a 24 well plate with electrode situated on the outer most region of wells. All rinse steps used a pipette tip in order to wash off loosely bound molecules. LCR meter was used to test the electrical response of electrodes in phosphate buffer. The impedance was measured using a 1V sine wave at 200 Hz. Re-calibration of the LCR meter and new fiber mat transducers were used in each testing cycle. Immobilization method was assessed by testing the electrical response of electrodes versus the initial bare impedance value found initially on the surface.

3.2E Immobilization of protein on polymicrospheres

The immobilization of polymicrospheres (PSMS) were done by simple adsorption. In order to assess the immobilization methodology of microspheres, 488 biotin was used as a target and streptavidin was used as a capture probe. The streptavidin coating process included 100µl of 50µg/ml streptavidin in PBS. Streptavidin solution was added to a 100µl solution of PSMS in PBS. For the 37ºC samples a 96 well plate and allowed to initiate the immobilization. Room temperature samples were placed in microcentrifuge tubes. PSMS were washed and spun down at 4400 rpm for 5 minutes and samples were then transferred to in 200µl PBS for a total of 3 times. Then 100µl of 50µg/ml biotin was added to each sample and allowed to react for 25 minutes at room temperature. An additional washing step was done prior to imaging fluorescent response. The response was captured utilizing a plate reader. The effects of the wash step were assessed as can be seen in Table 3.1. After 2 washes there was significant biotin loss. However, 4 washes still maintained biotin binding on PSMS surface.

Table 3.1 PSMS wash step optimization.								
	4 washes	**3 washes**	**2 washes**	**1 wash**	**No Wash**	**PBS**	**Uncoated PSMS**	Coated No Biotin
Sample 1	3002	7102	35875	292636	1234628	710	904	793
Sample 2	1527	8603	30685	248175	2852812			
Sample 3	2178	8052	21437	151630	1372350			

At 4 washes the values are still above the value for the uncoated and coated no biotin ones, though not too impressively especially in the case of sample 2. As the PSMS surface gets centrifuged and washed there is loss of microspheres with each wash. As noted by Bang's lab this is the easiest method to wash, but could potentially result in loss of PSMS due to the inability to form a proper pellet and removal of sample when decanting. (21) For further testing 3 washes were used. As can be seen in Figure 3.6, the microspheres incubated at 4 hours produced the highest response indicating a greater coating of streptavidin and biotin interaction with PSMS.

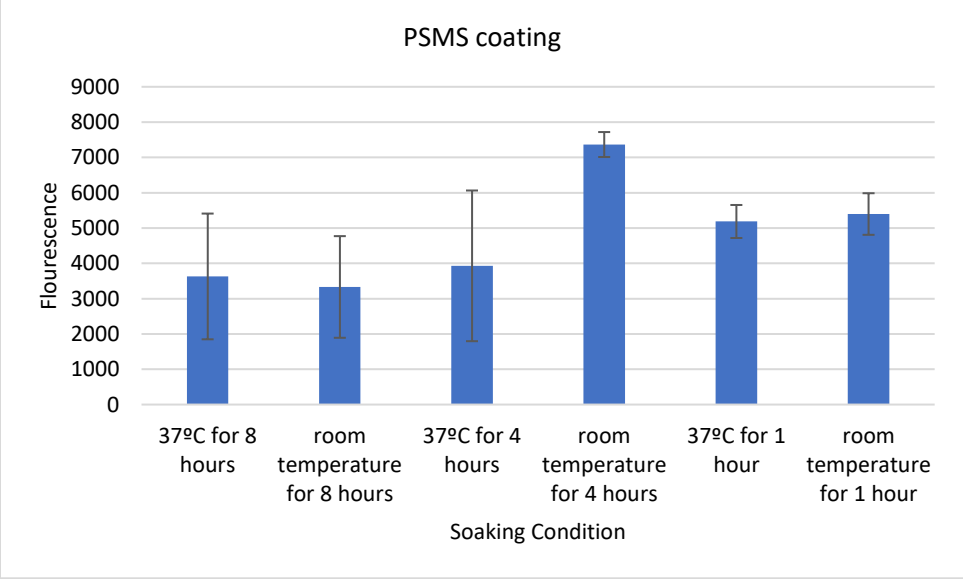

Figure 3.6. PSMS streptavidin-biotin incubation method.

3.2F Electrode response to protein coated polymicrospheres

The use of PSMS was tested to determine the electrical response with SBS nanofiber electrodes. The idea behind using the PSMS was that the use of a larger volume of material would increase the consistency and the magnitude of the impedance response. The use of microspheres was compared to the response seen with the use of only proteins without microspheres. The method used was similar to what was described above. 10 μm microspheres were first coated with streptavidin (50ug/mL) and allowed to incubate for 4 hours. After a wash step, biotin was added to the surface of streptavidin coated microspheres. During microsphere coating, streptavidin (50ug/mL) was immobilized on the surface of SBS electrodes. Electrical response was measured after the incubation of biotinylated microspheres on electrodes. As seen in Figure 3.7, Both groups showed variable electrical response to the addition of biotin (condition A) or biotinylated microspheres (condition B). Both conditions showed higher impedance modulation response for 5μg/mL over five different iterations. However, condition A showed a impedance difference of 5 ohms as opposed to only 3 out of 5 iterations for condition B showing 5 ohms or greater impedance change. The initial testing after five iterations shows that condition B did not increase signal response or consistency. Therefore, it was determined that the microspheres did not enhance overall impedance response of SBS electrodes. Condition A was used for subsequent testing and calibration curves.

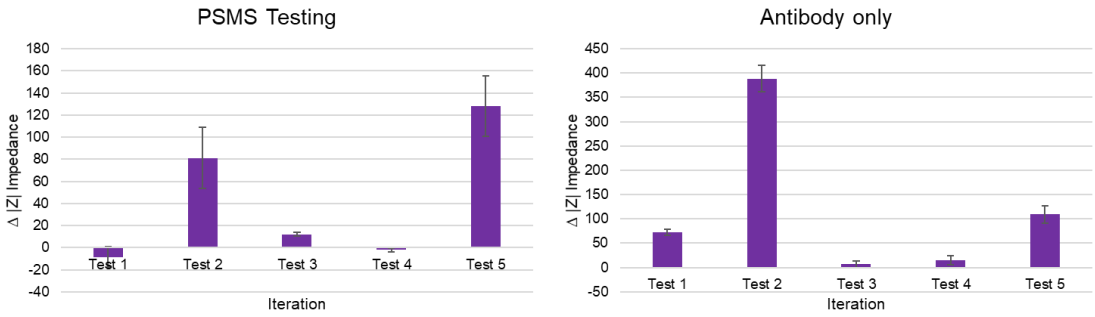

Difference in |Z| after adding 5ug/mL of antigen	Test 1	Test 2	Test 3	Test 4	Test 5
Spike Delta (5/5)	73	388	6.5	14	109
PSMS Delta (3/5)	-8	81	12	-2	128

Figure 3.7. Pilot PSMS impedance response.

3.3 Results and Discussion

3.3A Protein Adhesion

Results from initial protein immobilization study showed that the use of 10% GA provided a great response. However, this concentration also created an instable silane layer on MWCNT/PLA material where cracking and red silane precipitation was seen at this concentration. 10% group provided the generated the greatest protein adsorption with the exception to the 30min UV ozone treatment group. As seen in Figure 3.8, the 2% APTES treated samples provided a significantly higher protein adsorption than the 5% group. This was also seen over the 1-hour incubation time period as well. The effect of UV treatment can be seen qualitatively were increased exposure time significantly increased protein uptake. Initial impedance testing was done using the 2% APTES and 1 hour UV/ozone exposure time. Testing was also done via physical adsorption (0% APTES) with a 1-hour UV/ozone treatment.

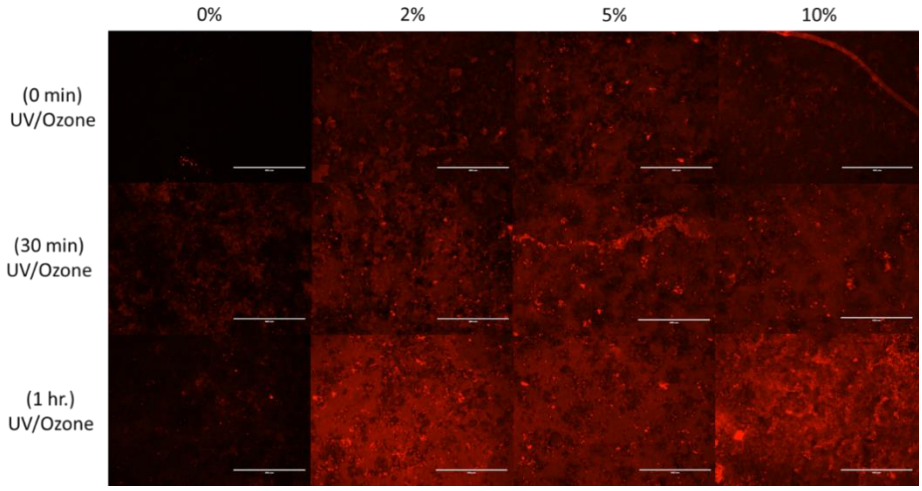

Figure 3.8. Fluorescent microscopy of MWCNT/PLA SBS nanofiber sheets. Scale bar equates to 400 microns. Protein used was Streptavidin Alexa-flour 594 with UV/Ozone treated SBS nanofibers.

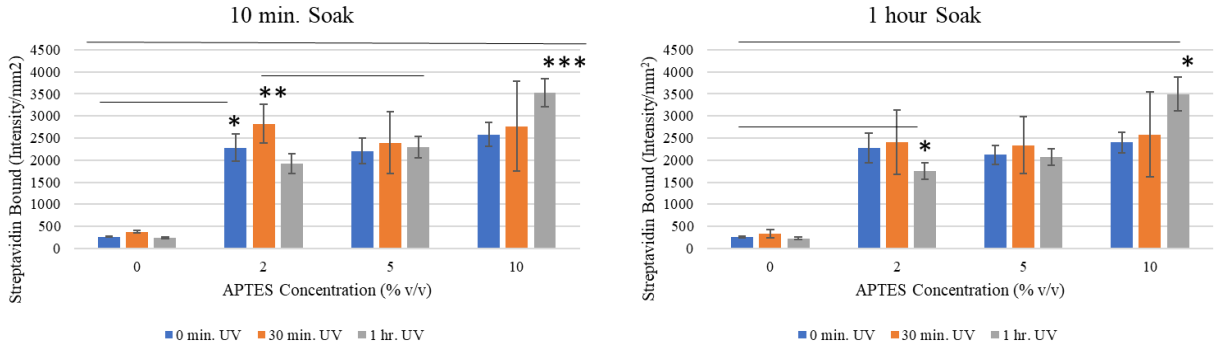

Figure 3.9. Streptavidin 594 UV/Ozone treated SBS nanofibers ImageJ data.

The samples were previously immobilized and allowed to soak in PBS for 1 hour over 0 – 200 ug/mL of Alexa Flour streptavidin. The results show that over a 1 hour soaking time the physically adsorbed samples desorbed proteins significantly more than the APTES treated samples.

3.3B Electrode performance

The immobilization of proteins depends on the surface properties of the solid support. Additionally, the impedance of the surface is also altered due to the introduction of functional hydroxyl and carboxyl groups, which increases the surface energy and improves the adhesion properties of surfaces as can be seen in the above study. The wettability of SBS MWCNT/PLA

nanofibers were altered with the use of a UV/Ozone system. The extent of wettability was tested using water contact angle and the corresponding impedimetric response can be seen in Figure 3.10. As shown in Chapter 2, SBS MWCNT/PLA nanofibers are predominantly hydrophobic in nature due to the presence of hydrophobic PLA material. This can be a good property due to the protein and surface bonding that can occur through hydrophobic forces. Soaking the samples in a solution of capture probe can allow for great interaction. However, for biosensor development sample and capture element concentration and volume can be limited. As a result, drop coat method of smaller volumes are typically used as a way to preserve capture probe and sample concentrations. Water contact angle of nanofibers were reduced from greater than 100 degrees (hydrophobic) down to less than 40 degrees (hydrophilic) with 0 to 120 min. treatment cycle, respectively. As a result of the UV treatment, the impedance response in PBS was also altered. The impedance of electrodes decreased with increasing exposure time where the response begins to plateau between 30 and 60 min. The reduction in the impedance response is a result of increase surface energy and the electrode surface adsorption of PBS unto the surface resulting in a lower impedance value.

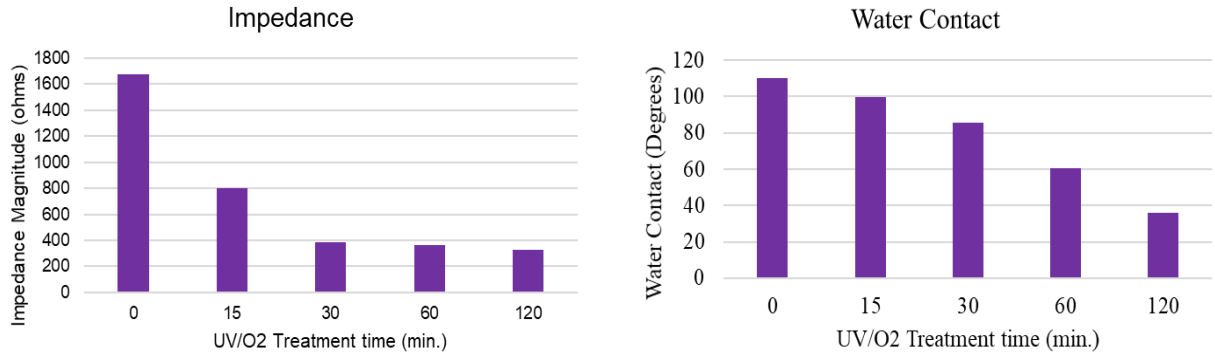

Figure 3.10. Water contact angle and corresponding impedimetric response of UV treated samples.

The electrode fabrication was examined in PBS to determine the amount of noise associated with carbon electrodes. As seen in Figure 3.11, the version 1 electrode utilizes a silver

backing layer that is then coated with SBS MWCNT/PLA whereas the version 2 design uses only carbon without the silver backing. Initial wash step and dry cycle was tested with version 1 electrodes. The first and second PBS wash step produced little to no percent change to the impedance response. Additionally, the dry time post PBS wash step also showed limited change in the electrodes. A 2 min. dry cycle was used for subsequent studies. A nitrogen dry step was used to determine the extent of change. The nitrogen step would be a faster dry process but provided considerable impedance change. Thus, a 2 min. RT dry cycle was used as opposed to the nitrogen drying process. Figure 3.12 shows that the dry cycle of the version 1 had a lower impedance change than that of version 2. One thing to consider here is that the use of carbon only (version 2) would provide a better insight to protein adsorption, but also increase the background noise due to the thin connection contacts of the carbon region. Version 1 electrodes utilize a silver pattern that is more mechanically stable and provides less background noise. Version 2 electrode generated a higher background noise upon each wash step and as a result the authors decided to utilize the version 1 setup with the silver backing.

Description of step	Percent difference	Delta
First PBS wash	0%	0.052733
Second PBS wash	1%	1.616667
2 min. dry cycle	1%	2.377067
5 min. dry cycle	2%	5.261867
First Nitrogen dry	9%	23.3458
Second Nitrogen dry	7%	21.73673
First DI water wash	1%	2.331733

*Values above measured with design 1 version 1

Design 1 version 1 Design 1 version 2

Figure 3.11. Electrode configuration and background noise with washing and drying step.

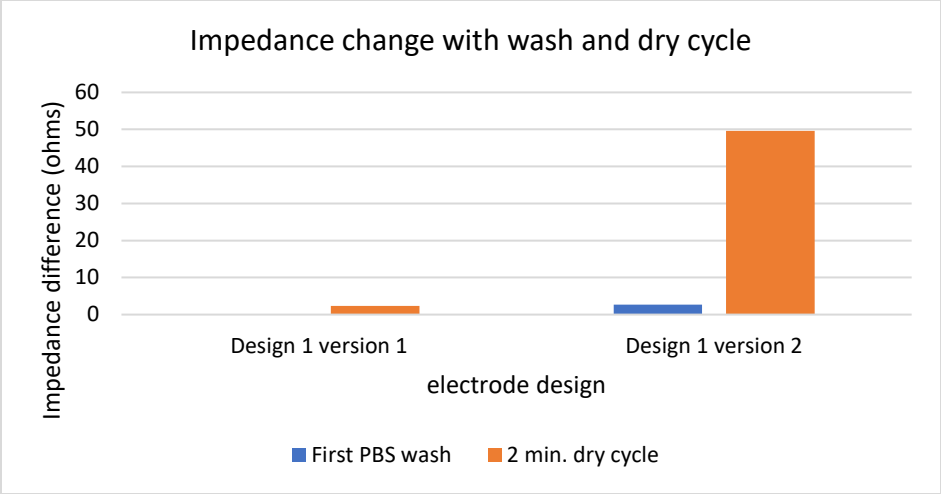

Figure 3.12. Background electrical noise in PBS.

3.3C Biosensor performance

The initial biosensor performance was done with the use of anti-spike:spike protein system. The initial impedance response of bare electrodes and anti-spike was tested over 200 – 2000 Hz to determine the optimal frequency to use with the LCR meter. There is a considerable change between each immobilization step at 200 Hz. This response diminishes over higher frequencies. Additionally, with each progression of immobilization the impedance response at 200 Hz gets smaller. This could be a function of protein concentration and also a function of surface coverage. As seen in Figure 3.13, the salinization step increases the impedance response. This is due to the formation of APTES film on the carbon surface that impedes the flow of current. Electrical response was tested over approximately 5 min.

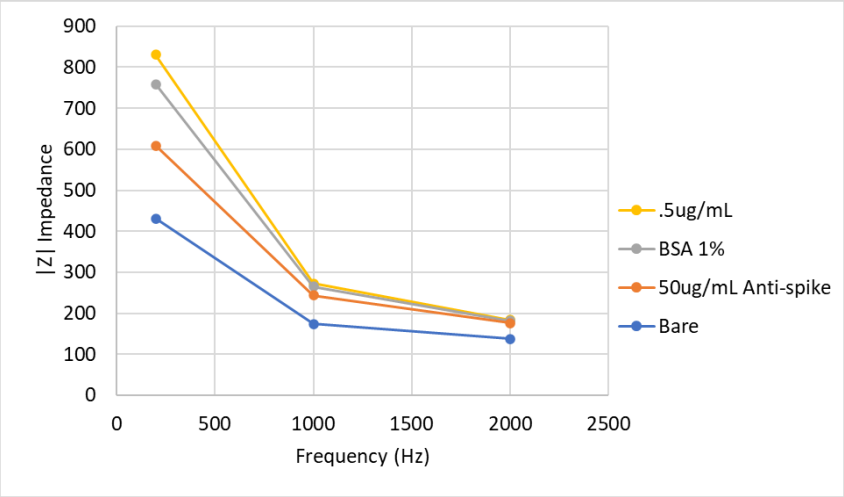

Figure 3.13. Impedance response of spike protein across various frequencies.

The curves in Figure 3.14. shows the response of electrodes to subsequent immobilization of spike proteins on the surface of electrodes over .5 – 1.5 ug/mL and a 1% BSA blocking step. The salinization of the carbon layer provides a good stable signal response over the testing range. The immobilization of the antibodies on the surface of electrodes caused an increase in signal response as was seen in earlier results. There is a considerable drift in the impedance magnitude upon immobilization of the antibodies on the surface. This could be a function of protein folding and also protein charges on the surface of the electrode causing a synergistic response to increase impedance (protein mass) and increase conduction (protein folding, surface charge). The PBS testing solution could also be an influence on the impedance drifting as there was a decrease in impedance with the negative control (NTC).

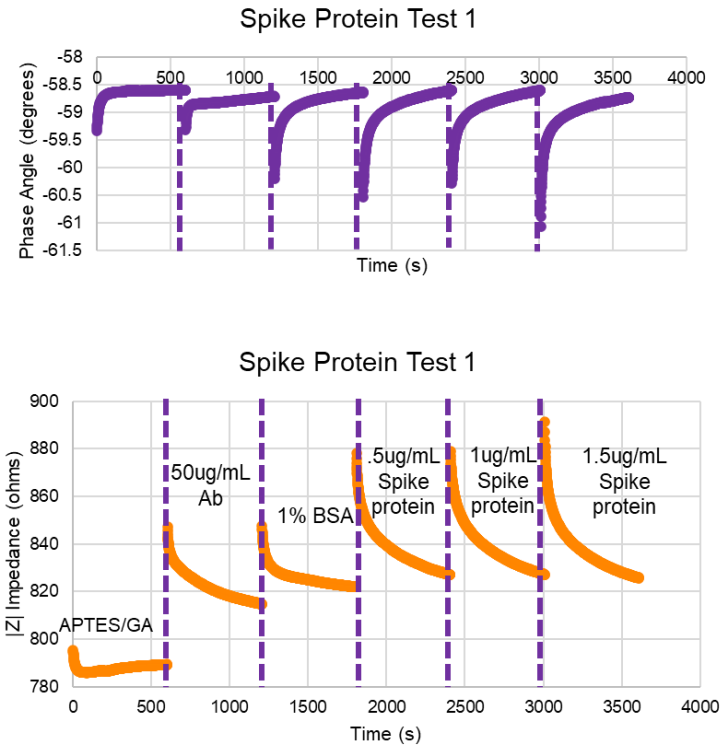

Figure 3.14. Real-time spike protein response.

The impedance response was averaged out over each concentration and can be seen in the curve below. The average response at each concentration was plotted over the tested concentrations. The impedance increased over 0.5 and 1 ug/mL. However, the response showed a slight decrease at 1.5 ug/mL. In order to test if the signal is saturating or found equilibrium at 1.5ug/mL, the authors tested a higher initial concentration with a negative control as seen in Figure 3.16.

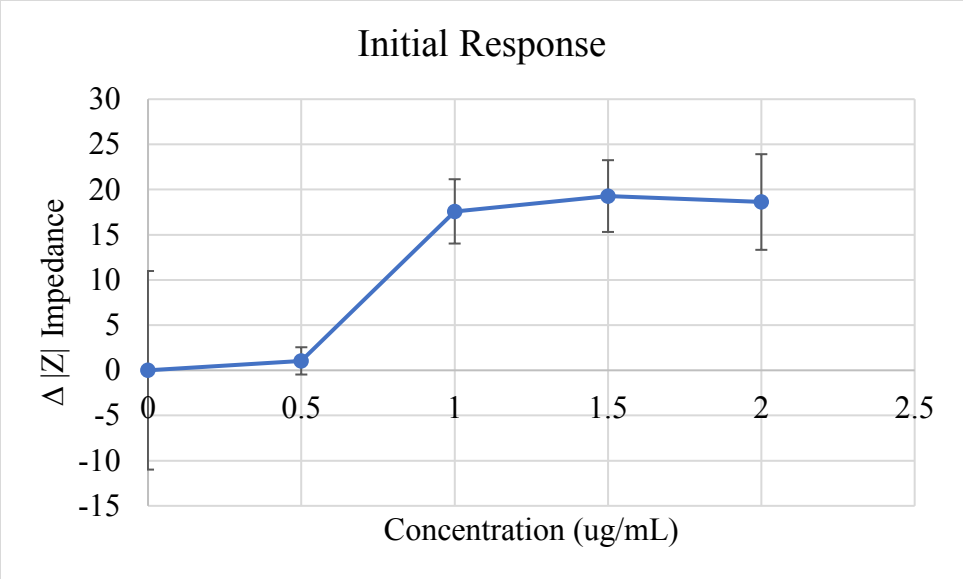

Figure 3.15. Corresponding standard curve of spike protein using chemically adsorbed antibodies.

The impedance response at .5 ug/mL increased and reached a plateau at approximately 1.5 ug/mL. 2.0 ug/mL was added and also followed the same trend. The NTC group saw a reduction in signal response over each immobilization step confirming the treatment group signal response. Overall, sensor performance against spike protein with the use of rabbit anti-spike was good as there was a significant difference between the control and treatment group. As seen in Figure 3.16, three calibration curves were generated to assess sensor performance across various electrodes. Calibration 1 shows a linear response to spike protein over 5-15 µg/mL with a slight saturation between 15-20 µg/mL. Calibration curve 2 increased in signal response at 5 µg/mL with a slight desorption at 10 µg/mL with a saturation region after subsequent concentrations of spike protein. As seen in the negative control response, there is a slight decrease over concentrations. The slight reduction in impedance response seen in calibrations 1 and 2 are simply indicative of inherent signal drift as seen in control. A similar response is seen in calibration 3 with 10 µg/mL being the equilibrium concentration and there is a slight drift in signal response over higher concentrations.

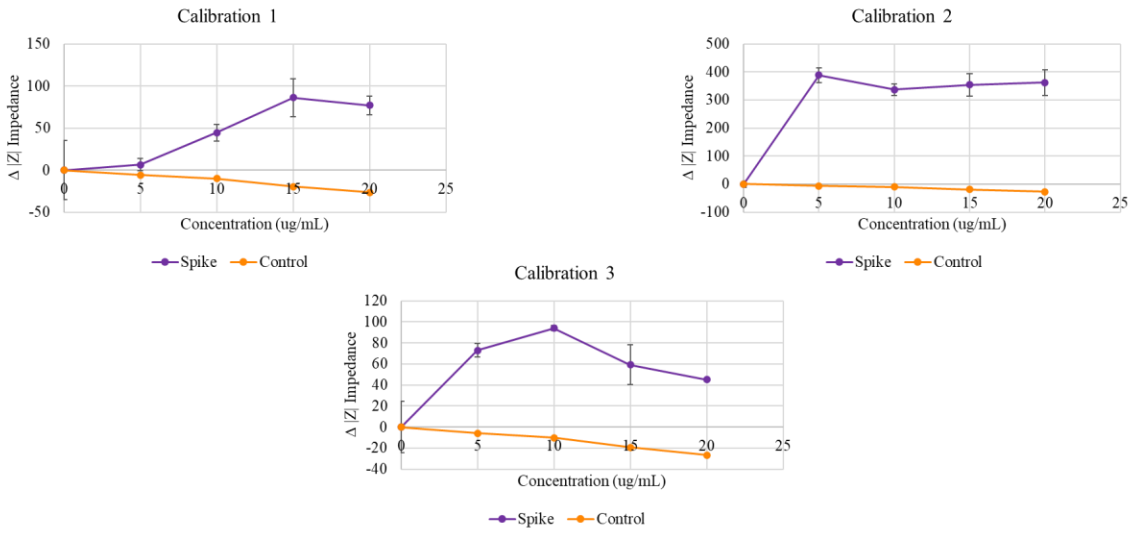

Figure 3.16. Corresponding standard curve of spike protein using chemically adsorbed antibodies.

The next goal of the study was to optimize the blocking step and determine if 1% BSA (10,000 µg/mL) is needed in order to perform as an effective block concentration. BSA concentration between 0-10,000 µg/mL was tested. Figure 3.17 shows that 1ug/mL BSA induced a 10-ohm difference from the control and 10ug/mL produced an additional 4-ohm difference in signal response to additional BSA. 100µg/mL produced an additional 20-ohm difference where it is suspected that this is where the equilibrium concentration lies. 1000 and 10,000µg/mL produced little to no impedance increase. This response indicates that 100 µg/mL is where the greatest impedimetric change is seen. Therefore, this is the concentration that is used for the optimized blocking step.

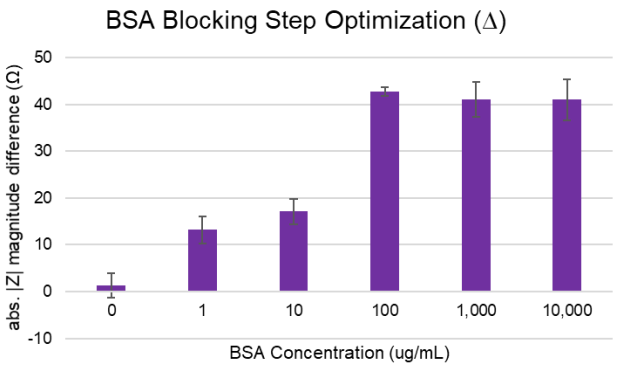

Figure 3.17. BSA block step optimization.

Antibody concentration was assessed to determine if there is a greater sensitivity to spike protein due to the availability antibody binding sites. 50 and 100 µg/mL was compared as seen in Figure 3.18. The signal response for the 100µg/mL group was much higher than that seen with 50µg/mL of anti-spike. Additionally, a saturation region is seen much earlier giving indication that the higher antibody concentration increased the binding sites for spike protein binding. The same response can be seen with Test 1 and 2.

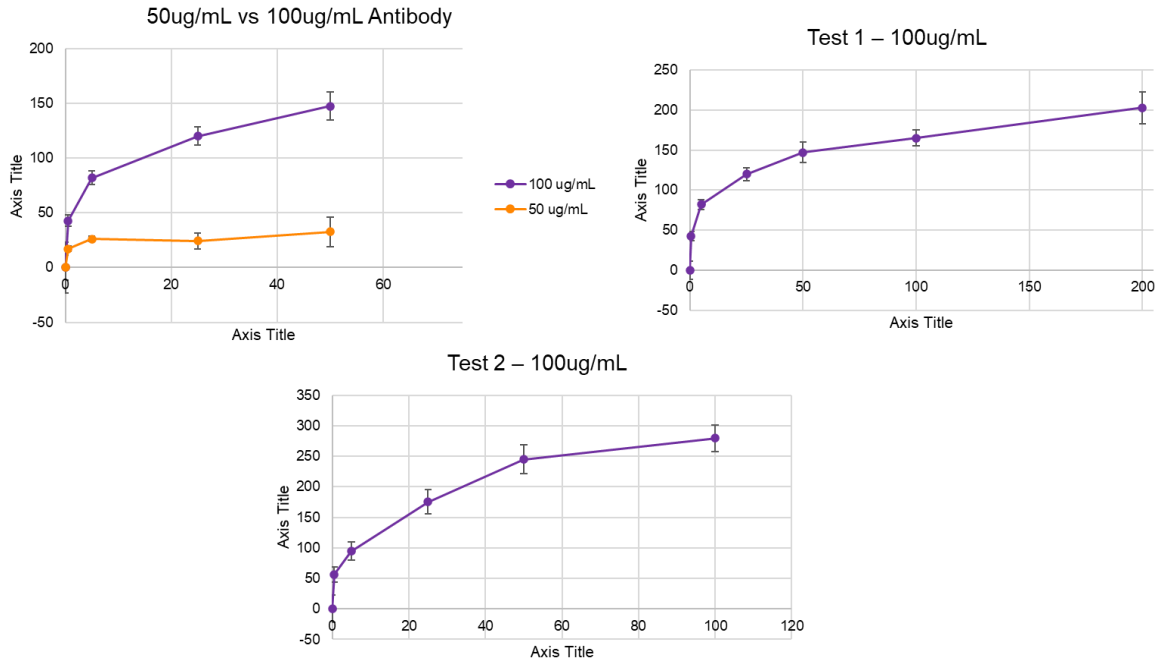

Figure 3.18. Antibody optimization and spike testing iteration 3.

Exclusivity testing was done with various proteins to assess specificity of SBS nanofiber interface to spike protein. Control group only consisted of PBS. As seen in the calibration curves, SBS nanofibers naturally drift. The impedance response in the control group decreased impedance response. Vascular endothelial growth factor (VegF) protein is a protein that is a signaling protein that increases the production of new blood vessels. This is a common protein that could be found in wearable applications. The SBS nanofiber interface was specific to spike protein as the VegF protein did not induce an impedance change higher than the threshold shown in Figure 3.19.

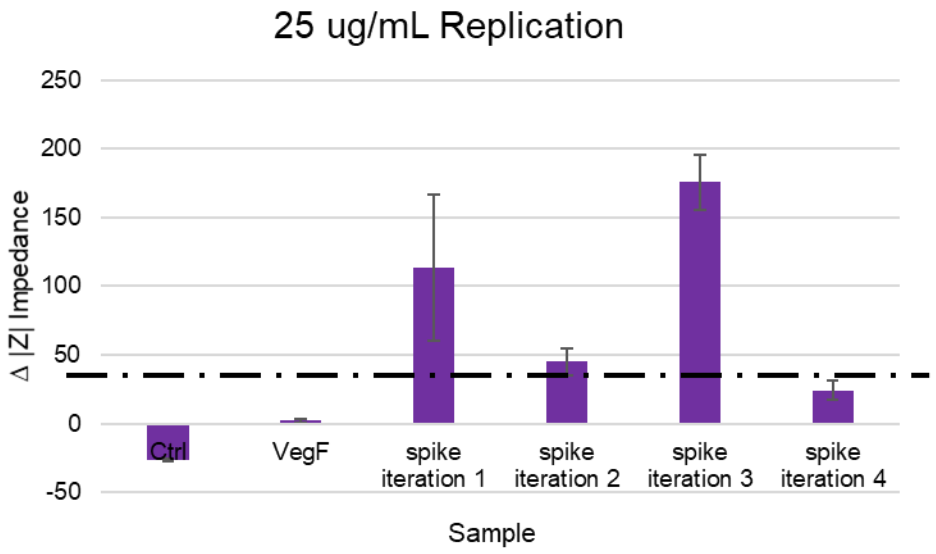

Figure 3.19. Exclusivity test

3.4 Conclusion

As scientist and engineers continue to advance low-cost material for electrochemical immunosensors, the application of solution blow spinning and similar nonwoven technologies remain a viable option for developing advanced low-cost biosensing interfaces. Due to the various factors involved in developing biosensing scaffolds, it is important to consider a nanofiber interface that can be modulated to address various applications such as wearables. The work outlined here shows that the surface medication, immobilization method, blocking, and antibody

concentration play key roles in the modulation of impedance response and protein uptake for SBS nanofiber PLA:MWCNT constructs. This nanofiber fabrication and immobilization technique may be successfully modified to address a multiple biosensing factors *in vitro* and *in vivo*. Results for impedance response to protein shows that protein binding creates an increase in the surface resistance and induces a noticeable impedance change. Not shown, there was a need to test several electrodes for each experiment/run. Thus, it is evident that the results obtained with the resistance-based sensor were not ideal. As some instances there was an impedance change and in other scenarios little to no impedance change was seen. There are a few possible explanations for this nonideal aspect. Small protein/antibody concentrations may not be large enough to induce an electrical response in impedance that were seen with BCA and fluorescent protein assay. Additionally, changes in the resistance response can be caused by temperature and/or pH fluctuations. Also, applied current to a PBS solution can increase electrons in a solution which could result in solution conduction modulation. Deionized water was tested (not shown) however a lack of conduction also produces even more signal variation. The further development of this work will serve as a way to build a nanofiber scaffold that could be used in a wearable biosensing platform for specific protein detection for various diseases such as diabetes or chronic infections.

3.5 References

1. Clark LC, Kaplan S, Mathews EC, Edwards FK, Helmsworth JA. Monitor and Control of Blood Oxygen Tension and pH During Total Body Perfusion. J Thorac Surg. 1958 Oct 1;36(4):488–96.
2. Layqah LA, Eissa S. An electrochemical immunosensor for the corona virus associated with the Middle East respiratory syndrome using an array of gold nanoparticle-modified carbon electrodes. Microchim Acta. 2019 Apr;186(4):1–10.
3. Welch NG, Scoble JA, Muir BW, Pigram PJ. Orientation and characterization of immobilized antibodies for improved immunoassays (Review). Biointerphases [Internet]. 2017 Mar 16 [cited 2021 Jul 8];12(2):02D301. Available from: https://avs.scitation.org/doi/abs/10.1116/1.4978435
4. Butler JE, Ni L, Brown WR, Joshi KS, Chang J, Rosenberg B, et al. The

immunochemistry of sandwich elisas—VI. Greater than 90% of monoclonal and 75% of polyclonal anti-fluorescyl capture antibodies (CAbs) are denatured by passive adsorption. Mol Immunol. 1993 Sep 1;30(13):1165–75.

5. Rashid JIA, Yusof NA. The strategies of DNA immobilization and hybridization detection mechanism in the construction of electrochemical DNA sensor: A review. Sens Bio-Sensing Res. 2017 Nov 1;16:19–31.

6. Hermanson GT. Enzyme Modification and Conjugation. In: Bioconjugate Techniques. Elsevier; 2013. p. 951–7.

7. Sabdin S, Azraie Mohd Azmi M, Azurin Badruzaman N, Zuriati Makmon F, Abd Aziz A, Azura Mohd Said N. Effect of APTES Percentage towards Reduced Graphene Oxide Screen Printed Electrode Surface for Biosensor Application. Mater Today Proc. 2019 Jan 1;19:1183–8.

8. Bayram L, Guler M. An ultra-sensitive non-enzymatic hydrogen peroxide sensor based on SiO2-APTES supported Au nanoparticles modified glassy carbon electrode. Prog Nat Sci Mater Int. 2019 Aug 1;29(4):390–6.

9. Badruzaman NA, Azmi MAM, Said NAM. Electrochemical immunosensor based on highly sensitive amino functionalized graphene nanoplatelets-modified screen printed carbon electrode. Key Eng Mater. 2020;833 KEM:171–5.

10. Parkash O, Yean CY, Shueb RH. Screen Printed Carbon Electrode Based Electrochemical Immunosensor for the Detection of Dengue NS1 Antigen. Diagnostics [Internet]. 2014 [cited 2021 Jul 10];4(4):165. Available from: /pmc/articles/PMC4665558/

11. Bartczak D, Kanaras AG. Preparation of Peptide-Functionalized Gold Nanoparticles Using One Pot EDC/Sulfo-NHS Coupling. Langmuir [Internet]. 2011 Aug 16 [cited 2021 Jul 10];27(16):10119–23. Available from: https://pubs.acs.org/doi/abs/10.1021/la2022177

12. Liu S, Zhang Z, Wang Y, Wang F, Han MY. Surface-functionalized silica-coated gold nanoparticles and their bioapplications. Talanta. 2005 Sep 15;67(3):456–61.

13. Serrano N, González-Calabuig A, Del Valle M. Crown ether-modified electrodes for the simultaneous stripping voltammetric determination of Cd(II), Pb(II) and Cu(II). Talanta. 2015 Jun 1;138:130–7.

14. Hermanson GT. Bioconjugate Techniques: Third Edition. Bioconjugate Tech Third Ed. 2013;1–1146.

15. S S, K G, M D, A S, N T, M F. A Comprehensive Review of the Covalent Immobilization of Biomolecules onto Electrospun Nanofibers. Nanomater (Basel, Switzerland) [Internet]. 2020 Nov 1 [cited 2021 Jul 10];10(11):1–39. Available from: https://pubmed.ncbi.nlm.nih.gov/33121181/

16. Zhao Y, Xiong J, Shi X, Ko F. Capturing cancer cells using hyaluronic acid-immobilized electrospun random or aligned PLA nanofibers. Colloids Surfaces A Physicochem Eng Asp. 2019 Dec 20;583:123978.

17. F K, J A, M S, J V, S MT, E S, et al. Improved human endometrial stem cells

differentiation into functional hepatocyte-like cells on a glycosaminoglycan/collagen-grafted polyethersulfone nanofibrous scaffold. J Biomed Mater Res B Appl Biomater [Internet]. 2017 Nov 1 [cited 2021 Jul 10];105(8):2516–29. Available from: https://pubmed.ncbi.nlm.nih.gov/27689849/

18. M M, S S, M S, S H, E E, M V. Efficient protein immobilization on polyethersolfone electrospun nanofibrous membrane via covalent binding for biosensing applications. Mater Sci Eng C Mater Biol Appl [Internet]. 2016 Jan 1 [cited 2021 Jul 10];58:586–94. Available from: https://pubmed.ncbi.nlm.nih.gov/26478348/

19. Cai Y, Kang K, Li Q, Wang Y, He X. Rapid and Sensitive Detection of Cardiac Troponin I for Point-of-Care Tests Based on Red Fluorescent Microspheres. Mol 2018, Vol 23, Page 1102 [Internet]. 2018 May 7 [cited 2021 Jul 10];23(5):1102. Available from: https://www.mdpi.com/1420-3049/23/5/1102/htm

20. Deregt D, Furukawa-Stoffer TL, Tokaryk KL, Pasick J, Hughes KMB, Hooper-McGrevy K, et al. A microsphere immunoassay for detection of antibodies to avian influenza virus. J Virol Methods. 2006 Oct 1;137(1):88–94.

21. Bang's Laboratory. Working with Microspheres. 2013;

22. Lin TY, Pfeiffer TT, Lillehoj PB. Stability of UV/ozone-treated thermoplastics under different storage conditions for microfluidic analytical devices. RSC Adv [Internet]. 2017 Jul 24 [cited 2021 Nov 15];7(59):37374–9. Available from: https://pubs.rsc.org/en/content/articlehtml/2017/ra/c7ra07435b

CHAPTER 4

DEVELOPMENT OF SOLUTION BLOW SPUN BIOSENSING INTERFACE FOR THE DETECTION OF VIRULENCE OF GRAM-NEGATIVE PATHOGENS

4.1 Introduction

Gram-negative bacteria passively release low molecular weight acyl-homoserine lactones (HSLs). HSLs are lipid molecules that possess a lactone ring with a carbon side chain that could range from 4 to 16 carbons. These molecules are hydrophobic in nature and their phobicity depends on the carbon chain length. *P. aeruginosa* utilizes the 3-oxo-C12-homoserine lactone (3OC12HSL) to upregulate quorum sensing dependent virulence factors. Figure 4.1 shows a diagram of the many virulent factors that this organism utilizes during infection. The LasR regulator sits at the top of the QS network and induces the transcription of the lasI gene (1). The 3OC12HSL-LasR complex creates a positive feedback loop for the production of additional HSL molecules (2). Additionally, the complex also controls the transcription of many genes that have virulence implications, such as biofilm formation LasA protease, LasB elastase, Apr alkaline protease and *Pqs* (1,3,4). The LasR complex upregulates the remaining three quorum sensing circuits in a hierarchical fashion as seen in Figure 4.2. 3OC12HSL is also a cross-kingdom signaling factor where it has been shown to alter gene expression in plants, create inflammation in mammalian cells, and impede fungal morphology such as hyphae in *C. albicans* (5–7). *P. aeruginosa* utilizes HSLs and a separate class of autoinducer called the pseudomonas quinolone signal (PQS). Once a critical threshold has been reached, HSLs bind to transcription factors in the cytoplasm or cell membrane to activate gene expression and modulate the production of additional signaling molecules (1).

The *las* and *rhl* quorum sensing systems in *P. aeruginosa* initiates the virulence and controls the entire system. Both *las* and *rhl* systems form a protein receptor complex with

3OC12HSL and C4-HSL. These complexes activate their respective promotors for each target gene for transcriptional expression. (1) Additionally, LasR induces the expression of RsaL system, which is a repressor of *lasI*. RsaL binding to *rsaL-lasI* complex promotor inhibits the expression of both *rsaL* and *lasI*. (1)

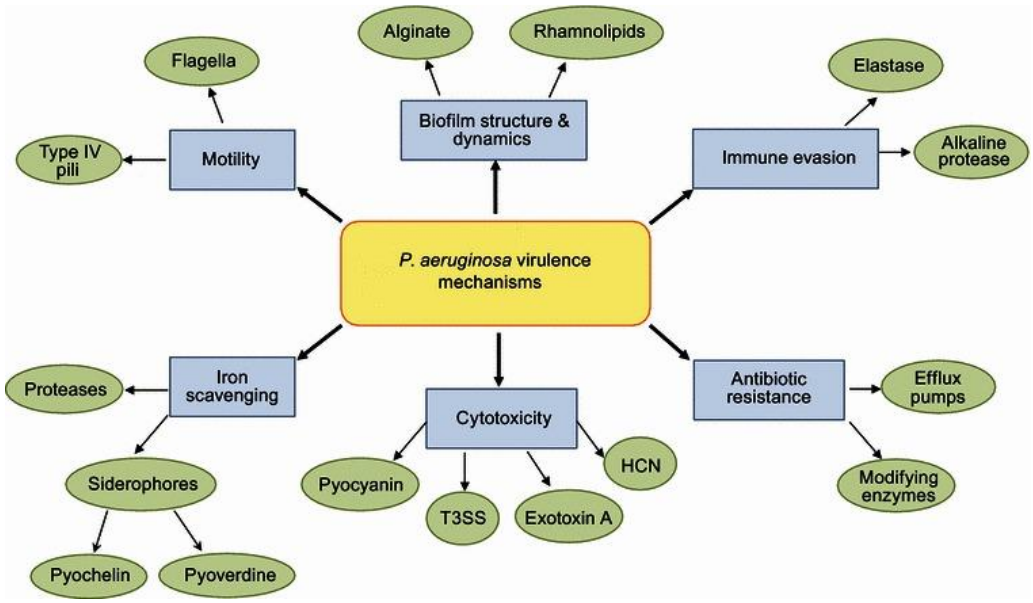

Figure 4.1. *P. aeruginosa* virulence factors. Figure reproduced from Ref. (1).

Point-of-care detection of these signaling molecules would provide clinicians with a great tool to determine the presence of *P. aeruginosa* and other virulent gram-negative bacteria. Conventional detection methods based on culturing and antimicrobial susceptibility testing are time-consuming and do not provide timely results for detection of bacteria. Molecular methods such as antibody, aptamer, or PCR based assays usually require sample preprocessing, expensive equipment, and a trained technician. This is not ideal for resource-limited settings. Biosensors have been developed for in vitro and in vivo applications to include synthetic or intrinsic plasmids or chromosomes from bacteria to detect an output signal (ex. Colorimetric or fluorescent). QS biosensors could be used to detect bacterial virulence prior to the expression of resistant genes,

which could help maintain antibiotic stewardship. Moreover, they could be used to screen novel antimicrobial agents such as quorum quenching molecules or bacteriophages. (2) Chromoproteins can be used as a reporter for transcriptional whole cell biosensors. AmilCP is a chromoprotein that is derived from the coral *Acropora millepora* and exhibits a strong blue/purple visible color at 588 nm. (8) The advantage of using chromoproteins is the ease of use and readout where there is no need for a substrate and a stop solution to end the reaction such as enzymatic detection schemes. Electropsun nanofibers and Whatman paper have been used in the past to immobilize bacteria for various applications. Zamel et al. used electrospun cellulose acetate and PEO nanofibers to immobilize *Bacillus paramycoides*. These nanofibers were used to remove methylene blue for potential wastewater treatment applications. (9) The James Collins group used flexible textiles to immobilize freeze-dried, cell-free biosenors for various applications such as SARS-CoV-2 detection at room temperature within 90 minutes. (10) Additionally, paper strips where used to immobilize biosenors for the detection of quorum signaling molecules such as HSLs.(11)

In addition to HSLs, *P. aeruginosa* specifically produces PYO which is a redox active molecule and virulence factor. There are two QS systems that are responsible for the upregulation of pyocyanin: Rhl and PQS. Briefly, pyocyanin is synthesized from a chorismate precursor that is converted to phenazine-1-carboxylic acid (PCA). Pyocyanin has a symmetrical peak around -.16 to -0.3 V and an irreversible oxidation peak at + 0.8V.(2) This redox molecule is responsible for persistent oxidative stress and premature senescence in mammalian cells. (12) *P. aeruginosa* is commonly found in both acute and chronic nosocomial infections found in burn wounds and patients with cystic fibrosis. (13,14) Additional efforts were made in the following chapter to produce inexpensive electrodes to detect PYO.

Research Questions:

1. To what extent does screen printed electrodes and SBS parameters affect electrochemical performance of redox reactions?
2. To what extent does SBS allow for electrochemical sensing of Pyocyanin from *Pseudomonas aeruginosa* cultures?
3. What is the reaction time and amilCP production of whole-cell bacteria on solid media versus suspended cultures?
4. To what extent does SBS constructs provide a scaffold for immobilized and functional amilCP-101 whole-cell biosensor?

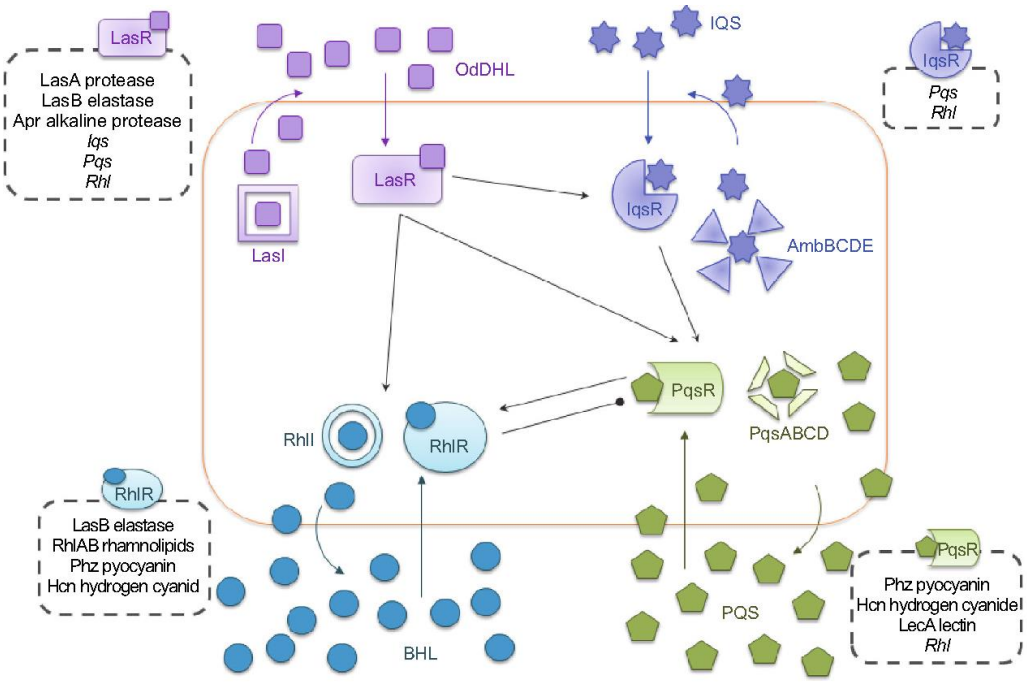

Figure 4.2. Hierarchy quorum sensing network utilized by Pseudomonas aeruginosa. (1).

4.2 Materials and Methods

4.2A Whole cell biosensor strain, medium and chemicals.

Biosensor containing a kanamycin resistant LasR-based plasmid (pFNK-503-qscrsaL). Plasmid constitutively expresses LasR from a *p(lacIq)* promotor. LasR forms a complex with

3OC12HSL which activates the *p(las)* promotor to express the GFP(LVA) (15,16). LasR Plasmid construct is contained within *E. coli E. coli* TOP10. This initial design was tested and used for the development of LasR system with amilCP reporter. Culture plates were made with Luria-Bertani (LB) Agar, Miller (Tryptone 10 g, yeast extract 5 g, sodium chloride 10 g, and Agar 15 g). 50 mg/mL kanamycin stocks were made using filter sterile water. A 1000-fold dilution of kanamycin (50 ug/mL) was used to make LB Agar, Miller plates. The *E. coli* glycerol stocks were T-streaked on Kanamycin plates and allowed to grow colonies overnight at 30 C. Desired colonies were cultured in 2 mL of LB broth containing 50 ug/mL kanamycin and allowed to grow overnight shaking at 30 C.

4.2B Homoserine stock solution and pathogenic bacteria strain

Biosensor response and performance was testing against synthetic and pathogenic homoserine lactones. Synthetic 3OC12HSL were reconstituted in DMSO and stored at -20 C. 100 uM stock solutions of 3OC12HSL were made in 30% ethanol solution for further analysis. Pathogenic bacteria *P. aeruginosa* PAO1 was used to assess biosensor functionality with pathogenic homoserine lactone production. Culture supernatant was collected by centrifugation after cells reached a concentration of OD_{600} between 1 – 3 in LB broth.

4.2C Construction of expressed plasmid

GFP(LVA) gene was removed from original pFNK-503-qscrsaL plasmid and the p15A origin of replication (ori) was amplified leaving the T1 terminus. Kanamycin and lasR regions were also amplified with complementary overlapping ends to the amplified BBa_K592009 insert. pFNK-503-qscrsaL and BBa_K592009 plasmids were both isolated using Zyppy-plasmid miniprep-kit (Zymo Research). Briefly, ceslls were grown and spun down in a 1.5 mL tube for 3 min at 6000 rpm. Pellets were placed on ice followed by prep protocol. The 260/280 OD reading

was taken and recorded for PCR and assembly steps. Primers used in this study were purchased from Eurofins and are shown in Table 4.1. Primers were provided in a dry salt-free lyophilization form that was reconstituted in TE buffer at a 250 uM stock. Stock solutions were diluted to 10 uM working stock. KAPA Taq ReadyMix PCR kit (kk1006) and iproof Hifi master mix were used and PCR cycling was completed according to manufacturer's recommendation. Gradient PCR was done for the annealing step in order to determine best amplification. After amplification, amplicons were ran on a gel with Bluegel minipcr to determine correct size prior to assembly step. As seen in Figure 4.3, the respective vector (3024 bp) and amilCP insert (700 bp) can be seen. DpnI digestion was used to remove methylenated DNA from reaction. The use of DpnI created sharper and brighter bands. NEB Hifi DNA assembly master mix was used to ligate complementary overlapping ends. *E. coli* DH5α cells were used for transformation of constructed plasmid. Competent cells were placed on ice for 20 min. 3 uL of assembled DNA was added to the cells and incubated on ice for 20 min. Cells were then heat shocked at 42 C for 30 sec. and placed back on ice for 2 min. 400 uL of LB agar (without antibiotics) was added to the cells and were allowed to outgrow by incubating for 1 hour. Cells were then plated and allowed to grow overnight, and colonies were screened using kanamycin 3OC12HSL loaded plates and chosen for further studies.

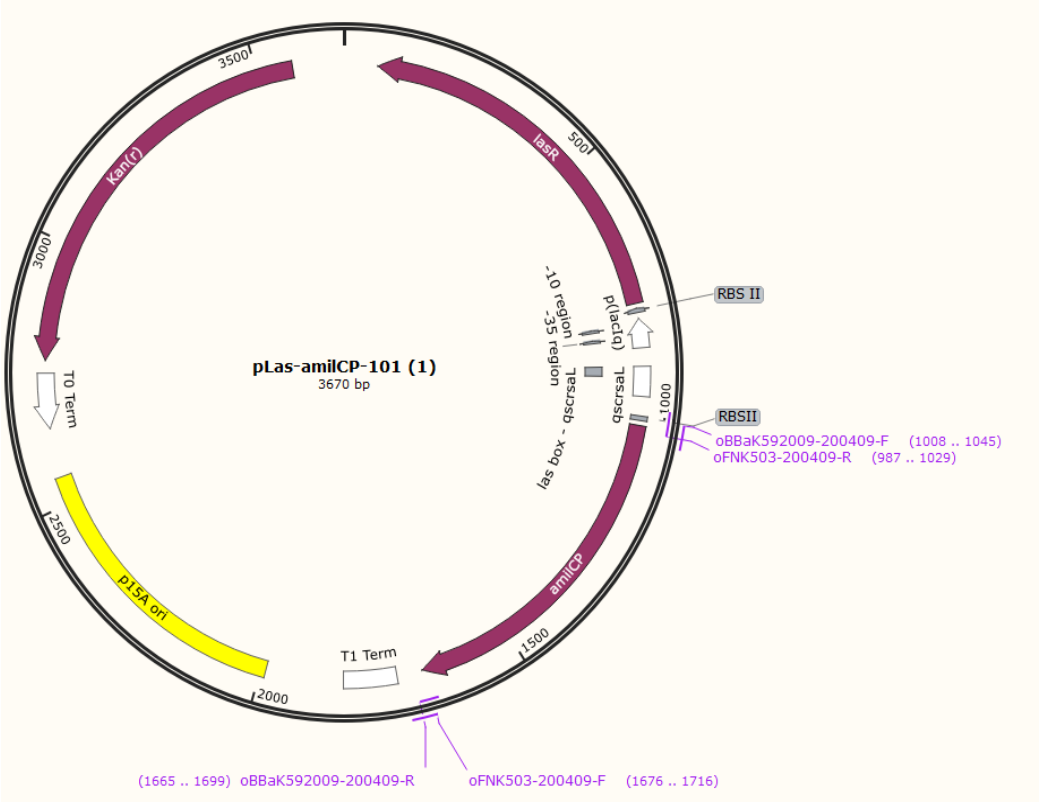

Figure 4.3. Schematic of the plasmid pLas-amilCP-101 constructed for 3OC12HSL detection with chromoprotein reporter.

Table 4.1. Primers used for amilCP reporter construction		
Name	**Sequence**	**Tm**
oFNK503-R	atcacactcatgcttaatttctcctctttaattctaggtaccc	69.4
oBBaK592009-F	agaaattaagcatgagtgtgatcgctaaacaaatgacc	70.4
oBBaK592009-R	taattaagcttattattaggcgaccacaggtttgc	66
oFNK503-F	gtcgcctaataataagcttaattagctgacctactagtcgg	67.3

4.2D Characterization of biosensor with GFP and AMILCP reporter

Single colonies of the initial pFNK-503-qscrsaL *E. coli* Top 10 biosensor were used before performing plasmid construction of amilCP reporter plasmid. Colonies were inoculated into 3 mL

of LB broth (20 ug/mL kanamycin) and incubated in a shaking incubator at 30 C and 250 rpm. The culture was then used in initial 3OC12HSL testing. 20 uL of culture was added to each of 2mL of twelve 3-fold serially diluted 100 uM of 3OC12HSL. 200 uL was then transferred to a well plate in triplicates and incubated at 37 C. Original pFNK-503-qscrsaL *E. coli* Top 10 biosensors were imaged and the relative fluorescence was measured and normalized to the OD_{600}. The amilCP-101 biosensor was imaged with a plate reader and the max absorbance at 588, 600, and 700nm was measured and used to monitor amilCP production quantitatively and visually.

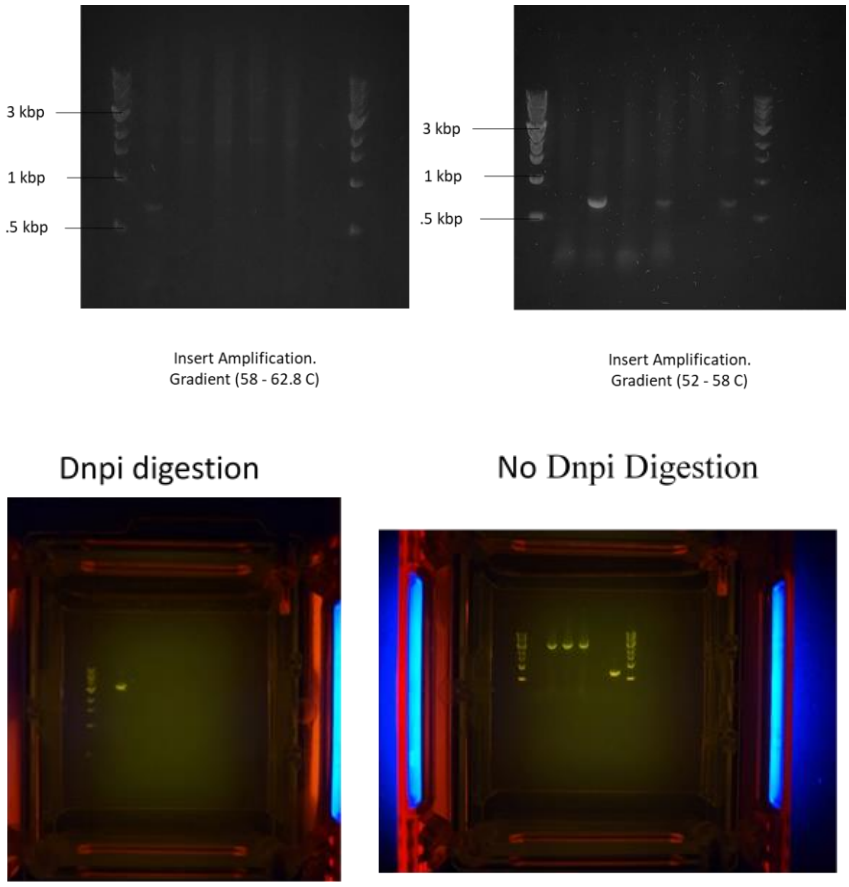

Figure 4.4. Gel runs of Plasmid.

4.2E Construction of SBS-based 3OC12HSL assay

12% PLA nanofibers were solution blow spun on PET film from solutions containing PLA and Chloroform using a feed rate of 100/hr., air pressure of 30 psi and deposited on glass slides fixated on a rotating collector drum. The fiber matrix was then used as a stabilizing matrix for bacterial immobilization. Similar to surface treatment done for $AgNO_3$ impregnation (Aim1), ethanol solution was used to introduce OH- groups to surface prior to bacterial immobilization. Overnight *E. coli* DH5α cultures were dropped on the mesh via dropwise method and incubated at 37^{o}C. Various 3OC12HSL concentrations in LB were then dropped on surface and allowed to react with cells overnight.

4.2F SBS electrodes for PYO detection

PLA pellets (Mn = 75,000 g/mol) were purchased from Jam Plast Inc., Ellisville, MO, USA. Chloroform (CHCl3 CAS 67-66-3), MWCNT (CAS 308068-56-6), Pyocyanin (CAS 85-66-5), Potassium Ferricyanide (CAS 13746-66-2), silver paste (901769) and Silver Nitrate (CAS 7761-88-8) were purchased from Sigma Aldrich, St. Louis, MO, USA. Phosphate buffer saline (PBS) was purchased and used for pyocyanin dilutions. Deionized water (18.2 M Ω.cm) was used for all media preparation. Lysogeny broth was purchased from Thermo Fischer. Custom made solution blow spinning apparatus was used to fabricate fiber mats.

The morphology of sensor construct was examined with the use of a scanning electron microscope (SEM). SEM 4800 was used to examine morphology of fiber mats. Platinum coating was deposited on samples to provide better imaging contrast.

SBS electrodes were made with a three-step process. First, PLA solution was deposited on a Polyester (PET) film to form a SBS PLA base layer. Flexible silver ink was used to screen print silver layer on SBS PLA base layer. In order to provide a carbon layer, an SBS-stencil based

method was explored. Briefly, PLA/MWCNT solution was dissolved in chloroform and mixed for 24 hours to encourage carbon dispersion. Versa laser printer was used to construct a three-electrode pattern mask. Mask was placed over SBS silver screen printed layer and SBS with PLA/MWCNT composite to form an SBS-based carbon electrode.

SBS-based sensors were characterized using IO Rodeostat potentiostat. Electrochemical characterization was done in a 50mM of ferricyanide in PBS (pH = 7.0) solution. Cyclic voltammetry was used between -1.0 to + 1.0 V to detect the change in peak current between 50 to 500 mV/s. Pyocyanin concentration ranging between 0- 300 μM was calibrated using square wave voltammetry (SWV) between -0.7 to -.1V with an amplitude of 50 mV. The current peak from each SWV graph was used for calibration curve. The repeatability of three electrodes were examined between 0 – 50 μM.

P. aeruginosa PAO1 was T-streaked on a petri dish and grown overnight at 37˚C. Cultures were resuspended in LB media (3 mL) and allowed to grow in the presence of silver nitrate (.1 – 10 μM). Optical density and SWV measurements were done on bacterial supernatant after 24 and 48 hours. Optical density measurements were done to detect a change in the peak absorbance at 311 nm to confirm the presence or absence of pyocyanin in bacterial supernatant.

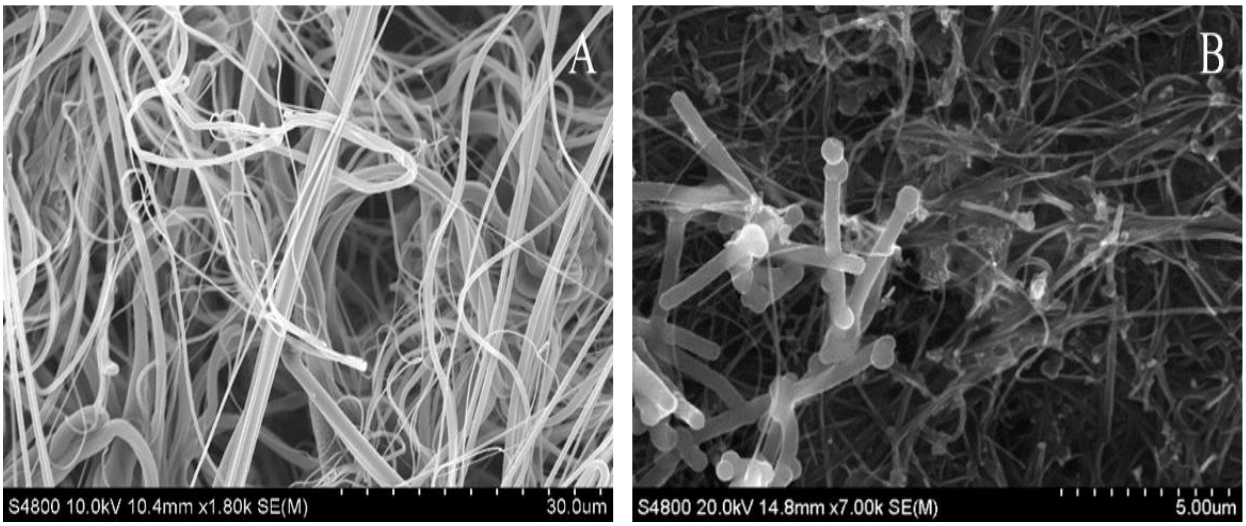

Figure 4.5. SEM of SBS electrode layers. (A) SBS PLA Layer (B) SBS Carbon sensing layer Electrode Fabrication.

Fabrication and Morphological features of SBS electrodes. Figure 4.5 shows the SEM of the SBS substrate (Figure 4.5A) and the Carbon Sensing layer (Figure 4.5B). The carbon sensing layer displayed smaller fiber diameter distribution and with a tighter porosity structure. Whereas the SBS substrate layer with 12% PLA displayed a higher fiber diameter distribution and wider fiber porosity. The electrode fabrication process can be seen in Figure 4.6. As outlined in the methods section. The fabrication of electrodes was done with a three-step process. Solution blow spinning of PET film with PLA, Screen printing silver pattern, SBS carbon layer via laser printed mask. Figure 4.7 and 4.8 shows the electrochemical performance of fabricated electrodes in 100 mM of potassium ferricyanide. The data showed a linear relationship between peak current and scan rate. Additionally, the electrochemical response of electrodes in hydrogen peroxide and ferrocene solution showed good electron transfer as seen in the CV on Figure 4.9.

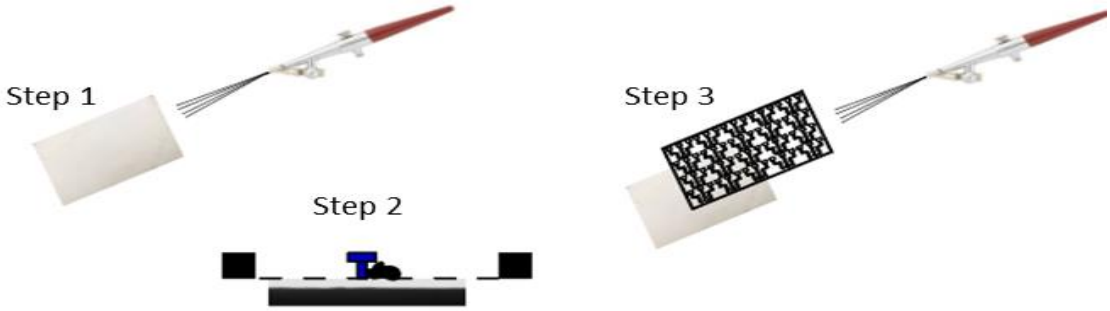

Figure 4.6. Fabrication of SBS-based electrochemical electrodes.

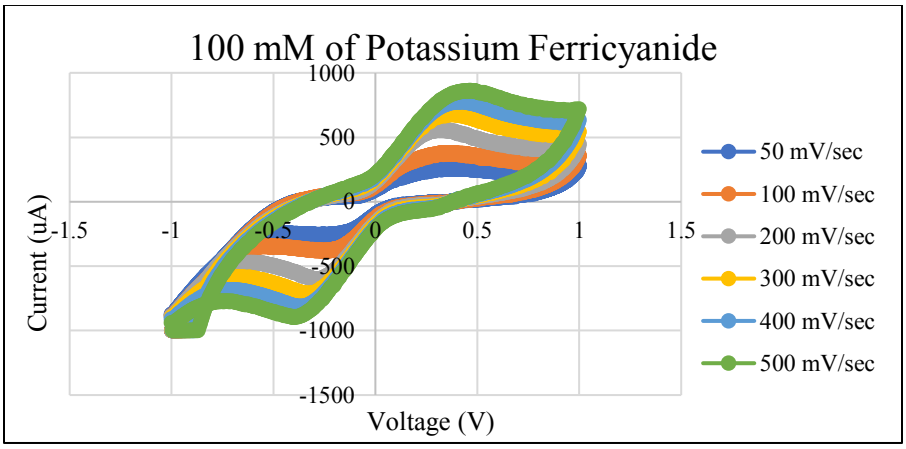

Figure 4.7. Electrochemical performance of SBS-based electrode in 100 mM of Potassium Ferricyanide. Cyclic Voltammetry of Potassium Ferricyanide (a) Current vs square root of scan rate (b)

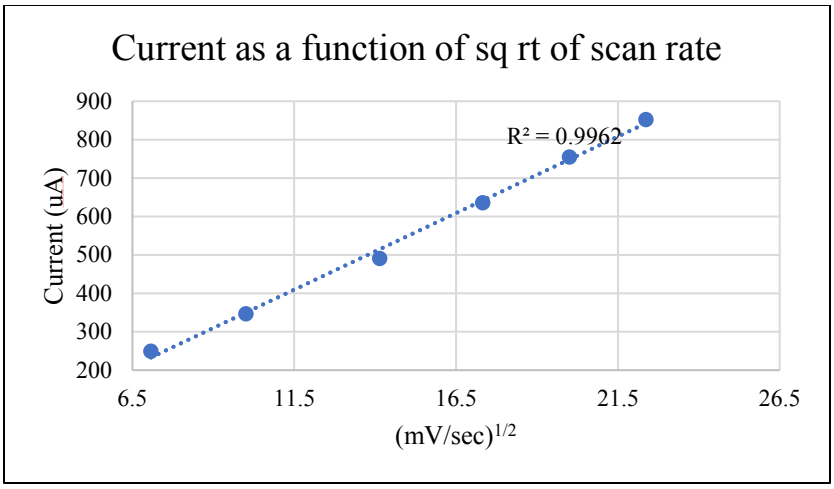

Figure 4.8. Electrochemical performance of SBS-based electrode in 100 mM of Potassium Ferricyanide. Cyclic Voltammetry of Potassium Ferricyanide (a) Current vs square root of scan rate (b)

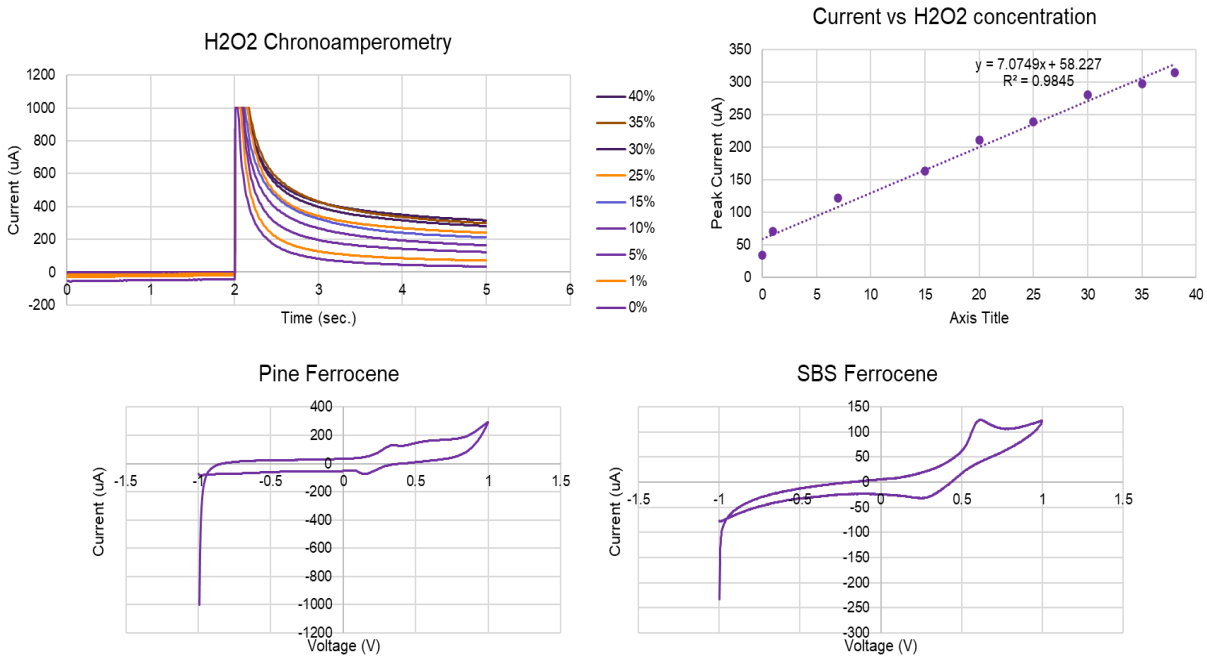

Figure 4.9. Electrochemical response of SBS electrodes in hydrogen peroxide (Top) and Ferrocene (bottom).

4.3 Results and Discussion

4.3A Pyocyanin detection via SBS electrodes

Conventional methods for the detection of pyocyanin molecules is the use of spectrophotometry and Mass Spect methods. As seen in Figure 4.8, the presence of pyocyanin exhibits a peak absorbance between 200 to 700 nM. The 311nM wavelength was chosen to measure the initial pyocyanin concentration in PBS. There is a linear correlation between the concentration of pyocyanin and the 311 nM wavelength in PBS. However, this was not seen in LB media as the peak absorbance at 311 nM saturates between at 75 uM and below.

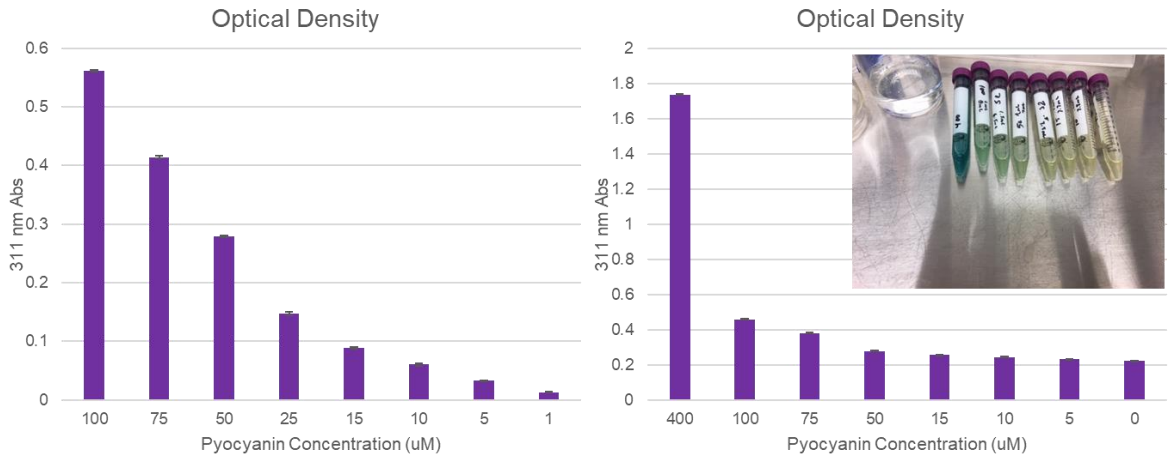

Figure 4.10. UV-vis Spectrum of PYO

4.3B Pyocyanin detection via SBS electrodes

Figure 4.11 shows the cyclic voltammogram of pyocyanin and the blank PBS control as can be seen from the graph there was little to no background noise from the control solution as there was a flat curve between the applied potential range. With the addition of 50uM of pyocyanin. The electrodes showed a reversible peak between -.5 and -.1 V. This is where the reversible redox reaction occurs with the molecule. The signal to noise ratio between the blank and 50 uM of

pyocyanin at -.3V was 8.3. Where the SNR using commercial pine electrodes under similar conditions was (8.7). This shows that the SBS electrodes can detect this molecule with a similar performance. Additional irreversible peaks can be seen at 0V and near +1V. These peaks are irrelevant as the calibration and further detection of pyocyanin will be done between -0.7 to -.1V.

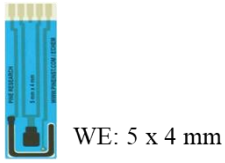

WE: 5 x 4 mm

Commercial Electrode. Pine research.[1]

WE: 6 x 4 mm

SBS PLA with Screen printed PET film and SBS carbon layer (2%-100% PLA:MWCNT)

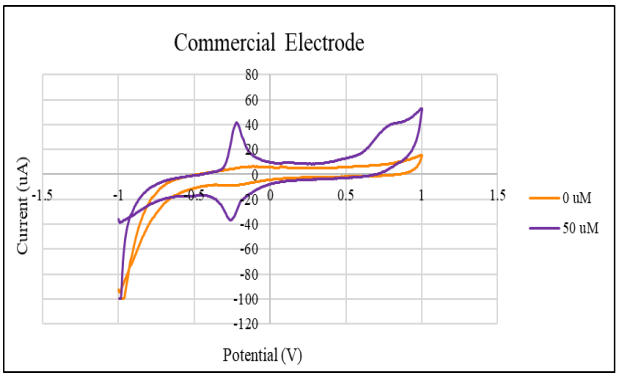

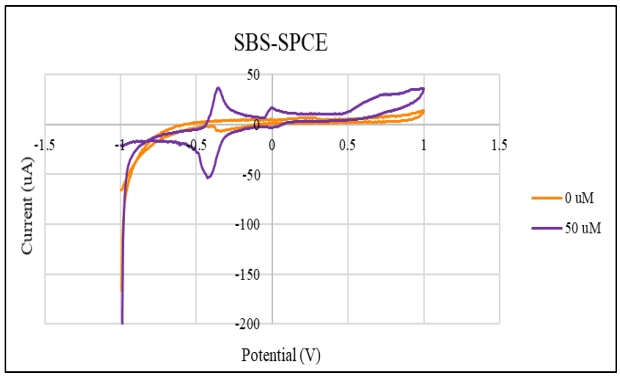

Figure 4.11. Cyclic Voltammetry of SBS electrodes in the presence of 50 uM of pyocyanin.
Cyclic Voltammetry of pyocyanin

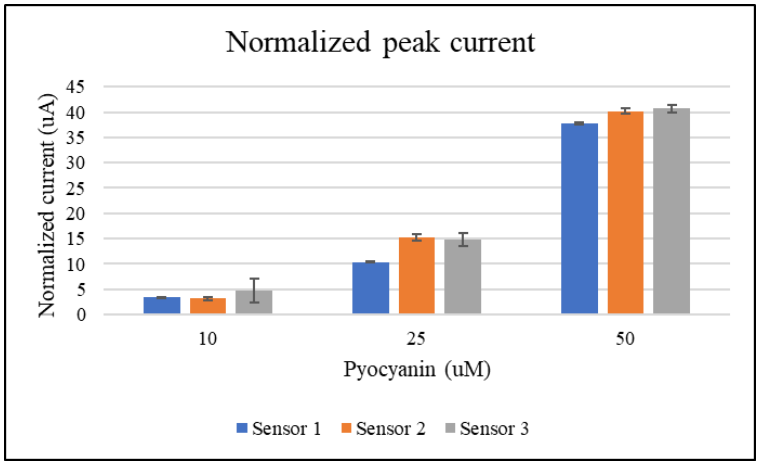

Figure 4.12. Reproducibility of electrodes

The reproducibility of electrodes was examined with 10, 25, and 50 uM of pyocyanin. As shown in Figure 4.12, there was no significant difference in the normalized peak current between three fabricated electrodes. Further work was done to examine the range of detection with fabricated electrodes. Square wave voltammograms of pyocyanin spiked PBS shows an increase in height with increasing pyocyanin concentrations (Figure 4.13). Thus, the peak change in peak current is directly proportional to the amount of pyocyanin in the given sample. Pyocyanin peak was apparent at -0.26 V. The detection range for fabricated electrodes was found to be 5 – 300 uM with a limit of detection of approximately 700 nM . All samples were tested in triplicates and their average was used to determine the standard curve equation, Y = 0.6198 + 3.9079 with a R^2 of 0.997. Calibration curve from peak current can be seen in Figure 6B. Concentration was also verified using spectrophotometry.

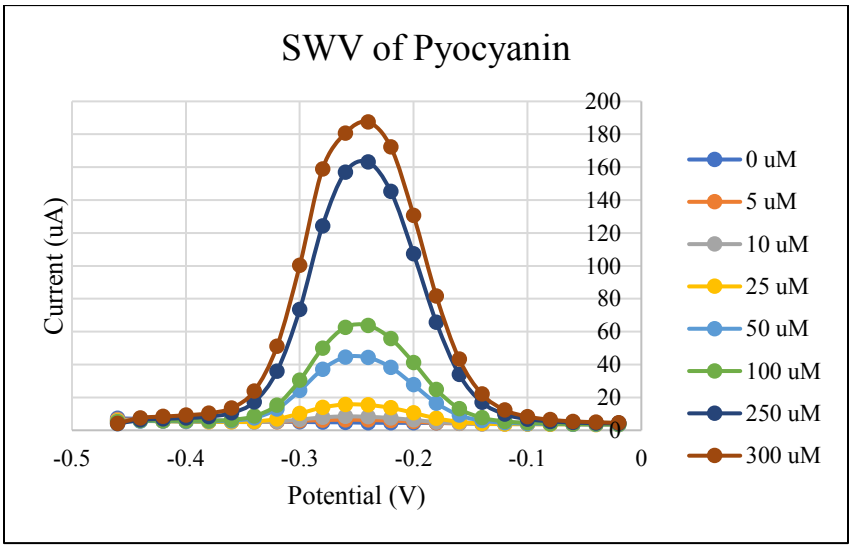

Figure 4.13. The detection of pyocyanin via square wave voltammetry.

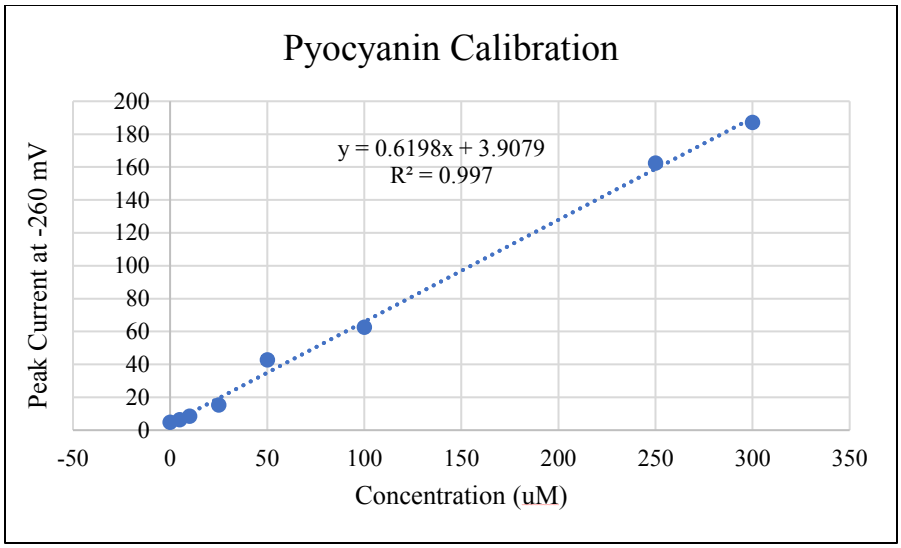

Figure 4.14. SWV peak current vs. pyocyanin concentration.

4.3C 48-hour P. aeruginosa pyocyanin detection.

P. aeruginosa (PAO1) cultures were grown over 48 hours in the absence and presence of silver nitrate. Silver is antimicrobial to most pathogens by interruption of ATP production, denaturation of ribosomes, DNA replication disruption, or by the degradation of the cell membrane. The production of Pyocyanin can be an indication of bacterial fitness in *P. aeruginosa* (PAO1). Peak current and the optical density of bacterial supernatants were measured at 24 and 48 hours to assess the bacterial fitness in the presence of antimicrobial silver. As seen in Figure 15, there was little to no pyocyanin production over 24 hours in the 10-uM silver treated group. The peak current in this group also reflects the lack of pyocyanin production from cultures (Figure 16). Over the next 24 hours, pyocyanin production was seen. This is an indication that the silver treatment disrupted the production of pyocyanin. The OD slightly decreased over 24 hours in the 1 uM group. However, there was no significant difference in the OD between the 10 uM treatment group after 48 hours and the 1 uM group at 24 and 48 hours. The electrochemical response showed a slight increase in from 24 hours to 48 hours in the 1 uM group. The OD and peak current responses were in agreement with the .1 uM and 0 uM treatment groups.

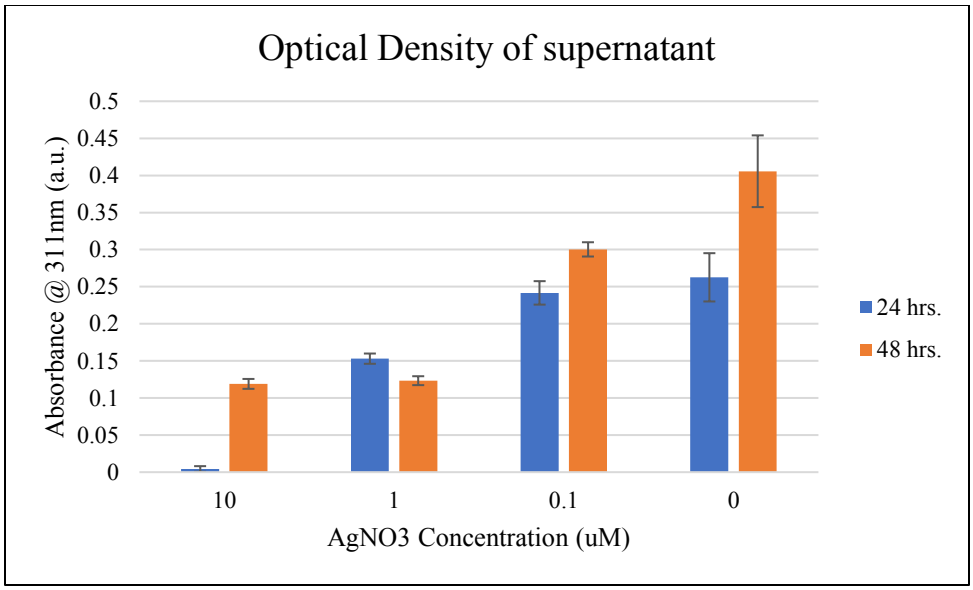

Figure 4.15. Optical density of culture supernatant.

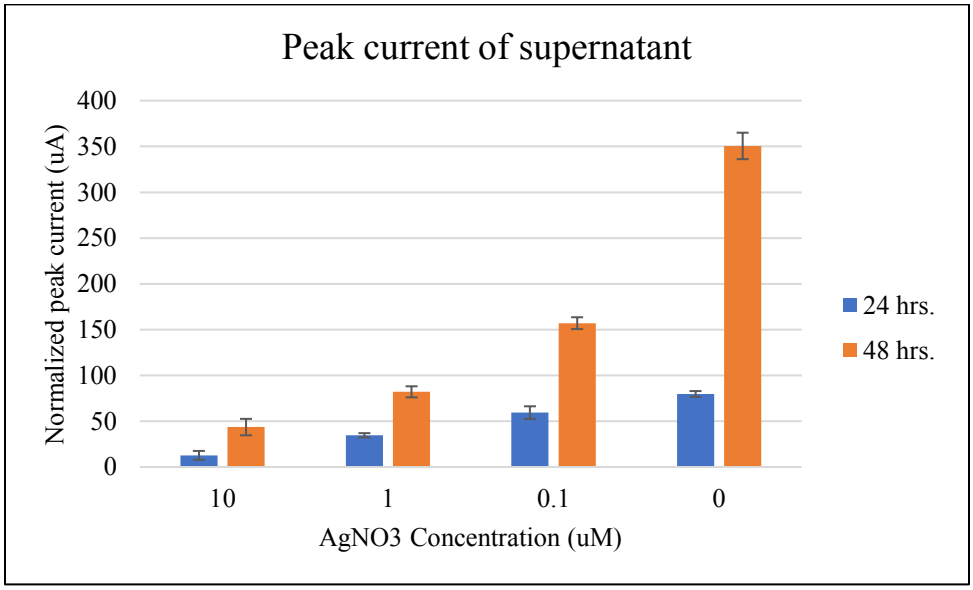

Figure 4.16. The detection of pyocyanin via square wave voltammetry.

As stated earlier in chapter, *P. aeruginosa* uses QS communication to regulate biofilm formation and virulence production. QS relies on the release and binding complex of transcriptional ligand-binding domains for the up/down regulation of genes. The contribution of

QS role in the development of infection has been demonstrated in the past. Thus, it is important to develop methods capable of detecting bacterial chemical molecules at low levels. The availability of point-of-care sensors to detect HSLs that would allow for in-field environmental and clinical applications. The aim of this chapter is to redesign a previously constructed LasR plasmid for the visual detection of 3OC12HSL. The chromoprotein amilCP reporter is used for visual detection. Biosensor construction and validation is discussed below, and the factors of bacterial immobilization was investigated in order to determine the functionality of amilCP biosensors in a hydrophobic PLA nanofiber mesh. To evaluate the performance of pFNK-503 qscrsaL biosensor, aliquots of previously grown bacteria was incubated with varying concentrations of 3OC12HSL. Briefly, Bacteria were grown on Agar/LB plates with kanamycin (concentration) via T-streak method overnight. Kanamycin (concentration) was added to LB media and inoculated with biosensor and grown to an OD of 0.279. Biosensor was then added to serially diluted 3OC12HSL in a 96 well plate to monitor gfp response overnight. In Figure 13A, there was an exponential gfp response from 150 pM to 10 nM of 3OC12HSL. The curve begins to flatten out between 10nM and 100nM. Additional 3OC12HSL caused an attenuation in gfp response. This could possibly be due to higher ethanol concentration that could cause a decrease in the signal response. The curve in Figure 4.17 shows the biosensor response to ethanol based on OD values. Higher 3OC12HSL included higher ethanol concentrations which could account for the tapper off response seen. However, the concentration of ethanol used is very low. which has not been shown to cause cell death or metabolic changes. Moreover, the cell fitness decrease at higher 3OC12HSL concentrations could be due to the cell membrane and HSL interaction. It was previously shown that the facilitation of longer carbon chain HSL is facilitated by efflux pumps and that of shorter chains are freely permeable through the bacterial cell wall. For example, Pearson et al. has shown

that *P. aeruginosa* freely diffuses 3OC12HSL, but also depends on an active MexAB-OprM efflux pump. (17) 3OC12HSL has also been shown to partition into the cell membrane due to its longer carbon side chains. Drug efflux also plays a major role in the resistance mechanism of bacteria, where the resistance-nodulation-division (RND) family is suspected to be more involved in the uptake of long chain HSLs. The downregulation of RND efflux pumps and cell membrane partitions could be the reasoning behind the decreased sensor response at higher dosages. There is a linear response between .1 – 20 nM of 3OC12HSL.

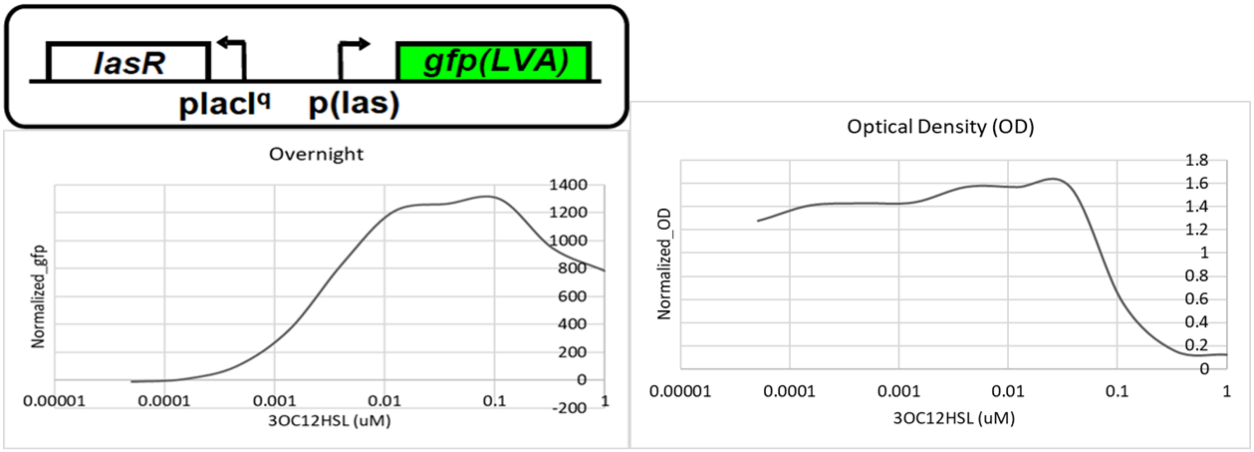

pFNK-503 normalized gfp response to exogeneous synthetic 3OC12HSL.

Optical Density as a function of exogeneous 3OC12HSL concentration.

Figure 4.17. Overnight response to 3OC12HSL molecules.

Initial pFNK-503 qscrsaL was verified in the above experiment. Further work was done to utilize the same vector and replace gfp reporter with the amilCP chromoprotein reporter. Gibson assembly method was used to develop the finalized plasmid construct. Gibson assembly utilizes site-directed mutagenesis and the assembly of DNA fragments upto 100 kb. This method was first introduced in 2009 by Daniel Gibson and colleagues (18). Since, many researchers have utilized this technique to construct plasmids and also to generate DNA libraries. (Thomas et al 2015; find karig paper; find paper of Weiss). As seen in Figure 4.18, The DNA fragments are designed such

that there are complementary overlaps at desired locations. The overlaps are typically 4-15 bp long. Amplified products are combined in a Gibson assembly master mix reaction in equimolar concentrations. All enzymes needed for the reaction is included within a single buffer. T5 exonuclease is used to chew back nucleotides on the 5' end of the amplified fragments and the resulting product are single-stranded 3' overhangs. Complementary fragments are then incubated at 50°C to subsequently anneal to each other. Phusion polymerase fills in gaps with nucleotides that are created in the previous steps. in one reaction tube in an isothermal reaction. Taq DNA ligase covalently join annealed complementary fragments.

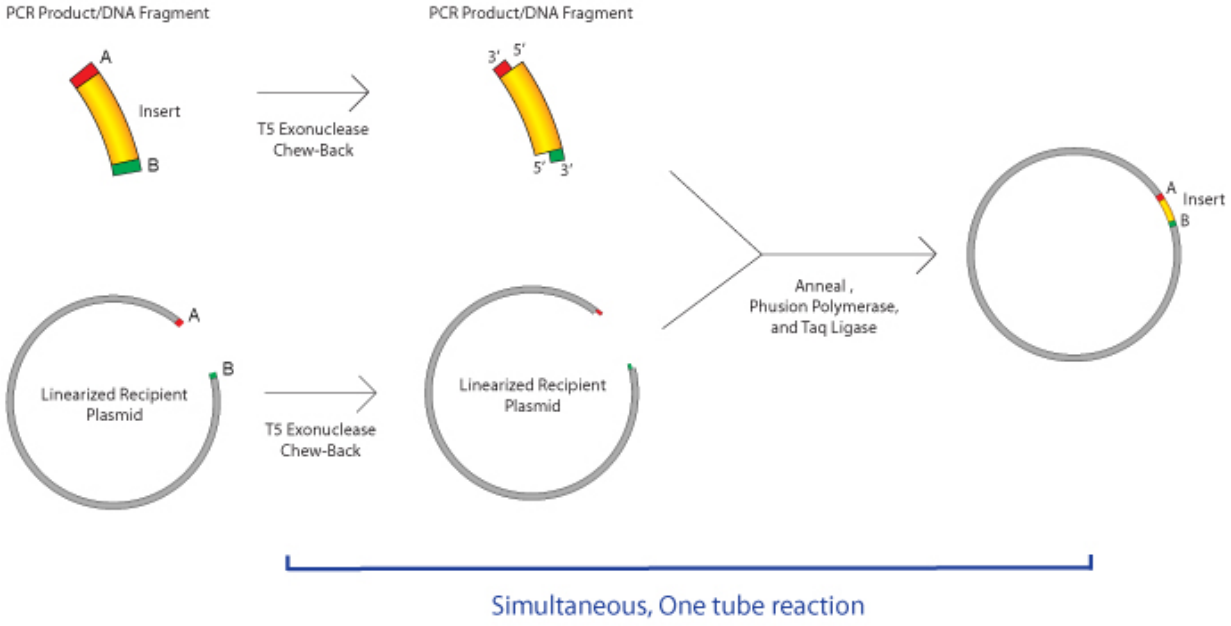

Figure 4.18 Illustration of Gibson Assembly method.

The designed pLas-amilCP-101 plasmid was derived from the pFNK-503-qscrsaL parent plasmid using Snapgene software. The parent plasmid was 3757 bp long with the gfp region located between location 1019-1774. This region was removed to create a 3024 bp linearized vector with the remaining backbone regions. AmilCP insert (692 bp) was amplified from

BBa_K592009 backbone. Complementary overlaps were added to both the vector and insert for Gibson assembly reaction step. After fragment amplification and assembly, the plasmid product is then used to transform. In this study, chemically competent E. coli DH5 alpha cells were used for transformation. As seen in Figure 4.19, transformed cells were plated on kanamycin agar plates and allowed to grow overnight for screening. Gibson assembly (GA) 9 and 10 were the transformed cells using the non-DpnI and DpnI digested reaction, respectively. Digestion was used in order to remove parent pLas-amilCP-101 from transformation reaction. DpnI digestion reaction cleaves to methylated sites and removes the cleaved DNA within a reaction. The DpnI treated products created larger colonies and more transformants than that of the non-DpnI treated cells.

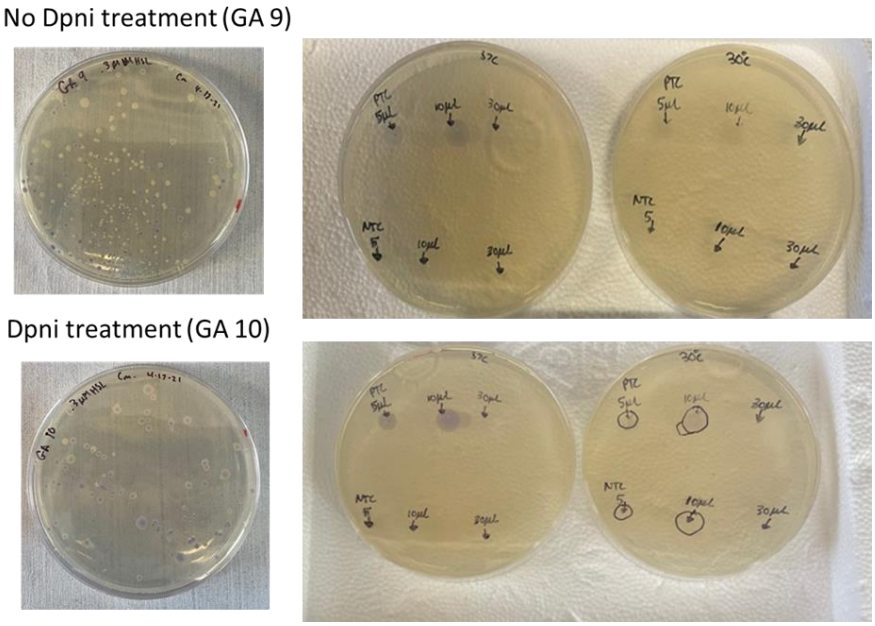

Figure 4.19. Screening of bacteria.

Random colonies from each group were used to inoculate LB-Kan media containing .3uM of 3OC12HSL. Both the DpnI and non-DpnI treated groups successfully transformed the constructed plasmid. However, only approximately half of GA9 colonies cells were transformants, whereas the majority of GA10 colonies successfully transformed the pLas amilCP plasmid.

Colonies from both groups were chosen and grown in the presence of 3OC12HSL overnight. The visual detection of HSLs can be seen in Figure 4.20. The lowest concentration that can be seen visually is approximately 1nM. This visual response can be used to screen for HSLs without the use of fluorescent microscopy, which utilizes highly expensive and large equipment.

Figure 4.20. Visual response of biosensor to 3OC12HSL.

The dosage curve response of biosensor in the presence of HSLs was measured with plate reader in order to quantify biosensor response. The designed sensor had a limit of detection of .5nM. The linear range was approximately between .1 – 75 nM with a saturation region above 100 nM. pLas amilCP response depends on the wavelength at 580nM due to amilCP maximal absorbance. Bacterial cells are commonly estimated at 600nM which is close to the maximal absorbance. As a result, researchers use a ratio of 580:700nM as an alternative to quantify the production of amilCP in bacteria. As seen in Figure 4.21, the response curve with the 580:600 ratio method is very low compared to the response curve developed with the use of 580:700 ratio method. Both GA 9 and GA 10 displayed a similar dosage response curve. This suggest that the

DpnI treatment did increase the transformation of plasmid but did not increase nor decrease the functionality and performance of biosensor in liquid suspensions. Response can be seen at a much earlier timepoint

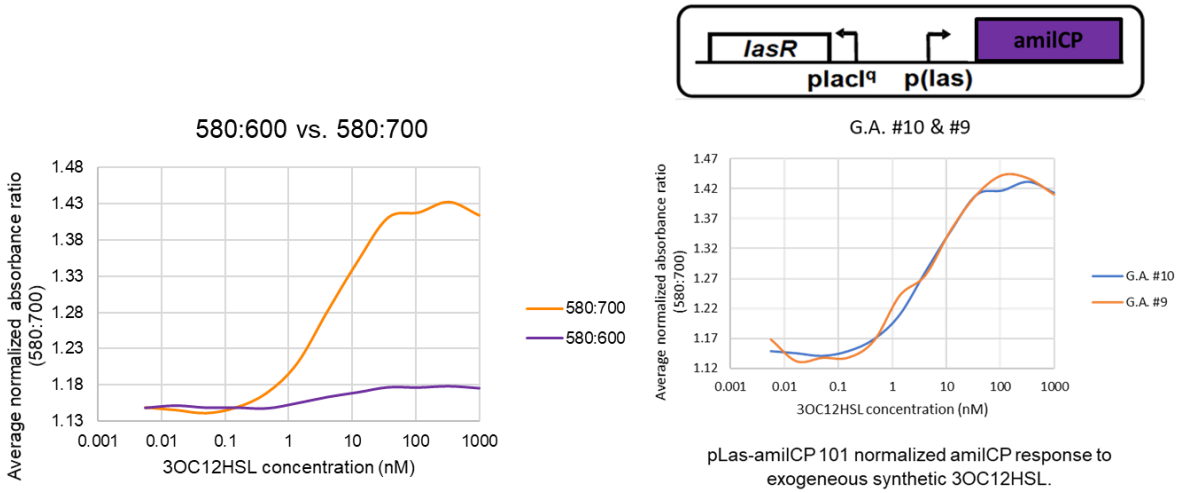

Figure 4.21. pLas amilCP-101 dosage response curve to 3OC12HSL.

Homoserine lactones have several analogs with various carbon chains that could potentially induce the developed sensor. Specificity of biosensor to 30C12HSL is shown in Figure 4.22. Where the biosensor showed a selected response towards the desired HSL molecule. Concentrations ranging from .01 to 10,000 nM was tested and there was little to no response seen in the absorbance ratio as seen below. Additionally, there was no appearance of amilCP production seen visually from cultures grown. The image below also shows the kinetic run of amilCP biosensor where sensor begins to respond to synthetic 3OC12HSL (33 uM) at around 15-hour mark. This was done in aqueous liquid cultures on a plate reader at 37ºC over 24-hours.

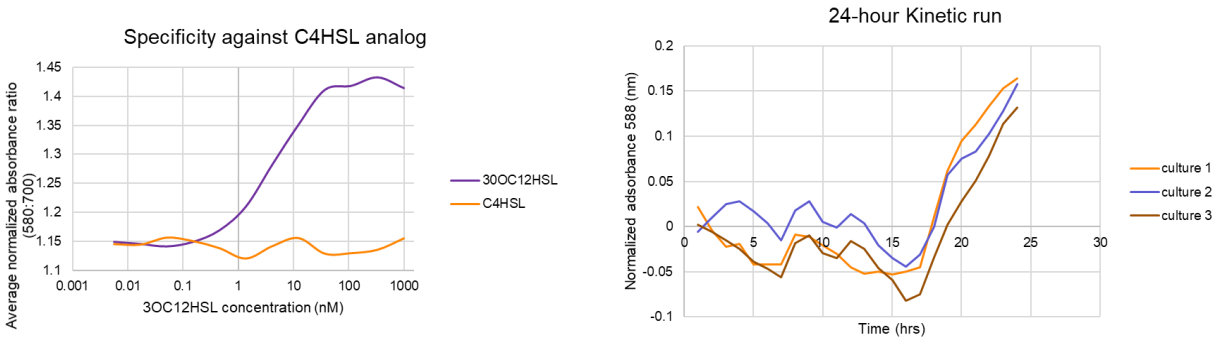

Figure 4.22. pLas amilCP-101 dosage response curve to 3OC12HSL in presence of C4HSL.

Pseudomonas putida KT2440 and *Pseudomonas aeruginosa* PAO1 cultures were grown and screened for HSL with amilCP visual detection scheme. As seen in Figure 4.23, KT2440 cultures induced a significant response as can be seen visually and detected via absorbance. KT2440 is a good model as it does not produce any visually interfering substances. PAO1 on the other hand displayed a lower response visually and it was not feasible to test for amilCP response via absorbance. In Figure 4.23, there is a clear distinct between PAO1 and control group. However, due to pyocyanin production there is an over lapping visual wavelength. Further testing was done with synthetic 3OC12HSL to assess performance on SBS nanofiber mesh.

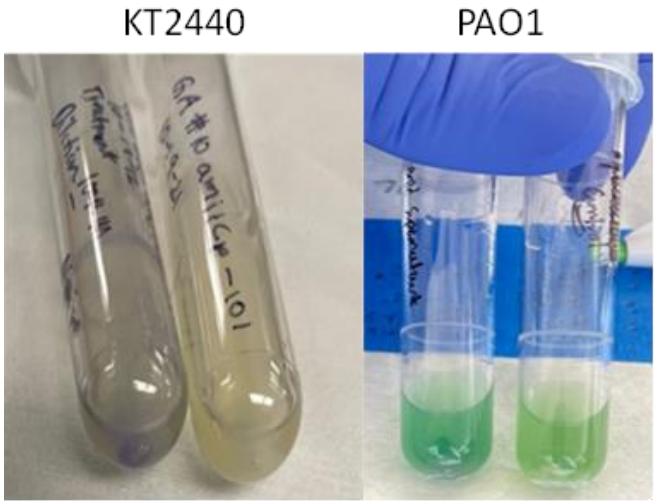

	580:700	580:311
PAO1 +amilCP	0.94	0.37
PAO1	1.02	0.312
KT2440 + amilCP	1.25	N/A
KT2440	1.169	N/A

Figure 4.23. Native 3OC12HSL detection from *P. aeruginosa* PAO1 and *P. putida* KT2440

As seen in Figure 4.24, cells were plated on LB-Agar Kan plates to test the time response over 24hours. This was done in an effort to see if there was a faster amilCP response. Compared to liquid cultures, the cultures grown on LB-agar kanamycin plates produced a faster response than the aqueous cultures. A distinct visual change can be seen after a 6-hour incubation period. The visual color intensity increased over the 24-hour period. Additionally, the cells grown at 37^{o}C produced a stronger color change than the cells incubated at 30^{o}C. This stronger signal seen on LB-agar could be due to increased diffusion of 3OC12HSL molecules in cell cultures. Figure 4.25 shows the amilCP-101 sensor response to 30 uM of 30C12HSL. The initial response shows a small visual deference in the control vs. the treatment sample. Additional efforts were made to address spreading of culture solution that can be seen in the first test (left). For this purpose double sided tape and acrylic sheets were laser printed and the corresponding response can be seen in Figure 4.25 (right). Three iterations of 30 uM of 3OC12HSL detection on SBS PLA nanofibers can be seen in Figure 4.26. In this iteration cell pellets were soaked on nanofiber scaffolds in an effort to enhance visual color. As seen in image, the sensor response is enhanced with the use of cell pellets.

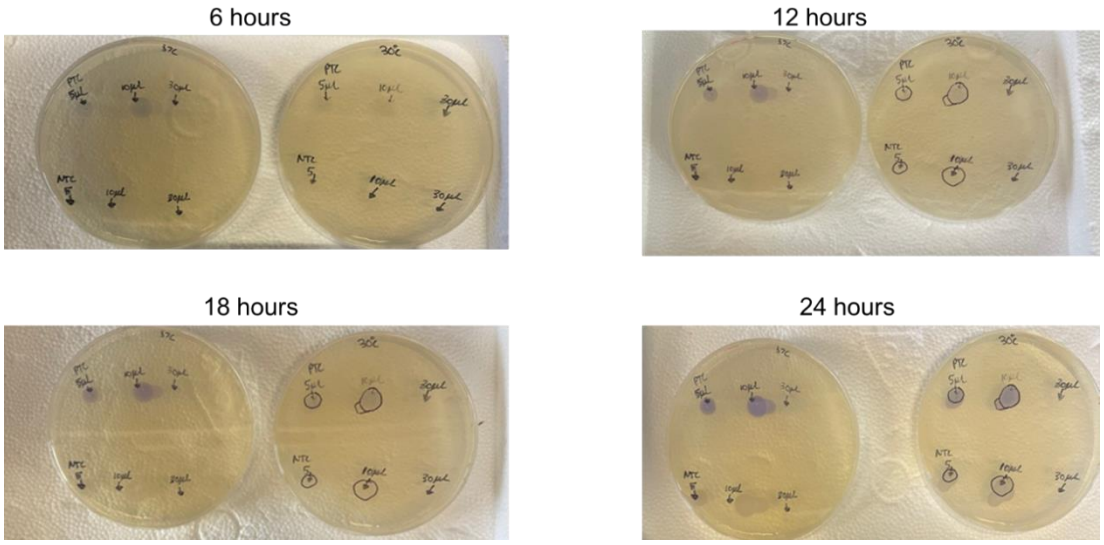

Figure 4.24. 24-hour Culture response to 3OC12HSL on LB-Agar Kan plates.

Figure 4.25. Immobilized amilCP-101 and synthetic 3OC12HSL detection on SBS nanofibers.

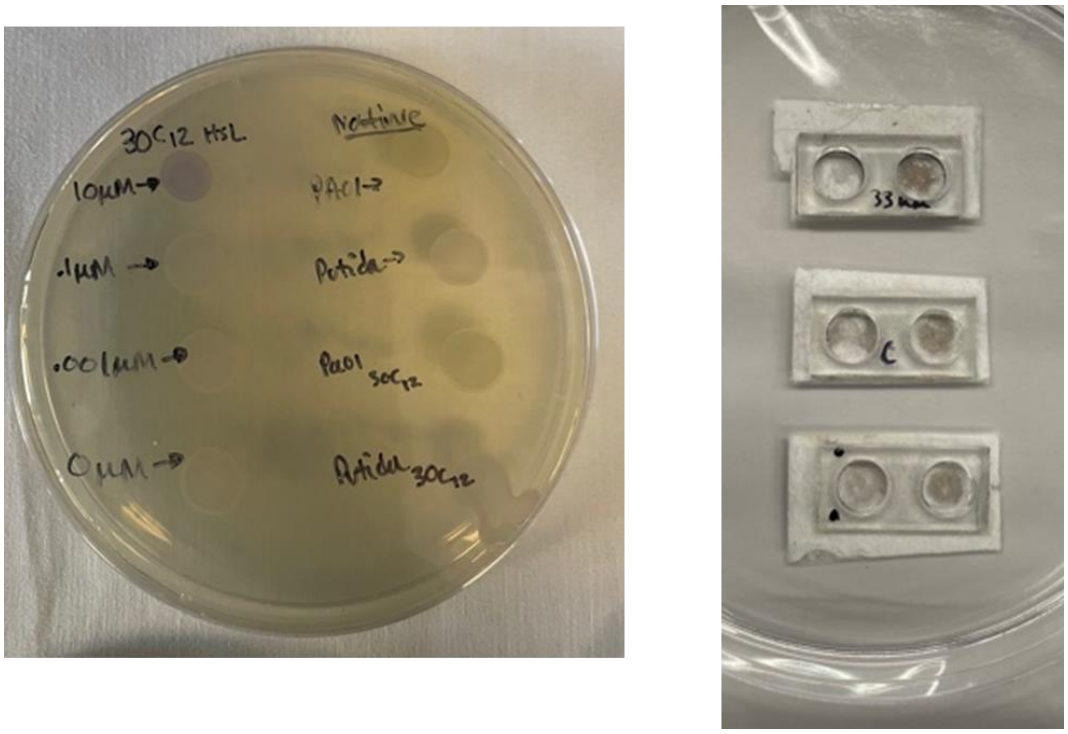

Figure 4.26 Visual LOD of amilCP-101 on LB agar and synthetic 3OC12HSL detection on SBS nanofibers.

4.4 Conclusion

SBS nanofibers have yet to be exploited for therapeutic and biomarker detection schemes. Here in this chapter, we demonstrate the use of a SBS PLA nanofiber mat with the use of screen-printing and a modified solution blow spinning scheme to produce electrode patterns for electrochemical applications. Clinically relevant pathogen, *P. aeruginosa* PAO1, was used to assess the use of SBS-based electrodes to detect pyocyanin. We also show the potential to electrochemically screen for novel drugs by the detection of pyocyanin in the presence and absence of $AgNO_3$ in cell cultures. Additional efforts were also made to develop an amilCP LasR reporter for the visual detection of 3OC12HSL. The reporter system was immobilized on SBS sheets to demonstrate potential for whole-cell biosensing immobilization. Future works could include the combine both immobilized bacteria biosensors on SBS PLA sheets to serve as a substrate for SBS PLA:MWCNT electrochemical electrodes for pyocyanin and/or electrochemical detection

schemes. Replacing amilCP chromogenic protein with a different color could help prevent pyocyanin wavelength overlap when testing for 3OC12HSL from *P. aeruginosa* PAO1.

4.5 References

1. Lee J, Zhang L. The hierarchy quorum sensing network in Pseudomonas aeruginosa. Protein Cell. 2014;6(1):26–41.

2. Miller C, Gilmore J. Detection of Quorum-Sensing Molecules for Pathogenic Molecules Using Cell-Based and Cell-Free Biosensors. Antibiotics [Internet]. 2020 May 16 [cited 2020 Dec 11];9(5):259. Available from: https://www.mdpi.com/2079-6382/9/5/259

3. VE W, D B, L P, AI B, BH I. Microarray analysis of Pseudomonas aeruginosa quorum-sensing regulons: effects of growth phase and environment. J Bacteriol [Internet]. 2003 Apr [cited 2021 Jul 29];185(7):2080–95. Available from: https://pubmed.ncbi.nlm.nih.gov/12644477/

4. M S, CP L, T O, EP G. Identification, timing, and signal specificity of Pseudomonas aeruginosa quorum-controlled genes: a transcriptome analysis. J Bacteriol [Internet]. 2003 Apr [cited 2021 Jul 29];185(7):2066–79. Available from: https://pubmed.ncbi.nlm.nih.gov/12644476/

5. Mathesius U, Mulders S, Gao M, Teplitski M, Caetano-Anollés G, Rolfe BG, et al. Extensive and specific responses of a eukaryote to bacterial quorum-sensing signals. Proc Natl Acad Sci [Internet]. 2003 Feb 4 [cited 2021 Jul 29];100(3):1444–9. Available from: https://www.pnas.org/content/100/3/1444

6. Hogan DA, Vik Å, Kolter R. A Pseudomonas aeruginosa quorum-sensing molecule influences Candida albicans morphology. Mol Microbiol [Internet]. 2004 Dec 1 [cited 2021 Jul 29];54(5):1212–23. Available from: https://onlinelibrary.wiley.com/doi/full/10.1111/j.1365-2958.2004.04349.x

7. Smith RS, Kelly R, Iglewski BH, Phipps RP. The Pseudomonas Autoinducer N-(3-Oxododecanoyl) Homoserine Lactone Induces Cyclooxygenase-2 and Prostaglandin E2 Production in Human Lung Fibroblasts: Implications for Inflammation. J Immunol [Internet]. 2002 Sep 1 [cited 2021 Jul 29];169(5):2636–42. Available from: https://www.jimmunol.org/content/169/5/2636

8. Part:BBa K592009 - parts.igem.org.

9. Zamel D, Hassanin AH, Ellethy R, Singer G, Abdelmoneim A. Novel Bacteria-Immobilized Cellulose Acetate/Poly(ethylene oxide) Nanofibrous Membrane for Wastewater Treatment. Sci Reports 2019 91 [Internet]. 2019 Dec 12 [cited 2021 Oct 23];9(1):1–11. Available from: https://www.nature.com/articles/s41598-019-55265-w

10. Nguyen PQ, Soenksen LR, Donghia NM, Angenent-Mari NM, de Puig H, Huang A, et al.

Wearable materials with embedded synthetic biology sensors for biomolecule detection. Nat Biotechnol 2021 [Internet]. 2021 Jun 28 [cited 2021 Oct 23];1–9. Available from: https://www.nature.com/articles/s41587-021-00950-3

11. Struss A, Pasini P, Ensor CM, Raut N, Daunert S. Paper Strip Whole Cell Biosensors: A Portable Test for the Semiquantitative Detection of Bacterial Quorum Signaling Molecules. Anal Chem [Internet]. 2010 Jun 1 [cited 2021 Oct 23];82(11):4457–63. Available from: https://pubs.acs.org/doi/full/10.1021/ac100231a

12. Muller M, Li Z, Maitz PKM. Pseudomonas pyocyanin inhibits wound repair by inducing premature cellular senescence: Role for p38 mitogen-activated protein kinase. Burns. 2009 Jun;35(4):500–8.

13. Preventrion. C for DC and. Healthcare-associated Infections. 2019; Available from: https://www.cdc.gov/hai/organisms/pseudomonas.html

14. Bielecki P, Glik J, Kawecki M, Martins Dos Santos VAP. Towards understanding Pseudomonas aeruginosa burn wound infections by profiling gene expression. Biotechnol Lett. 2008;30(5):777–90.

15. Karig DK, Siuti P, Dar RD, Retterer ST, Doktycz MJ, Simpson ML. Model for biological communication in a nanofabricated cell-mimic driven by stochastic resonance. Nano Commun Netw [Internet]. 2011 Mar [cited 2021 Jul 15];2(1):39. Available from: /pmc/articles/PMC3124924/

16. K B, DK K, R W, FH A. Engineered bidirectional communication mediates a consensus in a microbial biofilm consortium. Proc Natl Acad Sci U S A [Internet]. 2007 Oct 30 [cited 2021 Jul 15];104(44):17300–4. Available from: https://pubmed.ncbi.nlm.nih.gov/17959781/

17. Pearson JP, Van Delden C, Iglewski BH. Active efflux and diffusion are involved in transport of Pseudomonas aeruginosa cell-to-cell signals. J Bacteriol [Internet]. 1999 [cited 2021 Jul 31];181(4):1203–10. Available from: https://journals.asm.org/journal/jb

18. Gibson DG, Young L, Chuang R-Y, Venter JC, Hutchison CA, Smith HO. Enzymatic assembly of DNA molecules up to several hundred kilobases. Nat Methods 2009 65 [Internet]. 2009 Apr 12 [cited 2021 Jul 31];6(5):343–5. Available from: https://www.nature.com/articles/nmeth.1318

CHAPTER FIVE

VIRTUAL STEM OUTREACH PROJECT TO INCREASE STEM SELF-EFFICACY, INTERST AND KNOWLEDGE IN MIDDLE SCHOOL STUDENTS

5.1 Introduction

Science, engineering technology, and math (STEM) engagement has been highly encouraged amongst students worldwide over the past several decades. Due to the information age and technological advancements, STEM engagement requires students to get an early jump start on science and engineering-based activities. Additionally, the state of our national security relies on the advancement of technology and the ability to recruit and engage future leaders to pursue STEM careers. Efforts to engage the population would help stimulate the economy, improve innovation and increase our national defense. (1,2) Efforts are made by the Department of Defense (DoD) to increase the innovative capacity of its workforce by providing scholarships and internship opportunities. The Department of Education has made a clear effort to support and invest in STEM education at from k-12 to the graduate level. In 2019 alone, the U.S. Department of Education committed $540 million towards STEM educational initiatives to include computer science. (3) Additionally, there is a push, worldwide, to recruit more students in order to build up the STEM workforce. The STEM workforce is a very diverse group with many different sub-classes. The workforce is critical in order to maintain a competitive economy and innovative nation. Skills learned in STEM activities/curriculum are very diverse and could be used in non-STEM occupations and activities. This workforce does not only include individuals with a science or engineering-based background, but also STEM competent individuals with non-STEM degrees.

Overtime, cutting-edge and innovative STEM skills will evolve and become routine work. Hence, the important to teach scientific and technological skills among the entire STEM

workforce. (4,5) STEM jobs include scientists, engineers, architects, engineering technicians, STEM related sales and management. According to the US Bureau of Labor Statistics, there was a total U.S. workforce of over 140 million in 2012 across all educational level. Science and engineering (S&E) occupations made up approximately 5.9 million of the workforce across all levels. (4) As the U.S. economy and nation continue to expand into the informational age, the daily task and occupations will have to evolve and require more of a science and engineering baseline or competency. As new technologies are designed and created, new problems arise which will require better troubleshooting skills from a highly competent workforce. The idea of building a strong workforce at every level is very important. (4) Several reports have shown the need to improve and increase the sub-baccalaureate or the technical STEM workforce. (4,6,7) The technical STEM workforce comprises of mainly workers with high school or associate degree, or one with a certification with STEM requirements. This workforce is commonly overlooked, and most efforts are focused on supporting individuals with a four-year degree or higher. However, this population is an important group to the US STEM workforce as almost half of STEM jobs are available to workers without a four-year degree. (8)

Since the 1990, there has been a 79% employment growth (9.7 to 17.3 million). (9) There were over 8 million STEM jobs in May of 2015, which made up over 6 percent of the U.S. employment population. U.S. Bureau of Labor Statistics projects that, between 2022-2029, there is expected to be an 8.8% growth in STEM jobs, where computing, manufacturing, and engineering are projected to be at the top of the list. (10) Computer-based occupations made up the majority of this group, whereas engineering jobs were the second highest at 19%. (11,12) In 2017, the median salary of science and engineering (S&E) occupations, amongst all educational

levels, was more than $85,000. This figure is two times higher than non-S&E occupations. (12) The average salary for S&E occupations increase with higher education levels.

Although there is expected to be an 8% increase in STEM occupations, there is still a need to increase the STEM workforce for certain areas. There is debate whether there is a STEM shortage or surplus in the US. This shortage and surplus are something that constantly changes over a period of time. The need for workers with a bachelor's degree or higher in electrical engineering is slightly different than the demand for workers with bioengineering degrees. The STEM workforce shortage or surplus depends on degree level, industry, and location. For example, the demand for marine biologist in Florida will be different than that of Kentucky. Hence, Florida may experience a STEM crisis in this specific sector, but this would only be a STEM shortage due to locality. The Taxicab queuing metaphor developed by David George Kendall is one example to explain the current and future STEM workforce. (13) According to this metaphor, every taxi system represents a section of the STEM employment sector. STEM occupations and/or employers can be thought of as the individual taxi cabs within a particular system. The past, current and potential STEM workers to include recent and future graduates are the passengers in the system. There are several thousands of employers waiting for job applicants to apply for their opening. We also have individuals who already occupy STEM jobs in the current market. Similar fashion, taxicab drivers either have current passengers or they wait for passengers to occupy their taxi. Once the number of taxicab drivers (employers) is greater than the number of passengers, then we have a queue of taxis. This is manifested as a STEM shortage for this particular sector. Likewise, a higher supply of passengers would create a queue of passengers or STEM workers, which would create a STEM surplus for this sector. A no queue condition would mean that there are adequate jobs for STEM workers and there is little to no vacancies open on the STEM market. (13)

The STEM market is composed of three main sectors: government, industry (private sector), and academia with each sector having its own occupational categories (i.e. engineer vs. doctor). The academic sector employs individuals from technical colleges for research assistant or technician positions. Master's students could be employed as lectures or instructors. The most coveted position in academia is a tenured track position. These positions typically require a Ph.D. level degree. Additionally, Ph.D. graduate could also serve as a non-tenured or a lecture. Over the past several decades, the number of PhDs awarded in STEM has continued to increase. However, the demand for faculty positions available has remained relatively constant. (14–16) In 2010, less than 15% of STEM PhD graduates found a tenure-track position within 3 years of graduating. (17) Many PhD graduates decide to go into a non-academic field. More than half of PhD holders are employed in governmental or industry positions.(18–20) The governmental sector includes the various branches of armed forces and civilian sectors, such as the US Department of Energy or Defense, military, or research institutes. Governmental institutes are major employers of scientists and engineers. With the exception to contract work and bridge programs, this sector is limited to US citizens and those capable of obtaining proper clearance. In 2018, the RAND Corporation's National Defense Research Institute (NDRI) conducted a report to assess the governmental and private sector STEM workforce. According to the NDRI report, there were approximately 320,000 STEM workers in the federal government in 2018, which was about 17% of the total governmental workforce. This number has been reported to be consistent over the past decade. Each department in the government is different in size, but in terms of percentage, the Department of Navy followed by the Army and Agriculture had the highest percentage of STEM workers. (21)

Currently, there is not a STEM shortage or surplus crisis. However, there is still a lack of women and underrepresented individuals in the STEM workforce. According to a report by the

Department of Commerce, women filled approximately 50% of all US jobs. However, only 24% of STEM jobs. This number is not due to a lack of education or qualifications. Women make-up half of college educated workforce, but only make up 25% of the college educated STEM workforce. About 40% of men with a STEM degree has a STEM occupation. Additionally, it was found that women with a STEM degree are less likely to work in the STEM workforce than their male counterparts. (22) There is also a disparity in the type of STEM majors chosen. 59% of all women that major in STEM pursue a degree in the biosciences compared to 30% of men. Women were more likely to pursue a math or healthcare major/career than their male counterparts. The gains that women have made in the biosciences of STEM is encouraging, but they still remain underrepresented in other STEM fields, such as engineering and computer sciences. (22)

Minority ethnic groups are still underrepresented in the STEM workforce. The entire US workforce is made up of 11% of black workers, yet they only represent 9% of the STEM workforce. Additionally, the Latino community made up more than 15% of the total workforce, but only account for 7% of the STEM workforce. Overall, whites and Asians make up 69% and 13% of the STEM workforce, respectively. The number of Hispanic and black STEM workers has seen a small increase from 4% and 7%, but there still is work to be done to increase these numbers. (9) Early exposure, encouragement and STEM prep programs could help persuade students to pursue a STEM career. The STEM workforce depends on the diversification of its workers in order to find innovative ways to solve the world's most difficult problems.

There are many reasons for the hesitancy of students to pursue courses or a career in STEM. STEM self-efficacy, career knowledge and interests, and social support from family a role in the intent to pursue STEM. STEM career knowledge is the level of understanding that a student has about careers that are STEM. The level of knowledge that a student has can vary considerably

based on the school system's career education program. Additionally, certain students may also have a greater exposure to STEM careers through their family and community. The students with family members in the S&E community tend to have a head start in a baseline STEM career knowledge. A lack of career knowledge may lead to a decline in STEM careers interest due to a focus on more recognized occupations. (23) Many reports have shown that career knowledge can have a direct affect on their intentions to pursue a career in S&E. A lack of career information about potential careers was shown to limit students' ability to make a resilient plan towards a STEM career. (24,25) With a lack of knowledge in potential career opportunities, students may dismiss a STEM career option as an option to potentially pursue. This lack of knowledge could led to a negative outlook towards core classes required for STEM pathways and influence their desire to pursue opportunities to learn more and get involved with STEM activities. Increasing the STEM knowledge of prospective students have been shown to increase their desire to take more high school science and math courses. (26)

Students' interest in STEM careers and activities also affects the likelihood of pursuing a career in S&E. Studies have shown that students begin to take interest in STEM careers and are able to be influenced at a high level at the elementary and middle school level. Additionally, these students are more likely to pursue a STEM career, where eight graders are three times more likely to pursue a STEM major in college than students who lack interest. (27) However, this interest is time sensitive as studies have shown a drastic decline in STEM interest between ages 10 to 14. This decline in STEM interest could be due to a coursework, summer learning delays, or social economical factors. The executive report of 2010 has shown that students from low-socioeconomic backgrounds are at a greater risk for STEM interest decline due to a lack of access to STEM based programs. (28) Therefore, it is imperative to continue to employ STEM outreach and engagement

programs in order to maintain the interest of the students within this age group. Society greatly influences both STEM career/activity knowledge and interest. These include role models that the students may have access to or through social media, family members, and also the teachers they interact with on a daily basis. These social influences have a great impact on the STEM career knowledge and interest. Additionally, the social factors have been shown to greatly impact a student's self-efficacy about a particular subject. (29) Low socioeconomic status also has a negative affect on a student's interest level in STEM and could potentially hinder one's ability to pursue STEM activities and careers. (23) Early interest in STEM topics and subjects could be a good indication of learning and STEM career choice. Continued support and encouragement could greatly influence middle school student's desire to pursue a STEM career by increasing their self-efficacy.

Self-efficacy is the belief that a person has about their capability to succeed in a particular area. Math and science self-efficacy are considered major predictors of major and career selection, where higher self-efficacy tends to mean a greater chance that a student would pursue a STEM career. Grades 7-9 are very important in building science and math self-efficacy, similar to building a student's overall STEM career interest. (28) The Social cognitive career theory (SCCT), developed by Lent et al. demonstrates the importance of personal interest and intent to pursue STEM careers. The SCCT shows that career interests, intent to pursue, and personal goals are directly related to performance and self-efficacy. (30) Student academic performance is positively related to the self-efficacy level of each subject. This success could then give a confidence boost, which could enhance their overall STEM interest.

Informal or supplemental STEM outreach programs could increase the chances that a student will pursue a STEM career. Student's attitude towards STEM are affected by their

experiences, motivation and self-efficacy in mathematics and science related subjects. (31) Formal and informal school STEM intervention programs designed to engage underrepresented students have shown to increase overall interest, knowledge and self-efficacy in STEM careers. (32,33) Moreover, interventions provide STEM role models and mentors which could also increase students' self-efficacy and interest are enhance with these interventions. Studies have shown that middle school students have limited STEM career knowledge with respect to course related topics, which could create a disconnect between learning objectives and outlook on real-world value. (32) Supplemental outreach programs have the ability to connect with middle school aged students from underrepresented programs in a way that increases their self-efficacy. Additionally, such programs have the chance to help students understand the true value in common mathematics and scientific topics discussed at their grade level as it relates to STEM careers.

The objective of this project was to conduct a 5-day virtual STEM outreach program to examine and increase the self-efficacy of middle school aged students from two South Carolina middle schools. The project will attempt to increase the awareness of STEM careers and common mathematics and scientific topics to help increase the self-efficacy of students. Target schools will be Cane Bay and Sangaree Middle School. Additionally, this project is also a requirement for the call me doctor fellowship program, which requires fellows to participate in a community project during their PhD program.

5.2 Materials and Methods

The first day involved a pre-survey to assess the self-efficacy and interest in STEM careers and subjects along with an introduction to common career paths and higher educational options. Each aspect of STEM was outlined. In particular the scientific and engineering design process was discussed in detail with tangible examples as seen in Table 5.1. This was an effort to get the

students engaged and interested in STEM careers and activities. Table 5.2 was discussed in order to provide the students with an understanding of which career paths require an advanced level math/science curriculum and four-year degree. The first day was more of an introductory day for the outreach program to discuss program outline and administer the pre-survey.

Table 5.1. STEM examples for day 1 of outreach.

TECHNOLOGY	ENGINEERING	SCIENCE	MATH
Basketballs	Leather pattern and groves with round shape.	Laws of motion	Trigonometry, geometry, algebra
Iphone touchscreen	Transparent conductive film, LCD display design	Physics of capacitors	Calculus and algebra
Airplanes, spacecrafts, cars	Composites, landing gears, cabin temperature	Laws of motion	Trigonometry and algebra
Electrical grid	Substation/Power Design	Kirchovs laws	Algebra and Matrix Math
Polymerase Chain Reaction, Recombinant DNA technology	Synthetic Biology, Forensics	Biology	Differential equations and algebra

Table 5.2. STEM career requirements.	
Career	**Advance Math/Science Needed?**
Electrical Engineer	Y
Car Mechanic	N
Dental Hygienist	N
Civil Engineer	Y
Cosmetologist	N
Bioengineering Professor	Y
Registered Nurses	Y
Engineering Technician	Y
Plumber	N
Politician	N
School Counselor	N
Mechanical Engineer	Y
Mathematician	Y
Medical Doctor	Y
Biochemist	Y

The first day also included the integration of knowledge about STEM requirements for certain career opportunities. This module is designed to help increase the STEM career knowledge of the participants by providing a few familiar examples. The second day included an overview of DNA and central dogma theory with a small DNA isolation project. There was a review of key aspects about DNA and conduct a small exercise where I extract DNA from my cheek by mouth washing and dispensing water into a kit. An additional exercise was done to help provide a visual

to the students based on DNA base pairs and the concept of primer design and DNA assembly techniques. Figure 5.1 is an image from one of the participants.

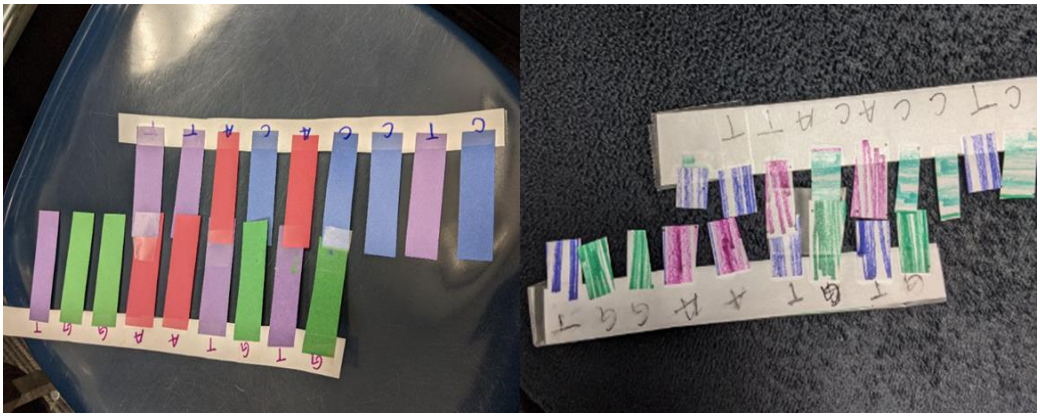

Figure 5.1. Images of DNA plasmid construction activity.

Day 3 overview of glucose and how it is used as a biomarker for diabetes. The participants received a small presentation about the central dogma theory and proteins as it relates to glucose homeostasis. An activity was done that utilized a commercial glucometer to measure the glucose concentration of common soft drinks and water containing glucose. Day 4 involved the use of a small Arduino project and discuss electronics and electricity theory. The students received a small overview of electrical circuit theory and the basics of electronics. Electricity and electronics theory was demonstrated through the use of LEDs and an Arduino controller circuit setup as seen in Figure 5.2. The final day will involve a small post-survey to assess the effectiveness of the program and a conclusion. Below is a table of the materials used for the virtual instruction.

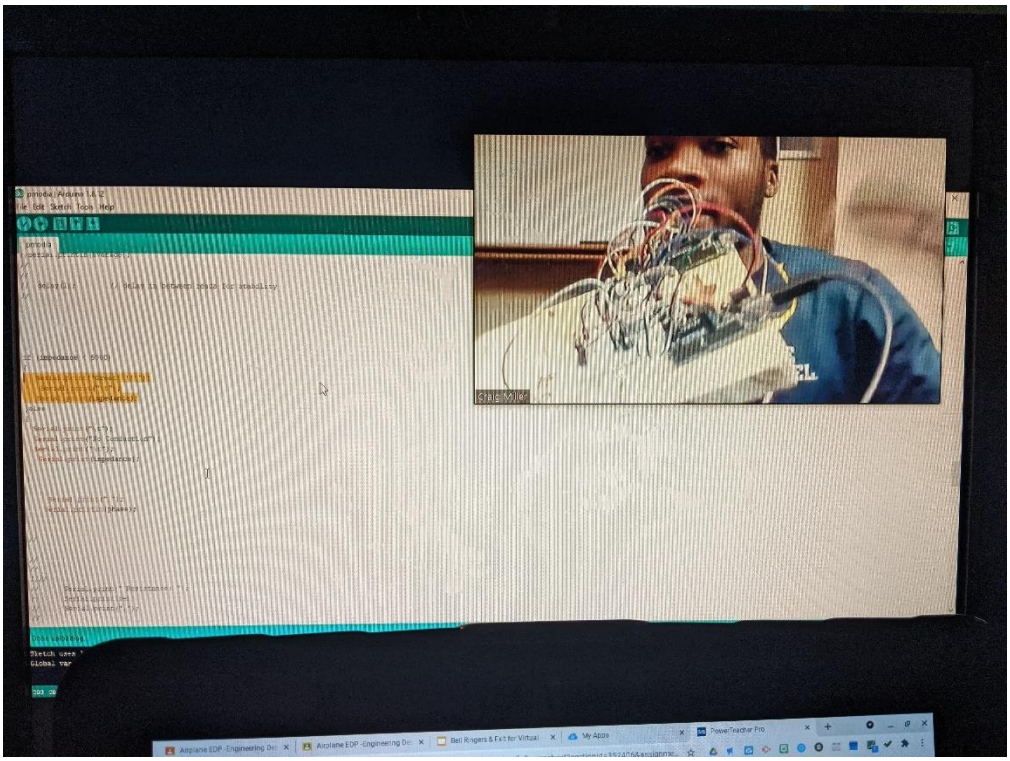

Figure 5.2. Images of DNA project.

Table 5.3. STEM outreach materials list	
DNA Module	
Item	**Supplier**
Construction Paper	Walmart
Scissors	Walmart
Scotch Tape	Walmart
Marker/Pen	Walmart
Glucose Module	
Glucose Meter	CVS
Gatorade	Walmart

Coca Cola	Walmart
Electrical Module	
Arduino Uno Kit	In-house
LEDs	In-house
Resistors	In-house
Breadboard	In-house

5.2A Instrument Development

A STEM Survey instrument was developed based on previous literature and feedback from program educators and STEM liaison officer. The literature review consisted of multiple searches for outreach studies examining the STEM career and activity interest. The search included studies addressing students' self-efficacy and their ability to pursue a STEM career. The search included the use of Google Scholar from the past 20 years. As discussed earlier, authors suggested that STEM career and activity interest was related to the overall self-efficacy and previous experiences of students. Additionally, the SCCT as seen in Figure 5.3 was used as a guide to help develop STEM instruments for the outreach project.

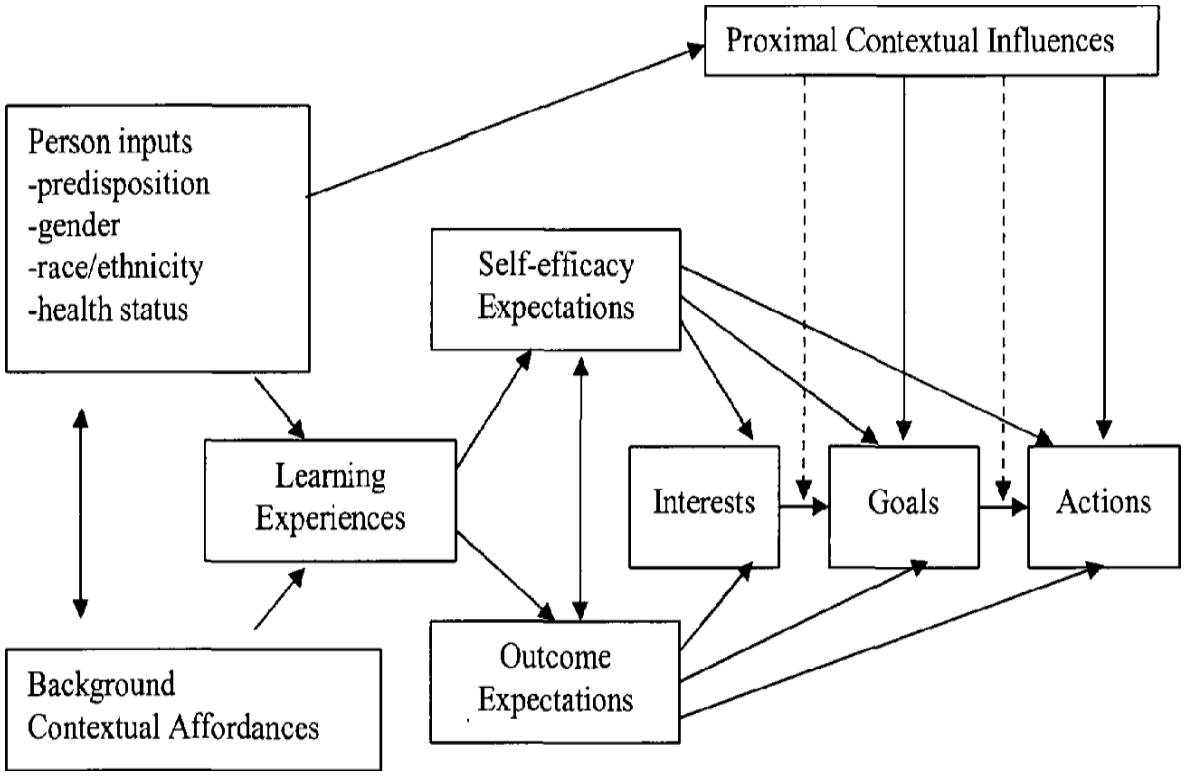

Figure 5.3. SCCT influences on career choice behavior. (34)

The outreach was 100% virtual and conducted across two different middle schools. Six total classes participated in the program. Two from Sangaree middle school and four from Cane Bay middle school. Below is a brief summary of the demographics of each group by class and school.

5.3 Results and Discussion

The sample population for this study consisted of predominately male population. Cane Bay consisted of a predominately white population, whereas Sangaree had a larger minority population. Minority being defined by most researchers as African American, Hispanic/Latino, or Native Americans. See Table 5.4 for demographics of participants. For all participants, it was the

first time they had the seen the items listed in the survey. Students took the survey online (Google Forms) using a school issued laptop.

Table 5.4: Demographics of Participants				
Variable	**Total**	**Class A**	**Class B**	**Class C**
Participants	130	44	38	48
Gender				
Male	69	24	23	22
Female	51	15	15	21
Other (decline to answer)	10	5	0	5
Ethnicity				
White	54	19	21	14
African-American	40	9	10	21
Hispanic	18	7	3	8
Native American	3	1	0	2
Asian American	9	4	4	1
Dominican	1	0	0	1
Other (decline to answer)	5	4	0	1

The participants were asked a series of question regarding their interest in pursuing a career in engineering, science, and mathematics. Most students at this grade level may understand what it means to be an engineer. However, many may not know many careers in mathematics. The reason for asking the same questions on each survey was to see if there would be an increased interest among participants for each career category. The level of interest in engineering increased

amongst participants from 20.93% to 32.06%. There was also a 5% reduction in the number of participants that listed that they "definitely did not" want to pursue a career in engineering. Compared to 1.24% reduction indicating that they were unsure. This indicates that the outreach may have persuaded

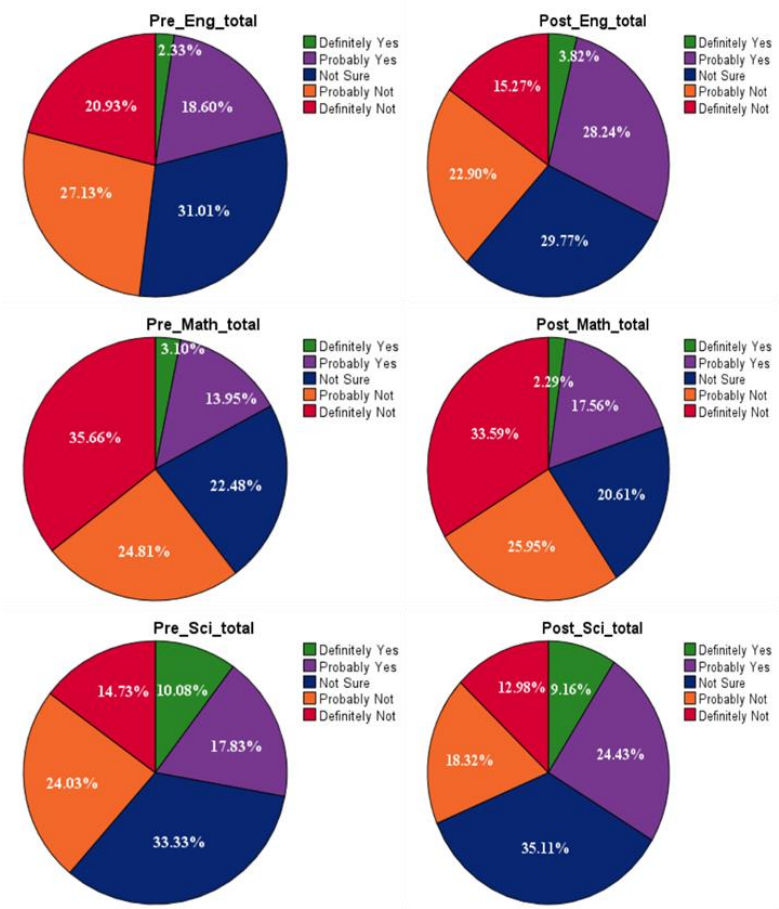

Figure 5.4. Compiled distribution of desire to pursue STEM career.

most participants to have an interest in pursuing a career in engineering as opposed to the lack of knowing what a career in engineering entails. Mathematics career interest was among the lowest on the pre survey where 60.47% indicated that they had no interest in pursuing a career in mathematics. There was a 2.8% increase in the desire to pursue a career in math compared to a 12% increase on the interest to pursue an engineering degree. The interest in a career in science

was initially 7% higher than that of engineering. Additionally, 10% fewer indicated that they did not want to pursuit a career in science. The number of students interested in science increased by 5.7%. The initial questions saw more variation in the interest and disinterest of students to pursue science and math. There were smaller differences seen within the unsure responses and within the entire mathematics group.

Cronbach's alpha is normally reported with the development of research scales intended to measure attitudes toward a particular subject. Alpha is a statistic used to demonstrate that a particular survey is fit for its intended purpose. A number of qualitative words have been used by authors to make an interpretation of Cronbach's alpha values. Alpha values can be labelled as excellent (0.93–0.94), strong (0.91–0.93), reliable (0.84–0.90), robust (0.81), fairly high (0.76–0.95), high (0.73–0.95), good (0.71–0.91), relatively high (0.70–0.77), slightly low (0.68), reasonable (0.67–0.87), adequate (0.64–0.85), moderate (0.61–0.65), satisfactory (0.58–0.97), acceptable (0.45–0.98), sufficient (0.45–0.96), not satisfactory (0.4–0.55) and low (0.11). (35)

STEM Career Knowledge

Questions were added to assess the knowledge of the participants and to understand how much general knowledge they had about some of the requirements needed to pursue a career in a STEM field. Initial Cronbach alpha was calculated on the survey questions for reliability. The STEM career knowledge portion included questions that asked if a specific STEM/non-STEM career required an advanced engineering/science curriculum. The answers were rated from 1, 2, and 3 for incorrect, unsure, and correct responses, respectively. A total of 14 measures were included where 6 involved questions that does not require advanced engineering curriculum such as plumber or politician occupation. The reliability of the construct with all 14 and the 6 questions

removed were tested. Table 5.5 of pre and post survey crons alpha pre and post screening of questions for all three classes are shown below.

Table 5.5. Cronbach's alpha summary of STEM career knowledge.

Class	**Measure Items**	**Cronbach's alpha (pre-survey)**	**Cronbach's alpha (post-survey)**
Class A	14	.775	.646
Class A*	8	.945	.935
Class B	14	.687	.607
Class B*	8	.868	.862
Class C	14	.320	.548
Class C*	8	.801	.902

The bioengineering professor measure in the SCK construct had a poor inter-item correlation matrix with the electrical engineering and mechanical engineering measure with a correlation of .072 and .055, respectively. Engineering technician had a poor correlation of .026 with civil engineering. Additionally, doctor had a poor correlation with electrical engineering of .055. This could be because some of the students were confused about what a professor means, and the requirements needed. The use of the original 14 question in the construct produced lower values where class C had a poor alpha. After screening out the six questions, the alpha improved to .801. For ANOVA analysis with this construct, the screened questions were removed. Class A and B both had acceptable alpha scores for both set of questions. Higher alpha scores with the

screened questions along with the slight increase in values with the post survey results was encouraging. This could be due to poor flexibility in construct or increased knowledge in STEM requirements from the given modules.

The average SCK from Class A, B and C was 19.8, 20.7, and 20.1, respectively. SCK score was relatively high where a maximal score was 24 points. The average scores can be seen in Figure 5.5. Approximately 73% of students had a high SCK score in the top quartile. This could be due to an increase in information on STEM and the importance of science and mathematics in the communities. ANOVA analysis was conducted on the SCK construct for the three classes along with the entire population. SCK from class B was significantly higher than both classes, where there was no difference between class A and C. The same relation was seen with the post-survey responses. Gender did not produce a significant difference in the SCK score.

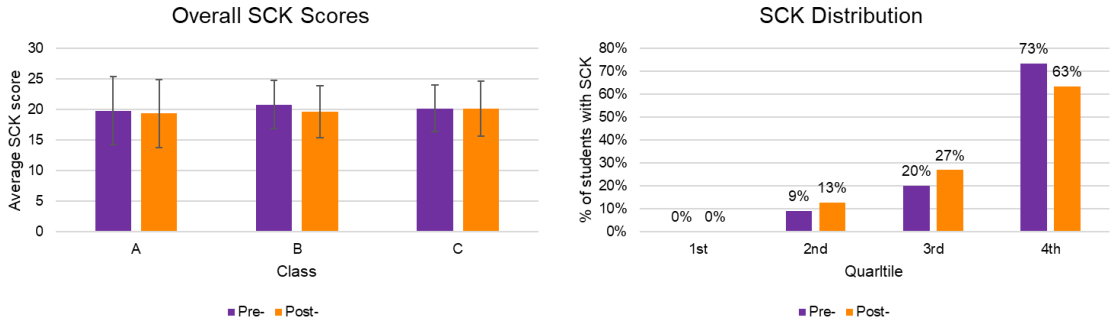

Figure 5.5. STEM career knowledge.

STEM self-efficacy

The Self-efficacy construct consisted of a math portion and science portion. The questions for each portion were similar with just a replacement of the word science with math. This construct was used to understand the level of self-efficacy of the students involved in the program. Initial

Cronbach alpha was calculated on the survey questions for reliability. The STEM science and math self-efficacy portion included questions that asked how confident the students were at performing a particular task. Other questions were added to determine their expected outcomes of a math and science course. The answers were rated from 1, 2, 3, 4, 5 for strongly disagree, disagree, unsure, agree, and strongly agree, respectively. A total of 17 measures were included where 6 involved questions that required an answer of strongly disagree in order to get the highest score. For example, strongly disagree for the measure "Math is hard" warrants a score of 5. Table 5.6 shows the reliability values for the pre and post survey for all three classes. Self-efficacy construct generated relatively high to excellent reliability values for both surveys.

Table 5.6. Cronbach's alpha summary of STEM math and science self-efficacy

Class	Self-efficacy	Cronbach's alpha (pre-survey)	Cronbach's alpha (post-survey)
Class A	Math	.854	.890
	Science	.900	.870
Class B	Math	.863	.854
	Science	.792	.797
Class C	Math	.941	.921
	Science	.918	.866

Overall, there was an increase seen in the science and mathematical self-efficacy of all three classes between the pre- and post- survey responses. Class A and B both had higher efficacy scores than Class C. Additionally, there was a significant difference seen between gender groups where the self-efficacy of male participants was higher than females ($\alpha < .05$). This was seen in the pre and post survey responses. No significant difference in science or mathematical self-

efficacy found with the pre or post survey responses between ethnical groups. However, minority groups (African American and Hispanic) had slightly higher science self-efficacy scores compared to Asian and white students. Asian American students had a higher math self-efficacy score in the pre-survey. The students were asked if they had a desire to pursue a career in Engineering, Math or Science. The responses were either definitely yes, yes, unsure, no, or definitely. Definitely yes and yes were grouped together as was Definitely no and no, where a score of 3 and 1 was given, respectively. Unsure was given a score of 2. The average SSE scores and MSE were graphed against the desire to pursue a STEM career. In the pre-survey responses, there was no significant difference between the SSE scores and the desire to pursue a Engineering or Math career. However, there was a significant difference in the SSE scores and the desire to pursue a career in science. The same response was seen in the post-survey response with the exception that there was a significant difference seen in SSE scores and desire to pursue engineering. The students that showed a desire to pursue a career in engineering or math had significantly higher MSE scores. However, there was no difference seen in the MSE scores and the desire to pursue a science career. The same was seen in the post-survey responses.

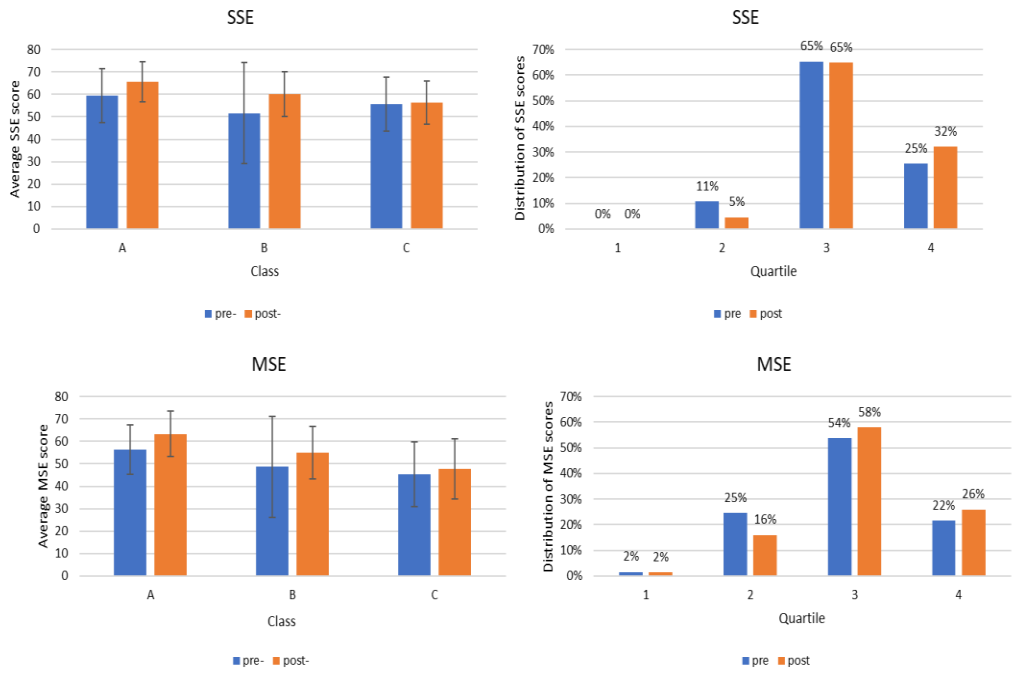

Figure 5.6. Compiled and distribution of Science and Math self-efficacy responses.

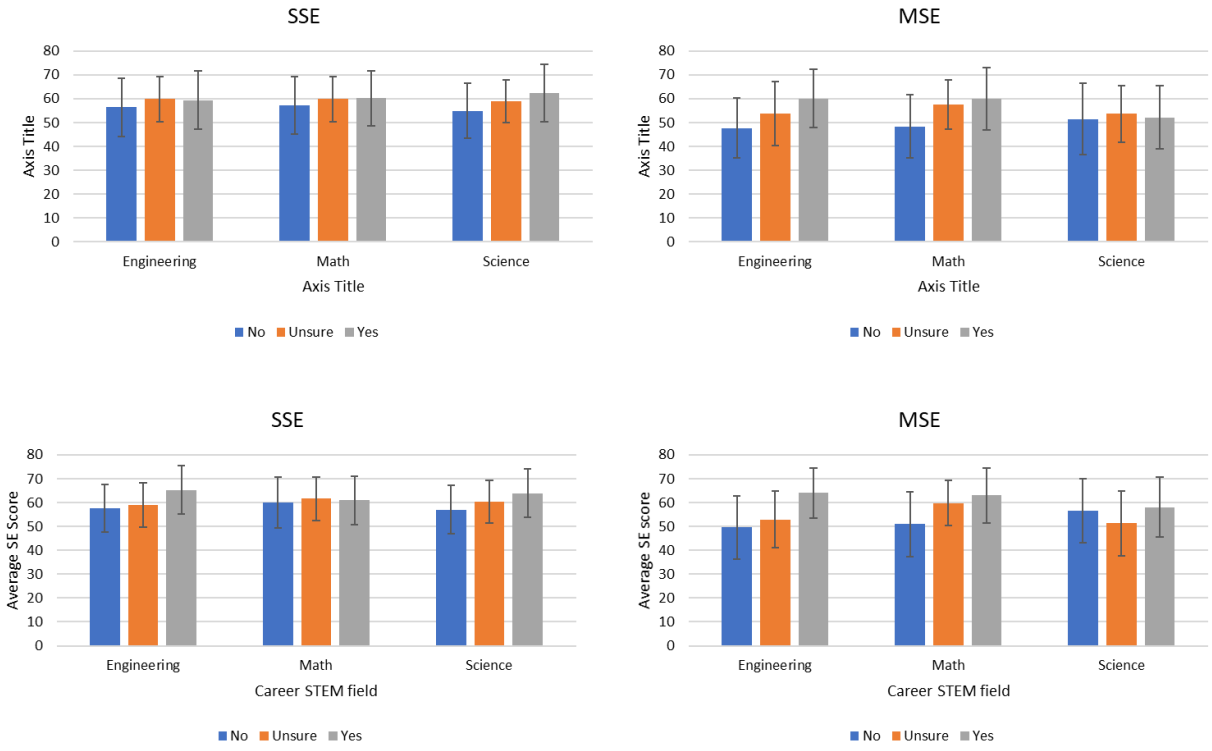

Figure 5.7. Pre- and post- self-efficacy vs desire to pursue a STEM career.

Table 5.7. Pre-Survey STEM Self-Efficacy: ANOVA alpha values				
		Engineering	**Math**	**Science**
SSE				
No Desire	Unsure	0.163	0.298	0.094
	Desire	0.289	0.254	0.002
Unsure	No Desire	0.163	0.298	0.094
	Desire	0.870	0.902	0.194
Desire	No Desire	0.289	0.254	0.002
	Unsure	0.870	0.902	0.194
MSE				
No Desire	Unsure	0.022	0.002	0.469
	Desire	0.000	0.000	0.803
Unsure	No Desire	0.022	0.002	0.469
	Desire	0.045	0.484	0.655
Desire	No Desire	0.000	0.000	0.803
	Unsure	0.045	0.484	0.655

Table 5.8. Post-Survey STEM Self-Efficacy: ANOVA alpha values				
		Engineering	**Math**	**Science**
SSE				
No Desire	Unsure	0.536	0.495	0.126
	Desire	0.000	0.651	0.002

Unsure	No Desire	0.536	0.495	0.126
	Desire	0.004	0.855	0.092
Desire	No Desire	0.000	0.651	0.002
	Unsure	0.004	0.855	0.092
MSE				
No Desire	Unsure	0.211	0.002	0.068
	Desire	0.000	0.000	0.606
Unsure	No Desire	0.211	0.002	0.068
	Desire	0.000	0.338	0.018
Desire	No Desire	0.000	0.000	0.606
	Unsure	0.000	0.338	0.018

There was a portion on the survey that asked the students various questions to determine their interest in pursuing a career in science, engineering, or Math along with their interest in STEM activities such as "I would like to use creativity and innovation in my future work." There were five responses between Strongly agree to Strongly disagree and were scaled from 5 to 1. The STEM activity interest (SAI) scores were correlated to the interests in the STEM career field. There was a significant difference between the SAI scores and the desire to pursue a career in all STEM fields on the survey with the exception of Math on the post survey. This shows that the interest in STEM activities are related to the participants desire to pursue a career in STEM.

Table 5.9. Cronbach's alpha summary of STEM career knowledge			
Class	**Measure Items**	**Cronbach's alpha (pre-survey)**	**Cronbach's alpha (post-survey)**
Class A	8	.935	.885
Class B	8	.908	.905
Class C	8	.872	.869

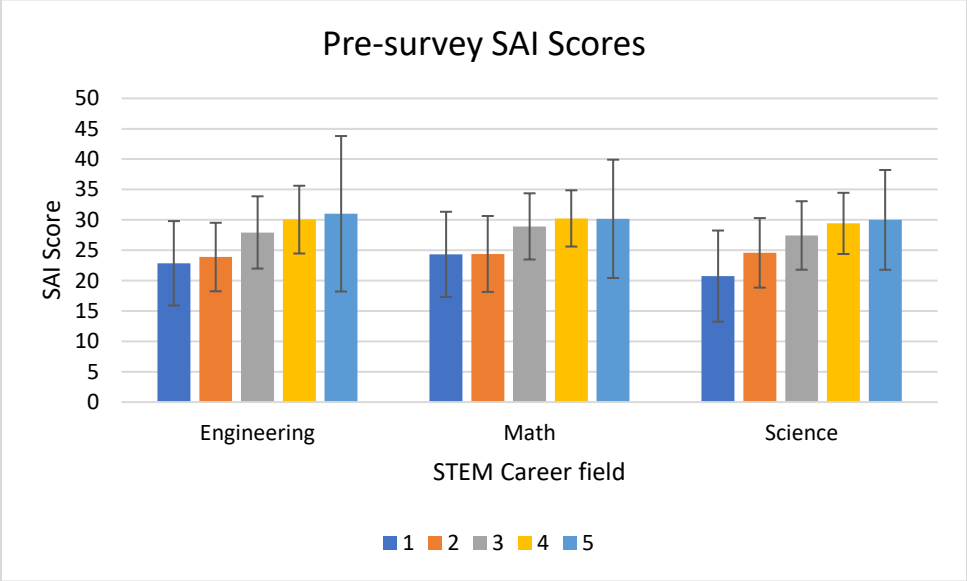

Figure 5.8. Pre- STEM activity interest score vs desire to pursue a STEM career.

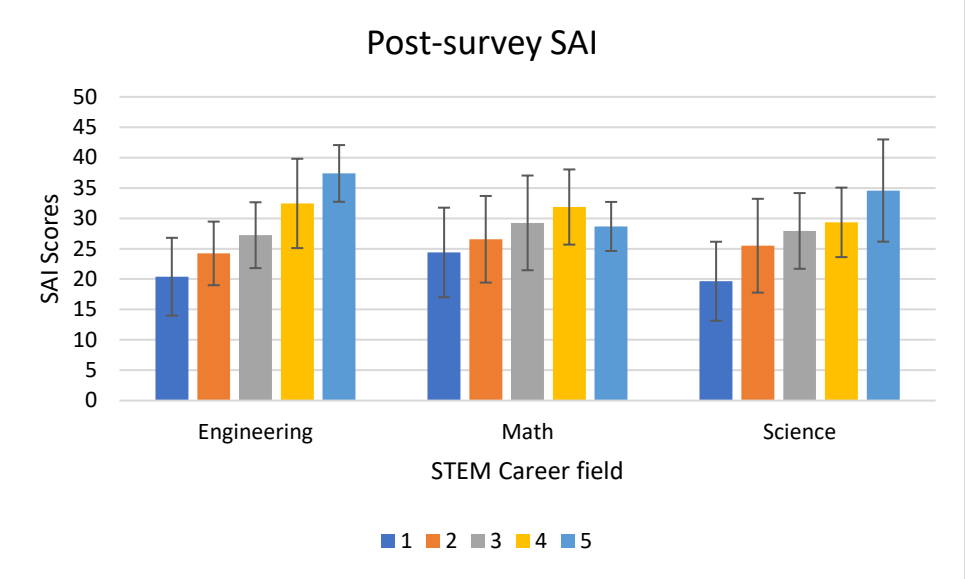

Figure 5.9. Post- STEM activity interest score vs desire to pursue a STEM career.

Table 5.10. Pre-Survey STEM Activity Interest: ANOVA alpha values

		Engineering	**Math**	**Science**
Strongly Disagree	Disagree	0.526	0.964	0.030
	Unsure	0.001	0.004	0.000
	Agree	0.000	0.001	0.000
	Strongly Agree	0.017	0.037	0.000
Disagree	Strongly Disagree	0.526	0.964	0.030
	Unsure	0.006	0.009	0.053
	Agree	0.000	0.003	0.003
	Strongly Agree	0.034	0.046	0.005

Unsure	Strongly Disagree	0.001	0.004	0.000
	Disagree	0.006	0.009	0.053
	Agree	0.193	0.513	0.229
	Strongly Agree	0.352	0.669	0.181
Agree	Strongly Disagree	0.000	0.001	0.000
	Disagree	0.000	0.003	0.003
	Unsure	0.193	0.513	0.229
	Strongly Agree	0.778	0.982	0.775

Table 5.11. Post-Survey STEM Activity Interest: ANOVA alpha values

		Engineering	**Math**	**Science**
Strongly Disagree	Disagree	0.032	0.187	0.006
	Unsure	0.000	0.006	0.000
	Agree	0.000	0.000	0.000
	Strongly Agree	0.000	0.319	0.000
Disagree	Strongly Disagree	0.032	0.187	0.006
	Unsure	0.046	0.146	0.149
	Agree	0.000	0.007	0.35
	Strongly Agree	0.000	0.626	0.000

Unsure	Strongly Disagree	0.000	0.006	0.000
	Disagree	0.046	0.146	0.149
	Agree	0.000	0.202	0.36
	Strongly Agree	0.001	0.892	0.003
Agree	Strongly Disagree	0.000	0.000	0.000
	Disagree	0.000	0.007	0.035
	Unsure	0.000	0.252	0.36
	Strongly Agree	0.093	0.468	0.022

Table 5.12. Item-total correlation of individual questions vs total category score.

Item number	**Item-total correlation**	**Question**
Test: Interest in STEM		
Q1	0.604	I am interested in learning more about Math
Q2	0.740	I am interested in learning more about science
Q3	0.829	I am interested in the engineering design process
Q4	0.811	I am interested in the engineering design process
Q5	0.668	I am interested in learning more about engineering
Test: Science Self-efficacy		

Q1	-0.212	I believe I can get an "A or B" in a Science Class
Q3	-0.35	I have a hard time understanding Science even if I try hard
Q5	-0.248	I feel confident when using Science outside of class
Q18	0.112	Doing well in Science will help me in my future career
Q19	0.14	I will work hard in my Science classes
Test: MATH Self-efficacy		
Q1	0.135	I believe I can get an "A or B" in a MATH Class
Q3	-0.661	I have a hard time understanding MATH even if I try hard
Q5	-0.509	I feel confident when using MATH outside of class
Q18	-0.341	Doing well in MATH will help me in my future career
Q19	0.435	I will work hard in my MATH classes

5.4 Conclusion

In conclusion, the outreach program was supposed to be an in-person event, but pandemic caused us to shift to a virtual platform. All participants in this outreach thoroughly enjoyed the online experience. The motivation to complete this work is to increase the number of minorities and underrepresented students to pursue STEM related studies and careers. Additionally, the middle schools targeted in this study are local school from my hometown region of in the low country. Participation in middle school outreach programs increases the development of self-efficacy in students. As seen in the survey responses, there was no significant difference seen in the self-efficacy scores. However, minority groups had a higher science self-efficacy score than

any other ethnic groups. This could be due to the fact that I am a minority that they possibly self-identify with. The outreach program was 100% online, but it included some hands-on experience with their respective teachers under my guidance. Self-efficacy and interest play a huge role in the intent of perspective students to pursue a STEM related career or field of study. Results from the survey showed that interest in STEM related activities has an influence on middle school students' intent to pursue a career in science, engineering, or math. Based on the survey results and feedback, we believe that programs as these provide a great experience for minority and majority middle school aged students.

5.5 References

1. O'Hanlon ME. Forecasting Change in Military Technology. Mil Technol 2020 [Internet]. 2018 [cited 2021 May 13]; Available from: https://www.worldpittsburgh.org/wp-content/uploads/2019/01/Forecasting-change-in-military-technology-2020-2040-Brookings-2018.pdf
2. Jentsch F. Human-Robot Interactions in Future Military Operations - Florian Jentsch - Google Books [Internet]. 2016 [cited 2021 May 13]. Available from: https://books.google.com/books?hl=en&lr=&id=3qGKDQAAQBAJ&oi=fnd&pg=PT9&dq=future+military+technology&ots=VyBAkimf4M&sig=jNG3uzpB8n2qXHjJr1KAL52naqU#v=onepage&q=future military technology&f=false
3. U.S. Department of Education Advances Trump Administration's STEM Investment Priorities | U.S. Department of Education [Internet]. [cited 2021 May 17]. Available from: https://www.ed.gov/news/press-releases/us-department-education-advances-trump-administrations-stem-investment-priorities
4. National Science Foundation. Revisiting the STEM Workforce: A Companion to Science and Engineering Indicators 2014 (NSB-2015-10) [Internet]. 2015 [cited 2021 May 17]. Available from: https://www.census.gov/dataviz/visualizations/stem/stem-html/
5. Camilli G, Hira R. Introduction to Special Issue-STEM Workforce: STEM Education and the Post-Scientific Society. 2018 [cited 2021 May 17]; Available from: https://doi.org/10.1007/s10956-018-9759-8
6. Hira R. U.s. policy and the STEM workforce system. Am Behav Sci [Internet]. 2010 Mar 9 [cited 2021 May 17];53(7):949–61. Available from: http://abs.sagepub.com
7. Cannady MA, Greenwald E, Harris KN. Problematizing the STEM Pipeline Metaphor: Is the STEM Pipeline Metaphor Serving Our Students and the STEM Workforce? Sci Educ [Internet]. 2014 May 1 [cited 2021 May 17];98(3):443–60. Available from: https://onlinelibrary.wiley.com/doi/full/10.1002/sce.21108

8. Rothwell J. The Hidden STEM Economy [Internet]. 2013 [cited 2021 May 17]. Available from: https://www.brookings.edu/research/the-hidden-stem-economy/

9. Funk C, Parker K. Diversity in the STEM workforce varies widely across jobs | Pew Research Center [Internet]. 2018 [cited 2021 May 17]. Available from: https://www.pewresearch.org/social-trends/2018/01/09/diversity-in-the-stem-workforce-varies-widely-across-jobs/

10. Zilberman A, Ice L. Why computer occupations are behind strong STEM employment growth in the decade [Internet]. Vol. 10. 2021 [cited 2021 May 17]. Available from: www.bls.gov/oes/

11. Fayer S, Lacey A, Watson A. STEM Occupations: Past, Present, And Future. 2017.

12. The State of U.S. Science and Engineering 2020 | NSF - National Science Foundation [Internet]. [cited 2021 May 14]. Available from: https://ncses.nsf.gov/pubs/nsb20201/u-s-s-e-workforce

13. Kendall DG. Some Problems in the Theory of Queues [Internet]. Vol. 13, Source: Journal of the Royal Statistical Society. Series B (Methodological). 1951 [cited 2021 May 18]. Available from: https://about.jstor.org/terms

14. Ghaffarzadegan N, Hawley J, Larson R, Xue Y. A Note on PhD Population Growth in Biomedical Sciences. Syst Res Behav Sci [Internet]. 2015 May 1 [cited 2021 May 18];32(3):402–5. Available from: /pmc/articles/PMC4503365/

15. Cyranoski D, Gilbert N, Ledford H, Nayar A, Yahia M. Education: The PhD factory. Nature. 2011 Apr 21;472(7343):276–9.

16. Fernandes JD, Sarabipour S, Smith CT, Niemi NM, Jadavji NM, Kozik AJ, et al. A survey-based analysis of the academic job market. Elife. 2020 Jun 1;9:1–30.

17. Xue Y, Larson RC. STEM crisis or STEM surplus? Yes and yes. Mon Labor Rev. 2015;2015(5).

18. Bowen RM, Arvizu DE, Bassler B, BENBOW Patricia CP, Hart R, BRUER President JT, et al. Science and Engineering Indicators 2012.

19. Austin J. Want to Be a Professor? Choose Math. Science (80-). 2013 Jul 24;

20. Kulis S, Shaw H, Chong Y. External Labor Markets and the Distribution of Black Scientists and Engineers in Academia. J Higher Educ. 2000 Mar;71(2):187.

21. Edwards KA, Mccollester M, Phillips B, Acheson-Field H, Leamon I, Johnson N, et al. Compensation and Benefits for Science, Technology, Engineering, and Mathematics (STEM) Workers: A Comparison of the Federal Government and the Private Sector [Internet]. 2021 [cited 2021 May 18]. Available from: www.rand.org/nsrd/frp

22. of the Chief Economist O, Administration S, Department of Commerce U. STEM Jobs: 2017 Update [Internet]. [cited 2021 May 18]. Available from: https://cew.georgetown.edu/cew-

23. Yerdelen S, Kahraman N, Taş Y. Low socioeconomic status students' STEM career

interest in relation to gender, grade level, and stem attitude. J Turkish Sci Educ. 2016;13(Specialissue):59–74.

24. Compeau S. THE CALLING OF AN ENGINEER: HIGH SCHOOL STUDENTS' PERCEPTIONS OF ENGINEERING.

25. Zhang L, Barnett M. How high school students envision their STEM career pathways. Cult Stud Sci Educ [Internet]. 2015 Sep 22 [cited 2021 May 24];10(3):637–56. Available from: https://link.springer.com/article/10.1007/s11422-013-9557-9

26. Harackiewicz JM, Rozek CS, Hulleman CS, Hyde JS. Helping Parents to Motivate Adolescents in Mathematics and Science : An Experimental Test of a Utility-Value Intervention. 2012 [cited 2021 May 24]; Available from: http://pss.sagepub.com/http://pss.sagepub.com/content/early/2012/07/02/0956797611435530

27. Full STEM Ahead: Afterschool Programs Step Up as Key Partners in STEM Education [Internet]. [cited 2021 May 24]. Available from: http://www.afterschoolalliance.org/aa3pm/STEM.pdf

28. (US). PC of A on S and T. Prepare and Inspire: K-12 Education in Science, Technology, Engineering, and Math (STEM) for America's Future: Executive Report. [Internet]. 2010 [cited 2021 May 24]. Available from: http://www.whitehouse.gov/ostp/pcast.

29. Mangu DM, Lee AR, Middleton JA, Nelson JK. Motivational factors predicting STEM and engineering career intentions for high school students. In: Proceedings - Frontiers in Education Conference, FIE. Institute of Electrical and Electronics Engineers Inc.; 2015.

30. Lent RW, Brown SD, Hackett G. Toward a Unifying Social Cognitive Theory of Career and Academic Interest, Choice, and Performance. Vol. 45, Journal of Vocational Behavior. Academic Press; 1994. p. 79–122.

31. Roberts T, Jackson C, Mohr-Schroeder MJ, Bush SB, Maiorca C, Cavalcanti M, et al. Students' perceptions of STEM learning after participating in a summer informal learning experience. Int J STEM Educ. 2018;5(1).

32. Blotnicky KA, Franz-Odendaal T, French F, Joy P. A study of the correlation between STEM career knowledge, mathematics self-efficacy, career interests, and career activities on the likelihood of pursuing a STEM career among middle school students. Int J STEM Educ. 2018;5(1).

33. Allen PJ, Chang R, Gorrall BK, Waggenspack L, Fukuda E, Little TD, et al. From quality to outcomes: a national study of afterschool STEM programming. Int J STEM Educ [Internet]. 2019 Dec 1 [cited 2021 May 25];6(1):1–21. Available from: https://doi.org/10.1186/s40594-019-0191-2

34. Ambriz J. Social cognitive career theory (SCCT) and Mexican/Mexican-American youth career development, with a special focus on STEM fields. undefined. 2016;

35. Taber KS. The Use of Cronbach's Alpha When Developing and Reporting Research Instruments in Science Education. Res Sci Educ. 2018;48(6):1273–96.

CHAPTER SIX
CONCLUSIONS AND FUTURE WORK

6.1 Summary of Findings

This chapter details the conclusions of various experiments done in the development of solution blow spun nanofibers for potential biosensing applications. Additionally, future directions are discussed for further developing point-of-care solution blow spun-based sensors for molecular, protein and pathogen detection schemes. After a two literature reviews and the completion of this work, it can be concluded that nonwoven nanofiber mats are capable of fulfilling most properties required of a biosensor interface material that could be used for chronic wound applications. This work focused on the conductivity, antimicrobial, adsorptive, and electrical response of solution blow spun nonwoven scaffolds. Overall, we have found that solution blow spun-based electrodes can be used for electrochemical detection schemes of small molecules and of whole cell pathogens. Initial results showed that MWCNT and $AgNO_3$ were both great materials for the development of conductive and conductive/antimicrobial filler material. These nanofiber mats were tested in the detection of whole cell bacteria (Aim 1) in an effort to determine bacteria concentration from aqueous solutions. Additional efforts were made to also assess material performance in protein adsorption in relation to surface treatment techniques (Aim 2). Enhanced protein adsorption was found with treated nanofiber surfaces for potential biosensing applications. Other work focused on the development of electrodes for the detection of pyocyanin, redox virulence factor, from *Pseudomonas aeruginosa* PAO1. Surface treatment techniques in this study, increased protein, and whole cell biosensor uptake.

The developed solution blow spun apparatus consisted of low-cost material that was capable of generating nanofibers of varying diameter and composition. The apparatus used a Paasche flow pencil, compressed nitrogen (N2) gas, stepper-motor driven collector spool, and an

Arduino for control. All materials were derived from the lab and allowed for the development of a low-cost fiber fabrication platform. Poly(lactic acid) (PLA), multi-walled Carbon nanotubes (MWCNT) and chloroform was used to generate conductive nano-fibers. The conductivity of the fiber mats was also modified by varying the concentration of MWCNT. In our initial analysis, conductive fiber mats reached conductivity values as high as 474 S/cm, which is 2x higher than the commonly used semiconductor, germanium. Furthermore, 4% weight/volume PLA and 20% weight/weight MWCNT produced the smallest fibers with a mean diameter of 74.25 ± 42.71 nm. MWCNT displayed great dispersion in higher PLA polymer loading solutions. Lower polymer concentrations showed superior conduction, but poorer solution dispersion which is a result of lower viscosity and less entanglement between MWCNT and PLA polymer.

Impedance spectroscopy testing of whole cell bacteria was done with the use of MWCNT nanofibers to explore its potential use in bacterial and pathogenic electrochemical detection. This study also explores the electrical potential of solution blow spun MWCNT:PLA composites for bacterial and pathogenic electrochemical detection. Testing was done to measure the change in media conduction due to the presence of bacteria. We conducted an in vitro study to examine the use of impedance spectroscopy to detect the presence and concentration levels of *Pseudomonas putida (P. putida)* in a petri dish containing solid LB (lysogeny broth) media. Solution Blow Spun (SBS) poly(lactic-acid)/multiwalled Carbon nanotube (MWCNT) composite nanofiber mats were used as the sensing element. 10cm x 25cm strips were used and plated in petri dishes according to experimental design. An LCR 6002 Meter was used to conduct real-time 24-hour measurements. Results from this study showed that a 10^{-5} dilution displayed an increase in the normalized impedance (measured/initial) response over the testing period. P. putida increased the impedance across the 10cm x 25cm mats greater than the control solid LB broth condition. Continuous

monitoring (24-hour testing) provided a way to simulate bacterial growth in a culture environment over a longer period, and may have applications in long term, remote patient monitoring and telehealth. Long-term monitoring allows for the time-wise characterization of the change in impedance as bacterial colonization and biofilm formation begin to surround transducers. Instantaneous measurements (1-minute testing) were able to detect the presence of bacteria within seconds and would be useful in point-of-care clinical applications where immediate quantification is important for diagnosis.

Many biosensors employ immobilization of proteins such as antibodies and other biorecognizing elements to yield specific signal transduction. Improving the binding strength of such elements to the target analyte increases the signal-to-noise ratio of such platforms. Immunodiagnostics and biosensors developed for pathogenic antigen detection and quantification from samples utilize recognition proteins such as antibodies. In this study we used physical and chemical adsorption to facilitate immobilization of capture antibodies on the surface of solution blow spun (SBS) nanofiber substrates in a modified enzyme-linked immunoassay (ELISA) approach. The immobilization of capture molecules such as proteins, antibodies, and aptamers play a vital role in the performance of immunoassays. Immunoassays depend on the orientation and availability of antibodies. Biosensor performance depends on the sufficient immobilization of the capture element on a solid support surface with sufficient surface density and the maximization of antigen capture event. Biosensing potential was examined with the use of the anti-spike and spike protein system.

A multi-layered, conductive nanofiber composite was used as the base biosensor. Specifically, a flexible conductive silver ink was screen printed on Polyethylene Terephthalate (PET) film to serve as the conductive base material. Poly (l-lactide acid) (PLA) and Multi-walled

Carbon Nanotubes (MWCNT) were solution blow spun (SBS) over the silver interdigitated electrode pattern to provide a hydrophobic scaffold for antibody immobilization. Physical adsorption via soaking was used to fix antibodies to the SBS PLA/MWCNT samples. Fluorescently tagged antibodies (Donkey anti-goat alexa flour 594) were used to verify protein adsorption along with bicinchoninic acid assay (BCA, Albumin Standard). SBS PLA and PLA/MWCNT fiber mats were dissolved in 2mg/mL of bovine serum albumin over 1hr., 30min, and 5min. BCA was used to assess BSA adsorption via UV-Vis spectroscopy at 480nm. Donkey anti-goat capture antibodies conjugated with Alexa Fluor 594 was successfully immobilized on SBS PLA/MWCNT nanofiber substrate (8ug/mL). Qualitative fluorescent signal verified the presence of proteins on the surface. Increasing the soak time from 5min. to 24 hours caused an increase in fluorescent signal as can be seen in Figure 1. BCA results showed that SBS scaffolds are capable of adsorbing protein (albumin), which is essential for proper biosensor immobilization techniques. The incorporation of Carbon generally decreases the adsorption of PLA scaffolds. However, the inclusion of more PLA in the composite allowed for more protein immobilization. Additionally, SBS PLA/MWCNT remained conductive post immobilization, which would indicate that an electrical signal could still be obtained from a functionalized electrode. The work outlined here shows that the surface medication, immobilization method, blocking, and antibody concentration play key roles in the modulation of impedance response and protein uptake for SBS nanofiber PLA:MWCNT constructs. This nanofiber fabrication and immobilization technique may be successfully modified to address a multiple biosensing factors *in vitro* and *in vivo*.

Gram-negative bacteria passively release low molecular weight acyl-homoserine lactones (HSLs). HSLs are lipid molecules that possess a lactone ring with a carbon side chain that could range from 4 to 16 carbons. These molecules are hydrophobic in nature and their phobicity depends

on the carbon chain length. *P. aeruginosa* utilizes the 3-oxo-C12-homoserine lactone (3OC12HSL) to upregulate quorum sensing dependent virulence factors. Point-of-care detection of these signaling molecules would provide clinicians with a great tool to determine the presence of *P. aeurignosa* and other virulent gram-negative bacteria. Chromoproteins can be used as a reporter for transcriptional whole cell biosensors. AmilCP is a chromoprotein that is derived from the coral *Acropora millepora* and exhibits a strong blue/purple visible color at 588 nm. [1] The advantage of using chromoproteins is the ease of use and readout where there is no need for a substrate and a stop solution to end the reaction such as enzymatic detection schemes. Additionally, chromogenic biosensor was developed via Gibson assembly. SBS nanofiber substrates were used as a site of immobilization for synthetic probes. Additionally, conductive SBS composites were used to develop transducers to electrochemically detect pyocyanin produced by Pseudomonas aeruginosa. Electrochemical properties of SBS-based electrodes were analyzed with potassium ferricyanide. The detection range of pyocyanin for fabricated electrodes was found to be 5 – 300 uM with a limit of detection of approximately 700 nM. Additionally, electrodes were used to conduct antimicrobial susceptibility testing with silver nitrate in pseudomonas cultures. This method could be used to screen novel drugs against Pseudomonas aeruginosa and detect the onset of virulence for chronic wound applications.

Being a Call Me Doctor Fellow® I was required to conduct an outreach project of my choosing. The objective of this chapter was to conduct a 5-day Outreach STEM project to examine and increase the self-efficacy of middle school aged students from a rural and underrepresented population. The project aimed to increase the awareness of STEM careers and common mathematics and scientific topics discussed at the middle school level that is required by the state.

Target school was previously Holly Hill, SC Middle. This would have been a more appealing option as the school district is from my hometown and the population is majority minority students. However, the opportunity to do a virtual program was not possible at the time. Therefore, we had the opportunity to conduct a virtual outreach through 5 total classes split into three sessions. Day 1 involved a pre-survey to assess the initial self-efficacy and interest in STEM careers and subjects along with an introduction to common career paths and higher educational options. Day 2 involved a gave an overview of glucose and how it is used as a biomarker for diabetes. Scientific and mathematic topics was integrated into the presentation and glucose detection project in an effort to show how their middle school curriculum fits into real-world applications. Day 3 included an overview of DNA and central dogma theory with a small DNA isolation project. Day 4 involved the use of a small Arduino project and discuss electronics and electricity theory. We concluded the program with a small post-survey to assess the effectiveness of the program and a conclusion.

6.2 Future Work

Chapter 1

1. More literature is needed on the application and development of whole-cell bacteria biosensors and textile integration.
2. The literature lacks publications on pure electrical properties of individual bacterial cells and textile electrode modeling and design.
3. More insight on the physics and electrical properties of non-conductive and conductive solution blow spun nanofibers.

Chapter 2

1. Assessment of chirality/structural changes in solution blow spun multi-walled carbon nanotubes during and after fabrication process.

2. Development of a working microfluidic channel with filtering properties to address need for in-situ testing and fluid stability.
3. Modeling and testing of electrical properties of various pathogenic bacterial cells on a molecular level in their planktonic and biofilm state.

Chapter 3

1. Assess the long-term stability of immobilized surfaces via Raman spectroscopy to determine if protein structural changes are occurring and at what point does this occur in relation to electrical response.
2. The development of alternative models for electrochemical detection of proteins via the development of redox labeled aptamers
3. The Development and modeling of Photolithographic patterning of solution blow spun films for nano/micro electrodes could help increase sensitivity of transducers.
4. The use of gold interdigitated electrode arrays to assess protein and/or aptamer structural changes with and without binding over time with the use of dielectrophoresis.

Chapter 4

1. The development of alternative reporter systems to enhance visual distinction within SBS textile mesh such as a enzymatic reporter with substrate.
2. Development of probiotic lactic acid non-model vectors for theragnostic chronic wound applications.
3. Incorporation of LAMP assay with solution blow spun nanofiber lateral flow for specific, in-situ detection of bacteria presence. See Figure 6.1.

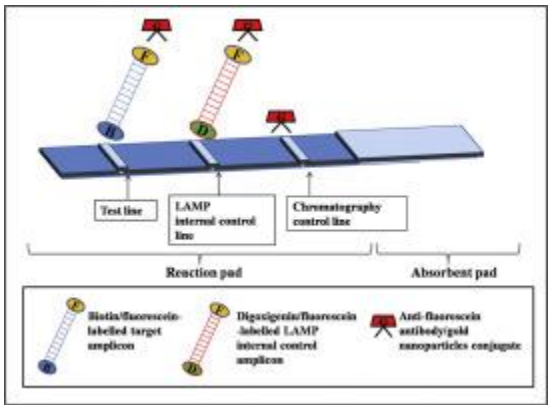

Figure 6.1. LAMP isothermal amplification lateral flow substrate.[2]

Chapter 5

1. Conducting the study with more students and schools would further validate program's efficiency along with tracking the performance of a small cohort of participants from middle school upto early college years.
2. Conduct an in-person study and compare to virtual platform in an effort to improve virtual platform for program dissemination.
3. Conduct more studies as these are needed to continue the contribution of giving back in an effort to increase the diversity and strength of our STEM workforce.

6.3 References

[1] "Part:BBa K592009 - parts.igem.org." .

[2] A. B. Nurul Najian, E. A. R. Engku Nur Syafirah, N. Ismail, M. Mohamed, and C. Y. Yean, "Development of multiplex loop mediated isothermal amplification (m-LAMP) label-based gold nanoparticles lateral flow dipstick biosensor for detection of pathogenic Leptospira," *Anal. Chim. Acta*, vol. 903, pp. 142–148, Jan. 2016, doi: 10.1016/J.ACA.2015.11.015.

Appendix A: Outreach Survey

Name: _____

Part I - Background Information:

A. Your sex is
   - Male
   - Female
   - I prefer not to answer

B. What is your racial or ethnic identification? (select one)
   - American Indian or other native person
   - Asian, Asian American or Pacific Islander
   - Black or African American
   - White (non-Hispanic)
   - Hispanic or Latino/a
   - Multiracial
   - Other: _____
   - I prefer not to answer

C. Do any of your immediate family members hold an engineering degree?
   - YES
   - NO
   - I prefer not to answer

D. What is the highest level of education that your mother completed? (Mark one)
   - Did not finish high school
   - Graduated high school
   - Attended college but did not complete degree
   - Completed an Associate degree
   - Completed a Bachelor degree (AA, AS, etc.)
   - Completed a Masters degree (MBA, MA, MS, etc.)
   - Completed a Doctoral or Professional Degree (JD, MD, PhD, etc.)
   - I don't know
   - I prefer not to answer

E. What is the highest level of education that your father completed? (Mark one)
   - Did not finish high school
   - Graduated high school
   - Attended college but did not complete degree
   - Completed an Associate degree
   - Completed a Bachelor degree (AA, AS, etc.)
   - Completed a Masters degree (MBA, MA, MS, etc.)

- Completed a Doctoral or Professional Degree (JD, MD, PhD, etc.)
- I don't know
- I prefer not to answer

F. Do you see yourself pursuing a career in Engineering?

- Definitely Not
- Probably Not
- Not Sure
- Probably Yes
- Definitely Yes
- I prefer not to answer

G. Do you see yourself pursuing a career in MATH?

- Definitely Not
- Probably Not
- Not Sure
- Probably Yes
- Definitely Yes
- I prefer not to answer

H. Do you see yourself pursuing a career in SCIENCE?

- Definitely Not
- Probably Not
- Not Sure
- Probably Yes
- Definitely Yes
- I prefer not to answer

I. Do you plan to go to college?
   - Yes
   - No
   - Not Sure

J. Do you know any adults that have a career in STEM?
   - Yes
   - No
   - Not Sure

Part II – **Efficacy** of STEM related activities and careers:

Directions: There are lists of statements on the following pages. Please mark your answer sheets by marking how you feel about each statement.

Please fill in on only one answer per question.

1. **SCIENCE**:

Self-efficacy	Strongly Disagree	Disagree	Unsure	Agree	Strongly Agree
I am believe I can get an "A or B" in a SCIENCE class.*					
If I work hard enough, I can learn difficult SCIENCE concepts.*					
I cannot understand SCIENCE even if I try hard.*					
I am confident that I can be successful in SCIENCE.*					
I feel confident when using SCIENCE outside of class.*					
I believe I am the type of person that can do SCIENCE.*					
I feel that I will do well in future SCIENCE classes.*					
I believe I can do well on a SCIENCE homework.*					
I believe I can do well on a SCIENCE test.*					
I am confident that I can learn new SCIENCE skills.*					
SCIENCE is hard.*					
I am sure I could take advance SCIENCE classes in high school.*					
I am considered smart in SCIENCE.*					
I get nervous when taking a SCIENCE test.**					
Working on SCIENCE homework is stressful.**					
I get nervous when asking a question in SCIENCE class.**					
I get nervous when I use SCIENCE outside of class.**					

2. **MATH**:

Self-efficacy	Strongly Disagree	Disagree	Unsure	Agree	Strongly Agree
I am believe I can get an "A or B" in a MATH class.*					
If I work hard enough, I can learn difficult MATH concepts.*					
I cannot understand MATH even if I try hard.*					
I am confident that I can be successful in MATH.*					
I feel confident when using MATH outside of class.*					
I believe I am the type of person that can do MATH.*					
I feel that I will do well in future MATH classes.*					
I believe I can do well on a MATH homework.*					
I believe I can do well on a MATH test.*					
I am confident that I can learn new MATH skills.*					
Math is hard.*					
I am sure I could take advance MATH classes in high school.*					
I am considered smart in MATH.*					
I get nervous when taking a MATH test.**					
Working on MATH homework is stressful.**					
I get nervous when asking a question in MATH class.**					
I get nervous when I use MATH outside of class.**					

II. STEM Career Knowledge

Knowledge	Advance Math/Science Needed?			4-year Degree Required?		
	Yes	No	Unsure	Yes	No	Unsure
Electrical Engineer	Y			Y		
Car Mechanic	N			N		
Dental Hygenist	N			N		
Civil Engineer	Y			Y		
Cosmetologist	N			N		
Bioengineering Professor	Y			Y		
Registered Nurses	Y			N		
Engineering Technician	Y			N		
Plummber	N			N		
Politician	N			Y		
School Counselor	N			Y		
Mechanical Engineer	Y			Y		
Mathematician	Y			Y		
Medical Doctor	Y			Y		
Biochemist	Y			Y		

1. Please name three careers that you see as ENGINEERING careers.

_____ _____ _____

2. Please name three careers that you see as SCIENCE careers.

_____ _____ _____

3. Please name three careers that you see as MATH careers.

_____ _____ _____

III. **STEM Activity/Career Interest:**

Here are descriptions of subject areas that involve math, science, engineering and/or technology, and lists of jobs connected to each subject area. As you read the list below, you will know how interested you are in the subject and the jobs. Fill in the circle that relates to how interested you are.

There are no "right" or "wrong" answers. The only correct responses are those that are true for you.

Interests	Strongly Disagree	Disagree	Unsure	Agree	Strongly Agree
I am interested in learning more about math	○	○	○	○	○
I am interested in learning more about science	○	○	○	○	○
I am interested in the engineering design process	○	○	○	○	○
I am interested in learning more about engineering	○	○	○	○	○
I enjoy learning science	○	○	○	○	○
I would like to use creativity and innovation in my future career.	○	○	○	○	○
I enjoy learning about new technology	○	○	○	○	○
I enjoy learning engineering	○	○	○	○	○

Interests	Not at all Interested	Not so Interested	Interested	Very Interested
Physics (Astronomer__)	○	○	○	○
Environmental Work (Environmental Engineer)	○	○	○	○

Biology and Zoology (add__	○	○	○	○
Veterinary Work (add __	○	○	○	○
Mathematics (add accountant)	○	○	○	○
Medicine (Doctor, Nurse)	○	○	○	○
Earth Science (	○	○	○	○
Computer Science	○	○	○	○
Medical Science	○	○	○	○
Chemistry	○	○	○	○
Energy	○	○	○	○
Engineering	○	○	○	○

Part III – Social Influences in STEM related activities and careers:

perceived discrimination and SCK, MSE/SSE, SI

Revise for header → "Many factors can either support or hinder students' college and career plans. We are interested in learning about the types of situations that could help or hinder your plans."

Supports and barrers	Yes	No	Unsure
Do you believe that your TEACHERS can help you with MATH?			
Do you believe that your TEACHERS can help you with SCIENCE?			
Do you believe your TEACHERS would be happy if you do STEM stuff?			
Do you believe that your FAMILY can help you with MATH?			
Do you believe that your FAMILY can help you with SCIENCE?			
Do you believe your FAMILY would be happy if you do STEM stuff?			
Do you believe your FRIENDS think you are good at MATH?			
Do you believe your FRIENDS think you are good at SCIENCE?			
Do you believe your FRIENDS can help you with STEM stuff?			
Has anyone ever told you that you are not smart enough for STEM?			